PROCESSES LEADING TO THE FORMATION OF TECTONIC FEATURES ON THE MOON AND MARS

by

Jennifer Lynn Hall

S.B., Massachusetts Institute of Technology
(1978)

SUBMITTED TO THE DEPARTMENT OF
EARTH, ATMOSPHERIC, AND PLANETARY SCIENCES
IN PARTIAL FULFILLMENT
OF THE REQUIREMENTS
FOR THE DEGREE OF

DOCTOR OF PHILOSOPHY

at the

MASSACHUSETTS INSTITUTE OF TECHNOLOGY

August 1985

Signature of Author _____
Department of Earth, Atmospheric, and Planetary Sciences

Certified by _____
Sean C. Solomon
Thesis Supervisor

Accepted by _____
Chairman, Department Committee

Table of Contents

PROCESSES LEADING TO THE FORMATION OF TECTONIC FEATURES ON THE MOON AND MARS

by

Jennifer Lynn Hall

Submitted to
the Department of Earth, Atmospheric, and Planetary Sciences
on August 5, 1985 in partial fulfillment of the
requirements for the degree of Doctor of Philosophy
in Geophysics

ABSTRACT

The surfaces of the terrestrial planets have been shaped by several distinct physical processes, in particular the exogenous process of projectile impact and the endogenous processes of volcanism, loading, and ductile flow. The stress fields produced by these processes led to the formation of many of the tectonic features on planetary surfaces. By constructing models for the physical processes governing the tectonic history of a region, and comparing the predictions made by those models with the available data, we can constrain the processes involved. In this thesis such an approach is applied to three problems in the tectonics of the Moon and Mars: the formation of lunar floor-fractured craters, the origin of tectonic features in the irregular maria, and the tectonic history of the Elysium volcanic province of Mars.

We evaluate the hypothesis that topographic modification of floor-fractured craters on the Moon was accomplished predominantly by viscous relaxation. Adopting the simple assumption that the Moon may be modeled as having a uniform Newtonian viscosity, we compare the observed topographic profiles for a number of floor-fractured craters with the profiles predicted from the viscous relaxation of topography of fresh craters of similar diameter. Despite the simplicity of the rheological model, the comparison is quite good. The floor uplift, the rim subsidence, and the apparent subsidence ouside the rim for the several floor-fractured craters considered are well matched by the viscous relaxation hypothesis. Floor fractures, while indicating that a purely viscous model is not strictly valid, can be explained by the effects of isostatic adjustment on a thin brittle lithosphere. The association of many floor-fractured craters with impact basins and with the

time of mare volcanism can be understood in terms of a pronounced acceleration of crater relaxation in local regions of anomalously high near-surface temperatures and therefore of low effective viscosity and thin lithosphere. The quantitative extent of relaxation of floor-fractured craters can be interpreted in terms of a limited time interval of substantial relaxation for each crater. That time interval ended for each crater after local cooling had been sufficient for the viscosity to rise, for the lithosphere to thicken, and for the present topographic relief to be "frozen in". Thus viscous relaxation can explain the topographic profiles of a number of lunar floor-fractured craters, and the extent of viscous relaxation of crater topography may serve as a tool to map lateral and temporal variations in the shallow thermal structure of the Moon and of other satellites and planets.

It has been shown that many of the tectonic features associated with the circular maria are the result of stresses generated by loading of the lunar lithosphere by mare basalt units. We test the assumption that the irregular maria share with the circular maria the processes leading to the formation of mare ridge systems and basin-concentric graben. To do this, we develop a general formulation of the lithospheric flexure problem to model the asymmetric basalt loads for the irregular maria. On the basis of the tectonic structures and geologic history of each of the major irregular maria, as well as models for the distribution of mare basalt for each region, we compare the predicted stress fields with the distribution of tectonic features for various assumed values of the thickness of the elastic lithosphere. Loading models are quite successful at predicting the orientations of ridges and graben for each region. For each mare we have found that the lithospheric thickness at the time of ridge formation appears to have been somewhat greater than that at the time of graben formation. Our lithospheric thickness estimates are generally consistent with previous estimates for the neighboring circular maria.

We compare the distribution of lunar floor-fractured craters with other factors related to lunar tectonic history, including basin age, ages of mare units, and lithospheric thicknesses. Floor-fractured craters are clustered around the edges of the maria, in particular around the old and intermediate-age basins Procellarum, Nectaris, and Smythii. There is no obvious correlation between the locations of floor-fractured craters and the lithospheric thicknesses beneath the maria at the time of formation of larger scale tectonic features. If the lowered viscosities producing relaxed crater topography are due to elevated near-surface temperatures (which seems likely), the presence and distribution of floor-fractured craters are in a general sense measures of the thermal state of each region relatively soon after basin formation.

The second largest volcanic province on Mars lies in the Elysium region. Like the larger Tharsis province, Elysium is marked by a topographic rise and a broad free-air gravity anomaly and also exhibits a complex assortment of tectonic and volcanic features. We test the hypothesis that the tectonic features in the Elysium region are the product of stresses produced by loading of the Martian lithosphere. We consider loading at three different scales: local volcanic loading (individual shields), regional loading of the lithosphere from above or below, and quasi-global loading by Tharsis; and we compare the predicted stress fields from such models with the distribution and orientation of tectonic features. A comparison of flexural stresses with lithospheric strength and the with inferred maximum depth of faulting confirm that concentric graben around Elysium Mons can be explained as the result of local flexure of an elastic lithosphere about 50 km thick in response to the volcano load. Volcanic loading on a regional scale, however, leads to predicted stresses inconsistent with all observed tectonic features, suggesting that loading by widespread emplacement of thick plains deposits was not an important factor in the tectonic evolution of the Elysium region, either because regional volcanic units were isostatically compensated without lithospheric loading or because the elastic lithosphere was sufficiently thick on a regional scale that it could support a broad load without surface stresses reaching levels which would cause fracture. A number of linear extensional features oriented generally NW-SE may be the result of flexural uplift of the lithosphere on the scale of the Elysium rise. A simple circularly symmetric uplift model is shown to predict appropriate orientations and magnitudes of principal stresses, but does not explain the preferred trends of the faults; the asymmetry could be the result of heterogeneities in lithospheric thickness over the region (with local thinning in the areas where fracturing occurs) or of unmodelled asymmetries in the extent of uplift. The global stress field associated with the support of the Tharsis rise appears to have influenced the development of tectonic features in the Elysium region, including Cerberus Rupes and the systems of ridges in eastern and western Elysium. The comparisons of stress models for Elysium with the preserved tectonic features supsport a succession of stress fields operating at different times in the region, but our ability to determine from present observations the order in which those stress fields operated is very limited. On thermal and mechanical grounds, however, we expect that flexural uplift of the lithosphere by a mantle thermal anomaly would have preceded or occurred contemporaneously with emplacement of the largest volcanic loads. We conjecture that the earliest volcanic activity in the Tharsis province may also have been the result of lithospheric uplift, but either the scale of such uplift was considerably smaller than the present horizontal extent of the Tharsis rise or the tectonic evidence of this uplift has been long since erased by subsequent volcanism and faulting.

ACKNOWLEDGEMENTS

First of all, I would like to thank my advisor, Sean Solomon, for providing me with generous financial support for the last seven years. I think it would have been only slightly more expensive to send me physically to the Moon or Mars than it has been to pay my tuition all these years. He also suggested the research projects that form this thesis. My admiration for his scientific abilities is truly unbounded.

Next, I would like to thank all the people who were my mentors at various stages of my time at MIT: David Adler of the Electrical Engineering Department, Ted Greenwood of the Political Science Department, John Filson of the US Geological Survey, Rae Goodell and Barbara Gastell of the MIT Writing Program, Sharon Begley of Newsweek, Steve Marcus of The New York Times, and Robert Jastrow of Columbia University and Dartmouth College. These people gave me advice and career counseling; they read my halting first drafts and edited my manuscripts. Most importantly, they believed in me and in my abilities. Their generous and unstinting support of my ego meant more to me than I can say.

As I leave MIT, the most precious thing I take with me is not my doctorate, but a truly remarkable collection of friends. My words can only begin to express the gratitude and love I feel for them. My friends suffered through the usual stormy weather of grad school along with me. They endured my too-frequent black moods with more grace and patience than I deserved, and accepted my transformation from scientist to writer with considerably more equanimity than I did myself.

My special thanks go to:

Eric Bergman, my surrogate advisor.

Roger Buck, comrade extraordinaire, who understands the narcoleptic value of a good stiff drink better than anyone.

Guy Consolmagno, whose two-year absence from the U.S. gave me an excuse to keep the verbal half of my brain alive by writing letters.

Dan Davis, who always liked the things I wrote.

Bob Grimm, who set the appropriate tone for my defense by sitting in the front row wearing an "Ask Mr. Science" t-shirt.

Sarah Kruse, who made me eat lunch before my defense.

The Late Shift, summer 1985 edition: Paul Huang, Multics wizard, who always stayed later than I did; Kiyoshi ("Spits Out the Truth") Yomogida, who, when the word processor on the 5th floor broke down at 11 p.m. the Sunday before my thesis was due, called the campus police and persuaded them to unlock the 9th floor word processor room; and Mark Murray, whose taste for fine literature influenced mine to such an extent that I may never be able to make my fortune writing trashy science fiction novels.

Jim Montanaro, who qualified for sainthood by loaning me a computer terminal for nearly two years, enabling me to do the majority of the program development for this thesis in the comfort of my own home while I watched late-night movies.

All present and former occupants of 54-410 (you know who you are!)

I'd also like to thank Dr. Peter Jenney of the MIT Medical Department, who helped me preserve the tattered shreds of my sanity as I struggled through this thesis.

Jimmy (of the MIT Physical Plant staff) kept close track of my progress through this thesis, and brought me cookies and candy to cheer me up when I was down. Thanks, Jimmy, and good luck!

My thanks also go to the people whose lives and works touched mine, and helped me find my way through 11 very long years at MIT: Fred Astaire, David Byrne and Talking Heads, Laurie Anderson, Stephen Sondheim, George Hearn, Ben Kingsley, Phillip Glass, David Horner, William Shatner and Leonard Nimoy, the Firesign Theater, Peter Elbow, and Harlan Ellison.

Next, I would like to express my gratitude to the commercial establishments in Boston, Cambridge, and New York City that allowed me to give them my money in exchange for the finer things in life: the Sack Cinemas, the Harvard Square Theater, the Brattle Theater, the Coolidge Corner Theater, the Nickleodeon Cinema, the Orson Welles Cinema, Off the Wall Theater and Cafe, the late lamented Exeter, Park Square, Kenmore, and Central Square Theaters; Mary Chung's Restaurant, Toscanini's Ice Cream ("the unsung key to health and beauty"), Miyako Restaurant, the Gandhi Restaurant, Smokey's Barbeque of New York, the Metropolitan Opera, the New York City Opera, the Brooklyn Academy of Music, the Boston Symphony Orchestra, the late Boston Shakespeare Company, and the American Repertory Theater.

Thanks to my support staff, who worked incredibly hard this summer to help me bring this thesis in on time: Linda Meinke did dozens of computer plots for me, and never lost her cool or her good humor even when I had to ask her to do things over. My sister, Leigh Hall, gave up her evenings and weekends

for the entire summer in order to do most of the drafting of the figures for this thesis. Pat McDowell did lettering on my moon maps for chapter 3; she did a great job on very short notice, and managed to get them done a day early! Jan Nattier-Barbaro is the most staggeringly competent technical typist on the planet. None of my weird typing requests (like consolidating six sets of references into one) ever seemed to faze her at all. Sharon Feldstein and Janet Sahlstrom were always ready with requisitions when I needed them, and never gave me grief about where the money went.

Thanks to my mother for putting up with me all these years. "Made it, Ma - top of the world!"

Finally, my thanks go to my husband, Rick Buxton. For the last two years he has been chief cook and bottle washer, laundryman, maid and butler, accountant, grocery shopper, assistant statistician, and therapist. And, when my struggles to complete this thesis on time brought me to the edge of physical, emotional, and mental collapse, he dropped his own job completely and dragged me through the final days. He also acted as editor in charge of semicolon eradication.

Rick, nothing has worked out the way we thought it would when we were married in 1978. We've both changed, and the future is as uncertain as it can be. I regard it as a major miracle that after all we've been through you'll still let me warm my icy feet against you at night. With you beside me, my love, I can face a thousand rejection slips!

The research on this thesis was supported by an Ida Green Fellowship (1978-1979), and by the NASA Planetary Geology and Geophysics Program under grants NSG-7081 and NSG-7297. thanks!

This page intentionally left blank.

CHAPTER 1

INTRODUCTION

You know,
I could write a book.
And this book
would be thick enough
to stun an ox.

-- Laurie Anderson, "Let X=X Tango"

The surfaces of the terrestrial planets have been shaped by several distinct physical processes, in particular the exogenous process of projectile impact and the endogenous processes of volcanism, loading, and ductile flow. The stress fields produced by these processes led to the formation of many of the tectonic features on the surfaces of the planets. The extent and style of tectonic features in each case are functions of the physical conditions in the planetary interior. The near-surface thermal environment is especially important because it is a controlling factor in the effective viscosity of near-surface material and determines the lithospheric thickness as a function of space and time.

Studies of the tectonic histories of the terrestrial planets other than the Earth are limited largely by the types of data available. Information on the gravity and topography of a planet constrains the present structure, but provides little clue to the processes that led to the present state. Important information on the stress history of a region is provided by photographic evidence of tectonic features. Photographic data also provide essential information on surface geology and stratigraphy. By constructing models for the physical processes governing the tectonic history of a region, and comparing the predictions made by those models with the available data, we can constrain the processes which have acted to shape the surfaces of the terrestrial planets.

In this thesis this approach has been applied to three problems in the tectonics of the Moon and Mars: the formation

of lunar floor-fractured craters, the origin of tectonic features in the lunar irregular maria, and the tectonic history of the Elysium volcanic province of Mars. In each of these problems a particular physical process has been modelled. In each case the model results are compared with photogeologic evidence to assess the ability of the model to account for the observed tectonic features and, if possible, to set limits on one or more important physical parameters such as near-surface viscosity or lithospheric thickness.

Approximately 200 craters on the lunar surface have visible fractures on their floors [Schultz, 1976]. Floor-fractured craters have generally shallow interior relief compared to fresh impact craters. Most (but not all) of them are clustered around the edges of the irregular and circular maria. Although floor-fractured craters have been explained as being entirely endogenic in origin [DeHon, 1971; Cameron and Padgett, 1974; Whitford-Stark, 1974], it is now generally believed that they are the product of endogenic modification of impact craters [Pike, 1968; Brennan, 1975; Bryan et al., 1975; Schultz, 1976]. The two models that have been most frequently proposed to explain the topography and fracture patterns of floor-fractured craters are (1) volcanic uplift and fracture of the crater floor by magmatic intrusion beneath the crater [Young, 1972; Brennan, 1975; Bryan et al., 1975; Schultz, 1976] and (2) viscous relaxation of crater topography [Masursky, 1964; Danes, 1965; Baldwin, 1968; Pike, 1968]. For both hypotheses, the distinctive characteristics of most

floor-fractured craters are related to their proximity to the maria, with their associated thermal anomalies and magma sources.

The tectonic history of the Moon has been dominated by the formation of large impact basins and by the formation and evolution of the lunar maria that fill many of these basins. The lunar maria can be divided into two groups: irregular and circular. The irregular maria occupy basins which are in general older than those filled by the circular maria and lack the well-defined basin ring structure [Stuart-Alexander and Howard, 1970] and large positive gravity anomalies associated with the circular maria [Muller and Sjogren 1968; Phillips and Lambeck, 1980]. The irregular maria, like the circular maria, contain extensive systems of tectonic features, both extensional and compresssional. For the circular maria, the basin-concentric graben and mare ridge systems have been interpreted as being the result of flexure of the elastic lithosphere under the load imposed by mare volcanic units, combined with modest global thermal stresses which are a function of time [Comer et al, 1979; Solomon and Head, 1979, 1980]. The fact that the tectonic features in the irregular maria are morphologically similar to those in the circular maria suggests that they may have formed in a similar manner.

On the planet Mars, the tectonic history has been dominated by the formation and evolution of several major volcanic provinces, rather than by the formation of impact basins and maria such as are seen on the Moon. The Tharsis volcanic province, which is the largest, has received the most

research attention; debate nonetheless continues on whether the Tharsis rise and associated tectonic features are principally the result of lithospheric uplift [Carr, 1974; Wise et al., 1979; Plescia and Saunders, 1979] or of volcanic construction and lithospheric loading [Solomon and Head, 1982]. Recent quantitative models for the Tharsis region have made it clear that loading of the lithosphere by volcanic units was an important process in the tectonic history of the region [Banerdt et al., 1982; Willemann and Turcotte, 1982].

The Elysium region is the second largest volcanic province on Mars [Malin, 1977]. Like Tharsis, Elysium is marked by a topographic rise and a broad free-air gravity anomaly [Sjogren, 1979; Janle and Ropers, 1983]. The Elysium region also exhibits a variety of tectonic and volcanic features. The tectonic features of the Tharsis region have been shown to be generally consistent with the response of the Martian lithosphere to the excess topography [Banerdt et al., 1982; Willemann and Turcotte, 1982]. By modelling the processes leading to the formation of tectonic features in the Elysium volcanic province, it should be possible to determine whether Elysium and Tharsis share a similar volcanic history.

In this thesis we combine photogeologic data and gravity and topographic data to model the formation of lunar floor-fractured craters (Chapter 2), the origin of tectonic features in the irregular lunar maria (Chapter 3), and the tectonic history of the Elysium volcanic province of Mars (Chapter 5).

In Chapter 2 we evaluate quantitatively the hypothesis that topographic modification of lunar floor-fractured craters was accomplished primarily by viscous relaxation. Adopting the simple assumption that the Moon may be modeled as having a uniform Newtonian viscosity, we compare the observed topographic profiles for a number of floor-fractured craters with the profiles predicted from the viscous relaxation of topography of fresh craters of similar diameter. We invert the difference in topographic profiles between floor-fractured craters and fresh craters to obtain the best-fitting value of the single free parameter t/η in the viscous relaxation model, where t is the time over which relaxation occurred and η is the viscosity of the near-surface material. Because most fracturing of crater floors occurred in proximity to mare basins or other mare deposits and within the time interval between mare basin excavation and cessation of mare volcanism [Schultz, 1976], it is likely that t/η is a measure of relaxation time and effective viscosity during the portion of that time interval when local temperatures were raised to their highest values by the combined effects of impact and volcanic heating. A version of this chapter was published as Hall et al. [1981]; several revisions to the text have been made for this thesis to update the arguments ~~for this thesis.~~

Like the circular maria, the irregular lunar maria exhibit a wide variety of both extensional and compressional tectonic features [e.g., Guest and Murray, 1976]. For the circular maria, most of these features have been interpreted as being

the result of flexure of the elastic lithosphere under the load imposed by mare volcanic units. Solomon and Head [1979, 1980] and Comer et al. [1979] used the thin-shell flexure model of Brotchie and Silvester [1969] and Brotchie [1971] for circularly symmetric loads to find the value of the lithospheric thickness for the circular maria at the time of formation of tectonic features. In Chapter 3 we extend their work to the major irregular maria, for which the basalt loads cannot be modelled with the assumption of cylindrical symmetry. Because the flexure equation is linear, the stresses due to any distributed load can be represented by the superimposed stresses due to an equivalent distribution of circular loads. We use this approach to determine the stress distributions predicted by loading models based on the near-side mare basalt thicknesses calculated by Bratt et al. [1985a] from lunar gravity and topography. By comparing the predicted stress fields to the observed tectonic features we determine the extent to which the observed features are the product of basalt loading. In addition, we also obtain a rough estimate of the elastic lithosphere thickness for each region during the time of tectonic activity. The chapter concludes with a comparison of the calculated lithospheric thicknesses for the irregular maria with those previously calculated for the circular maria and a discussion of the implications of the results for the thermal structure of the Moon.

Chapter 4 is a discussion of the possible relationship between the geographic distribution of lunar floor-fractured

craters and the history of formation and filling of the lunar maria. In particular we will discuss possible reasons for the clustering of floor-fractured craters around certain lunar maria.

In Chapter 5 we test the hypothesis that the tectonic features in the Elysium region of Mars are the result of stresses produced by lithospheric loading. We begin with a description of the physiographic features in the Elysium region which are of probable tectonic origin, based primarily on our own examination of the photogeology of the region. We then test the hypothesis that these features are products of volcanic loading of the lithosphere, considering loading at three different scales: local (individual volcanoes), regional (on the scale of Elysium Planitia), and quasi-global (Tharsis). For the loads of individual volcanoes we use the approximation of Brotchie and Silvester [1969] and Brotchie [1970] for flexure of a thin elastic shell overlying an inviscid fluid interior. To determine the stress distribution predicted by regional loading models we apply the generalized approach developed in Chapter 3. For the Tharsis load we use the spherical harmonic solutions of Banerdt et al. [1982] for displacement and stress in a thick elastic spherical shell given the topography and gravity. By comparing the predicted stress fields from these models with the distribution and orientation of the observed tectonic features, we evaluate the relative importance of of loading on the different scales.

In Chapter 6 we discuss some general conclusions of this

thesis relating to the formation of tectonic features on the terrestrial planets, in particular the importance of lithospheric loading as a process on the Moon and Mars. We then address questions generated by the analyses contained in this work. Finally, we suggest future work designed to help answer these questions.

CHAPTER 2

LUNAR FLOOR-FRACTURED CRATERS: EVIDENCE FOR VISCOUS RELAXATION OF CRATER TOPOGRAPHY

I'm checking it out
I'm checking it out
I've got it figured out
I've got it figured out
Some good points
Some bad points
It all works out
Some times I'm a little freaked out...

-- Talking Heads, "Cities"

INTRODUCTION

There are approximately two hundred craters on the lunar surface that have visible fractures on their floors (Figure 1). Floor-fractured craters have generally shallow interior relief compared to fresh impact craters and tend to be clustered around the edges of the maria; floor fracturing of such craters typically occurred between the time of formation of the nearest mare basin and the time when mare volcanism locally ceased [Schultz, 1976]. Many floor-fractured craters, for example, are located in the regions adjacent to northwestern Oceanus Procellarum, around Mare Nectaris, and along the southern border of Mare Smythii.

A number of workers have considered at some length the processes that could lead to modification of crater topography and to fracturing of crater floors [Masursky, 1964; Danes^{v}, 1965; Pike, 1968; Brennan, 1975]. General classification schemes for floor-fractured and modified craters have been proposed by Young [1972], Cameron and Padgett [1974], Whitford-Stark [1974] and Schultz [1976]. Detailed geologic studies of individual floor-fractured craters have been made for Humboldt [Baldwin, 1968], Goclenius [Baldwin, 1971a; Bryan et al., 1975], Ritter and Sabine [De Hon, 1971], and Haldane [Wolfe and El-Baz, 1976]. The groups of floor-fractured craters located within the large crater Aitken were discussed by Bryan and Adams [1974], and those within Mare Smythii were discussed by Greeley et al. [1977].

Although floor-fractured craters have been explained as being entirely endogenic in origin [De Hon, 1971; Cameron and Padgett, 1974], it is now generally believed that they are the result of endogenic modification of impact craters [Pike, 1968; Brennan, 1975; Bryan et al., 1975; Schultz, 1976]. The two models that have been most frequently proposed to explain the shallowness and fracture patterns found in floor-fractured craters are (1) volcanic uplift and fracture of the crater floor by magmatic intrusion beneath the crater [Young, 1972; Brennan, 1975; Bryan et al., 1975; Schultz, 1976] and (2) viscous relaxation of crater topography [Masursky, 1964; Danes, 1965; Baldwin, 1968; Pike, 1968]. For both hypotheses, the distinctive characteristics of most floor-fractured craters are related to their proximity to thermal anomalies or magma sources near mare units. It should be noted, however, that approximately 20 percent of floor-fractured craters occur at significant distances from the nearest major mare unit [Schultz, 1976].

In this chapter, we consider at length the hypothesis that topographic modification of floor-fractured craters was accomplished predominantly by viscous relaxation. We first address the principal objections raised in the literature to the importance of viscous effects, including the presence of fractures, the nonuniform distribution of floor-fractured craters both by region and locally with respect to crater size and age, and questions of time scale and viscosity. We argue below that none of these issues need stand as

objections when viewed in light of evidence for strong spatial and temporal variations in the temperature and rheology of the outer portions of the Moon during the time of mare volcanism.

The topographic profiles of floor-fractured craters allow us to pose specific and quantitative tests of the hypothesis that these profiles are the result of viscous relaxation. To accomplish such a test, we have determined the difference in topographic profiles between a number of floor-fractured craters and fresh craters of about the same diameter (Figure 2). These differences represent estimates of vertical displacement as functions of radial distance for the floor-fractured craters. Adopting a very simple rheological model for the Moon, a viscous half-space, we have inverted these displacement profiles to obtain the best fitting value of the parameter t/η, where η is the viscosity and t is the time during which important viscous relaxation occurred.

Our inversion method reveals that in six of the eight cases examined a surprisingly good fit to the observed floor-fractured crater topography may be obtained by using only this simple model of viscous relaxation. This result suggests that isostatic adjustment of craters in areas of anomalously high temperatures at shallow depth may be a more important source of deformation on the moon than has been generally appreciated.

VISCOUS RELAXATION MODEL

If the outer portions of the moon may be idealized as a viscous material of uniform Newtonian viscosity, then the topographic relief of a crater is a predictable function of the time since crater formation. We assume that crater topography at any time t is cylindrically symmetric about the crater center. Then the topography f is a function only of t and of the radial horizontal distance r from the center of the crater.

Regarding the Moon as a half-space of uniform viscosity η and density ρ, the solution for $f(r,t)$ for any $t > 0$ is given by [Cathles, 1975]

$$f(r,t) = \int_0^\infty F(k)e^{-\rho g t/2\eta k}J_o(kr)\, k\, dk \qquad (1)$$

were g is the gravitational acceleration, k is the radial wave number, J_o is the Bessel function of order zero, and

$$F(k) = \int_0^\infty f(r,0)J_o(kr)r\, dr \qquad (2)$$

is the Hankel transform of $f(r,t=0)$. Equation (1) has the form of an inverse Hankel transform, where each wave number component of F(k) has been reduced by the multiplicative factor $e^{-t/\tau(k)}$, and where the characteristic viscous relaxation time

$$\tau(k) = 2\eta k/\rho g \qquad (3)$$

is linearly proportional to viscosity and to wave number. Note that if f(r,0) is known, f(r,t) in equation (2) depends only on the single free parameter t/η. We adopt

ρ = 2.9 g/cm^3 and g = 162 cm/sec^2. In practice, the upper limit of integration in equation (2) was taken to be 2R, where R is the crater radius, on the grounds that crater-related topography at this range is small and that the contribution to topography from other lunar features is likely to dominate [Settle and Head, 1977].

From equation (3) it may be seen that long-wavelength features (small k) will relax more quickly than short-wavelength ones (large k). This means that the floor of a crater will rise more quickly than the rim will sink, because the floor is dominantly a long-wavelength variation of topography, while the crater rim and central peaks are short-wavelength features. These results are illustrated in Figure 3. Equation (3) also implies that large craters will relax more quickly than small craters. A number of workers have interpreted the observed decrease in the depth/diameter ratio for at least some large craters as a consequence of isostatic relaxation of a form similar to that described by equations (1-3) [Pike, 1968, 1976; Baldwin, 1971b].

Viscous relaxation of idealized fresh lunar crater topography has been modeled by Danes^v [1965], R.F. Scott [1965], and Kunze [1973]. Viscous relaxation models have also been used to explain the topography of craters on icy satellites [Johnson and McGetchin, 1973; Parmentier and Head, 1979, 1980; Passey and Shoemaker, 1982]. The predicted characteristics of a viscously relaxed crater [Danes^v, 1965] include the following:

(1) The interior relief of the crater decreases as the crater floor rises and the rim subsides. (Rim uplift can occur for a period prior to rim subsidence; see Figure 3.)

(2) The floor of the crater flattens as it rises. Depending on the initial crater topography, doming of the floor can occur at some stages in the relaxation.

(3) A shallow depression develops immediately outside the crater rim.

Although viscous relaxation has long been recognized as potentially providing a mechanism for producing the general shallowness of floor-fractured craters and other modified craters, the importance of the process has usually been discounted on one of several grounds:

(1) The very presence of fractures on the crater floors indicates that at least some portion of the lunar surface material does not always behave in a perfectly viscous manner. Viscoelastic and plastic rheologies have been applied to the problem of crater modification, though to explain the formation of features of significantly greater scale than typical floor fractures, by Melosh [1976] and McKinnon [1978], respectively.

(2) Not all lunar craters of a given size, age, or region are floor-fractured. If viscous relaxation has acted to modify only some craters, then the

process must vary drastically in efficiency both in time and over short horizontal distances [Pike, 1968; Schultz, 1976].

(3) A viscosity of 10^{22} poise, the value indicated for most of the Earth's mantle on the basis of glacial rebound analysis [e.g., Cathles, 1975], would allow the topography of even small craters (10 km diameter) to relax completely in an unreasonably short period of time, on the order of 10^6 to 10^7 years [R.F. Scott, 1967]. Therefore, if viscous relaxation is occurring to any considerable degree, the average viscosity of lunar near-surface material in the time since crater formation must be quite high, on the order of 10^{25} poise [Baldwin, 1971b]. Otherwise the observed crater shapes could not have been preserved for the necessary amount of time.

None of these objections to viscous relaxation as an important contributor to the topographic modification of floor-fractured craters stands, however, once it is recognized that the near-surface temperature, and thus the rheology of lunar material, varied strongly with space and with time during the several hundred million years following formation of the youngest major impact basins [Solomon and Head, 1979, 1980]. We consider these objections in turn.

The presence of fractures need not rule out viscous relaxation. If the lunar surface is treated as a thin brittle layer of some elastic strength overlying a

viscous interior, then the evolution of craters whose size is large compared to the local lithosphere thickness would be dominated, especially after a long period of time, by the isostatic adjustment taking place in the underlying viscous material [Pike, 1968; Melosh, 1976]. The fractures may then be attributed to stresses created by the mass deficiency within the crater itself; although these stresses are relieved at depth by viscous flow beneath the crater, stresses in excess of lithospheric strength must be relieved by fracturing near the surface [Melosh, 1976]. The presence of a surface brittle layer may alter the relaxation process somewhat, however, over that in a viscous half-space [Danes[v] and McNeely, 1971; Cathles, 1975]. Qualitatively, the effect of a thin brittle layer at the surface would be to impede the relaxation process for short-wavelength features, such as crater rims. However, the short-wavelength features relax much more slowly than the long-wavelength features even in the viscous half-space model. Thus, the presence of a thin brittle layer would not substantially alter the results of our models.

The location of the floor-fractured craters is far from random. The close association of such craters with the margins of mare basins suggests a connection between basin formation and filling and the modification of floor-fractured craters; many floor-fractured craters are themselves partially flooded with volcanic material [Pike, 1968, 1971; Schultz, 1976]. The locally elevated temperatures that would

be expected during mare volcanism, and the influence of heat remaining from the basin excavation event [Bratt et al., 1985] could preferentially lower the effective viscosity of lunar near-surface material within and at the periphery of flooded basins and other major mare units. The thickness of a lithosphere of finite elastic strength would also be substantially less than in areas far from recent heating. Thus the characteristic time for viscous relaxation of many near-mare craters during the era of mare filling may have been much less, and the tendency for the lithosphere to fail in response to uncompensated topography may have been much greater, than for craters of comparable age elsewhere on the moon. In some areas, floor-fractured and unmodified craters of similar size and apparent age occur side by side (although we note that the extensive modification of floor-fractured craters often makes it difficult to estimate their ages). In other regions relatively small craters have apparently undergone greater modification and floor fracturing than adjacent larger craters [Schultz, 1976]. These characteristics indicate that regions of high temperature and low effective viscosity may have been sometimes localized to the immediate vicinity of the involved crater. Several potential sources for such localization of heating include (1) volcanism and shallow igneous intrusion [Schultz, 1976], (2) thermal effects of the impact event itself [Bratt et al., 1985b], and (3) impact melt remaining in basin secondary craters [Schultz and Mendenhall, 1979].

Because the outer portions of the Moon cooled rapidly during and after the era of mare filling [Solomon and Head, 1979, 1980], the rheology of lunar near-surface material can be expected to have changed markedly with time. In particular, comparatively low values for effective viscosity of near surface material would have persisted only for the relatively short time interval of most extensive volcanism and shallow plutonism in each region. Following this time, cooling would raise the effective near surface viscosity (and thus the viscous relaxation times) rapidly and would lead to thickening of the outer lithosphere capable of supporting differential stress. Thus any partially relaxed topography would be "frozen in" as the outer portions of the Moon increased in viscosity and acquired greater elastic strength. For this "freezing in" to occur, the near-surface effective viscosity must become high enough to prevent crater topography from disappearing even after a billion years or more have passed.

On the basis of these considerations, the cited objections to viscous relaxation of floor-fractured craters are not sufficient to rule out the process. On the contrary, viscous relaxation appears to be a viable hypothesis for topographic modification of craters in regions of elevated near-surface temperatures on the Moon. Because crustal and upper mantle temperatures on the Moon showed pronounced spatial and temporal variations, there is a straightforward explanation of the spatial and temporal distribution of most

floor-fractured craters. The fractures in the floors may be attributed to the same topographically produced stresses that give rise to viscous uplift. And finally, as we show below, a viscous relaxation model can account quantitatively for the topographic profiles of many floor fractured craters.

Our use of the simple viscous half-space model may be at least qualitatively justified by the small size of the craters treated in this study. Decay of topography of a particular wavelength involves viscous deformation to a depth comparable to that wavelength [Parmentier and Head, 1979, 1981]. The largest crater modeled in this study has a radius of 20 kilometers; thus for these craters the material flowing in response to viscous relaxation of crater topography is confined generally to the upper half of the lunar crust. At larger scales, models involving variations in viscosity with depth due to thermal gradients and compositional layering are appropriate; such models have been applied to the relaxation of lunar impact basins [Solomon et al., 1982a], and to the estimation of the preservation time of impact basin topography on Venus [Solomon et al., 1982b].

CRATER TOPOGRAPHIC DATA

The basic data set we shall use to test the hypothesis that floor fractured craters result from viscous relaxation consists of topographic profiles of floor-fractured and of fresh craters of comparable size. The topographic data have generally been taken from Lunar Topographic Orthophoto (LTO) maps.

The difference between topographic profiles for a fresh crater and a floor-fractured crater of the same rim diameter is a measure of the vertical displacement as a function of radial distance from crater center for the modified crater. The two profiles may be used with equation (2) to test the viscous relaxation model and to find the value of t/η that best matches the observed difference in topography. In practice, it has not been possible to find a fresh crater with exactly the same diameter as any given floor-fractured crater. Thus for each floor-fractured crater in our study, we located a fresh crater of closely similar diameter, adjusted the horizontal scale for fresh crater topography by a multiplicative constant (near unity) so that the two craters have the same rim diameter, and then tested the viscous relaxation hypothesis as described. The zero elevation datum for both fresh and floor-fractured craters has been set equal to the level of the surrounding plain well removed from substantial ejecta deposits.

There are several uncertainties in the topographic profiles due not only to uncertainties in the basic data set but also to unmodelled irregularities in the topography of real craters. The LTO's have a precision of about ± 50 m, and a somewhat larger relative accuracy along a profile. Additional uncertainties of a small topographic amplitude are introduced by deriving profiles from elevation contour maps.

Further uncertainties arise in the comparison of two distinct craters, for several reasons. The major

characteristics of crater geometry (e.g., rim height, rim width, floor depth) even for fresh craters are not single-valued functions of crater diameter, but rather they are statistically distributed about well-established mean values [e.g., Pike, 1968, 1977, 1980]. In addition, for most craters, both fresh and fractured, the height of the crater rim above the surrounding plain and the topographic profile of the floor are not azimuthally symmetric [Settle and Head, 1977]. The variations of rim height, for instance, can be quite large; in the profiles for some craters in this study, the opposite rims had a difference in elevation of as much as 800 m. Probable causes of such azimuthal variations in rim height include variable slumping of original (transient) crater walls [Melosh, 1977]; erosion by subsequent impacts onto the crater or by infall of debris from impacts in the region [Head, 1975], the possible influence of precrater topography [Pike, 1977], and the angle of incidence of the crater-forming projectile [Settle and Head, 1977]. The variations in rim height for the fresh craters included in this study are, in general, larger than the variations for the floor-fractured craters [cf. Schultz, 1976]. Other asymmetries in topography which will affect the calculated displacement curves include a collection of slumped material on the crater floor and offset central peak complexes.

Additional factors that introduce uncertainties in the topographic profiles are the choices of the zero elevation datum and of rim location. The zero elevation datum is

difficult to ascertain if the area surrounding the crater is topographically irregular or if the topographic contour map does not include a sufficiently large area around the crater to enable a reliable estimate. As craters age, their rims become less sharp, wider and more subdued [Head, 1975]. For craters that are somewhat degraded, including the floor-fractured craters in this study, the choice of the exact rim location is not as precise as for the fresh craters with which they are compared. However, the rim crest diameter measurements for the floor-fractured craters of this study are believed to lie within 10% of the original crater diameters. In summary, the net effect of these uncertainties is likely to be minor, particularly considering the large size of the craters treated (crater radius 8-20 km).

INVERSION METHOD

We wish to invert the difference in topographic profiles between floor-fractured and fresh craters to obtain the best-fitting value of the single free parameter t/η in the viscous relaxation model. We first choose a trial value of t/η, apply equation (2) to the fresh crater topography to produce a predicted topographic profile for the modified crater, and then determine the difference between the observed and predicted profiles. The best model is taken to be the one that minimizes the integrated squared difference between the two profiles. By making a good initial estimate of t/η for use as the trial value, it is possible to use a linearized, iterative matrix inversion scheme to improve the fit.

We formulate the linearized inversion by following a simple approach to the general problem using model parameters P_j, observed quantities O_i, and calculated quantities $C_i(P_j)$. Given initial values for the parameters, we have

$$\sum_j \left[\frac{\partial C_i}{\partial P_j}\right] \Delta P_j = O_i - C_i \qquad (4)$$

which yields, after inversion, the corrections ΔP_j to the parameters that will improve the fit of the model to the observations. The above linear equation is of the form $\underset{\sim}{A}\underset{\sim}{x}=\underset{\sim}{b}$, where $A_{ij} = \partial C_i/\partial P_j$, $x_j = \Delta P_j$, and $b_i = O_i - C_i$.

In the problem considered in this paper, the vector $\underset{\sim}{b}$ is composed of the differences between observed and predicted topographic heights at n points equally spaced in horizontal distance r from crater center, from r = 0 to r = (N-1)Δr where Δr is the horizontal spacing. Equation (4) thus consists of N independent equations, $\underset{\sim}{A}$ is an N x 1 matrix and x is a scalar. That is,

$$\underset{\sim}{A} = \begin{bmatrix} \dfrac{\partial f(r=0,t)}{\partial (t/\eta)} \\ \vdots \\ \dfrac{\partial f(r=[N-1]\Delta r,t)}{\partial (t/\eta)} \end{bmatrix} \qquad x = \Delta(t/\eta)$$

$$\underset{\sim}{b} = \begin{bmatrix} h(r=0) - f(r=0,t) \\ \vdots \\ h(r=[n-1]\Delta r) - f(r=[N-1]\Delta r,t) \end{bmatrix} \qquad (5)$$

where h(r) is the observed floor-fractured crater topography and f(r,t) is the topography predicted using equation (2).

Because the system of equations is overdetermined, we use a least squares routine that gives the value of x that is most nearly consistent with the components of $\underset{\sim}{b}$, i.e., that minimizes Σb_i^2. After the linearized inversion, an adjustment $\Delta(t/\eta)$ to the trial value of t/η is calculated. By using the new value for t/η, a new linear inversion is performed. This process is repeated until the solution for f converges, or until the model fits the observed topography to within a specified uncertainty, e.g., an r.m.s. profile difference equal to the typical uncertainty in the measurement of topography. In practice, 5 to 10 iterations were generally sufficient in the present problem to achieve satisfactory convergence.

RESULTS OF INVERSION

The inversion method described above has been applied to the difference between topographic profiles for seven pairs of floor-fractured craters and fresh craters of nearly identical diameters. These craters and their diameters and geographic coordinates are given in Table 1. Our choice of craters was constrained primarily by the availability of good topographic data. We present the results of the inversions in a series of figures comparing predicted and observed topography for the floor-fractured craters under the hypothesis that the departure from fresh-crater topography is due to viscous relaxation. We discuss each crater pair in turn.

Dumas-Dawes. Dumas is a 16-km diameter fractured crater located just outside the southwestern edge of Mare Smythii (Figure 4a). Dumas has a narrow concentric fracture separating the crater wall and floor. The topography of Dumas is extremely subdued, with the crater floor at approximately the same height as the area exterior to the rim. The area immediately outside the crater appears to be somewhat lower than the zero datum plane.

The fresh crater Dawes (Figure 4b), also 16 km in diameter, lies on the boundary between Mare Serenitatis and Mare Tranquillitatis. The crater rim crest is slightly scalloped in appearance, owing to some wall slumping and floor-swirl formation. Dawes is typical of a crater lying in the transition between bowl-shaped and flat-floored morphologies [Pike, 1980].

The observed topographic profiles for Dumas and Dawes and the predicted profile for Dumas using the viscous relaxation model are shown in Figure 4c. The observed difference in topographic profiles between Dumas and Dawes and the predicted vertical displacements for Dumas are given in Figure 4d. The topography of Dumas is sufficiently subdued that substantial viscous relaxation is indicated by the model ($t/\eta = 3.7 \times 10^{-8}$ sec/poise). The fit of the observed topography to that predicted by the viscous relaxation hypothesis is quite good. The only important difference is that the rim of Dumas is somewhat wider than the rim predicted by the model.

Haldane-Timocharis. Haldane (40 km in diameter) is one of a large group of floor-fractured craters located in Mare Smythii [Wolfe and El-Baz, 1976; Schultz, 1976; Greeley et al., 1977]; see Figure 4a. The craters of this group are similar in appearance and are characterized by a flooded moat located within the crater rim and bounded by concentric fractures.

Timocharis, located in Mare Imbrium, is a classic example of a fresh crater (Figure 5a). It is nearly circular (34 km in diameter), has a sharp rim, a rough floor, central peaks, and other characteristics of fresh craters as discussed in Head [1975].

The observed topographic profiles for Haldane and Timocharis and the predicted profile for the floor-fractured Haldane are shown in Figure 5b. The fit of predicted and observed topography for Haldane is generally good, particularly over most of the floor area. The predicted wall and rim heights lie above those observed for Haldane (Figure 5b). The model does not account for the narrow minimum in the displacement curve due to the sunken 'moat' just inside the rim (Figure 5c).

Runge-Timocharis. Runge (40-km diameter) is another member of the group of fractured craters in Mare Smythii [Greeley et al., 1977]; see Figure 4a. The floor of Runge lies at an elevation comparable to that of the surrounding plain.

The predicted and observed topographic profiles for

Runge, using Timocharis as the fresh crater, are shown in Figure 6a. The inversion technique results in a predicted profile with a floor somewhat shallower and a rim height somewhat lower than that observed. The best fitting value for the extent of relaxation, $t/\eta = 5 \times 10^{-8}$ sec/poise, is the largest obtained for any of the crater pairs considered in this study.

It should be noted that the observed displacement curve (Figure 6b) has a minimum outside the crater rim. This is a feature that would be expected for a crater that has undergone viscous relaxation, but is generally not predicted by simple volcanic intrusion models.

Davy-Timocharis. Davy is a 34-km diameter floor-fractured crater located on the eastern edge of Mare Nubium (Figure 7a). The crater is somewhat polygonal in shape, and the floor is flat and shallow with concentric and polygonal fractures. The crater rim is, in most places, sharp and well-defined.

The observed and predicted profiles for Davy are shown together with the Timocharis profile in Figure 7b. The observed difference in topographic profiles between Davy and Timocharis and the predicted vertical displacement for Davy are given in Figure 7c. For this crater pair the observed rim height of the fractured crater is higher than that of the fresh crater, an unusual situation [Schultz, 1976] that is perhaps related to variability of rim height, as noted earlier. The general shape of the fit obtained is good. The

minimum in the observed displacement curve for Davy lies outside the crater rim, as would be expected if viscous relaxation were acting to modify the crater.

Sabine (W) - Lambert. Sabine is one of a pair of nearly identical floor-fractured craters (Figure 8a) located at the southwestern border of Mare Tranquillitatis [DeHon, 1971]. Sabine (30 km in diameter) and its companion Ritter (28 km in diameter) have circular features bordering an interior moat and uplifted and fractured floors. The fresh crater Lambert (31 km in diameter) is located in Mare Imbrium (Figure 8b). Mare lavas have covered portions of the ejecta deposits beyond about 1.5 -2.0 crater radii from the crater center.

Two profiles of Sabine were used; one extending westward from crater center (more or less parallel to the edge of the mare), designated W, and one extending southward from crater center (perpendicular to the mare edge), designated S. The W profile runs through an area in which the floor of the crater is significantly uplifted within a concentric fracture.

The topographic profiles for Sabine (W) and for Lambert and the predicted profile for the viscous relaxation model are shown in Figures 8c and 8d. The fit of the model is hampered in this case by the fact that the rim of Sabine along this profile lies higher than the rim of Lambert. The rim height is measured above the elevation of the surrounding, presumably flat, region. It is possible that the zero elevation datum is influenced by the southern extension of the rim of Ritter and by the comparatively poor

resolution of topographic data for the area around the crater. (The maps used were LM60 and a Ranger VIII Lunar Map of Ritter and Sabine, because no LTO was available.)

Sabine (S) - Timocharis. Along the Sabine Figure 8a profile in the the southward direction there is no moat and the profile is in general much more subdued (Figure 9a). The crater Timocharis (Figure 5a) was used as the fresh crater to test the viscous relaxation hypothesis. The displacement curve for Sabine (S) has a minimum almost exactly at the crater rim (Figure 9b), because the Sabine rim for this profile is lower than that of Timocharis while the floor of the fractured crater stands higher. The model provides a good fit to the topography with this exception.

Ritter-Lambert. Ritter, the companion crater to Sabine, contains a floor raised within a concentric moat (Figure 8a). Ritter is substantially deeper, for its size, than the other floor-fractured craters examined for this paper. Lambert is used as the corresponding fresh crater (Figure 8b).

Both the floor and the rim of the predicted Ritter profile (Figure 10a) lie higher than for the observed profile. A higher floor would normally indicate that the model topography has relaxed beyond the observed topography, while a higher rim would be expected to mean that relaxation has not progressed far enough. Thus the indicated model represents a compromise fit between the floor and the rim. The minimum in the observed displacement curve (Figure 10b) lies at and immediately outside the rim, as predicted by a viscous relaxation model.

DISCUSSION

The single parameter estimated from the viscous relaxation model applied to topographic profiles for floor-fractured craters is the ratio t/η. Derived values range over a factor of 10, from 0.4 to about 5×10^{-8} sec/poise.

The derived values of t/η should be interpreted with the understanding that the effective viscosity η has varied markedly with time in the vicinity of each floor-fractured crater. The observed modification to crater topography probably occurred primarily within the time interval over which the effective viscosity was at or near its minimum value. Thus η should be regarded as the value of effective viscosity during the time of most rapid viscous relaxation, and t should be regarded as the time interval between the onset of rapid relaxation of topography and the time when η grew large enough and the outer elastic lithosphere grew thick enough so that further viscous relaxation effectively ceased. Because most fracturing of crater floors occurred in proximity to mare basins or other mare deposits and within the time interval between mare basin excavation and cessation of mare volcanism [Schultz, 1976], it is likely that t/η is a measure of relaxation time and effective viscosity during the portion of that time interval when local temperatures were raised to their highest values by the combined effects of impact and volcanic heating. Note, however, that because t/η is derived from a comparison between two present-day crater

profiles, the derived parameter reflects only those processes that occur after transient cavity formation and after any dynamic phenomena associated with early cavity modification have ceased.

Since only the ratio t/η is obtained from the fit of predicted to observed topography, the quantities t and η may not be independently estimated. Nonetheless, the estimates of $(0.4 - 5.1) \times 10^{-8}$ sec/poise are reasonable in view of possible values of effective viscosity of the outer portions of the Moon in regions of abnormally elevated temperatures. Adopting, for instance, a value of $\eta = 10^{22}$ poise as representative of the bulk of the Earth's mantle [e.g. Cathles, 1975] gives $t = (0.4 - 5.1) \times 10^{14}$ sec, or about 1 to 10 m.y. Such values for t are quite consistent with the hypothesis that the majority of the relaxation occurs over a geologically short time interval, during which local temperatures were anomalously high and effective viscosities anomalously low.

The derived values of t/η, if slowly varying over scales of tens of kilometers for floor-fractured craters of similar age, would be a useful parameter with which to constrain the shallow thermal structure of the Moon during the time between basin formation and the close of mare volcanism. Unfortunately, many more calculations for individual fractured craters are necessary to assess with confidence the possibilty of using extent of relaxation as a mapping tool. At present we can compare estimated values of

t/η on only two small groups of nearby modified craters.

Three of the fractured craters included in this study are located within (Haldane, Runge) or on the edge of (Dumas) Mare Smythii (Figures 2 and 4a). Dumas and Runge, which are extremely shallow and have low rim elevations, yield high values of t/η: 3.7×10^{-8} and 5.1×10^{-8} sec/poise, respectively. Haldane, which has a rim crest-floor relief of approximately 0.5 km, is best modelled by a lower value of t/η, 1.1×10^{-8} sec/poise. Since t/η is larger for Dumas than for Haldane, the derived values of t/η are not simply a function of distance from basin center.

Two other fractured craters that are in the same area and are included in this study are Ritter and Sabine, which are imediately adjacent. Since Ritter is deeper than Sabine, it yields a lower value for t/η (0.4 versus about 1×10^{-8} sec/poise) than Sabine. The two profiles for Sabine, which differ substantially in topographic detail, yield somewhat different best-fitting values of t/η (0.8 versus 1.8×10^{-8} sec/poise), though the uncertainties in each estimate overlap (Table 1).

There may be some regions of the Moon where the effective value of t/η varies so drastically as to be of limited value as a mapping tool. Such regions include those where nearby craters of similar age and size show very different degrees of fracturing and topographic modification or where small craters have been extensively modified but larger nearby craters are not [Schultz, 1976]. For such

regions, the effective viscosity may have varied rapidly with spatial location as well as time; near-surface regions of high temperature may have been strongly localized by impact heating or by volcanism and plutonism. Whether there are, on the other hand, large regions of the moon with generally constant values for t/η, therefore indicating a regional-scale anomaly in near-surface temperature, remains to be demonstrated. On the basis of areal density of floor-fractured craters [Schultz, 1976], the Smythii basin and the area west of Oceanus Procellarum are obvious candidates for such regions.

In this paper the primary test of the hypothesis that topography of floor-fractured craters was modified by viscous relaxation has been made directly from the topographic profiles for a number of fractured craters. It is important to consider whether there are additional data that can independently test hypotheses for the origin of floor-fractured craters. The distribution and orientation of floor fractures indicate that at least a thin layer undergoes brittle failure, rather than viscous flow, in response to horizontal extensional stress. The sources of the extensional stress can include isostatic adjustment of crater topography, magmatic intrusion at depth, and regional stresses associated with mare basalt loading. The mass deficiency of the crater topography produces a system of stresses in an elastic lithosphere similar to the stresses produced by a mascon load [Solomon and Head, 1979, 1980],

except that the signs of all stresses are reversed. In particular, both horizontal stresses are extensional beneath most of the crater floor, with magnitudes that increase with increasing topographic relief and with decreasing lithosphere thickness. Thus the isostatic adjustment of crater topography in regions of elevated temperatures and thin lithosphere can lead naturally both to uplift and floor fracturing. The proximity of many floor-fractured craters to the edges of maria may subject these craters to additional extensional stress of regional scale. The mare-basalt loads, particularly in the mascon maria but also in Oceanus Procellarum and in similar irregular maria, produce horizontal bending stresses in the lunar lithosphere that are extensional at the mare edges [Solomon and Head, 1979, 1980; Head et al., 1980; Chapter 3]. That circumferential rilles near some maria cut through floor-fractured craters, such as in Goclenius [Baldwin, 1971a], provides confirmation of such an additional regional stress field.

Gravity data are potentially of use in distinguishing among possible mechanisms by which floor-fractured craters have been modified from their original forms, but the gravity anomalies over such craters are not well understood. Viscous relaxation of crater topography would be expected to reduce the free air gravity anomaly over the crater but it should not of itself alter any Bouguer anomaly for craters of the dimensions considered in this study. A number of large, young, unmodified craters have pronounced negative Bouguer

gravity anomalies [Sjogren et al., 1972; D.H. Scott, 1974; Janle, 1977; Dvorak and Phillips, 1977], thought to be due to a relatively low-density lens of brecciated material beneath the crater floor and walls [Innes, 1961; Janle, 1977; Dvorak and Phillips, 1977]. Older craters, including the floor-fractured craters Petavius and Humboldt, on the other hand, have at most very modest Bouguer anomalies [Dvorak and Phillips, 1978]. Dvorak and Phillips [1978] calculated that the excess mass at depth that could be accommodated by uplift of the floor of a floor-fractured crater is insufficient to remove a gravity anomaly equal to that observed for younger craters. Whether the older craters once had a negative Bouguer anomaly similar to that of the younger craters is currently an open question. It is possible that viscous flow of material at depth, occurring slowly over geologic time, could act to decrease the Bouguer anomalies of old craters.

CONCLUSIONS

The principal conclusion of this study is that viscous relaxation of topography is a viable hypothesis to explain the characteristics of many lunar floor-fractured craters. Differences between the topographic profiles of several pairs of floor-fractured and fresh craters of similar diameter can be quantitatively modeled by the very simple rheological model for the Moon of a uniform Newtonian viscosity. The general association of floor-fractured craters with mare regions, the apparently volcanic fill in many of these craters, and the quantitative extent of relaxation for the

floor-fractured craters considered here all support the hypothesis that substantial viscous relaxation of lunar crater topography and concomitant floor-fracturing was restricted in space and in time to regions and periods of anomalously high temperatures at shallow depths. The viscous relaxation of individual craters was probably restricted to fairly narrow time intervals (perhaps 10^7 yr) over which the effective viscosity was low and the thickness of an outer elastic or brittle lithosphere was small.

Both floor fracturing and viscous modification of crater topography have been observed on other planetary bodies. Floor-fractured craters on Mars have been described by Schultz and Glicken [1979]. A number of impact craters on the icy satellites of the outer planets show evidence for viscous relaxation of topographic relief [Smith et al., 1979; Parmentier and Head, 1981]. Quantitative modeling of the process of crater modification thus offers the promise of contributing to our understanding of lateral and temporal variations in the thermal structure of the Moon and of other planets and satellites as well.

Figure Captions

Figure 1. The floor-fractured crater Gassendi (110 km in diameter), located on the northern edge of Mare Humorum. (Lunar Orbiter pohotograph LO IV-143-H2.)

Figure 2. Locations of fresh and floor-fractured craters described in this study. Nonmare regions are shaded. Letters are keyed to Table 1.

Figure 3. (a) Oblique view of the fresh lunar crater Lalande (crater radius R = 12 km) (Apollo frame AS16-5396).
(b) Viscous relaxation of Lalande with time t. By the stage $t/\eta = 5.0 \times 10^{-8}$ sec/poise, the floor of the crater has relaxed completely, and only the shortest wavelength feature, the crater rim, is still visible. The apparent slight uplift of the crater rim for small values of t/η is a result of the more rapid relaxation of longer wavelength topography than shorter wavelength features.

Figure 4. (a) Vertical view of the floor-fractured craters Dumas (crater radius R = 8 km), Runge (R = 20 km), and Haldane (R = 20 km) (AS15-12991).
(b) Oblique view of the fresh crater Dawes (R = 8 km) (AS17-2767).
(c) Topographic profiles of Dumas, Dawes, and the model for Dumas predicted by viscous relaxation of the topography of Dawes for a best fitting value of t/η. Units for t/η are sec/poise. Vertical scale gives elevation in km measured from a zero-elevation datum

outside the crater; horizontal scale gives radial distance in units of R.

(d) Vertical displacement curves predicted for Dumas by the relaxation model in Figure 4c compared with the observed difference in the topographic profiles between Dumas and Dawes. Vertical scale gives displacement in kilometers; horizontal scale gives radial distance in units of R.

Figure 5. (a) Vertical view of the fresh crater Timocharis (R = 17 km) (LO IV-121-H3).

(b) Topographic profiles of Timocharis, the fractured crater Haldane (Figure 4a), and the model for Haldane predicted by viscous relaxation of the topography of Timocharis for a best fitting value of t/η.

(c) Predicted vertical displacement curve for Haldane compared with the difference in topography between Haldane and Timocharis.

Figure 6. (a) Topographic profiles of the fractured crater Runge, the fresh crater Timocharis, and the model for Runge predicted by viscous relaxation of Timocharis topography for the best fitting value of t/η.

(b) Predicted vertical displacement curves for Runge compared to the difference in topography between Runge and Timocharis.

Figure 7. (a) Vertical view of the floor-fractured crater Davy (R = 17 km) (LO IV-113-H2).

(b) Topographic profiles of Davy, the fresh crater

Timocharis (Figure 5a), and the model for Davy predicted by viscous relaxation of the topography of Timocharis for a best fitting value of t/η.

(c) Predicted vertical displacement curves for Davy with the difference in topography between Davy and Timocharis.

Figure 8. (a) Vertical view of the floor-fractured craters Ritter (left, R = 14 km) and Sabine (right, R = 16 km) (LO IV-85-H1).

(b) Vertical view of the fresh crater Lambert (R = 15 km) (LO IV-126-H3).

(c) Topographic profiles of Sabine (W), of Lambert, and the model for Sabine (W) predicted by viscous relaxation of Lambert topography for a best fitting value of t/η.

(d) Predicted vertical displacement curves for Sabine (W) compared with the difference in topography between Sabine (W) and Lambert.

Figure 9. (a) Topographic profiles of the fractured crater Sabine (S), the fresh crater Timocharis (Figure 5a), and the model for Sabine (S) predicted by relaxation of fresh crater topography for a best fitting value of t/η.

(b) Predicted vertical displacement curves for Sabine (S) compared with the difference in topography between Sabine (S) and Timocharis.

Figure 10. (a) Topographic profiles of the fractured crater Ritter (Figure 8a), the fresh crater Lambert (Figure 8b),

and the model for Ritter predicted by relaxation of fresh crater topography for a best fitting value of t/η.

(b) Predicted vertical displacement curves for Ritter compared with the difference in topography between Ritter and Lambert.

TABLE 1. Characteristics of Craters Used in This Study

Crater*	Radius, km	Latitude	Longitude	Topographic Data Source+	Profile Azimuth	t/η, 10^{-8} sec/poise
			Floor-fractured Craters			
Davy (A)	17.2	11°50'S	8°10'W	LTO77D1	W	1.1 (0.9-1.5)‡
Dumas (B)	8.0	5°25'S	81°55'E	LTO81B4	E	3.7 (3.0-4.8)
Haldane (C)	20.0	1°40'S	84°05'E	LTO81B1	N	1.1 (0.9-1.5)
Ritter (D)	14.0	1°55'N	19°15'E	RLC-7, LM60	W	0.4 (0.3-0.6)
Runge (E)	19.8	2°30'S	86°50'E	LTO81B2	NE	5.1 (> 2.0)
Sabine (F)	15.0 16.8	1°15'N	20°05'E	RLC-7, LM60	W S	1.8 (> 1.0) 0.8 (0.7-1.0)
			Fresh Craters			
Dawes (G)	8.0	17°15'N	26°20'E	LTP42C3S4	NW	
Lalande (H)	12.0	4°30'S	8°35'W	LTO77A4S1	SE	
Lambert (I)	15.4	25°45'N	21°00'W	LTO40A3	S	
Timocharis (J)	17.0	26°40'N	13°05'W	LTO40B3	S	

Notes to Table 1

*Letter in parentheses denotes location in Figure 2.

+Lunar maps are listed and described by Schimerman [1973]. LTO is Lunar Topographic Orthophotomap, scale 1:250,000, contour interval 100 m. LTP is Lunar Topophotomap, scale 1:50,000, contour interval 20 m. LM is Lunar Map, scale 1:1,000,000, contour interval 300 m. RLC is Ranger VIII Lunar Chart, scale 1:250,000, contour interval 100 m.

‡Range of t/η giving a mean squared difference between observed and predicted topography within 20 percent of its minimum value.

Figure 1

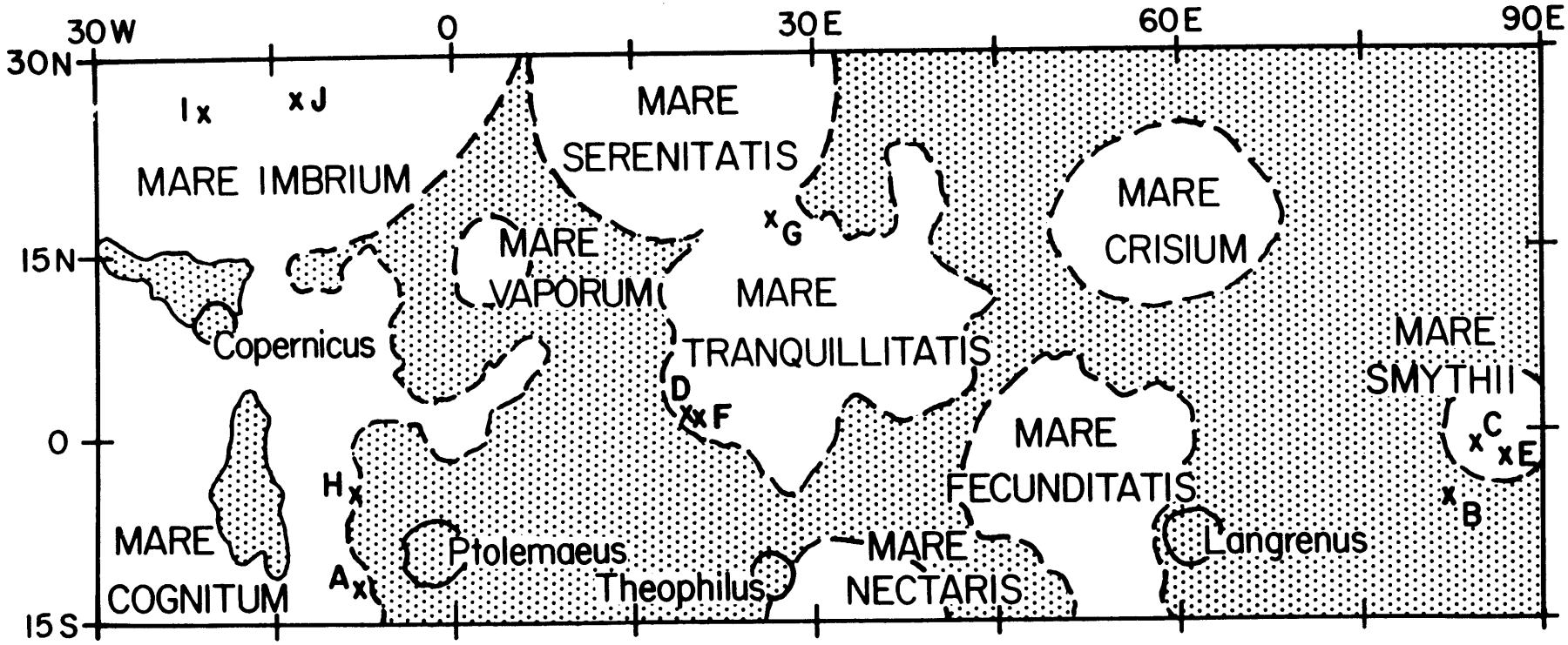
30W
0
30E
60E
90E
30N
15N
0
15S
I
J
MARE IMBRIUM
MARE SERENITATIS
MARE CRISIUM
MARE VAPORUM
MARE TRANQUILLITATIS
G
Copernicus
D
F
MARE SMYTHII
C
E
B
H
MARE FECUNDITATIS
A
Ptolemaeus
Theophilus
MARE NECTARIS
Langrenus
MARE COGNITUM

Figure 2

Figure 3a

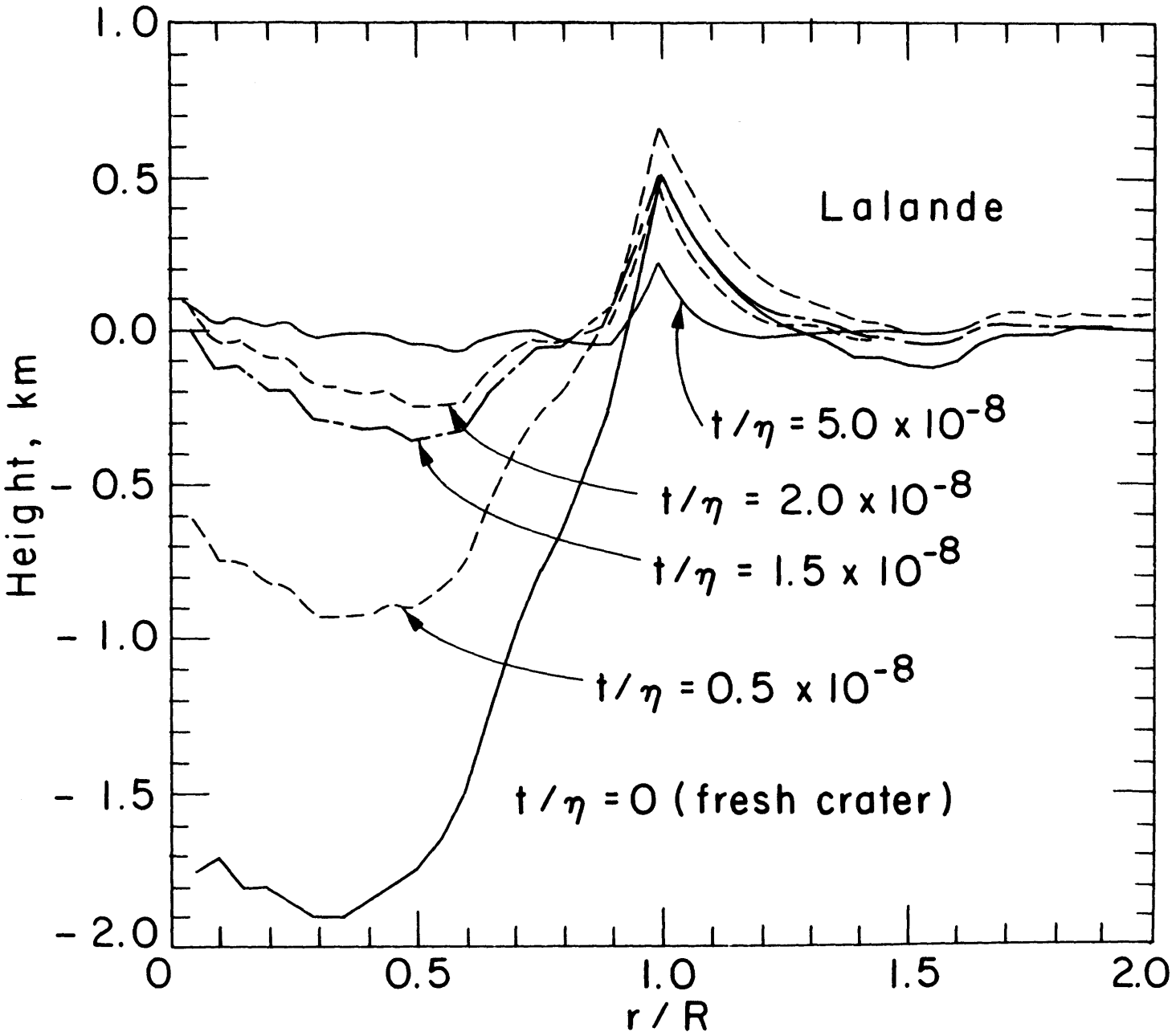
Lalande
Height, km
r / R
1.0
0.5
0.0
- 0.5
- 1.0
- 1.5
- 2.0
0
0.5
1.0
1.5
2.0
t/η = 5.0 x 10-8
t/η = 2.0 x 10-8
t/η = 1.5 x 10-8
t/η = 0.5 x 10-8
t/η = 0 (fresh crater)

Figure 3b

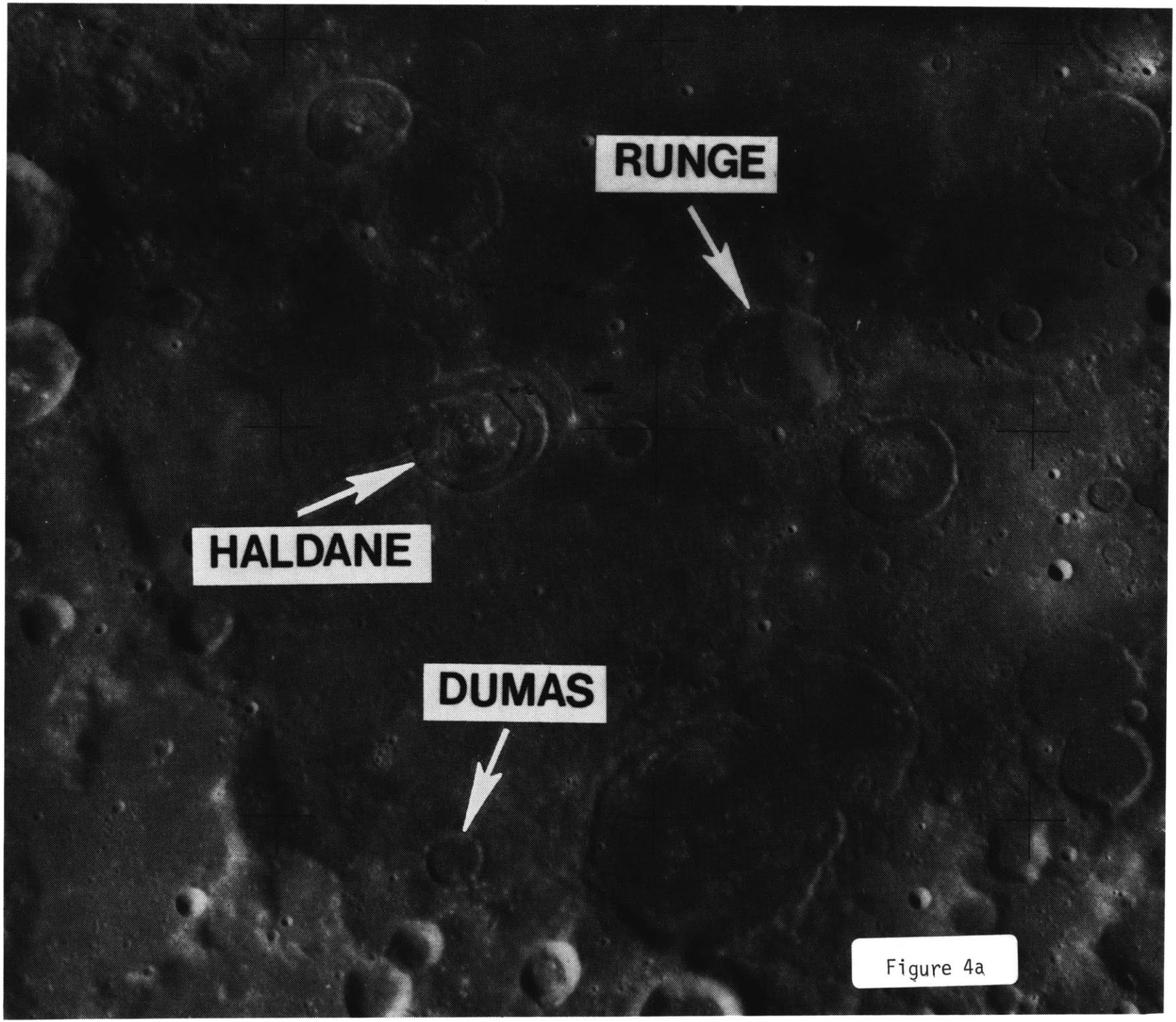

Figure 4a

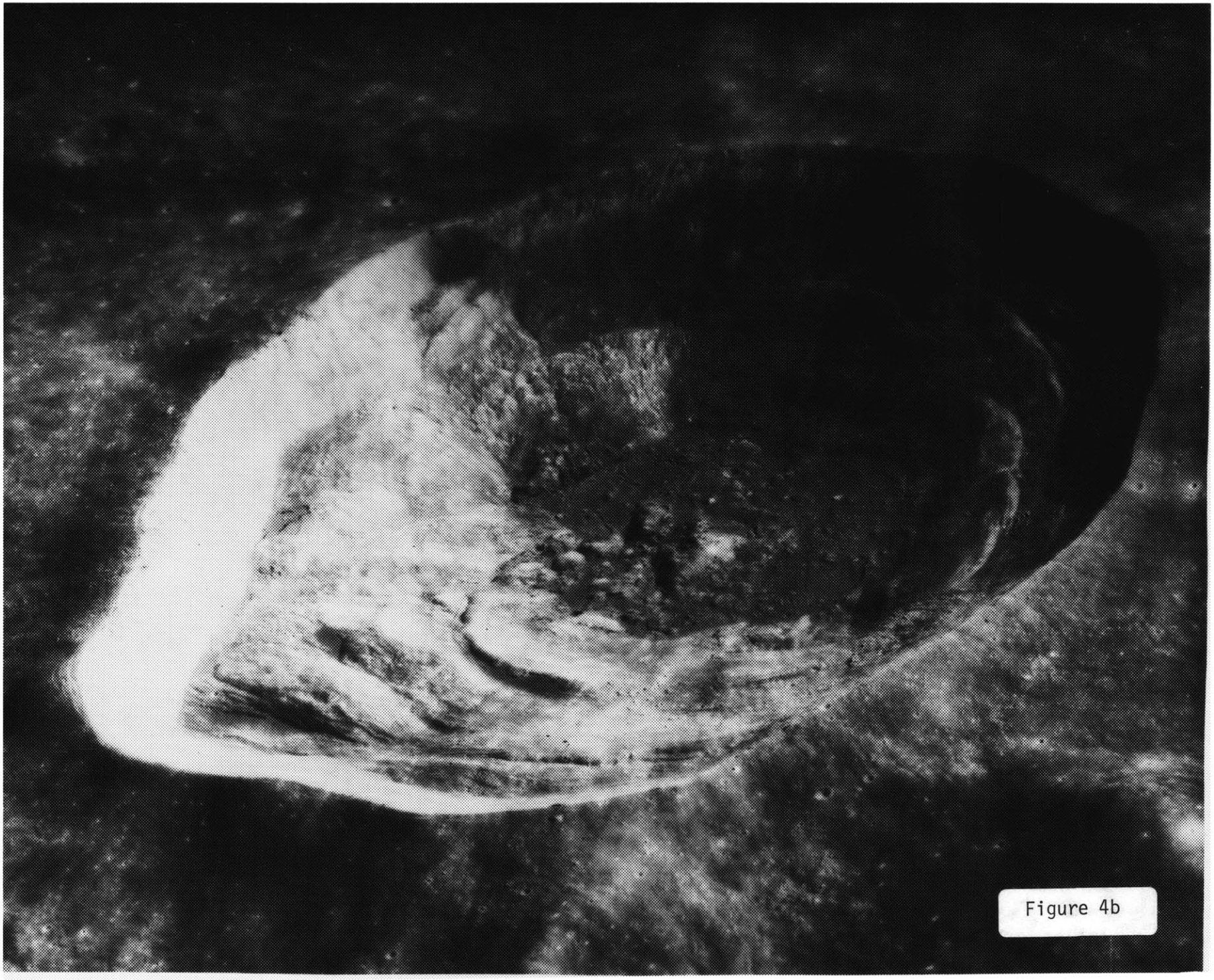

Figure 4b

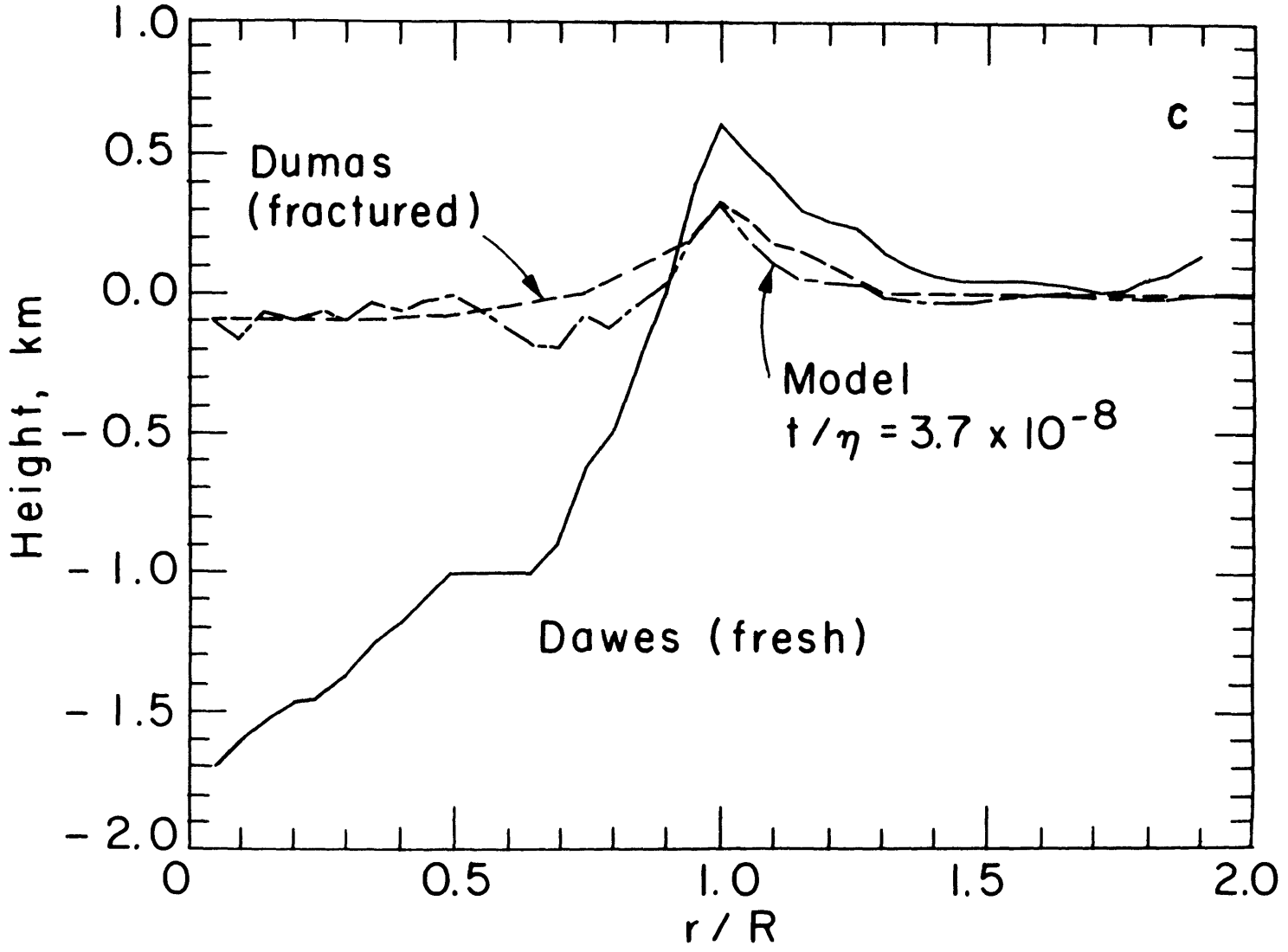
1.0
0.5
0.0
- 0.5
- 1.0
- 1.5
- 2.0
Height, km
0
0.5
1.0
1.5
2.0
r / R
c
Dumas
(fractured)
Model
$t/\eta = 3.7 \times 10^{-8}$
Dawes (fresh)

Figure 4c

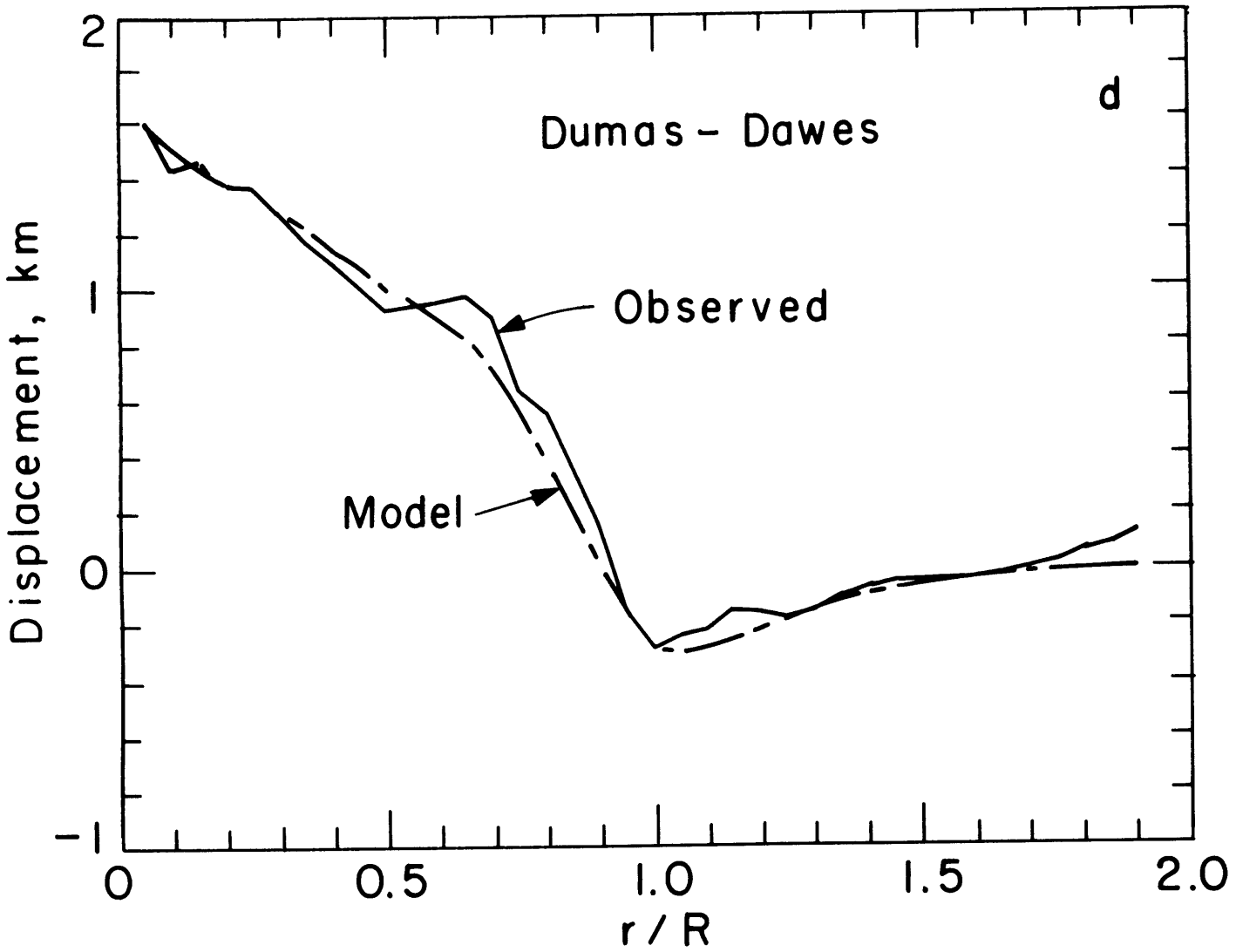
d
Dumas - Dawes
Observed
Model
Displacement, km
2
1
0
-1
0
0.5
1.0
1.5
2.0
r / R

Figure 4d

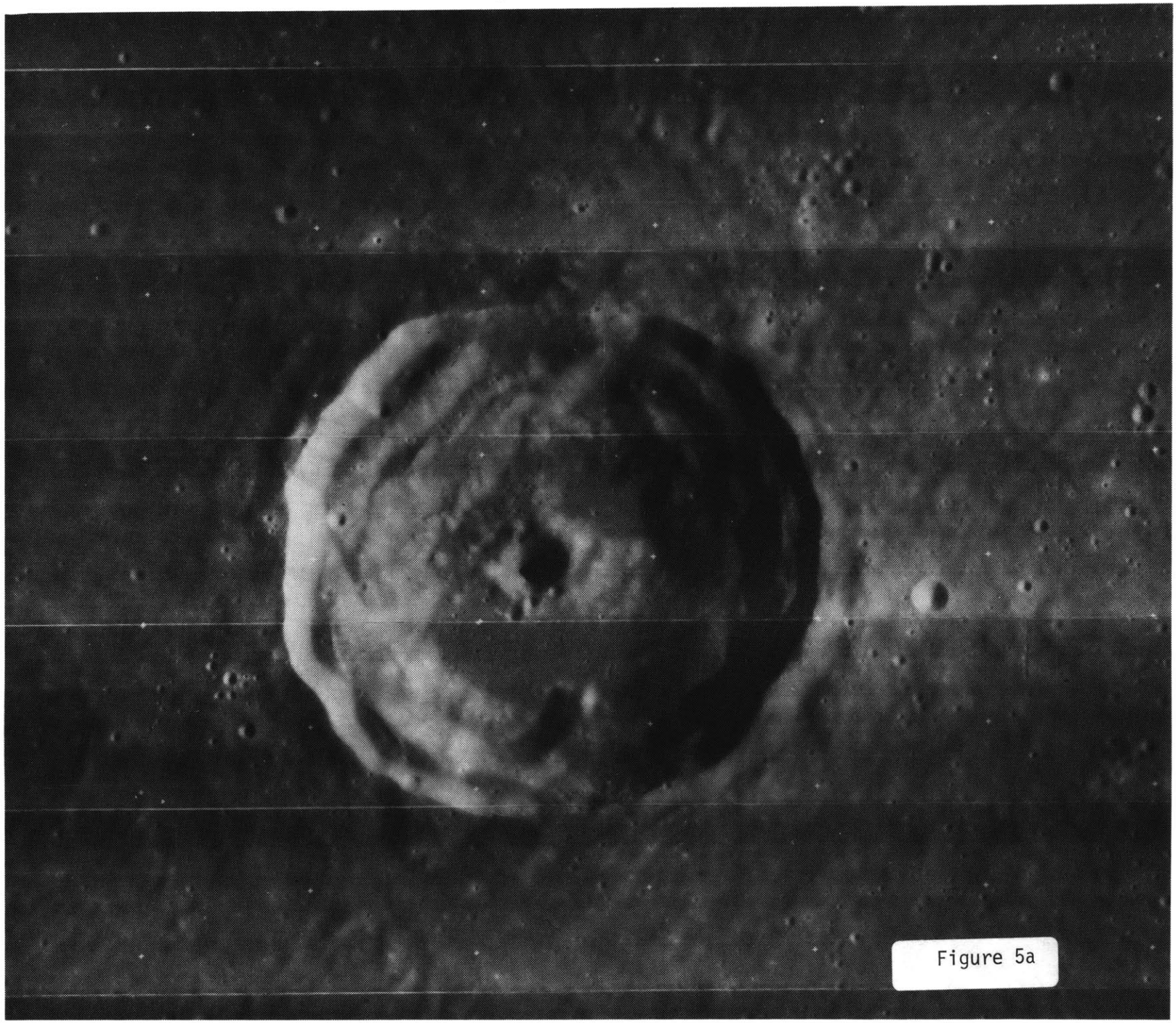

Figure 5a

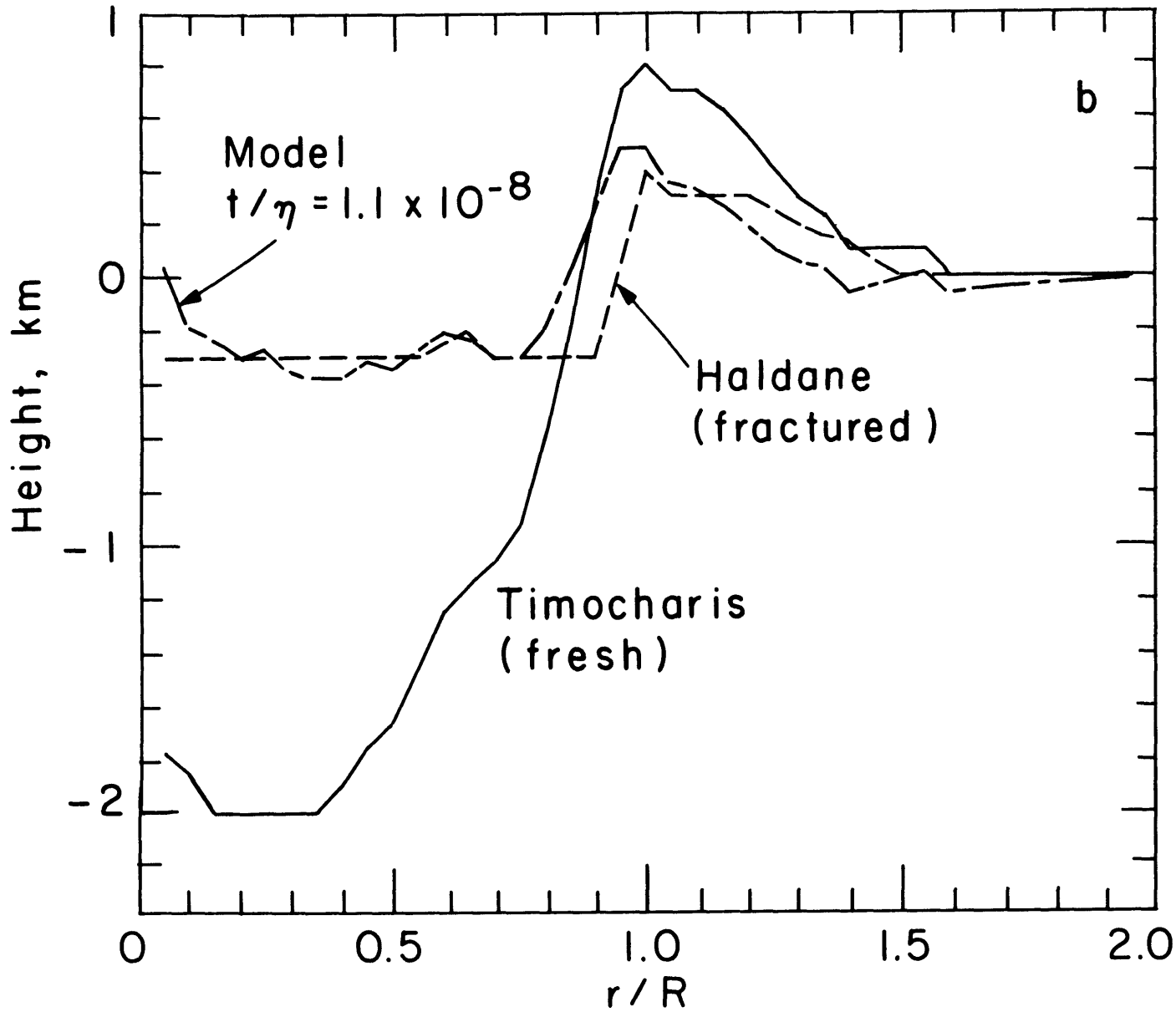
b
Model
$t/\eta = 1.1 \times 10^{-8}$
Haldane
(fractured)
Timocharis
(fresh)
Height, km
1
0
-1
-2
0
0.5
1.0
1.5
2.0
r/R

Figure 5b

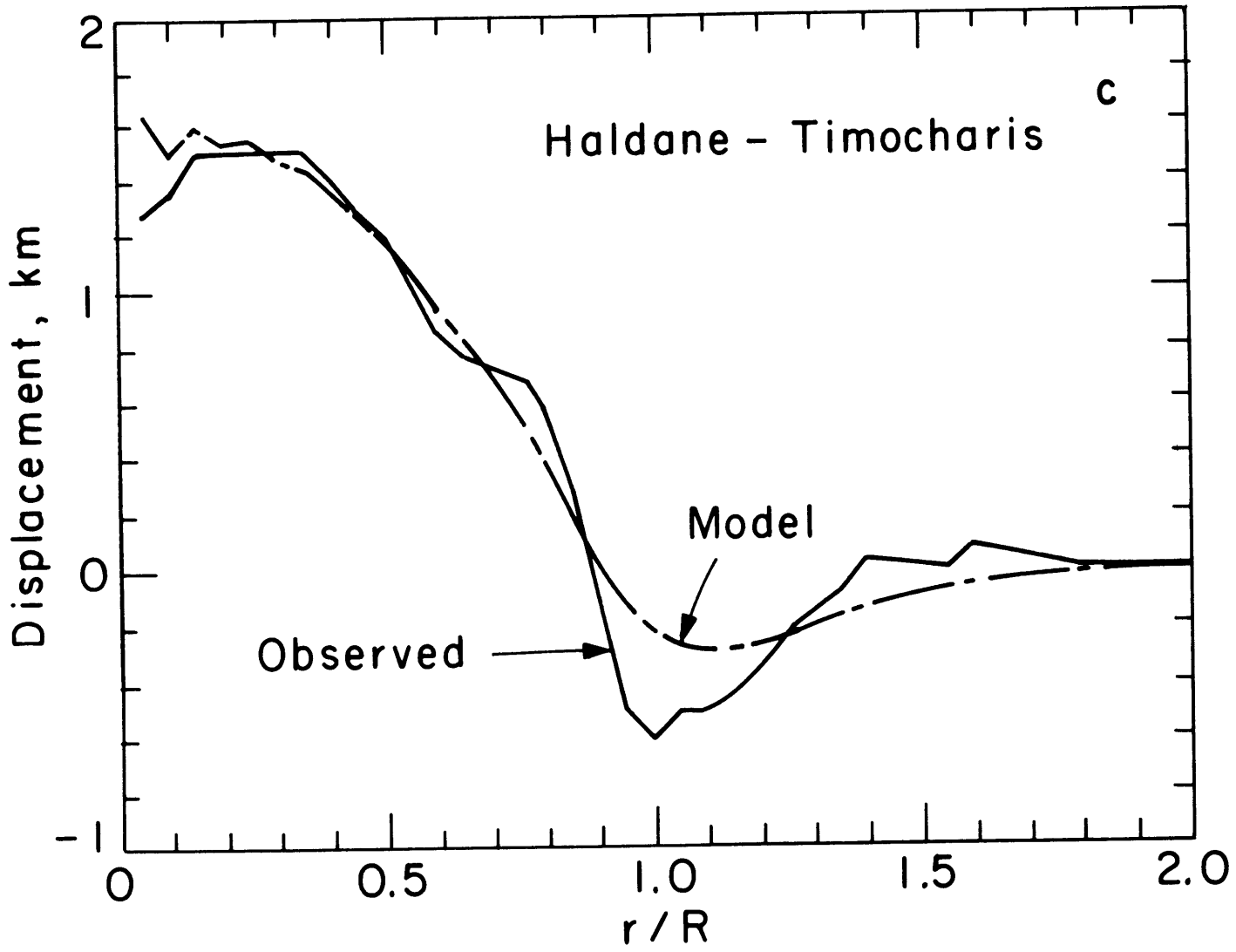
c
Haldane - Timocharis
Model
Observed
Displacement, km
2
1
0
-1
0
0.5
1.0
1.5
2.0
r / R

Figure 5c

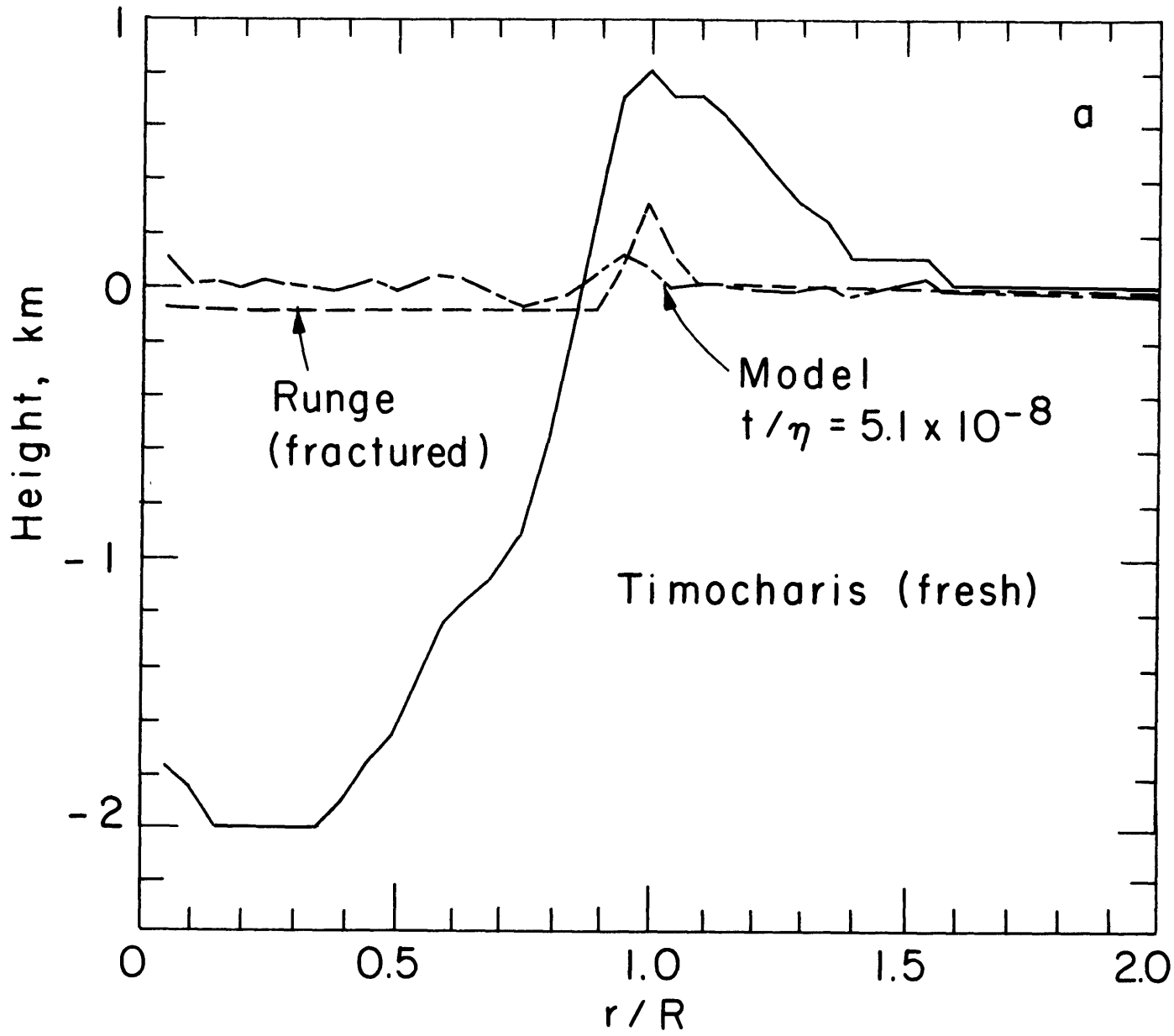
a
Height, km
1
0
-1
-2
Runge
(fractured)
Model
$t/\eta = 5.1 \times 10^{-8}$
Timocharis (fresh)
0
0.5
1.0
1.5
2.0
r / R

Figure 6a

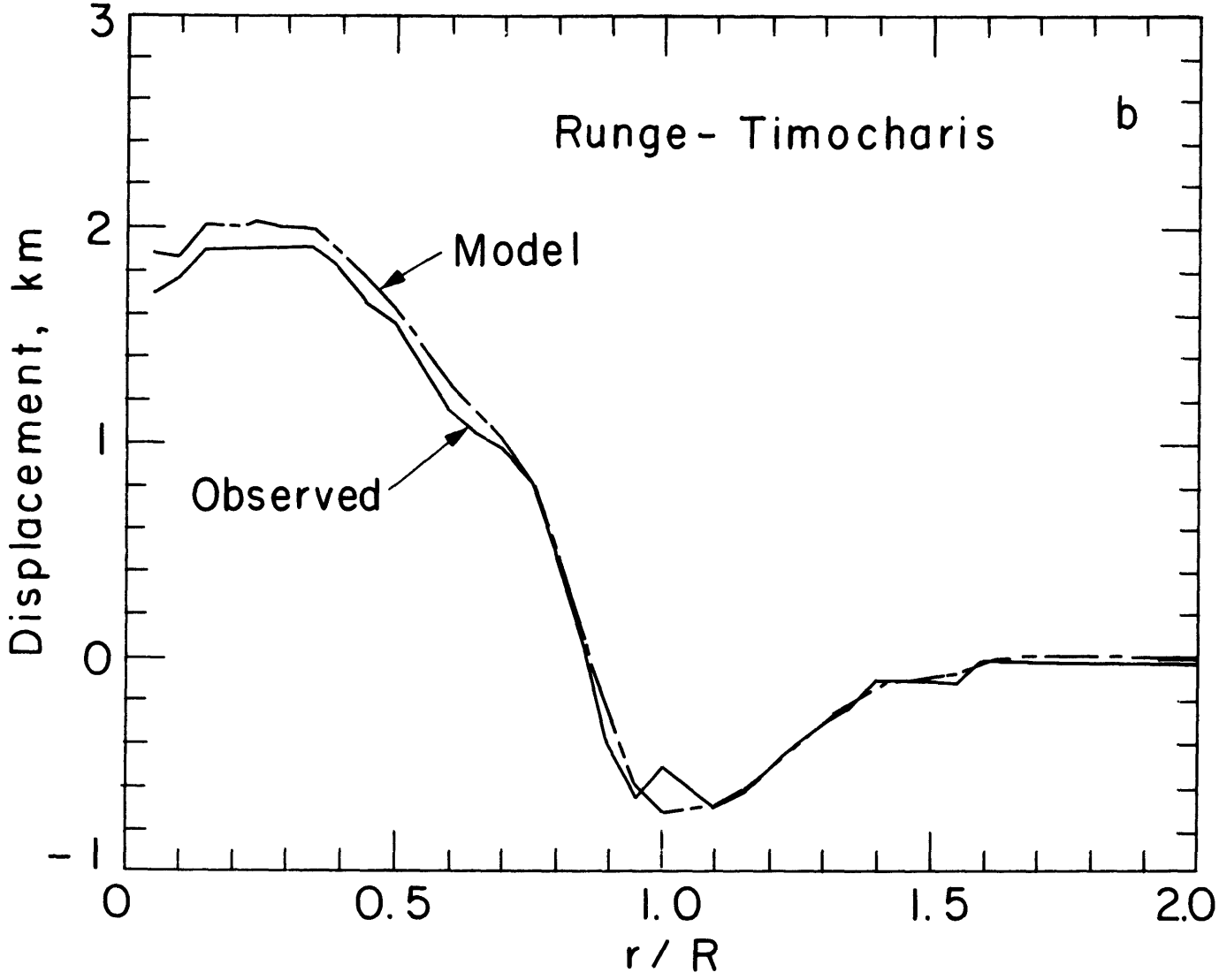
Runge- Timocharis
b
Model
Observed
Displacement, km
3
2
1
0
-1
0
0.5
1.0
1.5
2.0
r / R

Figure 6b

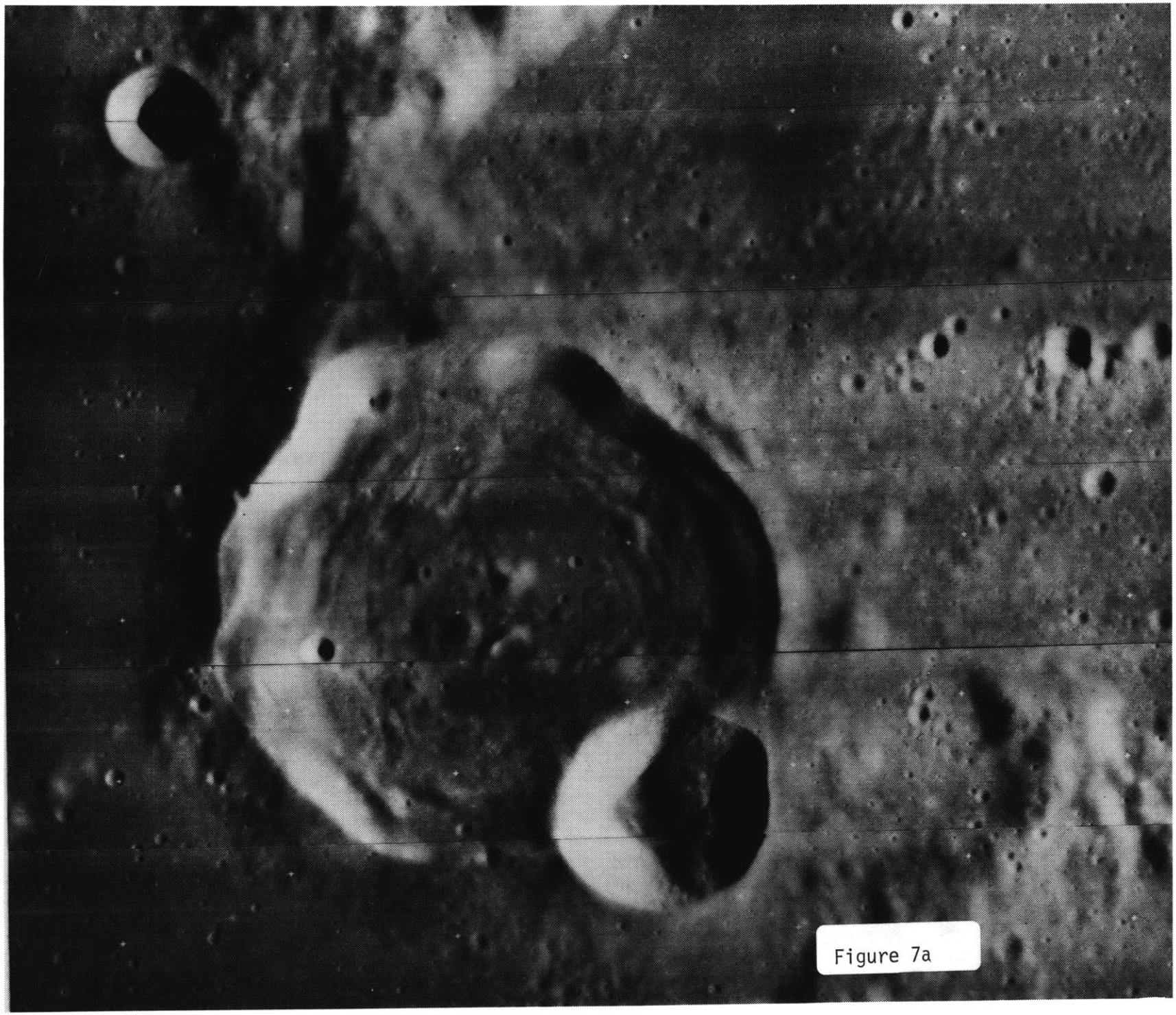

Figure 7a

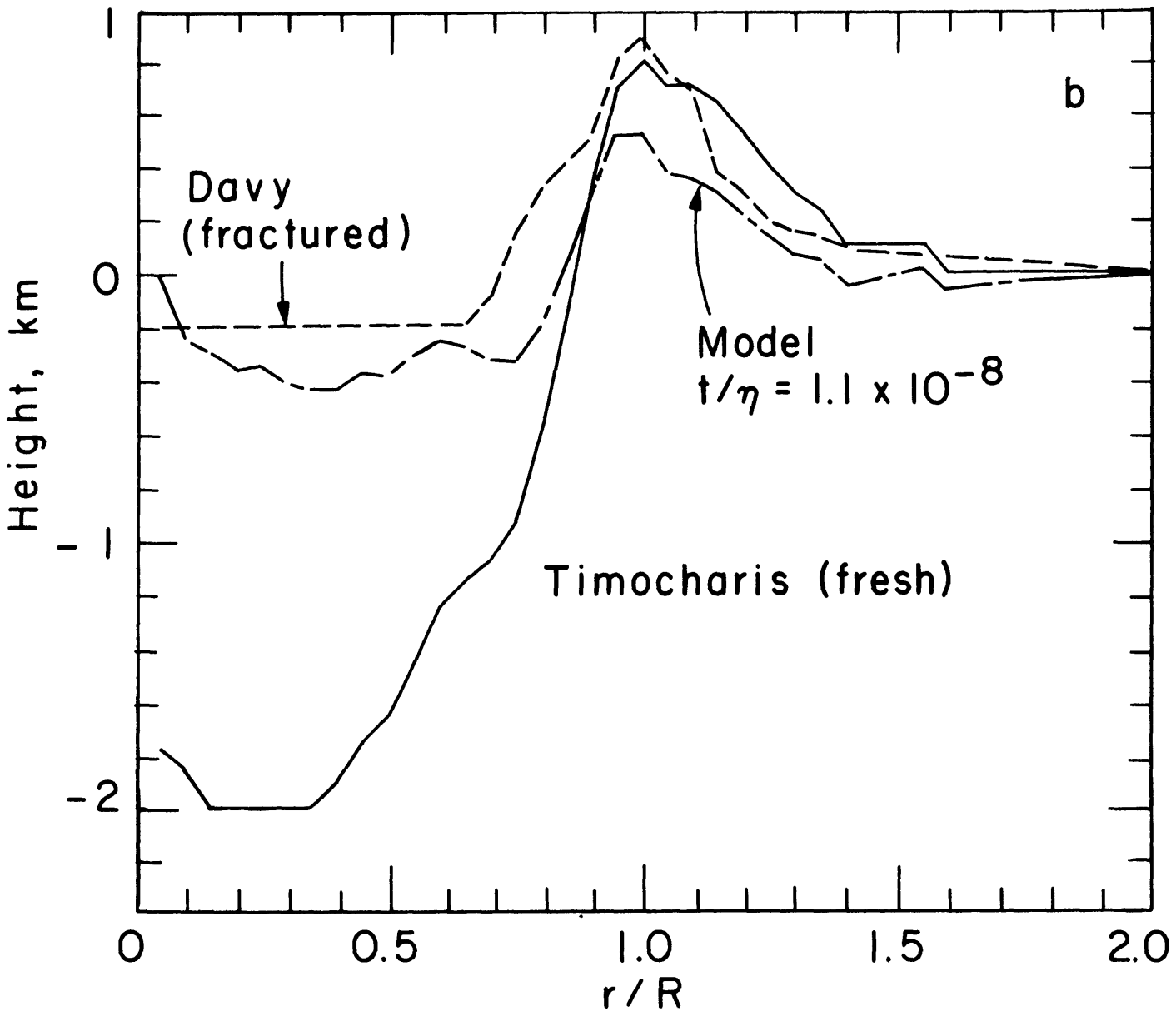
b
Davy
(fractured)
Model
$t/\eta = 1.1 \times 10^{-8}$
Timocharis (fresh)
Height, km
1
0
-1
-2
0
0.5
1.0
1.5
2.0
r / R

Figure 7b

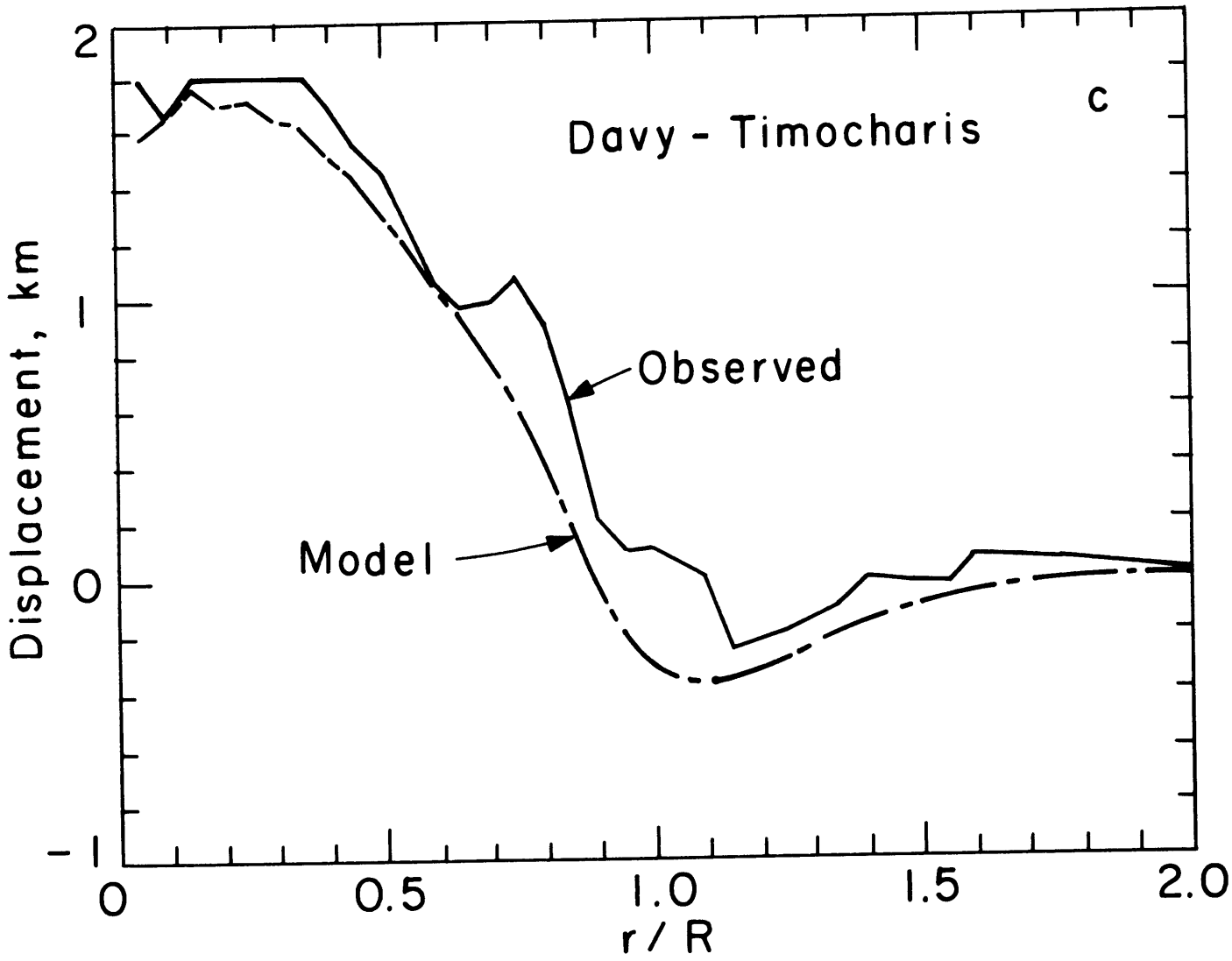
Davy - Timocharis
c
Observed
Model
Displacement, km
2
1
0
-1
0
0.5
1.0
1.5
2.0
r / R

Figure 7c

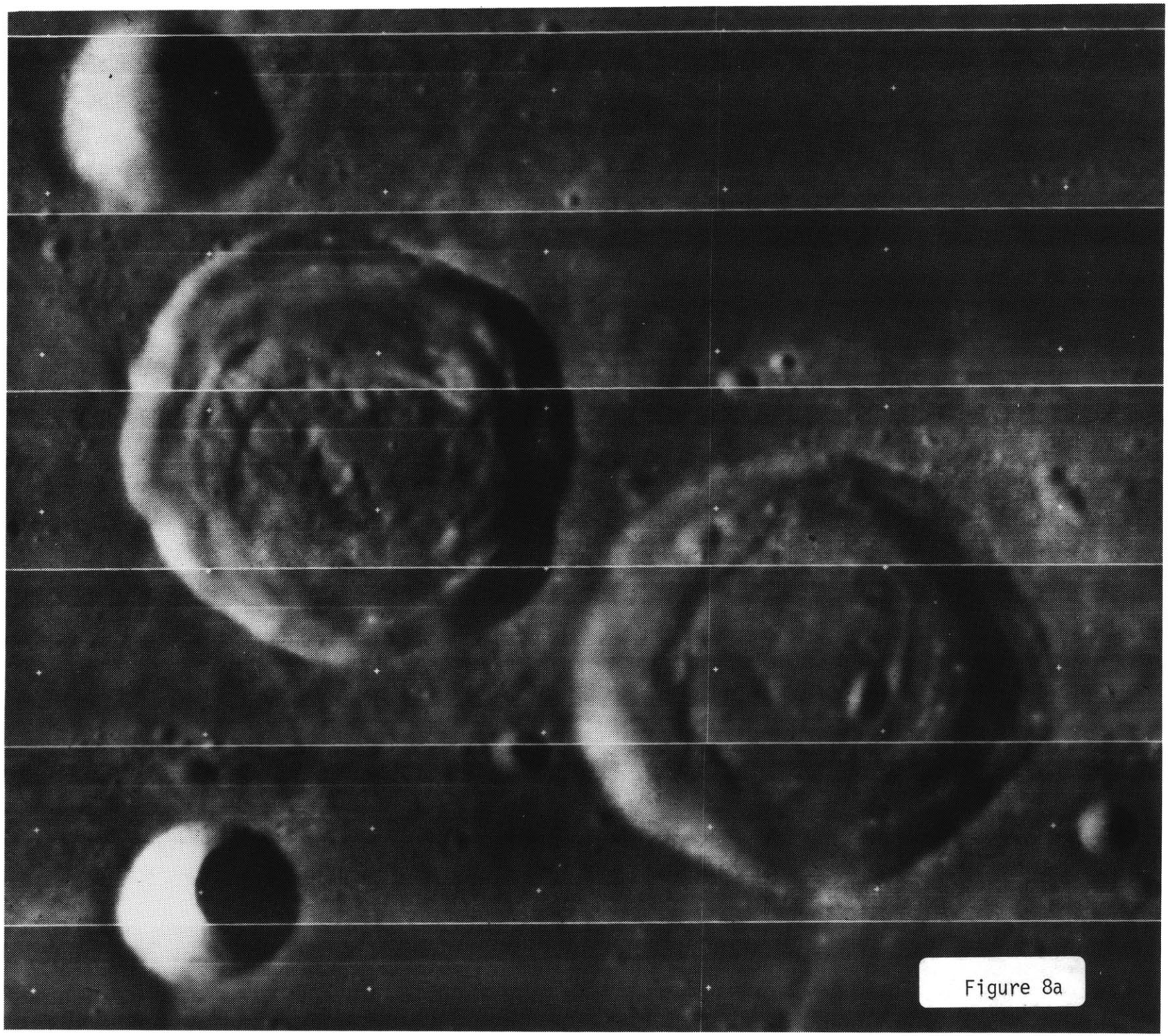

Figure 8a

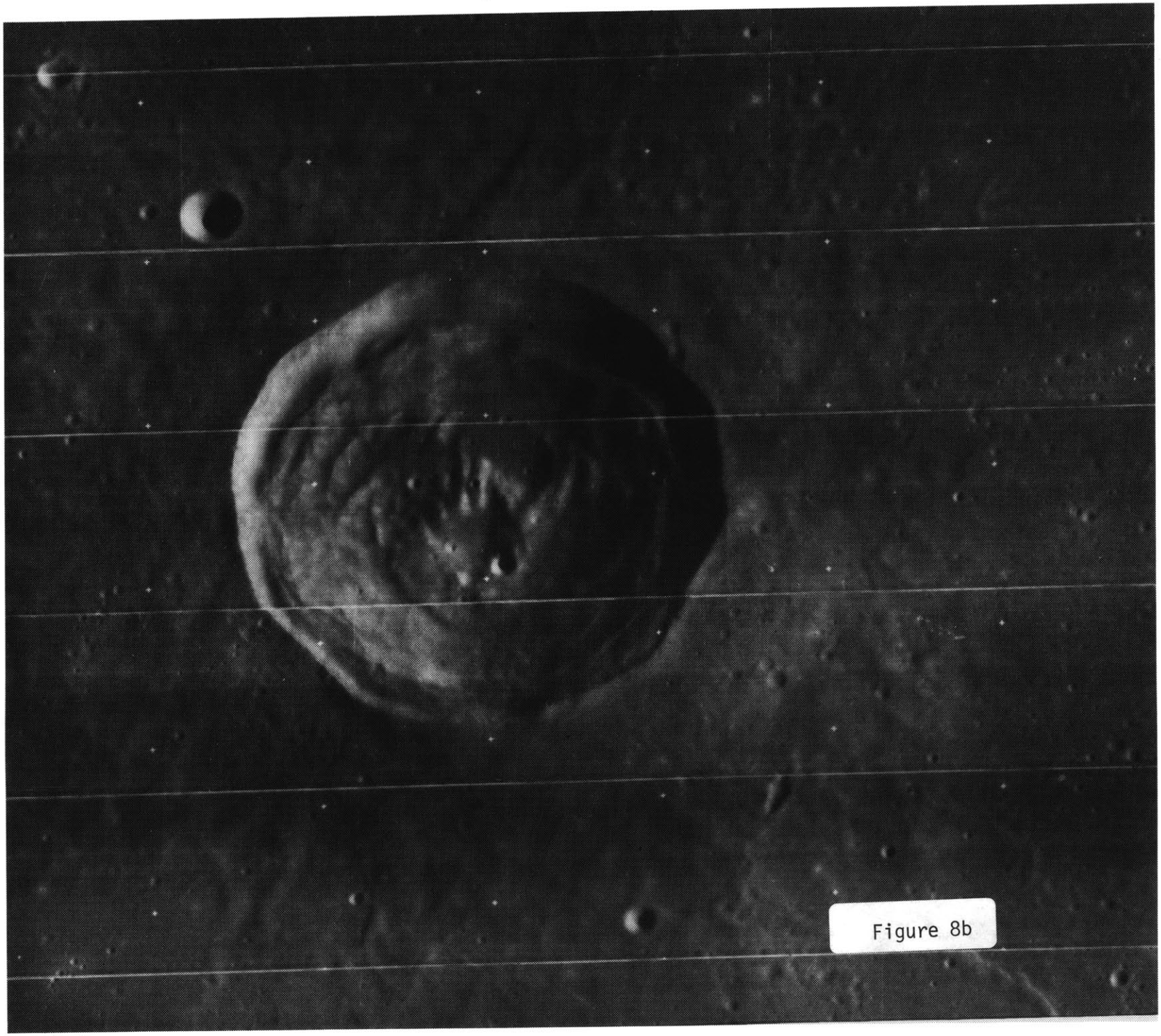

Figure 8b

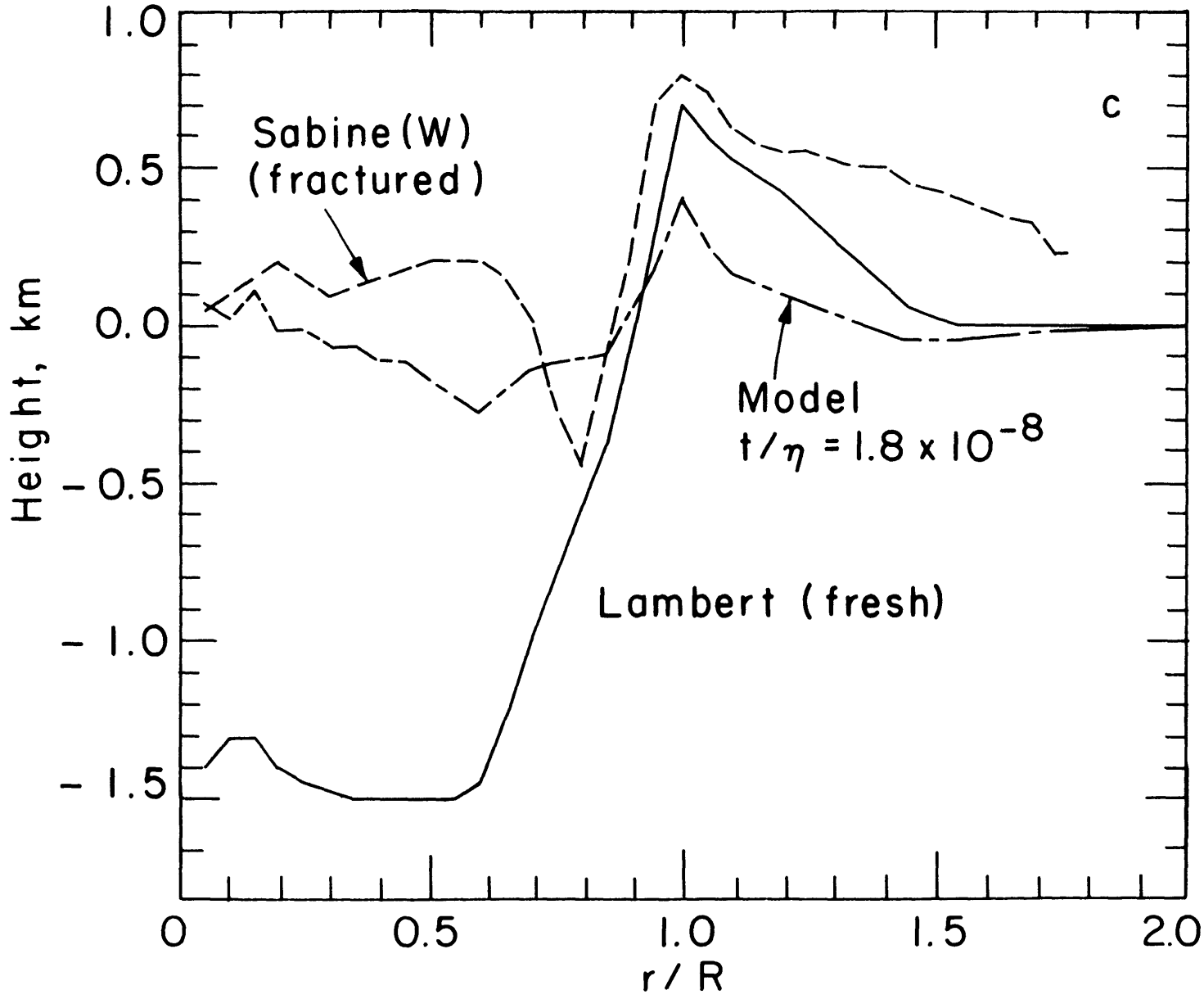
1.0
0.5
0.0
- 0.5
- 1.0
- 1.5
Height, km
Sabine (W)
(fractured)
c
Model
$t/\eta = 1.8 \times 10^{-8}$
Lambert (fresh)
0
0.5
1.0
1.5
2.0
r / R

Figure 8c

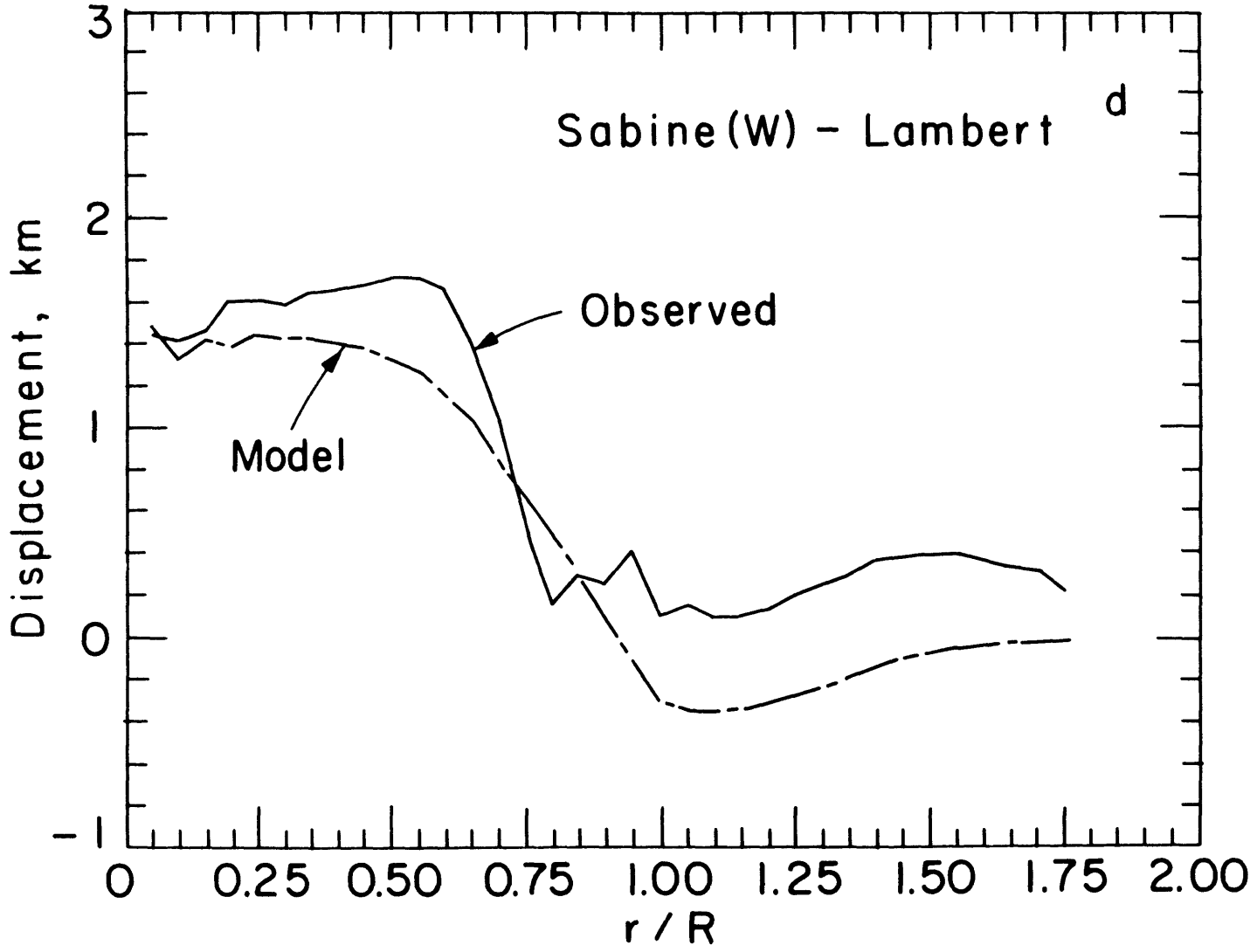
Sabine (W) - Lambert
d
Observed
Model
Displacement, km
3
2
1
0
-1
0
0.25
0.50
0.75
1.00
1.25
1.50
1.75
2.00
r / R

Figure 8d

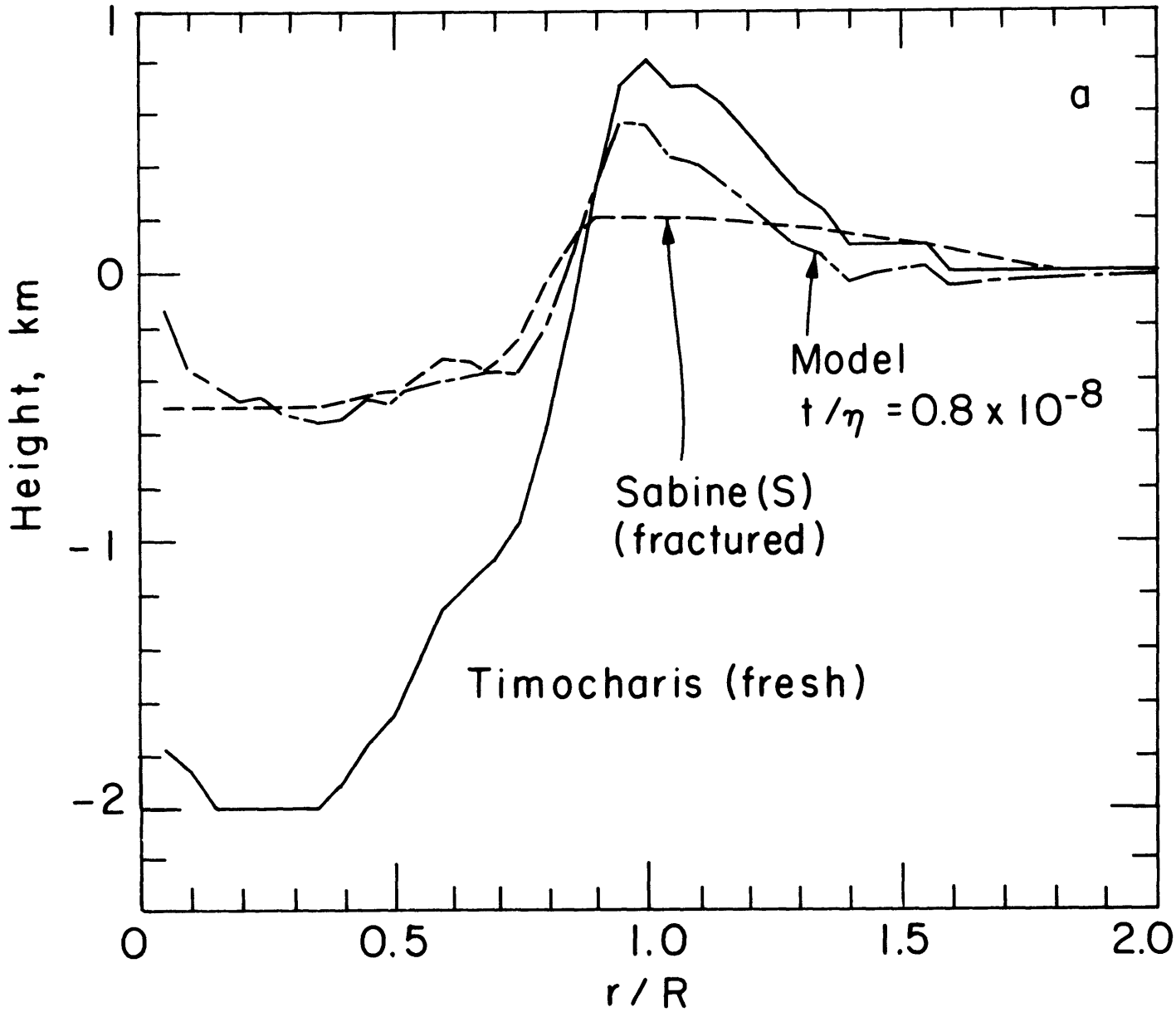
a
Height, km
1
0
-1
-2
0
0.5
1.0
1.5
2.0
r / R
Model
t / η = 0.8 x 10-8
Sabine (S)
(fractured)
Timocharis (fresh)

Figure 9a

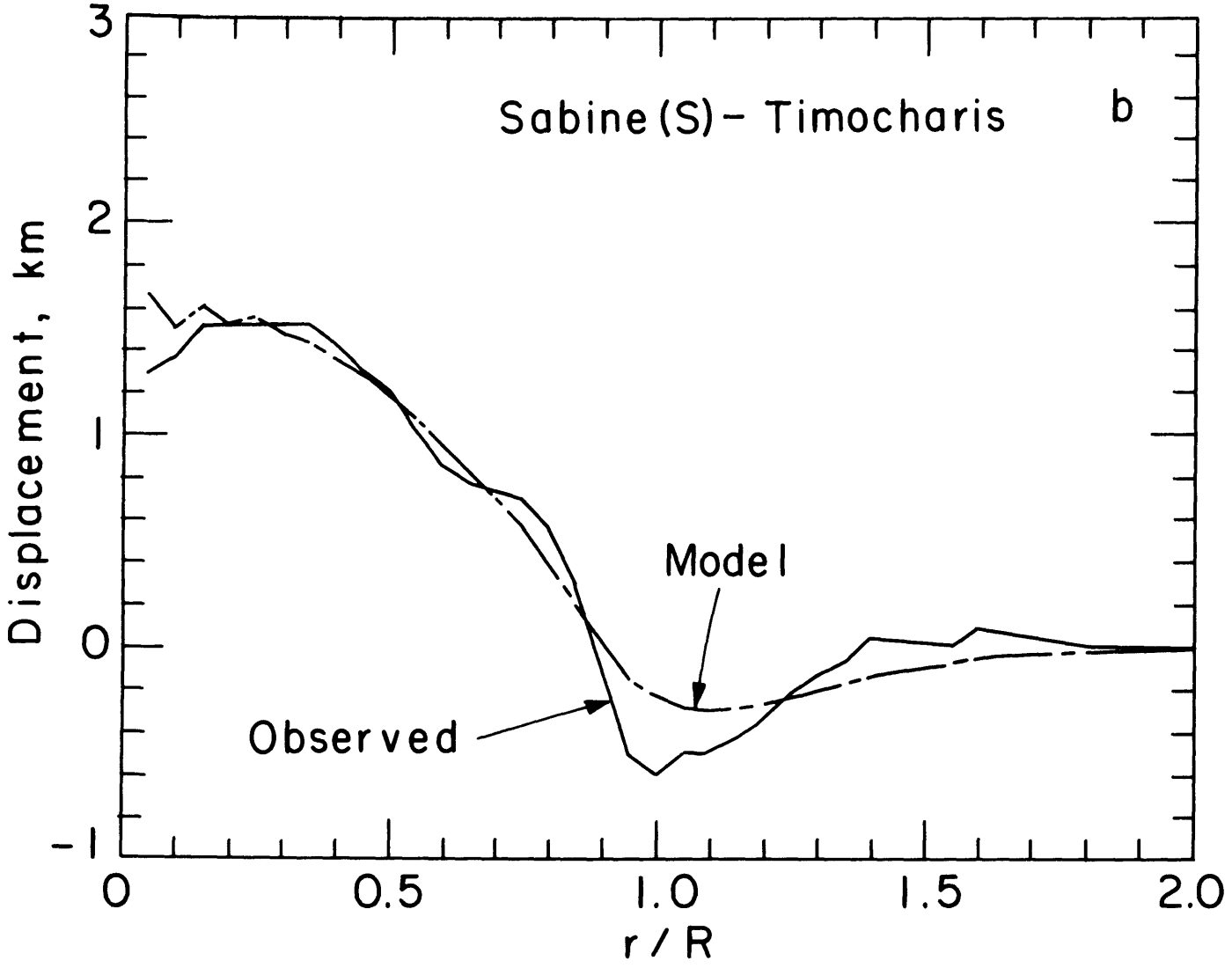
Sabine (S) - Timocharis
b
Displacement, km
3
2
1
0
-1
Model
Observed
0
0.5
1.0
1.5
2.0
r / R

Figure 9b

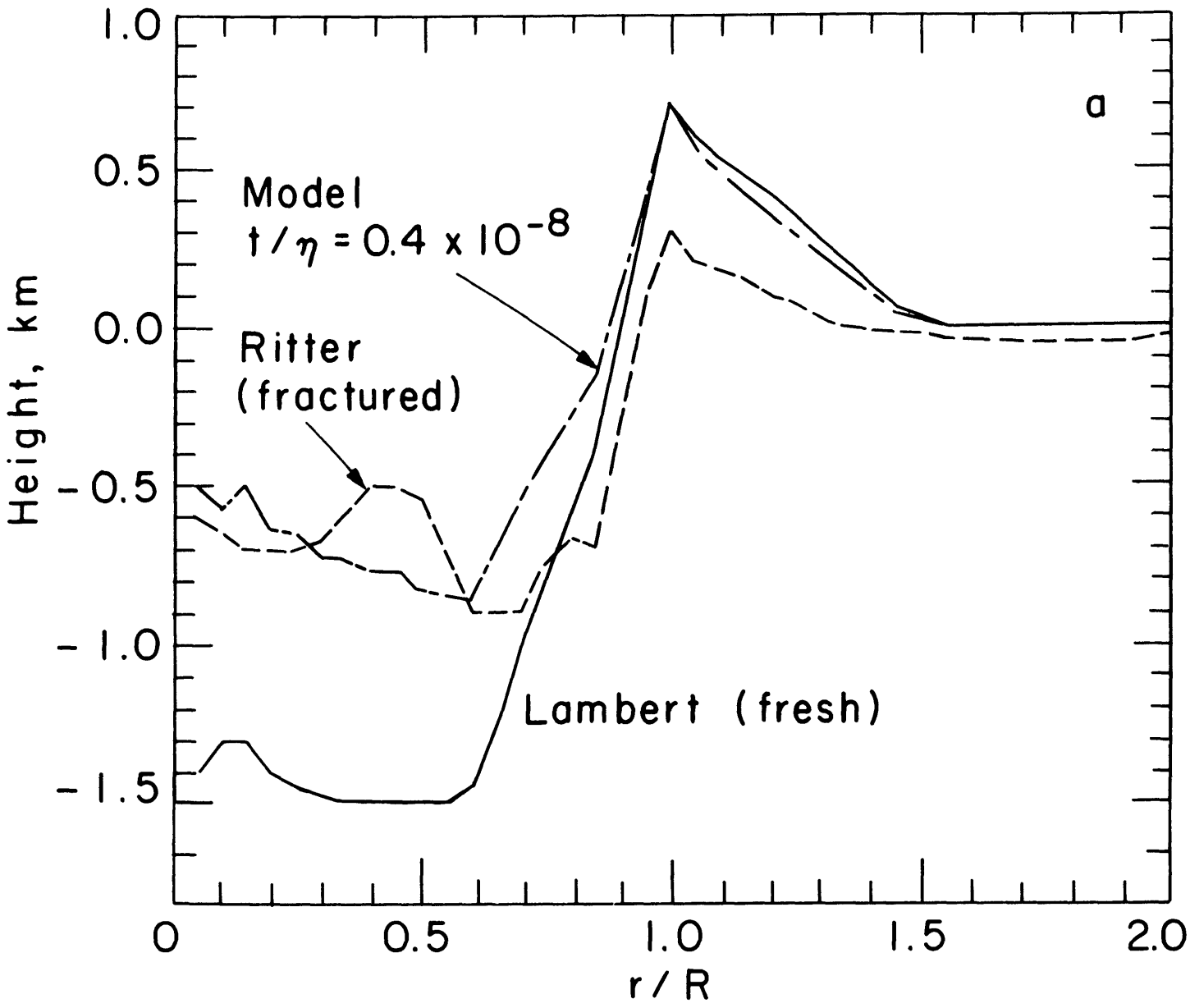
a
Model
$t/\eta = 0.4 \times 10^{-8}$
Ritter
(fractured)
Lambert (fresh)
Height, km
1.0
0.5
0.0
-0.5
-1.0
-1.5
0
0.5
1.0
1.5
2.0
r/R

Figure 10a

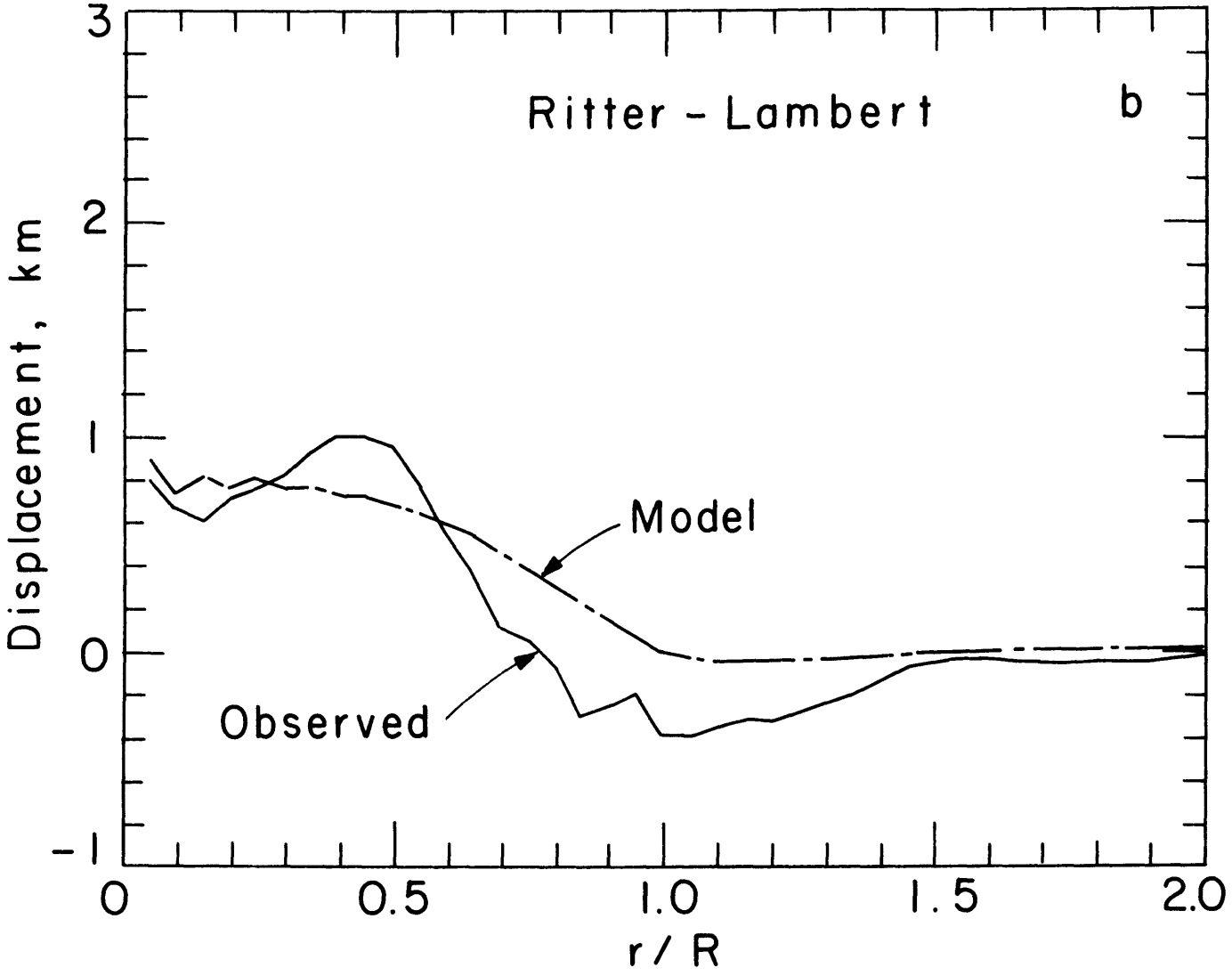
Ritter - Lambert
b
Displacement, km
3
2
1
0
-1
Model
Observed
0
0.5
1.0
1.5
2.0
r / R

Figure 10b

CHAPTER 3

LITHOSPHERIC LOADING MODELS AND THE TECTONICS OF THE IRREGULAR LUNAR MARIA

When we see the moon, we know that it is the moon, and that is enough.

-- D.T. Suzuki, Zen and Japanese Culture

INTRODUCTION

The geologic history of the Moon has been dominated by the formation of multi-ring impact basins and by the formation of the lunar maria that fill many of the basins. The impacts of large projectiles excavated the basins during the first billion years of lunar history [Wood and Head, 1976]. These impacts transferred large quantities of heat to the lunar interior [O'Keefe and Ahrens, 1977], and, in addition, the larger impacts probably led to widespread fracturing of the lunar surface [e.g., Fleitout and Thomas, 1982]. Between about 4 and 2.5 billion years ago, many of the nearside impact basins were filled by basalts to form the lunar maria [Boyce et al., 1974]. Most of the tectonic features on the Moon are closely associated with the lunar maria [Solomon and Head, 1979, 1980].

The lunar maria can be roughly divided into two groups, the circular and irregular maria. The circular maria include Imbrium, Serenitatis, Nectaris, Humorum, Smythii, Orientale, Crisium and Grimaldi. The major irregular maria include Oceanus Procellarum and the maria Tranquillitatis, Fecunditatis, and Nubium (Figure 1); there are also a number of smaller irregular maria and mare deposits, including the maria Frigoris, Undarum, and Spumans [Stuart-Alexander and Howard, 1970; Hartmann and Wood, 1971; Wilhelms and McCauley, 1971].

The circular mare basins are believed to be the result of individual large impacts [e.g., Baldwin, 1963; Stuart-Alexander and Howard, 1970; Head, 1976]. The irregular mare basins have

been attributed to various causes: overlapping impact features [e.g., DeHon, 1977, 1979], a degraded single impact basin [Stuart-Alexander and Howard, 1970], or irregular depressions of non-impact origin [Head, 1976].

The circular basins in general have well-defined basin ring structures; in the irregular maria the ring structures are degraded or absent entirely. For this reason the irregular mare basins are identified as being older than the basins filled by the circular maria [Stuart-Alexander and Howard, 1970]. The lack of prominent ring structures in the older mare basins may be the result of degradation of basin topography by subsequent impacts and ejecta deposition [Stuart-Alexander and Howard, 1970; McCauley and Scott, 1972; Hodges, 1973b] or to viscous relaxation of topography because of a thin local lithosphere [Solomon et al., 1982a]. Although the irregular basins are older than the circular ones, the mare units that fill the irregular basins range from among the oldest mare units (in Mare Tranquillitatis) to among the youngest (in Oceanus Procellarum) found on the Moon [Boyce et al., 1974; Boyce, 1976].

Most of the circular maria are associated with large gravity highs known as "mascons". These positive gravity anomalies indicate mass concentrations associated with the circular maria [Muller and Sjogren, 1968]. The mass concentrations are the result of both mantle uplift beneath the basin and the mare basalt load itself [Bowin et al., 1975; Thurber and Solomon, 1978; Phillips and Lambeck, 1980; Bratt et al., 1985]. There are

no mascons associated with the irregular maria, although there are smaller gravity anomalies found in them, the most outstanding example being the gravity high associated with the Lamont feature in Mare Tranquillitatis [Sjogren et al., 1973; Scott, 1974]. The lack of mascons in the irregular maria has been interpreted as being the combined result of isostatic compensation of the irregular mare basins before mare filling with relatively thin basalt fill [Phillips and Saunders, 1974; Bratt et al., 1985].

Despite these differences in age, appearance, and structure, the circular and irregular maria contain similar types of tectonic features. Both have systems of mare ridges, and sets of rilles or graben are found around the edges of both types of maria. Mare ridges are thought to be the result of horizontal compression of near-surface material [e.g., Lucchitta, 1976, 1977; Sharpton and Head, 1982a, 1983], while the rilles, like their terrestrial counterparts, are the result of horizontal extension [e.g., McGill, 1971]. For the circular maria, the basin-concentric graben and mare ridge systems have been interpreted as being the result of flexure of the elastic lithosphere under the load imposed by mare volcanic units. On the basis of this interpretation, Solomon and Head [1979, 1980] and Comer et al. [1979] applied the model of Brotchie and Silvester [1969] and Brotchie [1971] for flexure of a thin elastic shell over an inviscid fluid layer to infer the thickness of the elastic lithosphere beneath the circular maria at the time of formation of tectonic features.

The hypothesis that large-scale tectonic features

associated with volcanic regions of the terrestrial planets are products of the flexural response to loading of the lithosphere has proven to be a fruitful approach for constraining the tectonic history of circular lunar maria [Melosh, 1978; Comer et al., 1979; Solomon and Head, 1979, 1980] and the regions surrounding individual Martian volcanoes [Thurber and Toksoz, 1978; Solomon et al., 1979; Comer et al., 1985]. In this chapter we test the assumption that the irregular maria share with the circular maria the processes leading to formation of mare ridge systems and basin-concentric graben. To do this, we develop a more general version of the Brotchie formulation in order to model the asymmetric basalt loads found in the irregular maria. We discuss the geologic structure and history of each of the major irregular maria, and we derive load models from the distribution of mare basalt estimated by Bratt et al. [1985a] from lunar gravity and topography. From these models, and for various assumed values of the thickness of the elastic lithosphere, we compare the predicted stress fields with the distribution of tectonic features. We compare the best fitting values for lithospheric thickness beneath the irregular maria with those previously inferred for the circular maria. Finally, we discuss the implications of these new results for the thermal history of the Moon.

MARE TECTONIC FEATURES AND FRACTURE STRENGTH

There are two types of tectonic features found in association with the maria: mare ridges and linear and arcuate rilles. Several different mechanisms have been proposed for

mare ridge formation. Early workers favored volcanic intrusion or extrusion, controlled by global or basin-related tectonic patterns [e.g., Hartmann and Wood, 1971; Strom, 1972; Elston, 1972; Scott and Eggleston, 1973]. More recent studies indicate that ridges are tectonic features formed in response to horizontal compression of near-surface material [Bryan, 1973; Howard and Muehlberger, 1973; Muehlberger, 1974; Lucchitta, 1976, 1977; Fagin et al., 1978; Sharpton and Head, 1982, 1983]. Combinations of volcanism and tectonism have also been proposed [Colton et al., 1972; Young et al., 1973; Scott et al., 1975; Raitala, 1980]. We favor the interpretation that mare ridges are compressive tectonic features.

There is a long-standing consensus of opinion that rilles circumferential to the lunar maria are graben created by extensional stresses at the edges of the maria [e.g., Baldwin, 1963; Quaide, 1965; McGill, 1971; Young et al., 1973; Solomon and Head, 1979, 1980]. Some graben may be bounded by faults originally produced by major impacts, such as the Imbrium event, and later reactivated by regional stresses [Lucchitta and Watkins, 1978]. Basin-concentric graben may be plausibly attributed to the flexure of the lithosphere in response to the mare volcanic load. Graben radial to major maria, such as those adjacent to southwestern Oceanus Procellarum [McCauley, 1973; Whitford-Stark and Head, 1977a], however, may be at least partly the product of basin impact processes [Melosh, 1976; Mason et al., 1976; Schultz and Spudis, 1985], in particular the Imbrium impact, which has apparently left a near-planetwide

tectonic signature [Mason et al, 1976; Fleitout and Thomas, 1982].

In a number of locations it may be shown that ridge formation occurred more recently than rille formation. In particular, it appears that rille formation was confined to periods before about 3.6 ± 0.2 b.y. ago [Lucchitta and Watkins, 1978] while ridge formation continued until after the last major volcanic episode in each mare.

If we accept that ridges are formed by horizontal compression and that rilles are the result of horizontal extension, the question becomes how to model the horizontal stresses that led to the formation of these features. The loading models of Brotchie and Silvester [1970] and Brotchie [1971], taken alone, lead to stress fields which predict strike-slip faulting in many areas, with one horizontal principal stress compressional and the other extensional. Because neither the rilles nor the ridges on the Moon are the result of strike-slip faulting, it is necessary to invoke stresses in addition to those generated by mare basalt loading in order to predict the observed tectonic features.

One such source of stress arises from the thermal expansion and contraction of the Moon over its history [Solomon and Chaiken, 1976]. These horizontally isotropic stresses must be insufficient to produce tectonic features by themselves, because of the absence of evidence for pervasive lithospheric failure on a global scale, but when superimposed on the stresses produced by loading of the lithosphere by mare basalt units, they make it possible to account for the tectonic features observed in association with the lunar maria and for

the time dependence of formation of those features. An early period of thermal expansion promotes rille formation, and the later period of cooling and compression would favor ridge formation continuing past the time when rille formation had ceased [Solomon and Head, 1979, 1980].

The global thermal stress adds a constant to the local horizontal stresses arising from mare basalt loading; this can significantly change the magnitudes and possibly the sign of both the radial and azimuthal stresses around the maria, but not the directions of those stresses, which are controlled by the distribution of the basalt load. The lunar thermal history model of Solomon and Head [1980] predicts maximum horizontal thermal stresses of slightly less than 200 bars during the time of formation of mare tectonic features; this stress cancels out the small compressional tangential stresses found in the areas of maximum radial extensional stress outside the load; thus graben formation rather than strike-slip faulting is predicted. Later, when the planet cools and shrinks, the thermal model of Solomon and Head [1980] predicts global compressional stresses approaching 1 kbar. For the models of Solomon and Head [1980] these compressive stresses serve primarily to elevate the modest (200-400 bar) compressive loading stresses to levels considered consistent with the compressive strength of rocks (although the exact stress levels required for ridge formation are not known). For the models in this chapter, the global compressive stress field also cancels out occasional extensional stresses within mare units arising from the loading by nearby mare material. Because the time of ridge formation is not well known for most ridge features, we have made the

somewhat arbitrary assumption that approximately 400-500 bars of horizontally isotropic compression is available during the time of ridge formation.

STRESS MODELS

To model the stress field induced by volcanic loading, we use the theory of Brotchie and Silvester [1969] and Brotchie [1971] for flexure of a thin elastic shell overlying an inviscid fluid interior. Because the equation for flexure of a thin shell is linear, we can calculate the stresses due to an arbitrary surface load $q(\underline{r})$ by convolving the load with the stress tensor $\underline{\underline{\sigma}}_o$ resulting from a point load of unit magnitude:

$$\underline{\underline{\sigma}}(\underline{r}) = \iint \underline{q}(\underline{r}') \, \underline{\underline{\sigma}}_o(\underline{r}-\underline{r}') \, dA' \qquad (1)$$

where $\underline{r}$ and $\underline{r}'$ are position vectors on the planetary surface and dA' is a unit of surface area. As an approximation to (1), we replace $\underline{\underline{\sigma}}_o$ with the stress distribution $\underline{\underline{\sigma}}_d$ resulting from a finite disk load of unit magnitude [Brotchie, 1971; Solomon and Head, 1979], and we replace the integral in (1) with a sum over the number of disks:

$$\underline{\underline{\sigma}}(\underline{r}) = \sum_{i=1}^{N} q_i \, \underline{\underline{\sigma}}_d \, (\underline{r}-\underline{r}_i) \qquad (2)$$

where q_i and $\underline{r}_i$ are the load and the position of the center for the ith disk. Obviously the stress tensors $\underline{\underline{\sigma}}_d$ must be cast in terms of a global coordinate system before summation; standard spherical coordinates (r,θ,ϕ) with the polar axis at the geographic pole are used throughout. The principal horizontal stresses are found by means of the standard relations [e.g.,

Turcotte and Schubert, 1982]:

$$\sigma_{H1} = \sigma_{\phi\phi} \cos^2\alpha + \sigma_{\theta\theta} \sin^2\alpha + 2\sigma_{\theta\phi} \sin\alpha \cos\alpha$$
$$\sigma_{H2} = \sigma_{\phi\phi} \sin^2\alpha + \sigma_{\theta\theta} \cos^2\alpha - 2\sigma_{\theta\phi} \sin\alpha \cos\alpha \quad (3)$$

where α is the angle of rotation between the global coordinate system and the principal stress coordinate system and is given by

$$\alpha = \frac{1}{2} \tan^{-1} \left[\frac{2\sigma_{\theta\phi}}{\sigma_{\phi\phi}-\sigma_{\theta\theta}}\right] \quad (4)$$

The elastic theory used in these stress calculations is clearly an idealization of actual mechanical behavior, and it is important to realize the limitations of these simplified descriptions of the stress field. Several distinct limitations of the theory may be identified. The stress models are based on thin shell theory and are valid only for loads of horizontal dimension small compared to the planetary radius. For all models, perfect elasticity is assumed for the lithosphere. Further, for each model the lithosphere is taken to have a uniform thickness or flexural rigidity. Such time-dependent effects as viscoelasticity and load growth are ignored. In addition to these limitations on the theory, of course, are uncertainties introduced by errors in the load models and by imperfect and variable preservation of tectonic features. We discuss each of these limiting factors in turn.

The elastic flexure theory of Brotchie and Silvester [1969] and Brotchie [1971] is valid only for thin elastic shells and only for loads of small horizontal extent compared to the radius of curvature of the shell. The thin shell

approximation is not a serious source of error for local loading problems [Melosh, 1978; Pullan and Lambeck, 1981; Comer, 1983], even for a lithosphere several hundred kilometers in thickness, such as that in the vicinity of Olympus Mons on Mars [Thurber and Toksoz, 1978; Comer et al., 1985]. The approximation of horizontally limited loads in the Brotchie formulation in general presents no problem for the lunar maria, which with one exception have diameters much less than the radius of curvature of the lithosphere. The second largest lunar mare, Mare Imbrium, has an approximate load diameter of 900 km [Solomon and Head, 1980], compared to the lunar radius of 1738 km; loads of this size on the Moon are supported primarily by bending stresses rather than by membrane stresses [Turcotte et al., 1981], and thus for Mare Imbrium the Brotchie formulation will be acceptable.

The one lunar maria that appears to violate this approximation is Oceanus Procellarum, the largest lunar mare. The long axis of this mare is comparable in dimension to the lunar radius. However, there is evidence that the basalt flows over the region were deposited over an extended period of time, with the older flows coming into isostatic equilibrium before the youngest units were deposited [Whitford-Stark, 1980, 1983]. Thus, although Oceanus Procellarum taken as a whole does violate the assumption of small horizontal extent, it is in fact more appropriate to model Oceanus Procellarum as several individual loads, each of which taken separately is small enough to satisfy the approximation.

The assumption that the lithosphere behaves perfectly elastically does not take into account the fact that brittle fracture of the lithosphere (as demonstrated by the observed tectonic features) has acted to reduce stress. For plausible rheological models in which strength varies with depth [e.g., Goetze and Evans, 1979; Brace and Kohlstedt, 1980], however, even after near-surface faulting the stress differences induced by flexure are still supported by an elastic "core" of the plate and the effective flexural rigidity is similar to that of the elastic core.

There may also be significant lateral variations in strength or in lithosphere thickness [Solomon et al., 1979; Solomon and Head, 1982]. If there are important variations in the thickness of the elastic lithosphere, then estimates of lithospheric thickness derived from a comparison of model predictions to observed tectonic features will be intermediate between the extremes in actual values [Pullan and Lambeck, 1981]. The theories employed here neglect, moreover, any zones of weakness in the lithosphere, which can act to concentrate deformation and faulting [e.g., Sykes, 1978]. For the Moon we anticipate that large basin-forming impacts, such as the Imbrium impact, will have near-global tectonic effects [e.g., Fleitout and Thomas, 1982]; we may expect that impact-induced fault zones can affect the location and orientation of tectonic features created by loading.

The load models used in the stress calculations are based on estimates of the excess mass obtained from the mare basalt

thickness estimates of Bratt et al. [1985a]. These thicknesses were derived as part of a simultaneous inversion of nearside gravity and topographic data, using a procedure similar to that of Thurber and Solomon [1978]. In that method, the contributions of mantle relief and mare basalt load to the observed gravity anomalies are separated by assuming that the basin topography was isostatically compensated prior to mare basalt fill and that crustal subsidence in response to loading by mare basalts may be neglected. These assumptions lead to minimum values for the calculated mare basalt thicknesses [Thurber and Solomon, 1978].

The topographic and gravity data used by Bratt et al. [1985a] to derive the basalt thicknesses adopted for this study have errors and uncertainties associated with them. Bratt et al. [1985a] assume that the free air gravity anomalies at 100 km altitude have an associated error of ±10 mgal over the central nearside and ±20 mgal elsewhere. The most reliable Bouguer gravity data are also over the central nearside, in the areas beneath the orbital tracks of the Apollo spacecraft. These areas include the irregular maria Tranquillitatis and Fecunditatis.

Bratt et al. [1985a] used 5° x 5° block averages of topographic and gravity data to derive their models for crustal and basalt thicknesses. The estimates of errors on individual absolute topography measurements range from 0.3 km for Apollo laser altimetry and orbital photogrammetry [Bills and Ferrari, 1977] to 0.4 - 0.9 km for topographic measurements using

landmark tracking, earth-based photogrammetry, and limb profiling [Bratt et al., 1985a]. Because of the large number of topographic data points, uncertainties in the mean topography of blocks covered by Apollo orbital tracking data may be less than 0.1 km. However, in areas poorly covered by spacecraft tracking data, including portions of Mare Nubium, the estimated error in the average topography is nearly the same as that of the individual measurements [Bratt et al., 1985a]. In such cases errors in the measurement of topography are a major source of uncertainty in the Bratt et al. [1985a] model.

We also note that because Bratt et al. [1985a] derive their crustal and basalt thickness models in 5° increments over the lunar nearside, their models are somewhat limited in their ability to resolve small-scale fluctuations in their model parameters. The Bratt et al. [1985a] models also tend to overestimate the size of the mare loads slightly, compared to the sizes of the mare units shown on U.S.G.S. geologic maps. The radii of the disks in our load models are chosen to conform as closely as possible to the extent of the mare units shown on the quadrangle maps.

Although Bratt et al. [1985a] did not assign a formal error to their mare basalt thicknesses, we estimate that a typical uncertainty for mare thickness in the irregular maria is 0.25 km. This estimate is based on the constraint imposed by Bratt et al. [1985a] that mare basalt thicknesses be at least 250 m in areas with a very small Bouguer anomaly, including portions of the irregular maria (in particular

Oceanus Procellarum). This uncertainty is only that associated with the data and the formal inversion, however, and does not include that associated with the modeling assumptions, such as the assumption of premare isostasy.

Our primary objective in this chapter is to model the orientations and style (extensional or compressional) of the observed tectonic features in each region. Our load models give both stress orientation and stress magnitude, but the stress orientations are more reliable than the magnitudes because of uncertainties in the magnitude of the load. An error in the load magnitude will lead to a similar error in the calculated stress magnitudes, but will not alter the stress orientations or signs or the relative values of the stresses at different locations; these will be affected only by errors in the areal load distribution.

We have considered in several cases the effects of interactions between mare loads. For the circular maria we have used the load models of Solomon and Head [1980]. In cases where they estimated the load at two or more distinct stages of mare filling, we have used the load model corresponding most closely in age to the irregular mare load, based on ages of mare units estimated by Boyce et al. [1974], Boyce [1975, 1976], and Boyce and Johnson [1978]. For each of the irregular maria we have compared the stresses predicted by several different load combinations to determine which combination of loads and lithospheric parameters yields the best fit of the predicted stress field to the observed tectonic features.

For each model, stress fields were calculated for a range of values of the lithospheric thickness T. The results were then examined to determine the lithospheric thicknesses for which the predicted stress orientations corresponded most closely to the distribution of tectonic features. We further compared the locations of largest stress magnitudes to the areas of most extensive faulting. With this approach we generally obtain a range of lithospheric thicknesses consistent with each load model.

In addition to requiring the areas of maximum stress to coincide with the locations of observed faults, the stresses elsewhere should be insufficient to cause faulting. For extensional failure, following Solomon and Head [1980], we have required that the maximum stress difference be less than approximately 200 bars in areas lacking graben. This is in the range (200-400 bars) of the measured strengths of igneous rocks under extensional stress [Brace, 1964]. Further, Byerlee's [1968] frictional failure law gives an extensional strength of about 200 bars at 5 km depth on the Moon [Solomon, 1985], which is on the same order as the maximum depth of faulting on graben peripheral to the mascon maria Humorum and Serenitatis estimated by Golombek [1979]. Because stress magnitudes are sensitive to uncertainties in the load magnitude, the values of T derived from stress magnitudes have larger uncertainties than those based on locations and areas of maximum stress. In addition, because the magnitude of the basalt load used in the models is a minimum value, any upper bound on T assigned on the

basis of stress magnitudes is likely to be an underestimate.

This procedure has the advantage that even complicated models may be evaluated in a fairly straightforward way. The disadvantage is that it is difficult to assign a formal error to the calculated values for the lithospheric thickness. We may anticipate that the error will be larger for this method than for that of Comer et al. [1979], who obtained formal errors generally on the order of 10 km.

We also consider the basalt thicknesses estimated for the irregular maria by DeHon [1974, 1975a,b, 1977, 1979] and DeHon and Waskom [1976]. These basalt depths are based on measurements of rim heights and diameters of buried or partially buried craters in the maria; the rim heights are compared with those of unflooded craters of similar diameter to derive the depth of basalt fill in the crater. For each mare we discuss the differences between these basalt thickness estimates and those of Bratt et al. [1985a], and we evaluate qualitatively the differences in results for the two models. The crucial assumption made in the De Hon method is that the filled craters occur on the pre-mare surface, rather than on earlier basalt flows. Underestimates of the basalt fill using this technique can be caused by variations in crater rim crest topography and by the use of craters that postdate the beginning of mare fill. On the basis of these considerations, Head [1982] argues that this method may underestimate the true basalt thicknesses by more than a factor of two. Our primary interest in these alternative models is in the effect that

their different relative distribution of mass might have on the observed tectonic feature orientation and on the derived values of T.

DATA SOURCES FOR TECTONIC FEATURES

We have used the U.S. Geological Survey lunar geologic quadrangle maps for identification of tectonic features and mare unit boundaries. The later maps in the series use both Apollo and Lunar Orbiter photographic data. The earlier maps [e.g., Hackman, 1962; Marshall, 1963] were produced from earth-based telescopic photographs alone. However, based on a comparison of these maps with more recent published maps of lunar tectonic features [e.g., Guest and Murray, 1976; Whitford-Stark and Head, 1977a] it appears that that they are generally correct in their identification of major tectonic features. Some detail is lost on the earlier maps due to the poorer resolution of the photographic data, but the level of detail and accuracy, although at times less than ideal, is sufficient for the purposes of our models.

GEOLOGIC OVERVIEW AND LOAD MODELS

Mare Fecunditatis

Mare Fecunditatis occupies an irregularly shaped depression approximately 600 km by 900 km in size [DeHon and Waskom, 1976] (Figure 2a). It is surrounded by the circular maria Crisium (to the north) and Nectaris (to the southwest), and by the irregular mare Tranquillitatis (to the northwest)

(Figure 1). It is classed as a degraded circular basin by Stuart-Alexander and Howard [1970], Hartmann and Wood [1971], Wilhelms and McCauley [1971], McCauley and Scott [1972], Hodges [1973a], Scott et al. [1975], and Head [1976]. However, DeHon [1975b] and DeHon and Waskom [1976] argue that even if a degraded circular impact basin exists in northern Fecunditatis, the present configuration of the basin is a composite resulting from multiple overlapping structures related to both local and external nearby impacts.

The graben found around Mare Fecunditatis (Figure 2b) are located adjacent to the northwestern margin of the mare [Elston, 1972; Scott et al., 1975]. Because these graben are also approximately radial to the Imbrium basin [Elston, 1972], graben formation due to flexural subsidence of the mare load may have taken place preferentially on faults originally produced by the Imbrium impact.

A small positive gravity anomaly is located in west-central Mare Fecunditatis, at around longitude 51°E [Sjogren et al., 1972; 1974a,b]. This anomaly corresponds closely to an approximately semicircular ridge system, about 150 km in diameter (Figure 2c) [Sjogren et al., 1974b; Scott, 1974; Scott et al., 1975]. More ridge sets are found throughout northern Mare Fecunditatis; in some places the ridges appear to outline mantled pre-mare features [Elston, 1972; DeHon and Waskom, 1976]. The southern part of the mare contains essentially no tectonic features, either graben or ridges.

The basalt thicknesses estimated by DeHon [1975a,b] and DeHon and Waskom [1976] reach a maximum of 1000-1500 m in the area corresponding to the gravity high (Figure 3). Basalt thicknesses in northern Fecunditatis range from less than 250 m (near the edge of the mare) to more than 1500 m [DeHon, 1975a]. In southern Fecunditatis the basalt thicknesses inferred by DeHon [1975a,b] are quite thin (less than 250 m), although his estimates are limited by a lack of buried craters and by the accuracy of the available topographic data.

In northern Fecunditatis, the basalt thicknesses calculated by Bratt et al. [1985a] (Figure 4) are somewhat less than those of DeHon [1975a,b] and DeHon and Waskom [1976], reaching a maximum of approximately 1000 m in the central part of the mare. In the southern half of the mare, the basalt thicknesses of Bratt et al. [1985a] reach a maximum of 500 m.

In attempting to model the tectonic features of Mare Fecunditatis we have considered the following load combinations: Fecunditatis alone; Fecunditatis and Tranquillitatis; Fecunditatis, Nectaris, and Crisium; and all of the above plus Serenitatis. Our load model for Mare Fecunditatis, based on the basalt thicknesses of Bratt et al. [1985a], consists of three load centers, the northern center containing five disks, the central one, and the southern two (Table 2 and Figure 5).

The best fit of the predicted stress orientations and areas of maximum stress to the observed extensional features is obtained for the combination model including Nectaris and

Crisium (Figure 6). This model provides the best fit of stress directions to the observed graben distribution around the southeast and northeast edges of Fecunditatis, and the areas of maximum extensional stress generally correspond to the graben locations. The Fecunditatis load taken alone predicts stress directions that are only slightly worse than the Nectaris-Crisium-Fecunditatis load combination, but the maximum extensional stress occurs between the north and south loads, where no graben are seen. Also, an area of high extensional stress extends around the entire northern load center, and thus would predict graben formation in the north-northwest and in the east, where no concentric graben are seen. We note, however, that in these areas it is likely that any early episodes of fracturing would have been obscured by ejecta from the craters Langrenus to the east and Taruntius to the north; these craters are substantially younger than the mare units covered by their ejecta [Wilhelms, 1972; Hodges, 1973a]. Uncertainties in the relative basalt load distribution across the mare may also affect the predicted graben distribution. The model of DeHon [1975a,b] and DeHon and Waskom [1976] is relatively heavier in the western part of the mare, compared to the Bratt et al. [1985a] model, and would generate somewhat higher stresses on the western boundary of the mare. Extensional stresses around the southern Fecunditatis load center are significantly smaller, because of the reduced size of the load in this area; this difference may be sufficient to account for the lack of extensional features around the

southern part of the mare. For the DeHon model (Figure 3), the basalt thicknesses in southern Fecunditatis are also very thin, and formation of extensional features would not be predicted unless the lithospheric thickness was very small.

In order to estimate the lithospheric thickness at the time of graben formation, we examined the locations of maximum extensional stresses over the Fecunditatis region. The areas of maximum extensional stress, not surprisingly, occur between Fecunditatis and the mascon maria Nectaris and Crisium. The best fit of the areas of maximum stress difference to the observed graben locations is for values of T between approximately 40 and 75 km. Figure 7 shows stresses and stress difference contours for T=50 km. For comparison, we also show the contours of maximum stress difference for lithospheric thicknesses T=30 km and T=100 km. For T=30 km, the areas of maximum stress are substantially larger than the areas over which rilles are located (Figure 8); for T=100 km, the areas of maximum stress are smaller than the areas over which rilles are found (Figure 9).

One problem with this model is that it predicts graben formation over most of the area between Mare Fecunditatis and Mare Nectaris, but graben actually are found over only a portion of the area. It is possible that many of the graben around western and northern Fecunditatis originated on the sites of preexisting structural trends (as discussed previously).

The other combination models tested predict stresses less

consistent with the observed graben. The Tranquillitatis-Fecunditatis combination predicts formation of graben between the two mare (and concentric to both), which is not observed. The ejecta from Taruntius covers only a portion of the area between Tranquillitatis and Fecunditatis and thus cannot entirely account for the absence of graben in this region if load interactions have occurred. The combination including Serenitatis leads to a stress field which is not significantly different in style from that of the Tranquillitatis-Fecunditatis combination. Again, the region of high stresses is predicted to lie between Tranquillitatis and Fecunditatis.

At this time we can offer no simple explanation for why the tectonics of the Fecunditatis region appear to have been affected by load interactions with Crisium and Nectaris, but not by Tranquillitatis, which has a mare load comparable in age to that of Nectaris. It is possible that pre-existing structural trends, such as fracturing due to the Imbrium impact, have strongly influenced the formation of tectonic features around Fecunditatis and led to a preferred direction for graben formation. Our model assumes that the tectonic features associated with the maria are the result of loading-related stresses; using this model we cannot quantitatively predict the result of combining pre-existing fractures with the stress field due to loading.

In direction, the compressive stresses predicted by the Fecunditatis-Nectaris-Crisium load model combination are roughly consistent with the directions of ridges in Mare

Fecunditatis. The model predicts NS-trending ridges in the southern part of the main part of the mare; directions of maximum compressive stress vary from NE-SW to NW-SE across the northern part of the mare. Over the southern load center the predicted stresses are somewhat lower than over the northern load center, but this difference alone may not be sufficient to account for the absence of ridges in the southern half of the mare (Figure 2c). The areas of maximum stress difference coincide with the observed ridges in Fecunditatis most closely for lithospheric thicknesses in the range T=50-100 km. Figure 10 shows stresses and stress difference contours for T=75 km.

Mare Tranquillitatis

Tranquillitatis (Figures 11 and 12) is one of the oldest identifiable basins on the lunar nearside [Stuart-Alexander and Howard, 1970; Hartmann and Wood, 1971; McCauley and Scott, 1972; Wilhelms, 1981] and contains mare units that are among the oldest on the Moon [Boyce et al., 1974; Boyce, 1976; Boyce and Johnson, 1978]. Stuart-Alexander and Howard [1970] identified two degraded circular impact basins partially filled by Mare Tranquillitatis, with the western basin being the older. Wilhelms and McCauley [1971] and Wilhelms [1972] identify only a single impact basin; their identifications are based on remnants of an apparent basin ring structure and on the presence of linear and arcuate rilles peripheral to western Mare Tranquillitatis. They also note that the basin has been modified by the emplacement of ejecta from younger basins in

the vicinity, including Nectaris, Crisium, Serenitatis, and Imbrium. Pre-mare volcanism may also have modified this region [Morris and Wilhelms, 1967], but it is difficult to assess its presence and significance.

The topographic relief of the Tranquillitatis basin, after removing the effect of mare basalt fill, is consistent with significant viscous relaxation of basin topography prior to the emplacement of the oldest preserved mare surface unit [Solomon et al., 1982a]. Such relaxation could have occurred in an environment of elevated near-surface temperatures (and thus lowered viscosities) in the time period after basin formation [Solomon et al., 1982a; Bratt et al., 1985a].

The tectonic features in the Tranquillitatis region are shown in Figure 12. The extensional tectonic features associated with Mare Tranquillitatis are concentrated on the western side of the basin [e.g., Scott et al., 1975], where there is a well-developed concentric graben system (Figure 12b). These concentric graben occur in a narrow band at the mare boundary, extending from the southwest to the northwest side of the mare. The other major extensional tectonic feature of the region is the Cauchy fault system (Figure 12b), which begins near the eastern edge of Mare Tranquillitatis and cuts across the north-western portion of the mare [Quaide, 1965; Wilhelms, 1972; Scott et al., 1975]. Because these faults are radial to the Imbrium basin, Wilhelms [1972] has argued that they were produced by the Imbrium basin impact event and later reactivated.

There are a number of small ridges in eastern Mare Tranquillitatis (Figure 12c); most of these are preferentially oriented north-south [Fagin et al., 1978]. The most concentrated ridge system is that associated with the feature Lamont (Figure 12a) which is also the site of a prominent gravity high [Sjogren et al., 1973; Scott, 1974; Dvorak and Phillips, 1979]. Lamont is characterized by a double ring of ridge segments, surrounded by a set of radial linear mare ridges [Guest and Fielder, 1968; Scott, 1974; Dvorak and Phillips, 1979]. Although DeHon [1974] and DeHon and Waskom [1976] identify Lamont as the surface expression of a buried crater filled with mare material, Scott [1974] points out that other buried craters of comparable size do not have comparable associated gravity anomalies; for this reason he considers Lamont to be a small mare-filled multi-ringed basin, possibly located at the source of much of the mare fill for Mare Tranquillitatis. Dvorak and Phillips [1979] and Janle [1981] use models based on gravity and topography to argue that Lamont may be an igneous intrusive body rather than a filled basin.

There is a trough-like topographic low in western Tranquillitatis, aligned approximately north-south, with elevations some 1500 m less than the surrounding mare. The linear ridges of the Lamont region are within the trough while the rilles developed in western Tranquillitatis occur on the edge of the trough [Dvorak and Phillips, 1979].

On the basis of the topography, gravity, and ridge system associated with Lamont, Dvorak and Phillips [1979] present a

model for the structure in which the stress field due to a small circular mascon (diameter approximately 120 km) is superimposed on a regional east-west compressional stress field associated with the formation of a north-south-trending syncline; they do not attempt to determine the source of the regional compressive stress field.

Rather than invoke a regional compressive stress field of unknown origin to explain the linear ridges in Lamont, we will attempt to model the observed tectonic features by loading by basalt units alone. We note, however, that it is not possible to produce simultaneously the linear ridges and the ridge rings, which in places are perpendicular to one another. This means that if all the ridges in Lamont are the result of loading, that loading must have occurred in at least two separate episodes, with the circular ridges forming in one episode and the linear ridges in another.

DeHon [1974] and DeHon and Waskom [1976] map basalt depths in Mare Tranquillitatis from measurements of partially buried crater rim heights (Figure 3). Using this method, the deepest basalt thicknesses in the mare are along an axis extending from the "neck" of mare material connecting Mare Nectaris and western Mare Tranquillitatis northward through the Lamont region. The basalt depths in the vicinity of Lamont are estimated to be 1000-1500 m [DeHon, 1975b]. Although it is reasonable to expect that the positive gravity anomaly over Lamont may correspond, at least in part, to the deepest mare basalt load, DeHon [1974] bases his depth calculation in this

area on the assumption that the Lamont ridge ring marks a buried crater rim. As previously discussed, this assumption may not be valid.

The basalt depths calculated by Bratt et al. [1985a] (Figure 13), like those of DeHon [1974] and DeHon and Waskom [1976], indicate maximum basalt thicknesses in the western half of the basin. However, the thickness estimates of Bratt et al. [1985a] are somewhat smaller than those of DeHon [1974] and DeHon and Waskom [1976]. This is particularly noticeable in the area of Lamont, where Bratt et al. [1985a] give a maximum basalt depth of 800 m, compared with the 1500 m estimate of DeHon [1974]. In the "neck" between Mare Tranquillitatis and Mare Nectaris, Bratt et al. [1985a] give basalt thicknesses of roughly 1200 m, compared with about 1500 m by DeHon [1974]. In terms of relative mass distribution, however, the two models are roughly similar.

For Mare Tranquillitatis we have tested the following load combinations: Tranquillitatis alone; Tranquillitatis and Fecunditatis; Tranquillitatis and Serenitatis; and all of the above plus Nectaris and Crisium. Our arrangement of disk loads for Mare Tranquillitatis, chosen to approximate the basalt thicknesses of Bratt et al. [1985a], contains four load centers, as given in Table 1 and Figure 14. (The load magnitudes are expressed in Tables 1 through 5 in terms of the thickness h of mare basalt; the equivalent load magnitude is given by ρgh, where $\rho = 3.4$ g/cm^3, and $g = 162$ cm/s^2. Table 6 gives the load magnitudes and distributions for the circular

maria, from the models of Solomon and Head [1980]; the circular mare loads are assumed to be located at the centers of the basins as given by Wilhelms [1981].)

The best fit to the observed locations of extensional tectonic features is obtained for the load model consisting of Tranquillitatis alone. For this model, the stress orientations correspond closely to the concentric graben found around the western part of the mare. The areas of maximum extensional stress are around the edges of the southern load and along the western mare boundary; the stresses thus predict formation of concentric graben around the southern extension of Tranquillitatis (where none are observed) as well as in the west (where they are).

In order to estimate the lithospheric thickness at the time of graben formation, we examined the location of maximum extensional stresses in western Tranquillitatis as a function of lithospheric thickness. In general, as T increases, the location of maximum extensional stresses moves outward from the center of the load. The fact that the Tranquillitatis graben are located quite close to the edge of the mare boundary suggests that the lithosphere was relatively thin at the time they formed. The best fit of the area of maximum stress difference was obtained for T = 30-60 km. Figure 15 shows stress orientations and stress difference contours for T=40 km.

All the combination models tested give poorer fits of stress orientations and areas of maximum stress difference to the observed graben in the region. Combining the

Tranquillitatis and Fecunditatis loads does not change the orientations of stresses in western Tranquillitatis significantly, but the largest stresses for this model are found in the area between Tranquillitatis and Fecunditatis, where no graben of the correct orientation are observed. The combination of Tranquillitatis and Serenitatis changes the orientation of stresses in the northwestern part of the central load area, and would predict the formation of graben more nearly concentric to Serenitatis than Tranquillitatis. The model including Crisium and Nectaris in addition to the above loads shares the problems of the other combination models, and in addition predicts an area of high extensional stress between southern Tranquillitatis and Nectaris, where no graben are seen.

Because Tranquillitatis is surrounded by other mare loads, it is somewhat surprising that these other loads appear to have had little effect on the tectonic history of the region. Several scenarios can be constructed to explain this result, although none of them taken alone offer an entirely satisfactory explanation. Because Tranquillitatis is surfaced by mare units generally older than those of nearby maria (the exception being Nectaris) [Head, 1976], it is possible that relief of loading stresses by fracturing and perhaps also by viscoelastic relaxation prior to emplacement of most of the load in each nearby maria. This does not account for the lack of graben between Tranquillitatis and Nectaris, which contain mare units very close in age [Boyce and Johnson, 1978]. As

discussed below, however, the lack of graben around southern Tranquillitatis is difficult to predict for any model using a uniform lithospheric thickness beneath the entire Tranquillitatis load.

The large southernmost load (Figure 14) leads to large radial extensional stresses around the southern extension of Tranquillitatis; these stresses would predict the formation of concentric graben which are not observed. A possible explanation for this disagreement would be if the lithosphere in the "neck" of material extending toward Mare Nectaris were thicker than beneath the main portion of the mare. Although we cannot directly model a lithospheric thickness heterogeneity using this model, modest local thickening of the lithosphere in the southern part of Mare Tranquillitatis would qualitatively account for the absence of concentric graben in that area.

The compressive stresses over the loads are consistent in direction with the linear ridge systems passing through Lamont and with the ridges found in the southern part of the mare. However, the Tranquillitatis load model cannot reproduce the double ring of ridges at the center of Lamont. It has not been possible, using any combination of loads, in fact, to predict simultaneously the ridge rings and the north-south trending ridges oriented perpendicula ao them. Of course, Lamont is a relatively small-scale feature, while our load models are based on a fairly coarse 5° grid of basalt thicknesses Thus we cannot exclude the possibility that the Lamont ridge rings are related to loading; their circular form is very similar to,

although much smaller in scale than, the loading-related ridges associated with the circular maria.

For ridge formation, the area of maximum stress difference coincides with the region of observed ridges for lithospheric thickness in the range roughly 60 < T < 150 km. Figure 16 shows stresses and stress difference contours for T=75 km. We note that the area of maximum stress difference is displaced slightly to the east of the westernmost Lamont ridges. This may be due partly to the particular load model used. The disks chosen to represent the areal extent of the mare produce a load in the central part of the mare slightly greater than that of Bratt et al. [1985a] because of disk overlap.

Mare Nubium

Mare Nubium is located at the southern end of Oceanus Procellarum (Figures 1 and 17a). Stuart-Alexander and Howard [1970] placed the Nubium basin in their oldest category, based on its lack of a well-defined ring structure and on the number and condition of superposed craters in and around the basin.

The most striking tectonic feature of Mare Nubium is the Straight Wall (Rupes Recta), near the eastern edge of the mare (Figure 17b). It is an essentially straight scarp, 120 km long, with the inner side downthrown [DeHon, 1977]. The average height of the scarp is approximately 300 m [DeHon, 1977]; the maximum vertical displacement is approximately 400 m [Holt, 1974]. The Straight Wall has been interpreted as a normal fault [Fielder, 1963; Quaide, 1965]; Holt [1974]

suggests that the scarp results from recent movement along a pre-existing structural trend. DeHon [1977] suggests that it may be the result of settling of mare material over the buried rim of an impact basin forming part of the Nubium basin. Because it does not resemble the rilles and graben commonly found around the maria, it is likely that the Rupes Recta was not created only by loading stresses; it may be a previously existing structural feature reactivated by loading in the mare.

Mare Nubium contains several sets of mare ridges (Figure 17c). In the northern part of the mare the ridges are oriented almost north-south (slightly NNE-SSW). In the southern part of the mare there are separate ridge sets oriented WNW and ENE, and in the north-central region the ridges are generally oriented NW-SE. In the western central region, where these ridge sets intersect, the ridge pattern is, not surprisingly, irregular.

DeHon [1977] estimated basalt thicknesses in Mare Nubium from the rim heights of partially buried craters. His model for the basalt fill in the mare (Figure 18) contains several thick lenses; the two largest are one more than 750 m thick at 25°S, 21°W, and one in excess of 1500 m thickness at 22°S, 10°W. He estimates that the average thickness of basalt in Mare Nubium is slightly greater than 500 m. Based primarily on these calculated mare basalt depths, DeHon [1977] hypothesized that Mare Nubium occupies an area of four overlapping basins, with the west Nubium basin forming first and being

substantially modified by subsequent impacts in West Nubium and Humorum, which deposited a substantial amount of ejecta in the first basin. This differs from the analysis of Stuart-Alexander and Howard [1970], who characterized Nubium as a single, highly degraded circular basin.

The mare basalt thicknesses calculated by Bratt et al. [1985a] (Figure 19) from gravity and topographic data differ significantly from those of DeHon [1977]. The basalt thicknesses reach a maximum of 0.8-1.0 km depth in an elongate area on the western side of the mare, which corresponds roughly to one of the basalt lenses of the DeHon [1977]. However, the Bratt et al. [1985] model for Mare Nubium has no equivalent to the deep basalt lens postulated by DeHon [1977] in the eastern part of the mare.

We have tested three models for this region: one consisting of Mare Nubium alone; a combination of Nubium and Humorum loads; and a combination of Nubium with a load representing the southernmost portion of Oceanus Procellarum. The model for the Mare Nubium basalt load (Table 3 and Figure 20), derived from the Bratt et al. [1985a] model, contains three load centers. The orientations of the observed graben around Mare Nubium are most nearly consistent with the model consisting of Nubium alone. The directions of the stresses predicted by this model are consistent with the distribution of graben in western Nubium (not including the graben concentric to Humorum) and approximately consistent with the orientation of Rupes Recta in eastern Nubium. The graben along the

southern boundary of Mare Nubium are concentric to the western Nubium load center but not to the stresses predicted by the total load; this suggests the possibility that the Nubium load was emplaced in stages. Considering the areas of maximum extensional stress, the main problem with all Nubium models is that it is difficult to predict the formation of Rupes Recta and not predict other graben around the eastern load center. One possible explanation for this would be if the Rupes Recta had originated in a process other than loading (such as impact stresses), and was merely reactivated by loading stresses. We consider this to be likely, particularly because this feature does not closely resemble typical basin-concentric extensional features (it is in the form of a scarp rather than a graben).

Radial extensional stresses comparable to those in western Nubium are also predicted along the northern border of Mare Nubium, where no extensional features are seen. There are several possible explanations for this discrepancy. Much of the area, which lies between Mare Nubium and Oceanus Procellarum, is covered by relatively young geologic units [Whitford-Stark, 1983] which might have covered an early episode of faulting. It is also possible that because our models are based on the current gravity and topography of the region, we have overestimated the size of the basalt load in that area at the time of rille formation.

In order to estimate the lithospheric thickness under Mare Nubium at the time of graben formation, we examined the locations of maximum extensional stress over the region for a

range of values of T. The best fit of the areas of maximum stress to the observed graben was obtained for values of T in the range 30 to 75 km. Figure 21 shows stresses and stress difference contours for T=50 km.

The other load combinations tested for the Nubium region provide a worse fit to the observed extensional tectonic features. In terms of principal stress directions, the Nubium-Humorum combination offers no improvement on the Nubium load taken alone. In addition, the Humorum load generates large extensional stresses to a significant distance inside Mare Nubium; for this load combination, the area of maximum extensional stress is very broad, and it is essentially impossible to account for the graben between Nubium and Humorum without also predicting graben inside Nubium for any value of the lithospheric thickness. The vast majority of the surface basalt units in Humorum were emplaced about 3.6 b.y. ago [Boyce, 1976; Boyce and Johnson, 1978]. Crater density data for Nubium basalts give ages in the range 3.0-3.5 b y. [Boyce and Johnson, 1978]. It is thus possible that evidence of any early episodes of Humorum-induced fracturing inside Nubium would have been covered by younger basalts.

The combination of Nubium with a south Procellarum load leads to very large extensional stresses between the two regions, in areas where no graben are seen. Because young lava flows originating within Procellarum cover much of this region, however, we cannot completely exclude earlier faulting episodes.

The compressional stress field for the Nubium load model is consistent with the formation of ridges in much of Mare Nubium; in particular, the NE-SW-trending ridges in southern Nubium (25°-28°S, 20°-25°W) are consistent with the orientations of maximun compressive stresses in that area. The predicted directions of maximum compressive stress are also consistent with the NE-SW-trending ridges in northeastern Mare Nubium, and with the formation of both NW-SE-trending and NE-SW-trending ridges in the central part of the mare. The exact orientation of the maximum compressive stress, however, depends strongly on the details of the distribution of the basalt load.

The lithospheric thickness at the time of ridge formation is not tightly constrained by this model. For each value of T, the maximum stress differences in the vicinity the load itself change fairly slowly; this makes it difficult to choose a preferred value of T strictly on the basis of the location of maximum stress differences. Our estimate of lithospheric thickness at the time of ridge formation is T=50-150 km. Figure 22 shows stresses and stress difference contours for T=75 km.

Oceanus Procellarum

Oceanus Procellarun is located on the western nearside of the Moon (Figures 1 and 24a). It is the largest lunar maria, covering about 1.7 x 10^6 km^2, about 25% of the total lunar mare area [Whitford-Stark and Head, 1977a, 1980]. Oceanus Procellarum contains three volcanic complexes: the Marius

Hills, the Rumker Hills, and the Aristarchus Plateau/Harbinger Mountains; these volcanic complexes appear to be the source for many of the lavas that form Oceanus Procellarum [Whitford-Stark and Head, 1977b, 1980].

Because Oceanus Procellarum is so large and had a long volcanic history, we present a relatively detailed overview of the geology of the region. Oceanus Procellarum is characterized by four major geologic formations, described in detail by Whitford-Stark and Head [1980] (Figure 23). In order of increasing age, these include: the Sharp Formation (2.7 ± 0.7 b.y.), the Hermann Formation (3.3 ± 0.3 b.y.), the Telemann Formation (3.6 ± 0.2 b.y.), and the Repsold Formation (3.75 ± 0.05 b.y.) [Whitford-Stark and Head, 1980]. The oldest formation, the Repsold formation, is exposed primarily in northern Oceanus Procellarum, although it is thought to underlie younger formations over much of Oceanus Procellarum. The youngest formation, the Sharp formation, covers much of eastern and southern Oceanus Procellarum [Whitford-Stark and Head, 1980]. These flows are among the youngest on the Moon [Boyce et al., 1974; Boyce, 1976]. Thus, it is apparent that the volcanic activity that created Oceanus Procellarum occurred over an extended period of time and in several distinct episodes.

Various theories have been proposed to explain the formation of the depression filled by Oceanus Procellarum. These scenarios include overlapping small impact basins [DeHon, 1979] and the suggestion of Whitford-Stark [1983] that the

depression forming Oceanus Procellarum is an immense tectonic structure (essentially an enormous graben) whose formation was initiated by the Imbrium impact event. Perhaps the most provocative proposal is that Oceanus Procellarum occupies the remnants of a gigantic impact basin that originally covered much of the lunar near side [Cadogan, 1974, 1975; Whitaker, 1981; Wilhelms 1982,1983]. This proposal was originally presented by Cadogan [1974, 1975], based largely on the distribution of KREEP basalts (enriched in potassium, rare-earth elements, and phosphorus), which Cadogan interpreted as early volcanic materials produced during and immediately after the formation of the Procellarum basin. McCauley [1973] had previously noted the apparent remnants of an ancient multi-ring basin structure controlling the Oceanus Procellarum shoreline in the area near Grimaldi. Whitaker [1981] and Wilhelms [1983] used structural arguments (identifying supposed ring structures and examining orientations of nearside mare ridge systems) to argue in favor of the Procellarum basin idea. It has recently been suggested, however, that the geochemical evidence in support of the Procellarum basin is inconclusive [Spudis and Schultz, 1985], and that the ridge ring structure is more nearly concentric around the Imbrium impact site than around the supposed Procellarum impact location (which also lies in the Imbrium basin) [Schultz and Spudis, 1985].

Such an immense impact would have had a profound effect on lunar geologic history. Wilhelms [1983] argued that lithospheric thinning caused by the Procellarum impact would lead to

the preferential formation of the maria on the lunar nearside. Bratt et al. [1985a,b] point to the possible effect of the thermal anomaly of the Procellarum impact on the evolution of the major irregular maria (Nubium, Fecunditatis, and Tranquillitatis); the high heat flow generated by the impact would have led to lower viscosity in the near-surface material, which would promote viscous relaxation of basin topography. It has been shown that the inferred present topography of the Tranquillitatis basin is consistent with the viscous relaxation of initial relief comparable to that of better preserved young basins [Solomon et al., 1982a]. An impact of the size required to create the proposed Procellarum basin would also have generated enough heat to affect the generation of lunar magmas [Hubbard and Andre, 1983].

The surface of Oceanus Procellarum is topographically low, even lower than the other irregular maria [Head et al., 1980]. Western Procellarum is characterized by a trough-like topographic low; other lows are associated with the Rumker Hills in northern Oceanus Procellarum and with an area southwest of the Marius Hills [Whitford-Stark, 1983]. In these locations sinuous rilles generally run tangent to, rather than perpendicular to, the direction of maximum topographic slope; this suggests that the topographic lows in these locations are the result of subsidence occurring after the sinuous rilles formed [Whitford-Stark, 1983].

Although Oceanus Procellarum lacks major gravity anomalies, it does contain several small anomalies. There is a

slight positive anomaly whose location appears to correlate with the Sharp formation, the youngest of the major geologic units [Whitford-Stark, 1980, 1983; Pieters et al., 1980]. Small-scale positive anomalies also appear to correlate with major ridge locations; these have been attributed by Scott [1974] to dike intrusions beneath mare ridges.

The fact that the most widespread positive gravity anomalies in Oceanus Procellarum occur only in areas of relatively young lava flows may indicate [Whitford-Stark, 1980, 1983] that the earlier units have undergone significant isostatic compensation, while the later units did not. This could be due to cooling and thickening of the elastic lithosphere over the time in which volcanic activity occurred; regional variations in lithospheric thickness are another possible explanation.

Two major groups of tectonic features dominate the Oceanus Procellarum region: a series of linear rilles in the uplands adjacent to the mare (Figure 24b) and sets of ridges within the mare (Figure 24c). The linear rilles formed after the Imbrium and Orientale basins and after the earliest mare units were deposited, but before the emplacement of the youngest mare units in Oceanus Procellarum and the neighboring Grimaldi basin [McCauley, 1973; Whitford-Stark and Head, 1977].

The ridge patterns in Oceanus Procellarum vary from region to region in the mare [Whitford-Stark, 1983]. In southeast Oceanus Procellarum, the ridges are aligned preferentially NE-SW and NW-SE. In central Oceanus Procellarum the ridges in

general are aligned roughly parallel to the mare shoreline [Whitford-Stark, 1983]. The complicated ridge pattern in northern Oceanus Procellarum may be to some extent a reflection of pre-mare topography [Maxwell et al., 1975; Schultz and Spudis, 1985]. Scott and Eggleton [1973] argue that the directions of ridges in northern Oceanus Procellarum are controlled by faulting concentric (not radial) to the Imbrium basin.

Tectonic rilles and graben are developed most strongly around central to southern Oceanus Procellarum [McCauley, 1973; Guest and Murray, 1976; Whitford-Stark and Head, 1977a]. Graben both parallel (concentric) and perpendicular to the mare shoreline are observed. The fact that graben are preferentially developed in one area of the mare may be related to variable lithospheric thickness beneath the mare [Whitford-Stark, 1983], or to variations in the size of the volcanic load, or to both.

The fact that both radial and concentric graben overlie one another in some locations has suggested to some workers that at least two different stress regimes were dominant at different times in the history of the region [Whitford-Stark, 1983]. It has been proposed that the perpendicular graben, and possibly some of the concentric graben, may be related to the Imbrium impact event [Mason et al., 1976; Fleitout and Thomas, 1982; Whitford-Stark, 1983].

Rille formation in Oceanus Procellarum apparently occurred up to the time of deposition of the Hermann Formation

(3.6 ± 0.2 b.y.) and has been largely insignificant since then [Whitford-Stark and Head, 1980]. Mare ridges are found on the youngest formation (the Sharp formation), although the major period of ridge development was earlier [Whitford-Stark and Head, 1980].

Head et al. [1980] argued that the abundant ridge and rille systems associated with Oceanus Procellarum despite its thin basalt fill indicate that the elastic lithosphere in the region was quite thin (less than 25 km) at the time of tectonic activity. The thin lithosphere implies a high subsurface temperature at the time of mare emplacement and tectonic feature formation; this predicted high temperature is consistent with other aspects of the regional geology, including the extent and variety of volcanic activity and the presence of volcanic complexes such as Marius and Rumker.

The basalt thicknesses estimated by DeHon [1979] from buried crater rim heights (Figure 18) indicate generally thin basalts in northern Oceanus Procellarum, although the scarcity of data points in the region makes it difficult to generalize these estimates. In eastern Procellarum, DeHon [1979] inferred a relatively thick lens of basalt, while in western Oceanus Procellarum he inferred a long, irregular prism of basalt reaching a thickness of 1000-1500 m in at least three centers of accumulation. Other estimates of the average fill thickness in southeastern Oceanus Procellarum range from 500-750 m [Horz, 1978] to 1.1 km [Marshall, 1961].

The basalt thicknesses derived by Bratt et al. [1985a] for

Oceanus Procellarum (Figure 25) are roughly similar to those of DeHon [1977], with basalt thicknesses less than 400 m over most of the northern part of the mare and with several thicker lenses in the southwest. The thickest basalt fill is found along an axis running northwest-southeast, north of Mare Humorum. Maximum thicknesses in the region are inferred to be approximately 1.2 km.

Rather than attempt to model Oceanus Procellarum as a single large collection of loads, which (as discussed above) is not appropriate in view of the geologic history of the region, we have chosen to model the loading history of the region by dividing the mare into western and eastern sectors, with each region modelled seperately by an elongated collection of loads. Our eastern Procellarum load model corresponds approximately to the area covered by the youngest geologic unit (the Sharp Formation) while the western Procellarum model corresponds approximately to the exposed portions of the Hermann Formation. Although this is clearly still an oversimplification of the loading history of the region (for example, the Hermann formation may underlie portions of the Sharp formation [Whitford-Stark, 1983]) it is a reasonable first approximation; in addition, the Bratt et al. [1985a] model can be broken down into these two sets fairly straightforwardly. For western Procellarum, we have tested load models both including and excluding the Grimaldi mascon load. Because Grimaldi is too small to be resolved in the basalt thickness model of Bratt et al. [1985a], we have adopted the Grimaldi load model of Solomon

and Head [1980].

Our model (including Grimaldi) for the western portion of Oceanus Procellarum (Table 4 and Figure 26) predicts an area of maximum extensional stress in regions approximately coincident with the locations of graben adjacent to southwestern Procellarum, for values of elastic lithosphere thickness T less than approximately 25-35 km. Figure 27 shows the stress distribution for T=25 km. The results of this model are consistent with the formation of graben around Grimaldi and graben close to the edge of the mare in southwestern Procellarum. Somewhat surprisingly, our model is also consistent with the formation of several of the graben oriented perpendicular to the southwestern Procellarum shoreline"; these features are consistent with the stresses produced by superposition of extensional stresses from several loads, which (depending on the exact load arrangement) can produce a total stress field in which the maximum extensional stresses near the load are oriented parallel to an axis joining the load centers. This suggests that these features may be at least in part a product of the irregular shape of the mare load, though perhaps reactivating faulting originally produced by the Imbium impact event.

The only area in which our model noticeably fails to match the observed extensional features is in the region just northwest of Grimaldi, where extensional features oriented parallel to the mare shoreline are found in the area between roughly 5°S and 5°N, 74°W and 77°W. We were unable to devise a

load model that can account for both the graben located very near the mare edge (consistent with a thin lithosphere) and graben located at a significant distance from the mare without additional faulting at intermediate distances. Fleitout and Thomas [1982] argue that a major basin impact in a body that is warming and expanding at the time of impact and then cooling and shrinking will lead to formation of fractures both radial and concentric to the basin. It is thus possible that at least some of each type of graben around Procellarum originated in a major basin impact, either Imbrium or the proposed Procellarum impact.

Without the Grimaldi load, the Procellarum load model is much less successful at predicting the location and orientation of extensional features. This is not surprising, because the basalts constituting the Grimaldi load are much thicker than the Procellarum load, and thus the stresses generated by the Grimaldi mascon are the dominant influence on the extensional tectonics in the vicinity of the Grimaldi basin.

In general, the ridges in western Oceanus Procellarum are oriented NW-SE. Because our load model has maximum compressive stresses oriented perpendicular to the long axis of the total load, we can reproduce the general orientations of the western Procellarum ridges reasonably well. Both with and without the Grimaldi load, the largest compressive stresses are found in the southern part of the mare, where the Procellarum load is deepest.

The lithospheric thickness at the time of ridge formation

in western Oceanus Procellarum, as for Mare Nubium, is not well constrained by the location of the area of maximum stress difference. The stress difference contours change fairly slowly for values of T between roughly 25 and 50 km; the magnitude of the stress differences decrease substantially between T=50 and T=75 km. A rough estimate of the value of T at the time of ridge formation is that it lies in the range $25<T<75$ km. Figure 28 shows stresses and stress difference contours for T=50 km.

In eastern Oceanus Procellarum the mare basalts are essentially continuous with mare units of Mare Imbrium (to the northeast) and Mare Cognitum and Mare Nubium (to the southwest), as well as with those of western Oceanus Procellarum. The only extensional features appearing in the region are at the far southeastern edge of the mare, just north of Mare Nubium. We presume that if loading in eastern Oceanus Procellarum led to faulting early in the history of this mare, such fractures would have been covered by younger lava flows. The main constraints on our models are thus the mare ridges, which are found throughout the region. The ridge pattern in eastern Oceanus Procellarum is somewhat more complicated than in the west: there are irregularly branching ridges in the southern portion, NW-SE-trending ridges in the central portion, and both NE-SW and NW-SE-trending ridges in the north.

Our load model for eastern Oceanus Procellarum (Table 5 and Figure 29) consists of four load centers, with from two to five disks in each load center. We also tested a combination

model including a Mare Imbrium load (Table 6), but this did not significantly alter the predicted ridge orientations and stress differences within Oceanus Procellarum itself.

The extensional features on the eastern edge of Oceanus Procellarum are consistent in direction with extension around the southernmost load in our model. The value for the lithospheric thickness is, unfortunately, virtually unconstrained by the distribution of the observed tectonic features. This is because most of the surface of eastern Oceanus Procellarum is covered with very young lava flows which would have obscured any early fracturing episodes.

The best match of the predicted stress difference contours to the observed distribution of ridges is obtained for values of the lithospheric thickness T in the range 50 km < T < 100 km. Figure 30 shows stresses and stress difference contours for T=75 km.

DISCUSSION AND CONCLUSIONS

In this chapter we have tested the hypothesis that many of the tectonic features found in and around the irregular lunar maria are the result of loading of the lithosphere by mare basalt units. Our lithospheric loading models have been quite successful at predicting the orientations of ridges and grabens for each region. For the Lamont region of Mare Tranquillitatis, the linear ridges can be the product of compression induced by a linearly extended load. For Oceanus Procellarum, the presence and orientation of many of the graben in the western part of the mare are consistent with the superposition

of the loading stresses due to the Procellarum load with those of the Grimaldi mascon load.

We have estimated values for the lithospheric thickness beneath each of the major irregular lunar maria from a comparison of predicted stress trajectories with the observed distribution of tectonic features. We allow for the likelihood that the majority of graben and mare ridges may have formed at distinct times. For each mare we have found that the lithospheric thickness at the time of ridge formation appears to have been somewhat greater than that at the time of graben formation. Since ridge formation continued well after graben formation ceased, these results are generally consistent with the gradual cooling and thickening of the lithosphere over time, as well as with a change in the global thermal stress field from early heating and expansion phase to later cooling and contraction phase [Solomon and Head, 1979, 1980].

We have attempted to account for possible interactions of mare loads, but in most cases the directions of stresses resulting from load interactions do not fit the observed graben as well as those resulting from single mare loads. An exception to this is Mare Fecunditatis, where we found that a combination model consisting of Fecunditatis, Nectaris and Crisium loads predicted principal stresses whose directions matched the observed graben around Fecunditatis better than those predicted by the Fecunditatis load alone.

It is likely that a number of factors are involved in

determining the presence or absence of mare load interactions. These factors may include relative timing of load emplacement, pre-existing structural trends (such as fractures related to basin impacts) which can serve as preferred sites for graben formation, deviations of lithospheric mechanical properties from the idealized elastic model used here, and possibly regional variations in lithospheric thickness.

For each of the irregular maria studied, we have estimated elastic lithospheric thicknesses based on a comparison of locations of maximum stress difference with the locations of rilles and ridges. There are no clear correlations between lithospheric thickness and factors such as basin age or size. Our results, however, are generally consistent with those of Solomon and Head [1979, 1980] and Comer et al. [1979] for the mascon maria. The values of T estimated for each mare are comparable among adjoining maria (i.e., Serenitatis-Tranquillitatis-Fecunditatis, and Nubium-Humorum). Oceanus Procellarum, and in particular western Oceanus Procellarum, appears to have had an unusually thin elastic lithosphere at the time of rille formation, a result in agreement with the earlier result of Solomon and Head [1980] for the Grimaldi basin region

Table 1. Mare Tranquillitatis Load Model.

Load Center		Load Geometry	
Latitude	Longitude	Radius, km	Thickness, km
2.8°S	27.6°E	45	0.3
		75	0.25
		105	0.3
		119	0.25
10.0°N	34.9°E	257	0.25
14.5°N	27.7°E	119	0.2
		194	0.2
		245	0.25
5.8°N	24.6°E	114	0.25
		152	0.15
		191	0.1
		233	0.25

Table 2. Mare Fecunditatis Load Model.

Load Center		Load Geometry	
Latitude	Longitude	Radius, km	Thickness, km
5.0°S	50.3°E	76	0.1
		121	0.2
		166	0.2
		212	0.2
		254	0.25
18.8°S	52.9°E	72	0.3
		109	0.25
14.3°S	56.1°E	85	0.3

Table 3. Mare Nubium Load Model.

Load Center		Load Geometry	
Latitude	Longitude	Radius, km	Thickness, km
22.1°S	14.7°W	147	0.2
		194	0.3
		237	0.25
23.0°S	21.0°W	120	0.1
		180	0.1
		240	0.25
14.5°S	10.5°W	128	0.25

Table 4. Oceanus Procellarum (West) Load Model.

Load Center		Load Geometry	
Latitude	Longitude	Radius, km	Thickness, km
29.0°N	68.0°W	77	0.1
		116	0.2
		154	0.2
		360	0.25
4.0°N	57.5°W	91	0.2
		136	0.2
		182	0.2
		212	0.2
		242	0.25
17.5°N	64.0°W	100	0.1
		180	0.2
		260	0.25
6.0°S	51.5°W	136	0.2
		181	0.2
		226	0.25
5.5°S	68.5°W*	65	1.0
		70	1.5
		75	1.1

*Grimaldi load model from Solomon and Head [1980]

Table 5. Oceanus Procellarum (East) Load Model.

Load Center		Load Geometry	
Latitude	Longitude	Radius, km	Thickness, km
29.0°N	58.5°W	135	0.2
		270	0.2
17.0°N	51.5°W	87	0.2
		145	0.2
		261	0.2
2.5°N	44.0°W	106	0.2
		151	0.2
		212	0.2
		363	0.2
7.0°S	38.0°W	90	0.2
		120	0.2
		151	0.2
		181	0.2
		211	0.2

Table 6. Circular Mare Load Models, from Solomon and Head [1980]

Serenitatis (I): 27°N, 19°E

Radius, km	Load, 10^8 dyn/cm^2
115	0.54
140	0.43
200	0.21
295	0.22

Humorum (I): 24°S, 40°W

Radius, km	Load, 10^8 dyn/cm^2
65	0.56
100	0.28
130	0.28
170	0.14
200	0.14

Imbrium(II): 38°N, 19°W

Radius, km	Load, 10^8 dyn/cm^2
195	0.14
235	0.10
335	0.07
405	0.12
475	0.11
540	0.12
605	0.12
670	0.12

Table 6, continued.

Crisium (I): 18°N, 59°E

Radius, km	Load, 10^8 dyn/cm^2
100	0.53
125	0.42
185	0.21
220	0.24

Nectaris: 16°S, 34°E

Radius, km	Load, 10^8 dyn/cm^2
110	0.72
130	0.29
160	0.29

Note: All loads are assumed to be located at the centers of the basins as given by Wilhelms [1983].

FIGURE CAPTIONS

Figure 1. Distribution of mare deposits on the Moon. M denotes Mare; O, Oceanus; S, Sinus; P, Palus; and L, Lacus. From Head [1976].

Figure 2. Mare Fecunditatis geologic and tectonic structure, compiled from Elston [1972], Stuart-Alexander and Howard [1972], Wilhelms [1972], Hodges [1973a,b], and Olson and Wilhelms [1974]. (a) Principal mare units. (b) Major linear rilles. (c) Major mare ridges.

Figure 3. Basalt thicknesses, in m, on the eastern side of the Moon estimated by DeHon [1975b] from the heights of buried crater rims.

Figure 4. Mare basalt thicknesses in Mare Fecunditatis, in km, from Bratt et al. [1985a].

Figure 5. Load model for Mare Fecunditatis based on the basalt thicknesses of Bratt et al. [1985a]. Locations, dimensions, and magnitudes of the assumed loads are given in Table 2. The mare boundary is also indicated.

Figure 6. Load model for combination of loads for Mare Fecunditatis, Mare Nectaris and Mare Crisium. The Mare Fecunditatis load model is that shown in Figure 11. Magnitudes and dimensions of the assumed Nectaris and Crisium loads are from Solomon and Head [1980]; Nectaris and Crisium load locations are from Wilhelms [1981]. For load details see Table 6.

Figure 7. Principal horizontal stress orientations (a) and maximum stress differences (b) for the Fecunditatis-

Nectaris-Crisium combination load model detailed in Tables 2 and 6. crosses indicate directions of horizontal principal stresses; arrowheads denote deviatoric extension. Contours indicate the magnitude of the maximum stress difference (σ_1-σ_3) in kbar. The thickness of the elastic lithosphere is 50 km.

Figure 8. Maximum stress differences for the Fecunditatis-Nectaris-Crisium combination load model detailed in Tables 2 and 6. The thickness of the elastic lithosphere is 30 km. See Figure 7 for further explanation.

Figure 9. Maximum stress differences for the Fecunditatis-Nectaris-Crisium combination load model detailed in Tables 2 and 6. The thickness of the elastic lithosphere is 100 km. See Figure 7 for further explanation.

Figure 10. Principal horizontal stress orientations (a) and maximum stress differences (b) for the Fecunditatis-Nectaris-Crisium combination load model detailed in Tables 2 and 6. The thickness of the elastic lithosphere is 75 km. See Figure 7 for further explanation.

Figure 11. Mare Tranquillitatis. Earth-based photograph; plate C2571D8 from Kuiper et al. [1967].

Figure 12. Mare Tranquillitatis geologic and tectonic structure, compiled from Carr [1966], Morris and Wilhelms [1967], Milton [1968], Elston [1972], Scott and Pohn [1972], and Wilhelms [1972]. (a) Principal mare units. (b) Major linear rilles. (c) Major mare ridges.

Figure 13. Mare basalt thicknesses, in km, in Mare Tranquillitatis and adjacent areas estimated by Bratt et

al. [1985a] from an inversion of gravity and topography.

Figure 14. Load model for Mare Tranquillitatis, based on the basalt thicknesses of Bratt et al. [1985a] shown in Figure 5. Locations, dimensions, and magnitudes of the assumed loads are given in Table 1. The mare boundary is also indicated.

Figure 15. Principal horizontal stress orientations (a) and maximum stress differences (b) for the Mare Tranquillitatis load model of Table 1. The thickness of the elastic lithosphere is 40 km.

Figure 16. Principal horizontal stress orientations (a) and maximum stress differences (b) for Mare Tranquillitatis load model of Table 1. The thickness of the elastic lithosphere is 75 km. See Figure 7 for further explanation.

Figure 17. Mare Nubium geologic and tectonic structure, compiled from Marshall [1963], Eggleton [1965], Trask and Titley [1966], Titley [1967], Howard and Masursky [1968], Holt [1974], and Saunders and Wilhelms [1974]. (a) Principal mare units. (b) Major linear rilles. (c) Major mare ridges.

Figure 18. Basalt thicknesses, in m, on the western side of the Moon, estimated by DeHon [1979] from the rim heights of buried craters.

Figure 19. Mare basalt thicknesses, in km, in Mare Nubium and adjacent areas, from Bratt et al. [1985a].

Figure 20. Load model for Mare Nubium, based on the basalt thicknesses of Bratt et al. [1985a]. Locations, dimensions, and magnitudes of the assumed loads are given in Table 3. The mare boundary is also indicated.

Figure 21. Principal horizontal stress orientations (a) and maximum stress differences (b) for the Mare Nubium load model of Table 3. The thickness of the elastic lithosphere is 50 km. See Figure 7 for further explanation.

Figure 22. Principal horizontal stress orientations (a) and maximum stress differences (b) for the Mare Nubium load model of Table 3. The thickness of the elastic lithosphere is 75 km. See Figure 7 for further explanation.

Figure 23. Distribution of geologic units in Oceanus Procellarum and Mare Nubium; from Whitford-Stark and Head [1980].

Figure 24. Oceanus Procellarum geologic and tectonic structure, compiled from Hackman [1962], Marshall [1963], Eggleton [1965], Moore [1965], Trask and Titley [1966], Schmitt et al. [1967], Titley [1967], Scott and Eggleton [1973], Saunders and Wilhelms [1974], and Scott et al. [1977]. (a) Principal mare units. (b) Major linear rilles. (c) Major mare ridges.

Figure 25. Mare basalt thicknesses (in km) in Oceanus Procellarum, from Bratt et al. [1985a].

Figure 26. Load model for western Oceanus Procellarum, based on the basalt thicknesses of Bratt et al. [1985a] and

including the Grimaldi load model of Solomon and Head [1980]. Locations, dimensions, and magnitudes of the assumed loads are given in Table 4. The mare boundary is also indicated.

Figure 27. Principal horizontal stress orientations (a) and maximum stress differences (b) for the western Oceanus Procellarum model of Table 4. The thickness of the elastic lithosphere is 25 km. See Figure 7 for further explanation.

Figure 28. Principal horizontal stress orientations (a) and maximum stress differences (b) for the western Oceanus Procellarum model of Table 4. The thickness of the elastic lithosphere is 50 km. See Figure 7 for further explanation.

Figure 29. Load model for eastern Oceanus Procellarum, based on the basalt thicknesses of Bratt et al. [1985]. Locations, dimensions, and magnitudes of the assumed loads are given in Table 5. The mare boundary is also indicated.

Figure 30. Principal horizontal stress orientations (a) and maximum stress differences (b) for the eastern Oceanus Procellarum load model of Table 5. The thickness of the elastic lithosphere is 75 km. See Figure 7 for further explanation.

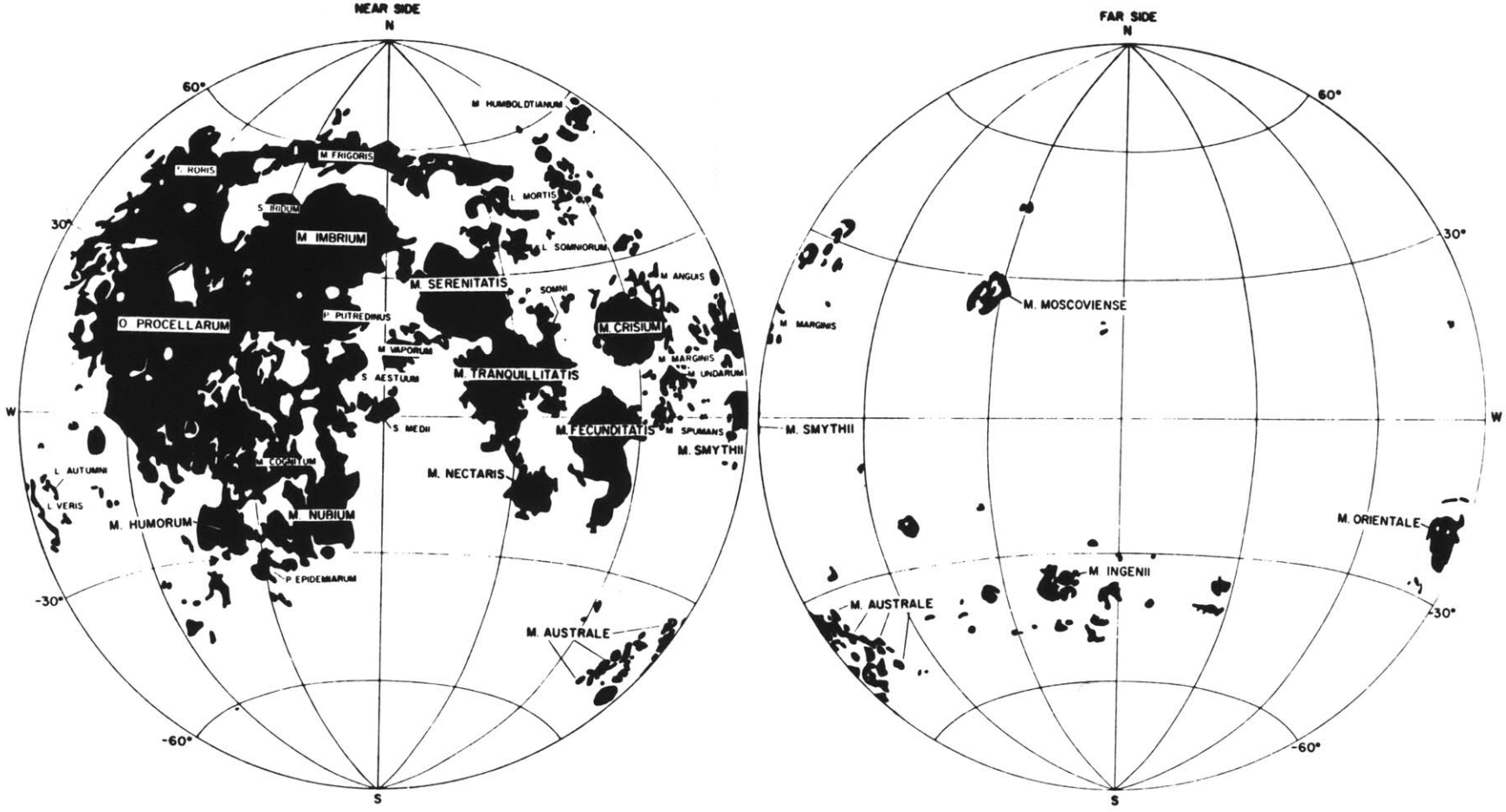
NEAR SIDE
N
60°
30°
W
-30°
-60°
S
M. HUMBOLDTIANUM
M. FRIGORIS
M. IMBRIUM
L. MORTIS
L. SOMNIORUM
M. SERENITATIS
M. ANGUS
P. SOMNI
P. PUTREDINUS
O. PROCELLARUM
M. CRISIUM
M. VAPORUM
M. MARGINIS
M. UNDARUM
S. AESTUUM
M. TRANQUILLITATIS
S. MEDII
M. FECUNDITATIS
M. SPUMANS
M. SMYTHII
M. NECTARIS
L. AUTUMNI
L. VERIS
M. HUMORUM
M. NUBIUM
P. EPIDEMIARUM
M. AUSTRALE
FAR SIDE
N
60°
30°
W
M. MOSCOVIENSE
M. MARGINIS
M. SMYTHII
M. ORIENTALE
M. INGENII
M. AUSTRALE
-30°
-60°
S

Figure 1

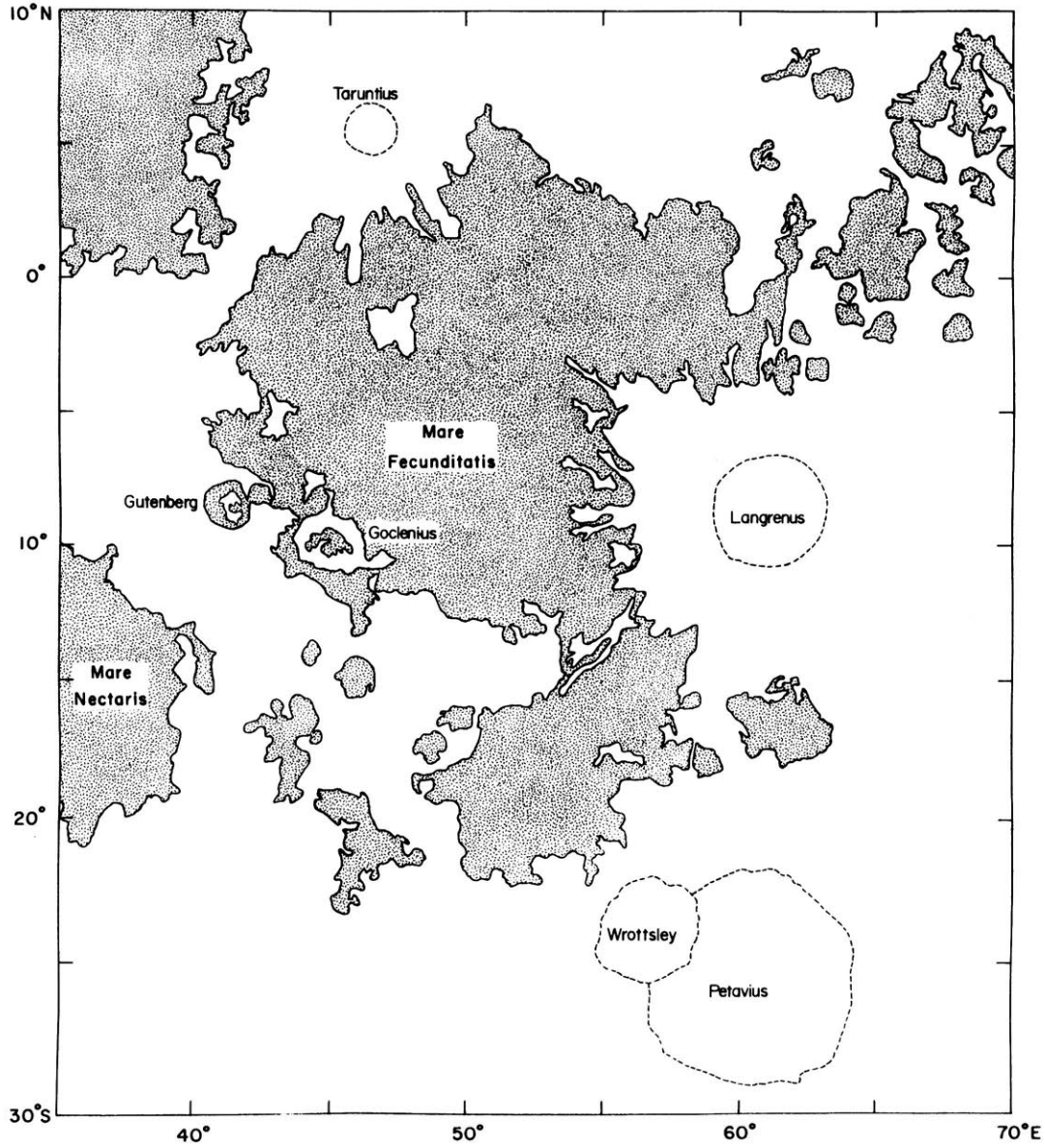
10°N
0°
10°
20°
30°S
40°
50°
60°
70°E
Taruntius
Mare
Fecunditatis
Gutenberg
Goclenius
Langrenus
Mare
Nectaris
Wrottsley
Petavius

Figure 2a

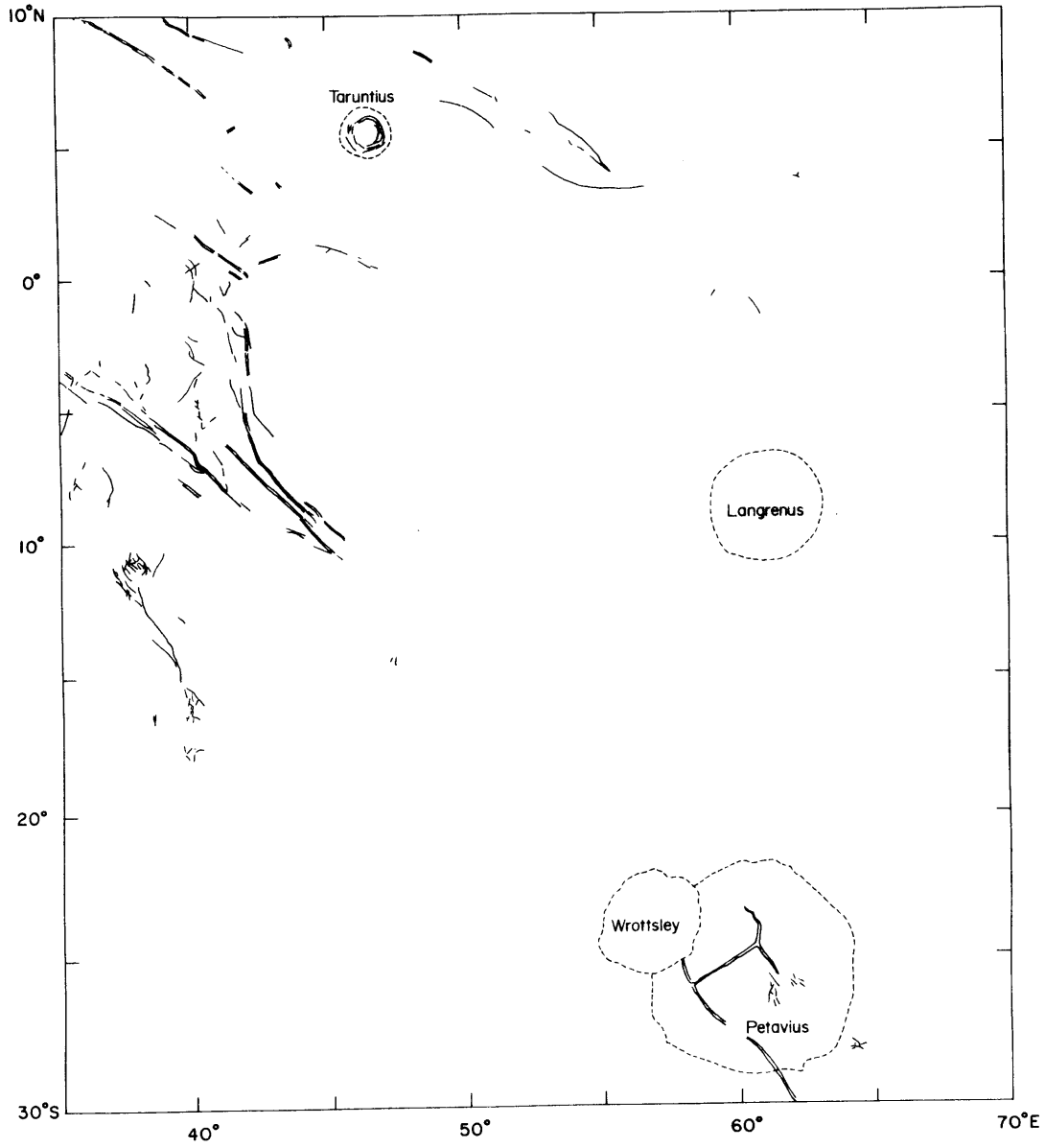
10°N
0°
10°
20°
30°S
40°
50°
60°
70°E
Taruntius
Langrenus
Wrottsley
Petavius

Figure 2b

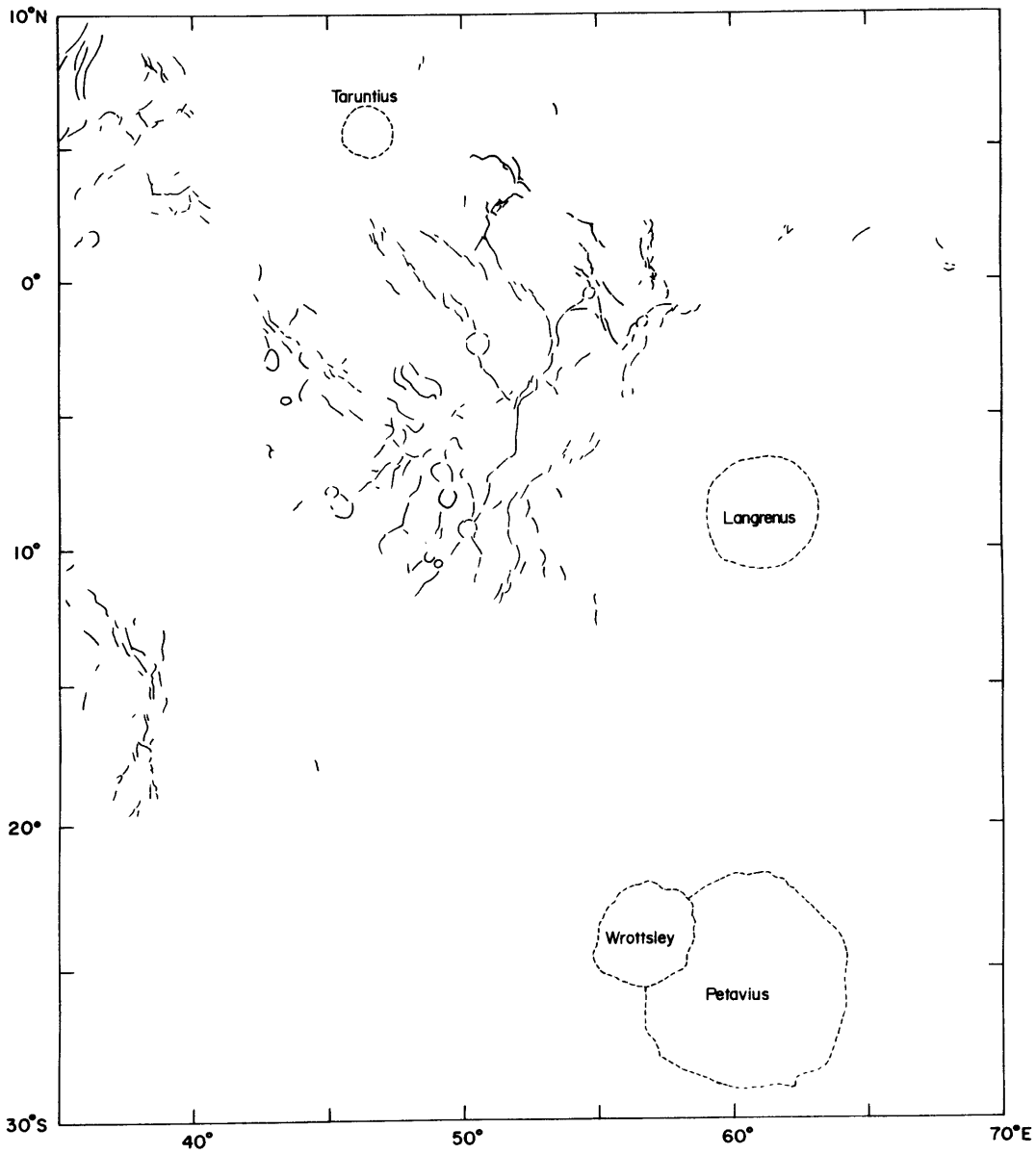
10°N
0°
10°
20°
30°S
40°
50°
60°
70°E
Taruntius
Langrenus
Wrottsley
Petavius

Figure 2c

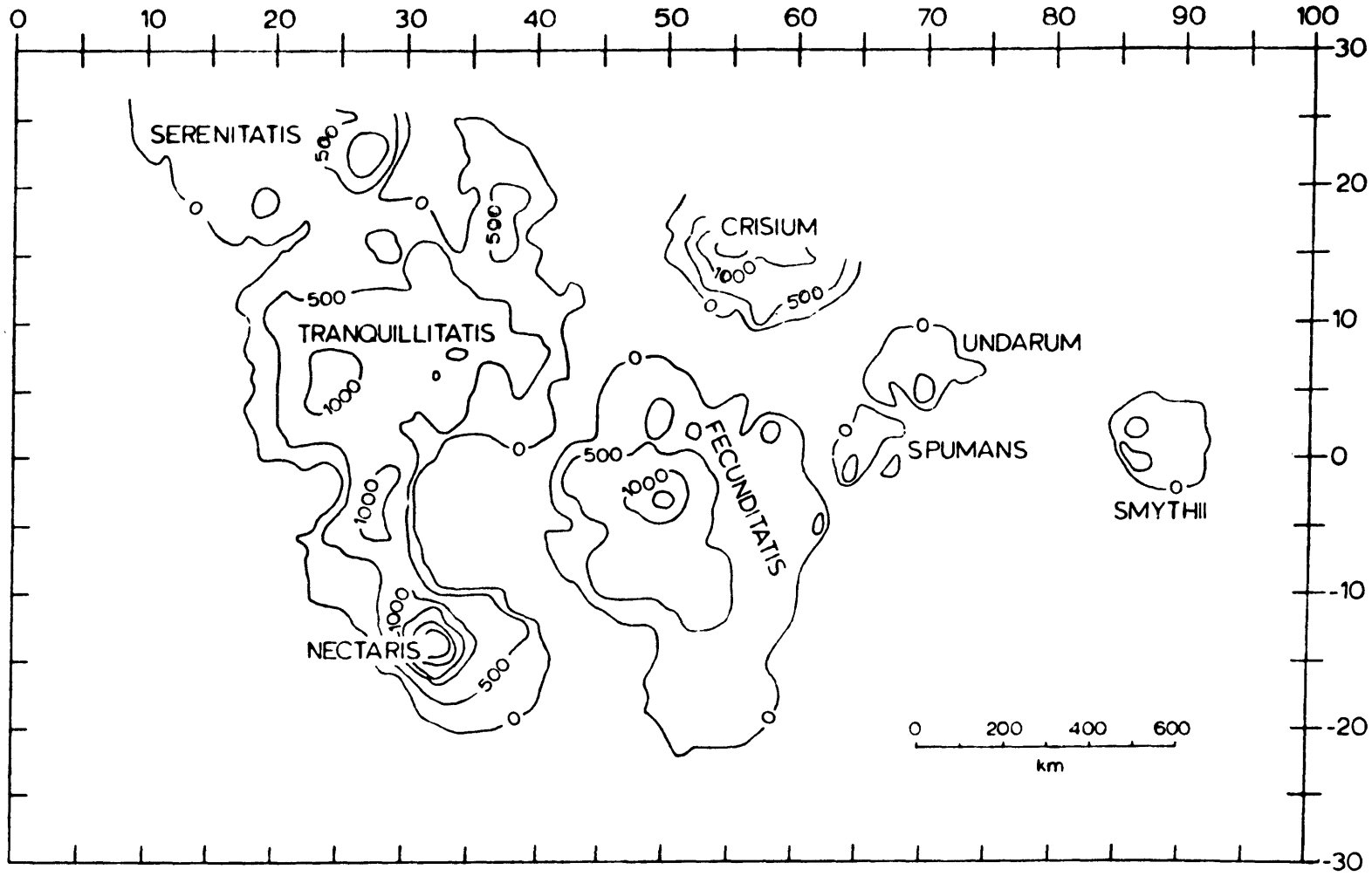
0
10
20
30
40
50
60
70
80
90
100
30
20
10
0
-10
-20
-30
SERENITATIS
500
0
500
500
TRANQUILLITATIS
0
1000
1000
0
CRISIUM
1000
500
0
UNDARUM
0
SPUMANS
0
SMYTHII
0
500
1000
FECUNDITATIS
0
1000
1000
500
NECTARIS
0
0
200
400
600
km

Figure 3

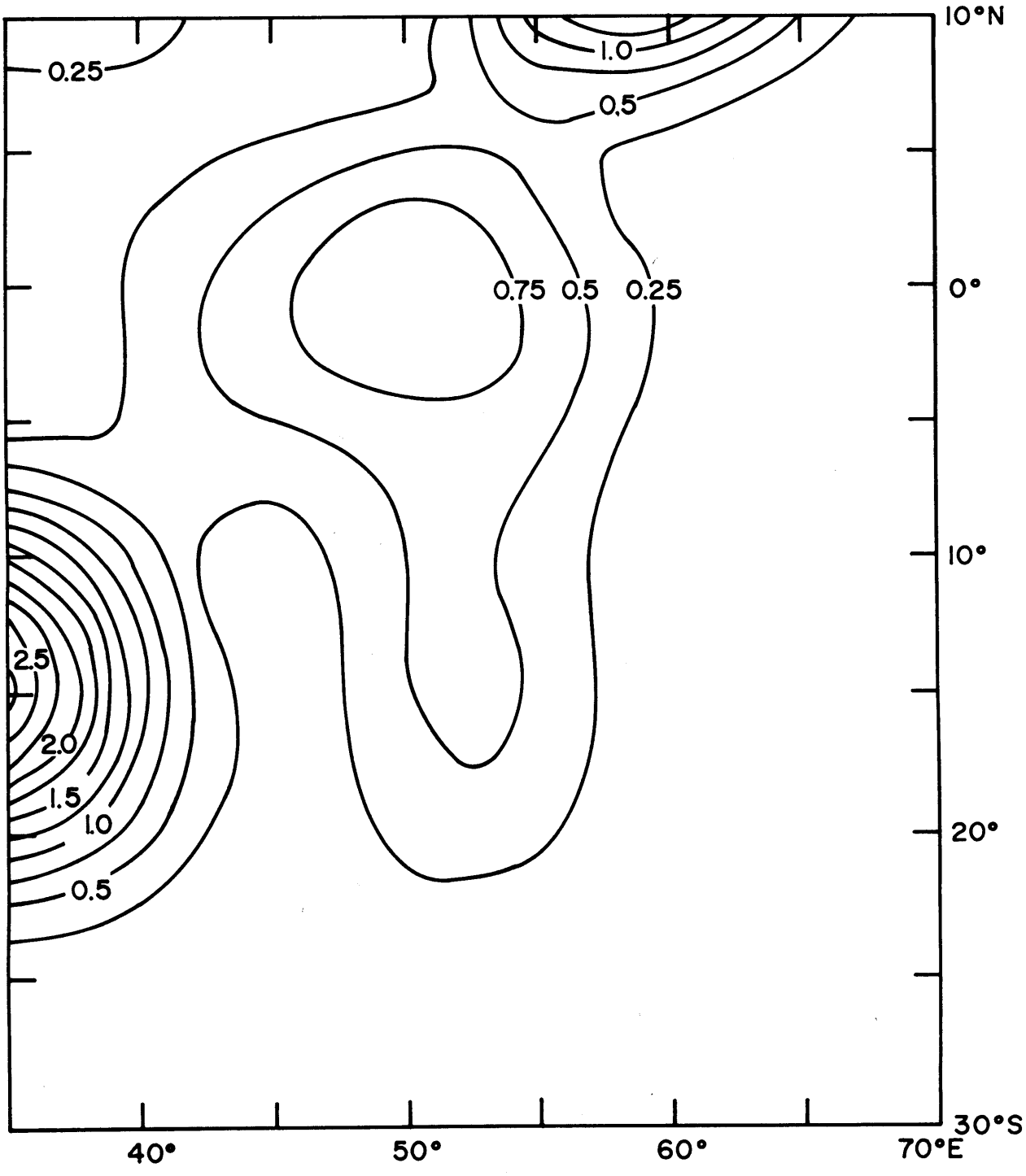

Figure 4

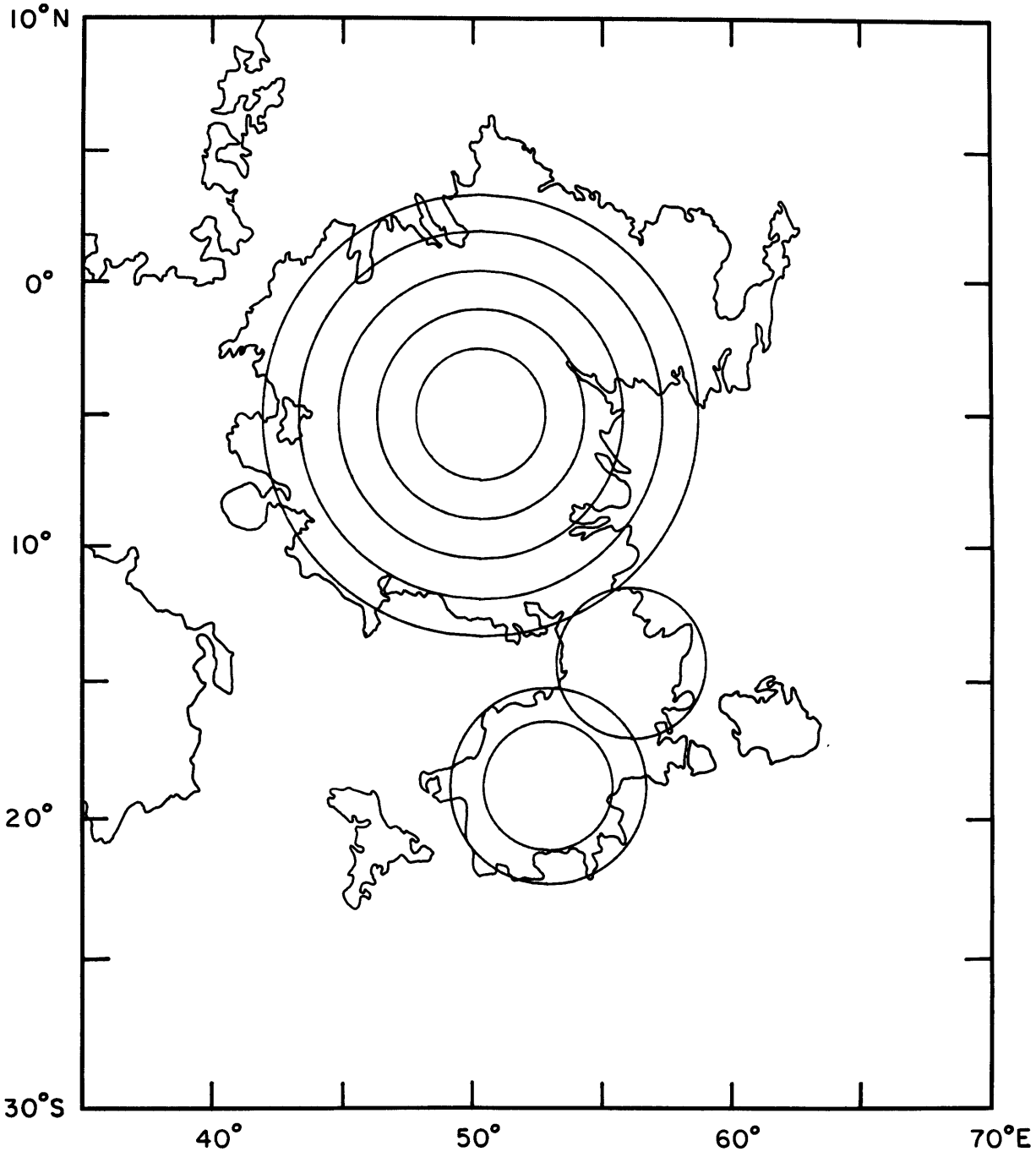

Figure 5

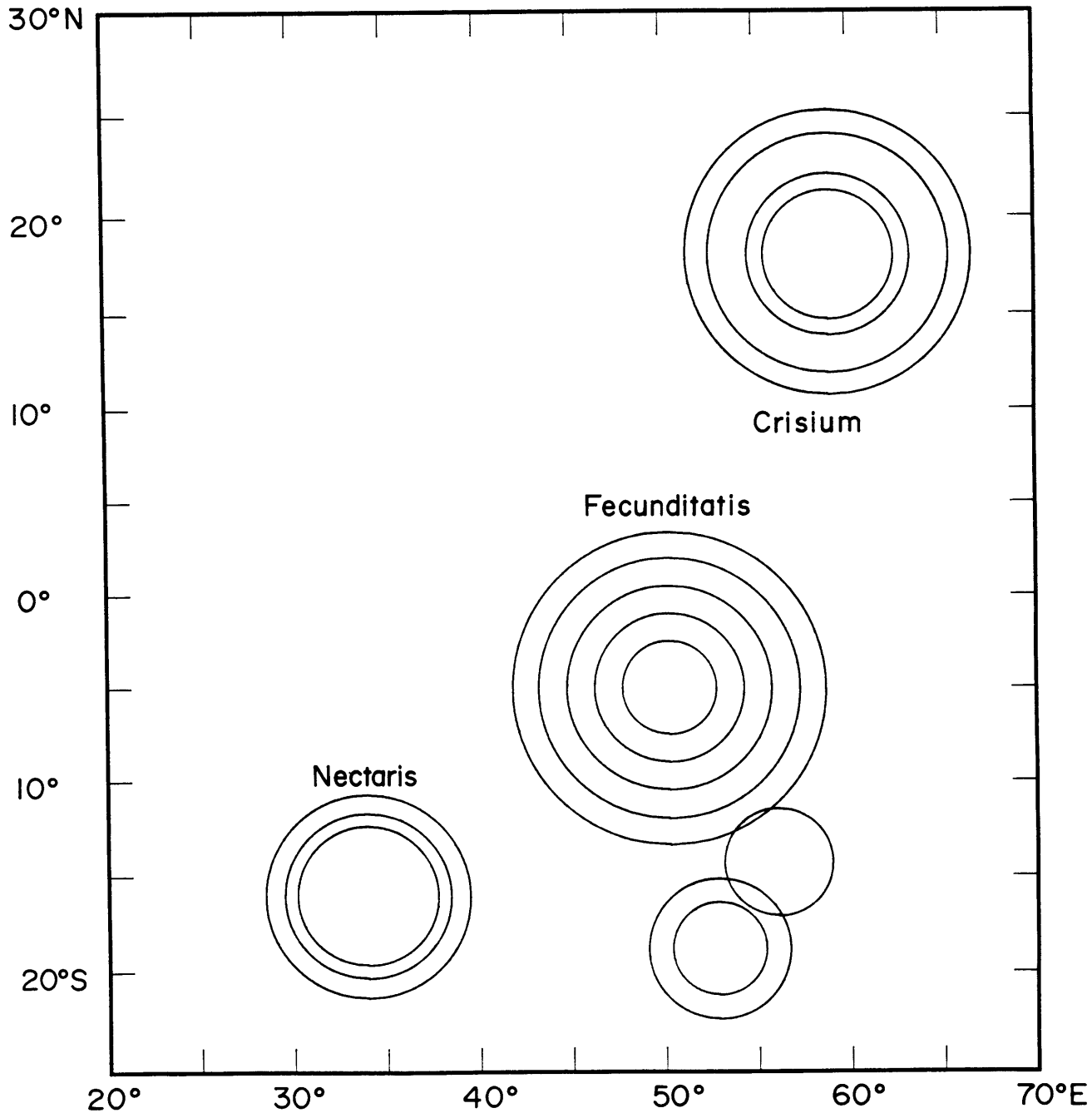
30°N
20°
10°
0°
10°
20°S
20°
30°
40°
50°
60°
70°E
Crisium
Fecunditatis
Nectaris

Figure 6

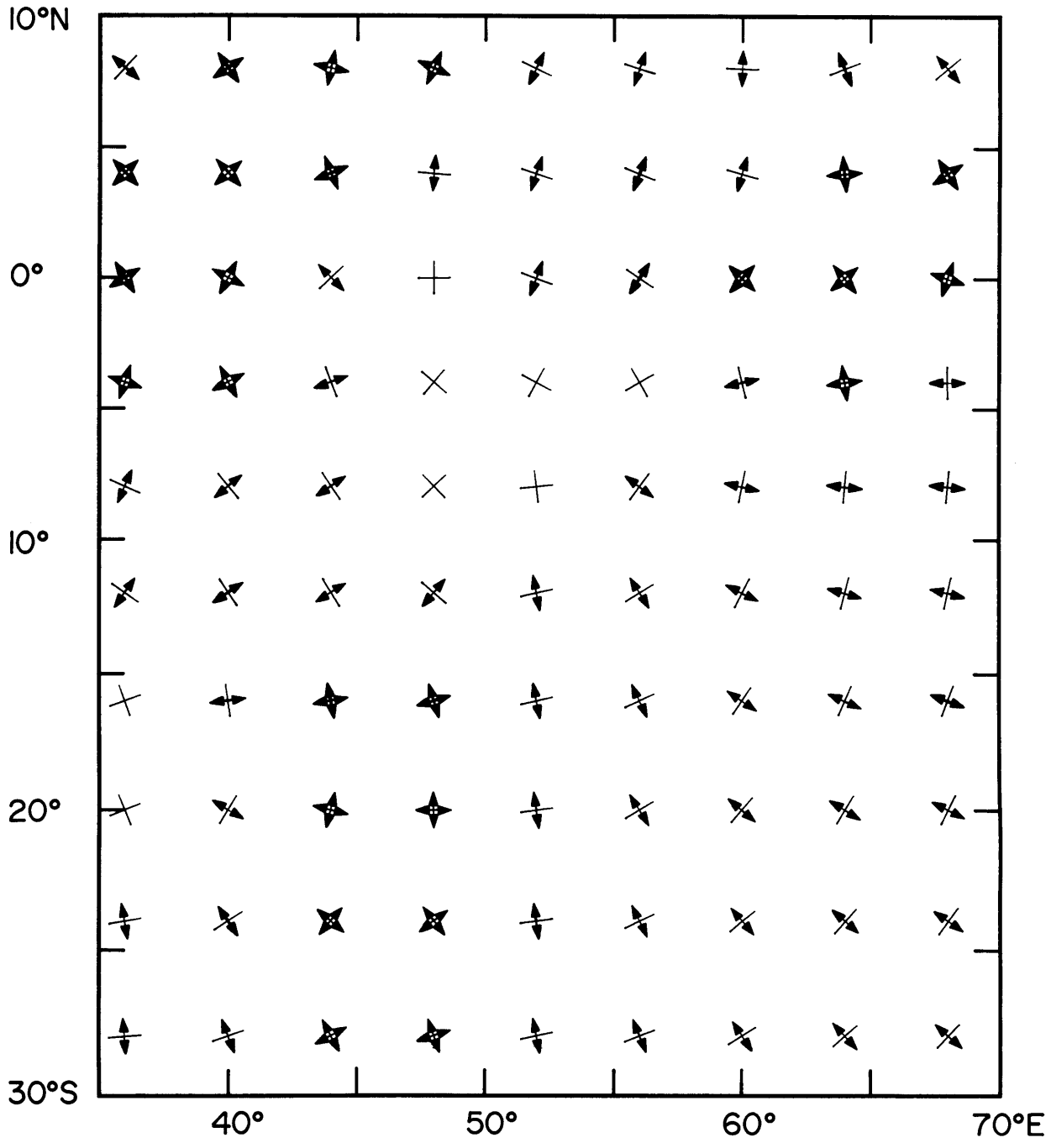

Figure 7a

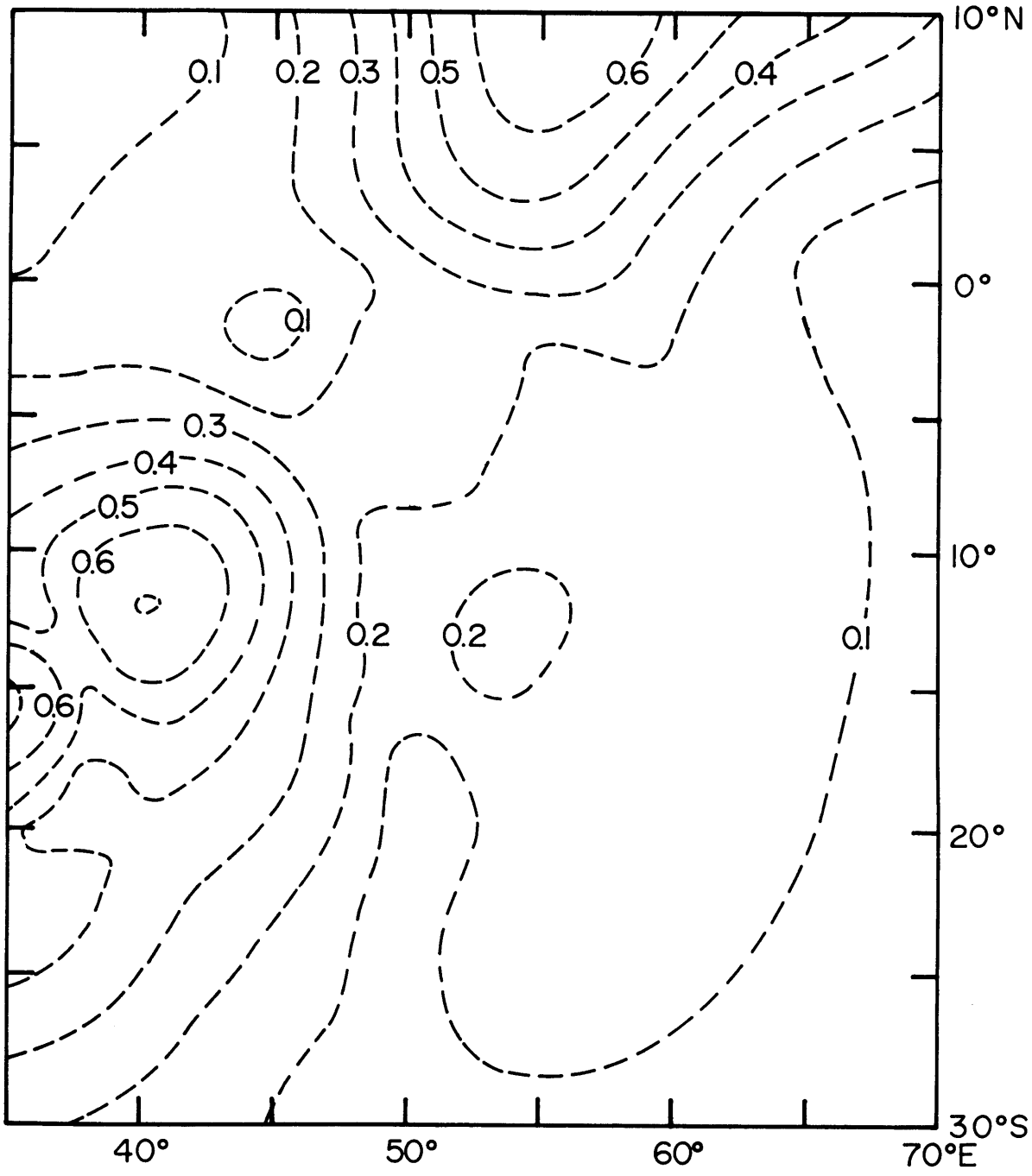
10°N
0°
10°
20°
30°S
40°
50°
60°
70°E
0.1
0.2
0.3
0.5
0.6
0.4
0.1
0.3
0.4
0.5
0.6
0.2
0.2
0.1
0.6

Figure 7b

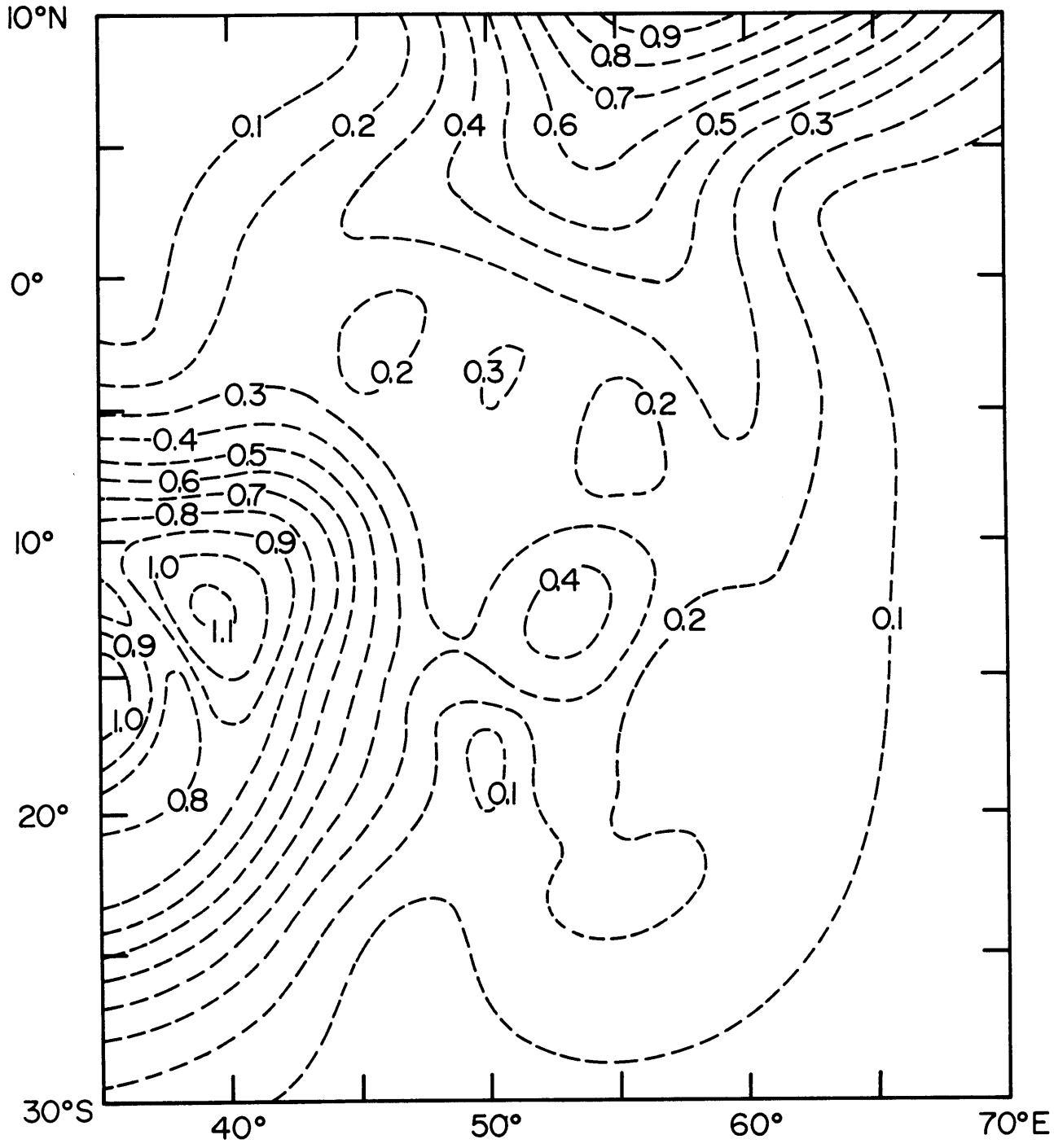
10°N
0°
10°
20°
30°S
40°
50°
60°
70°E
0.1
0.2
0.4
0.6
0.8
0.9
0.7
0.5
0.3
0.2
0.3
0.2
0.3
0.4
0.5
0.6
0.7
0.8
0.9
1.0
1.1
0.9
1.0
0.8
0.4
0.2
0.1
0.1

Figure 8

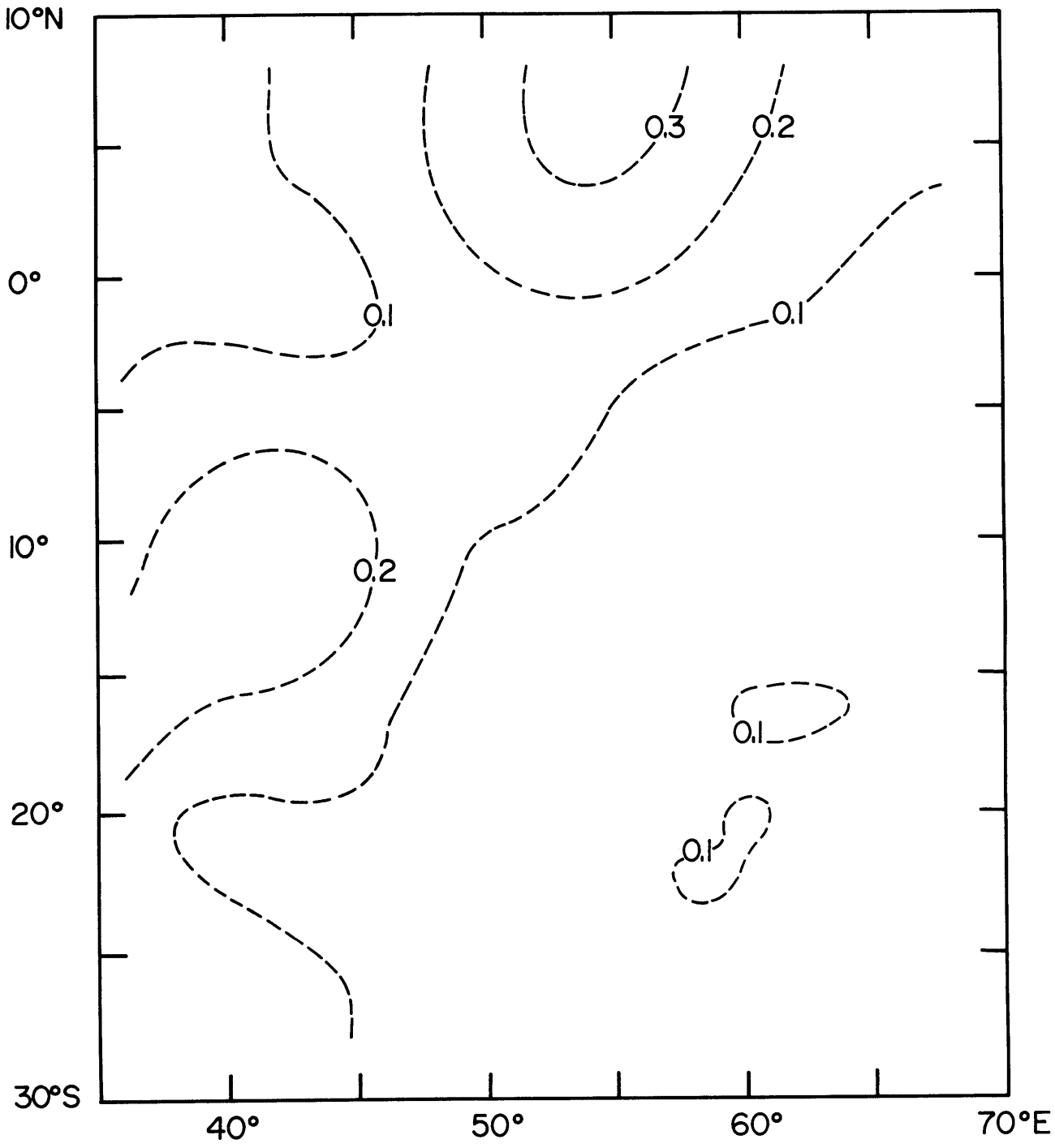

Figure 9

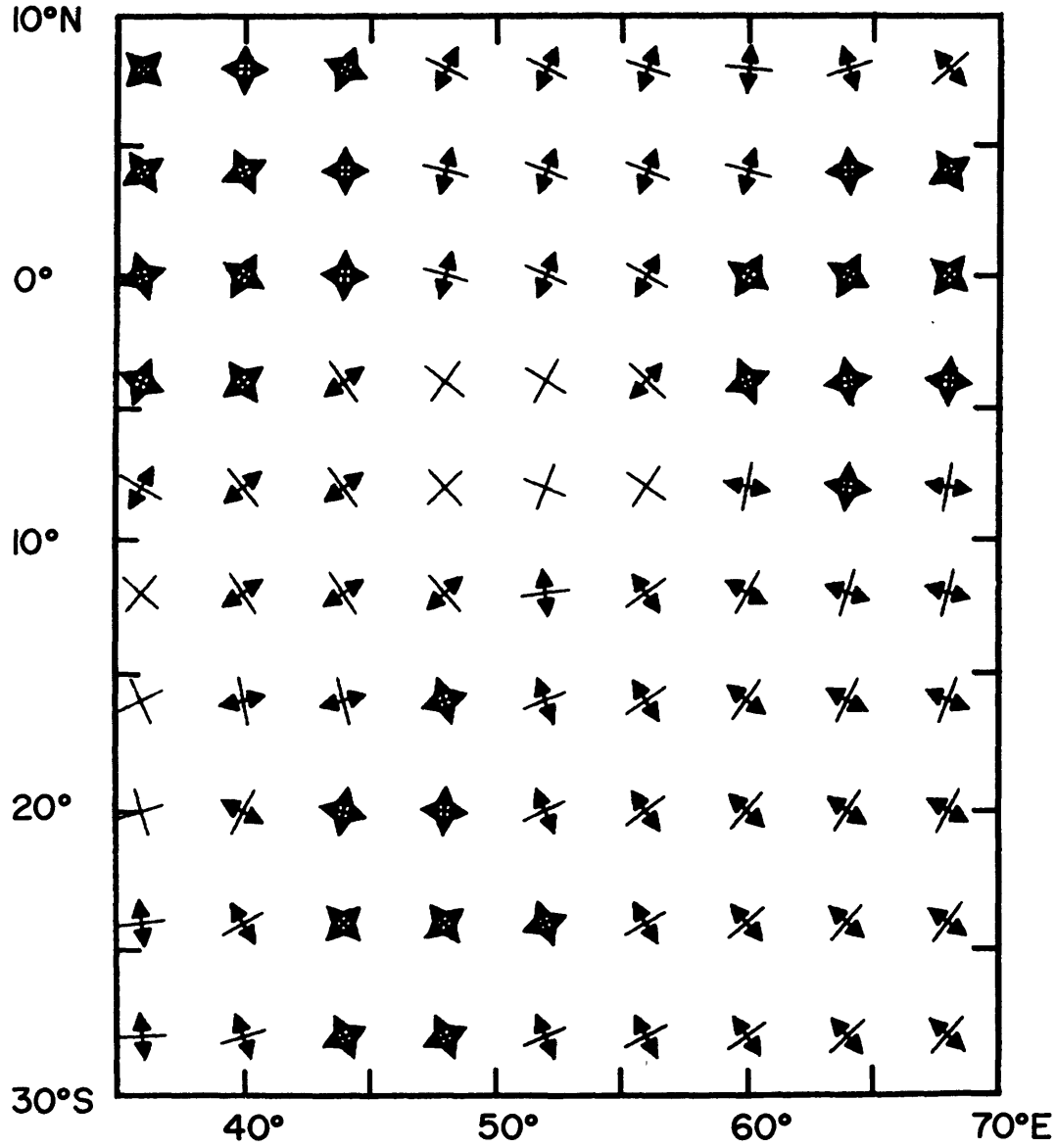

Figure 10a

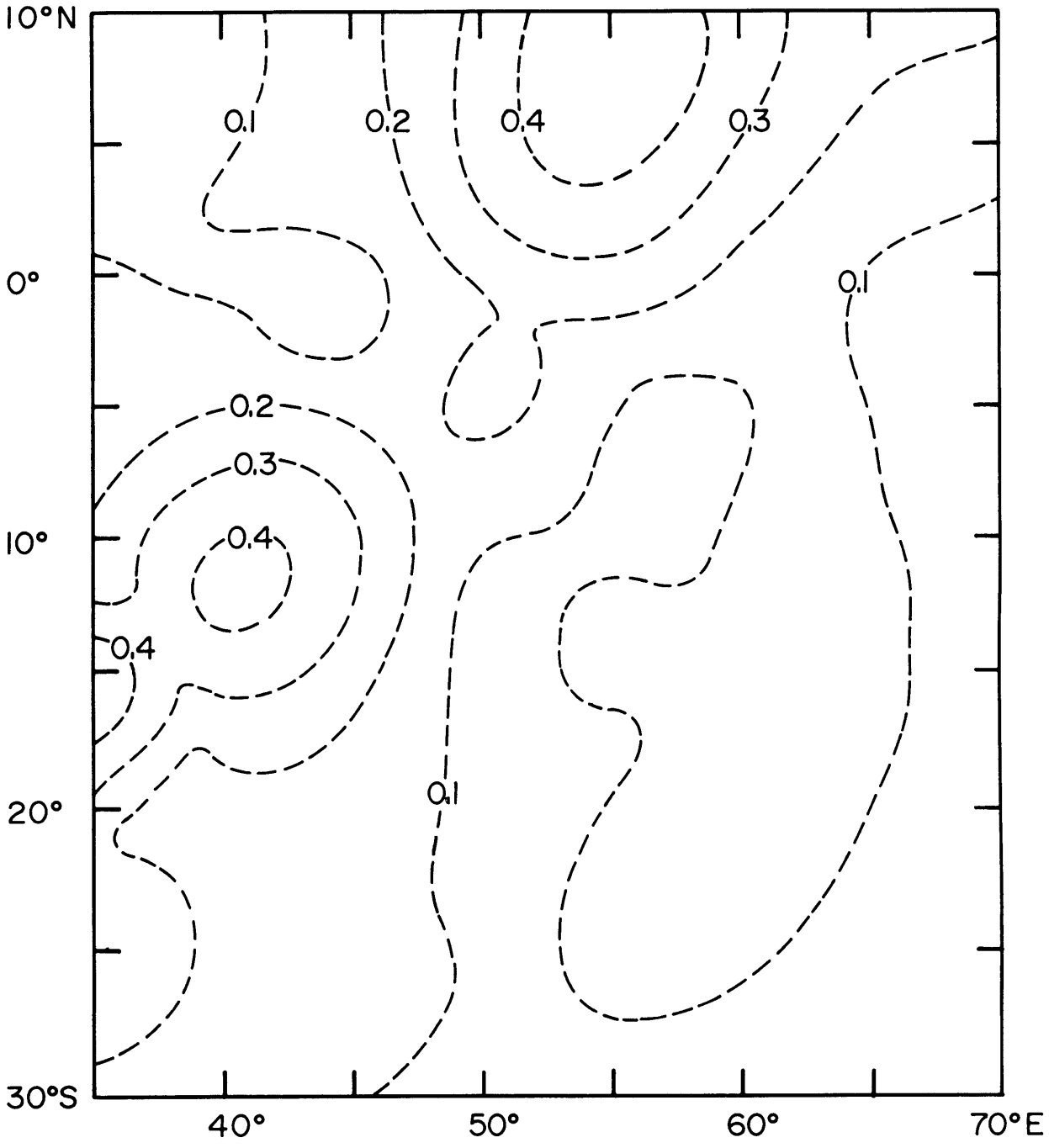

Figure 10b

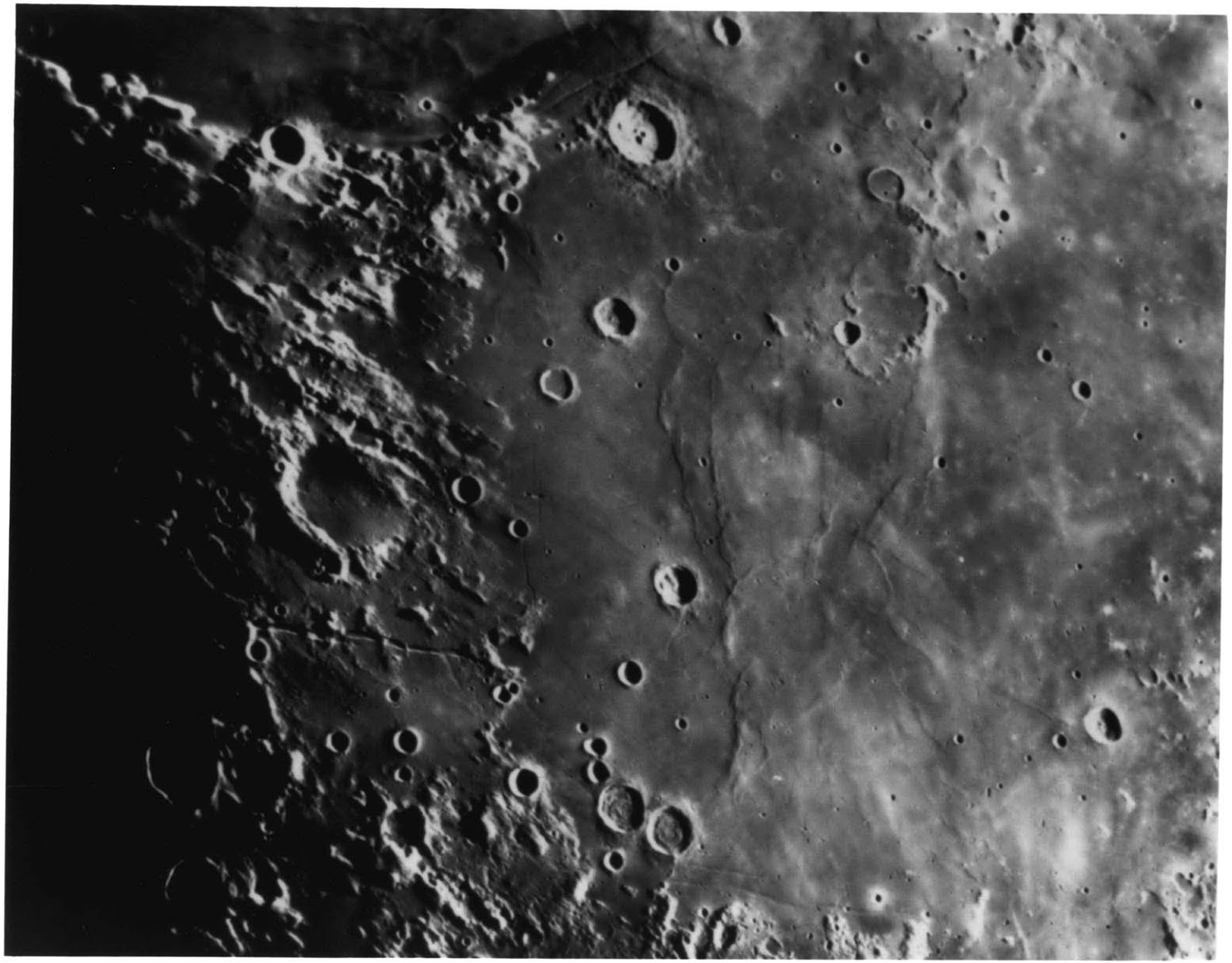

Figure 11

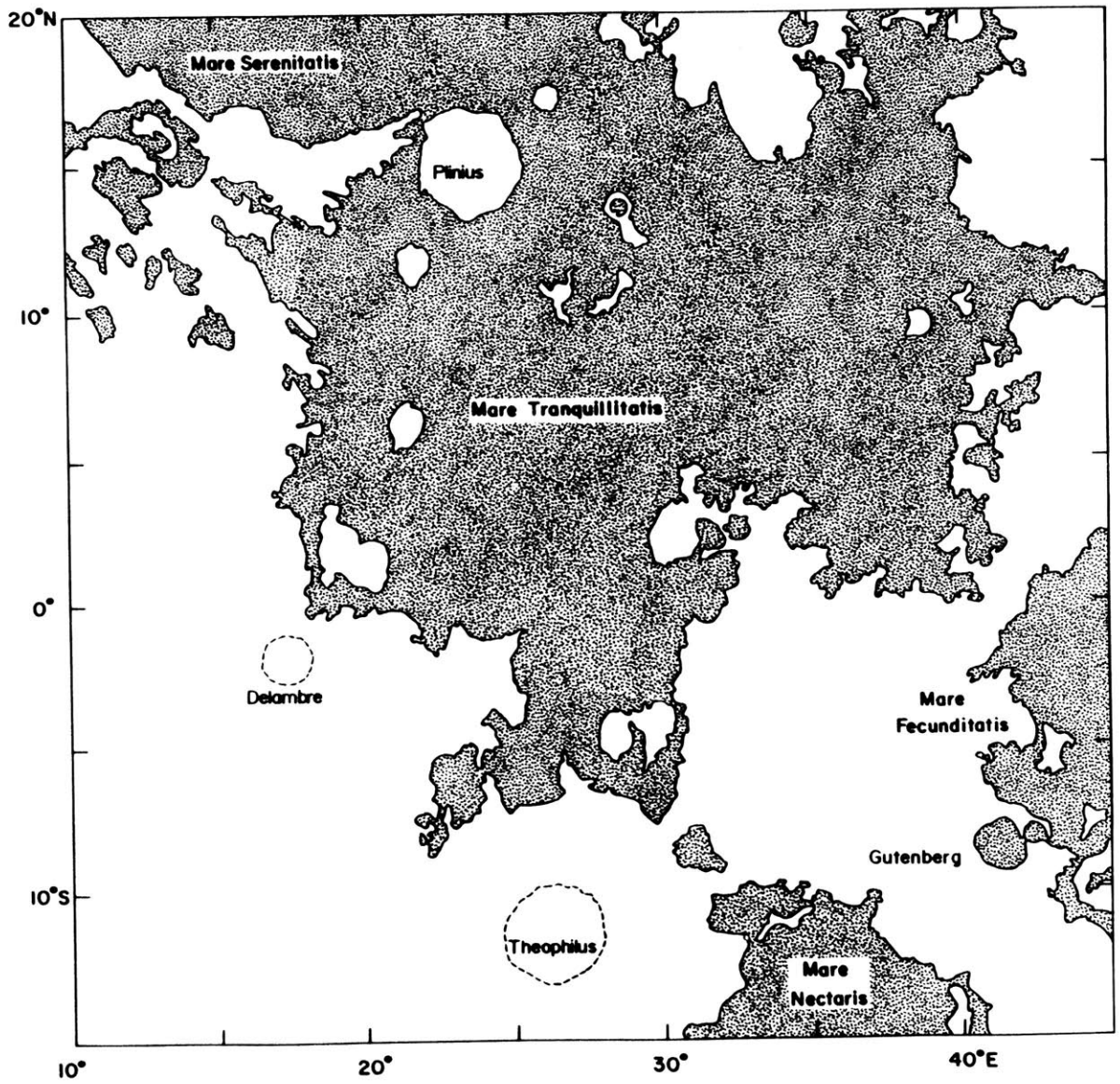
20°N
10°
0°
10°S
10°
20°
30°
40°E
Mare Serenitatis
Plinius
Mare Tranquillitatis
Delambre
Mare
Fecunditatis
Gutenberg
Theophilus
Mare
Nectaris

Figure 12a

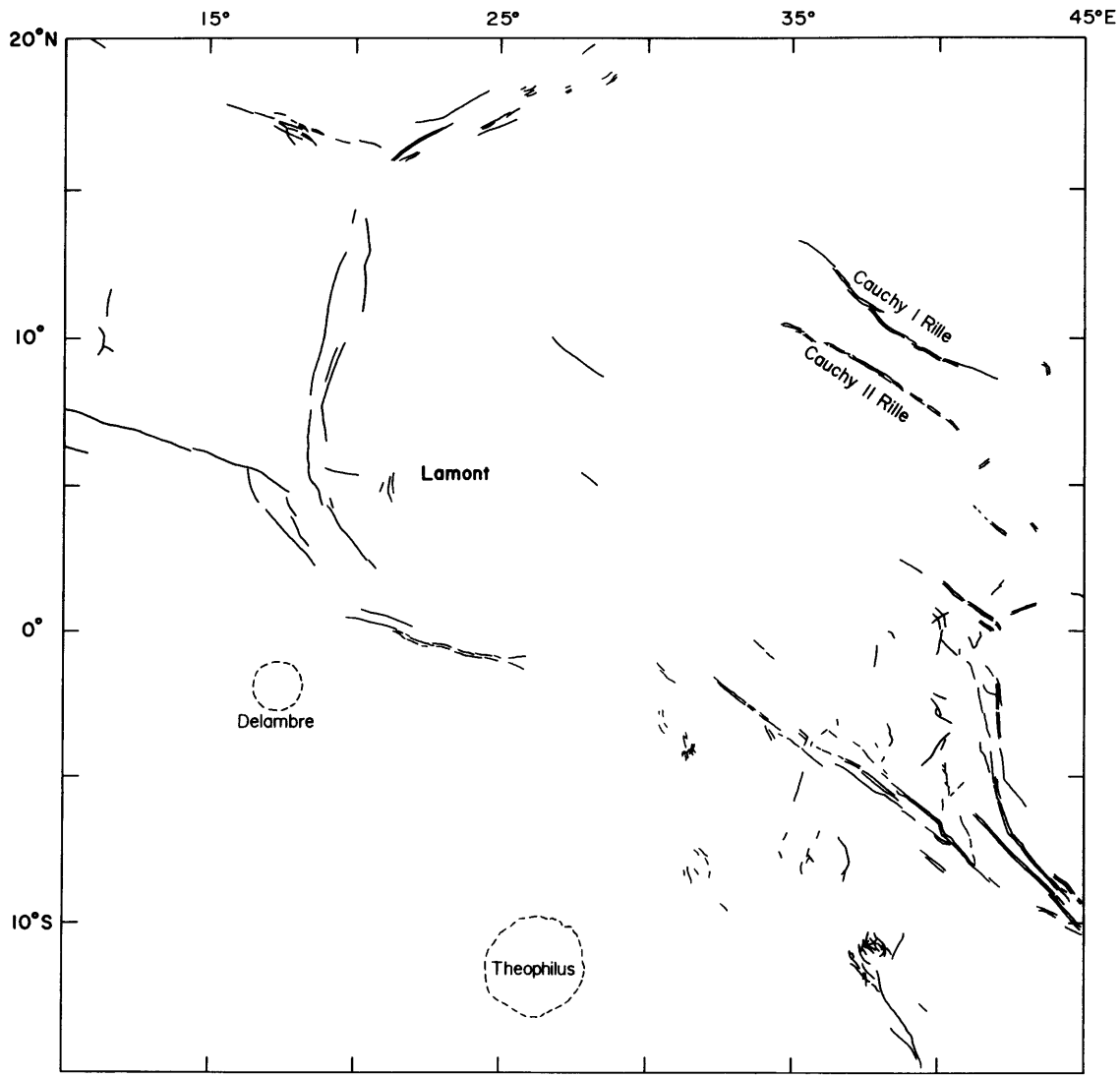
15°
25°
35°
45°E
20°N
10°
0°
10°S
Cauchy I Rille
Cauchy II Rille
Lamont
Delambre
Theophilus

Figure 12b

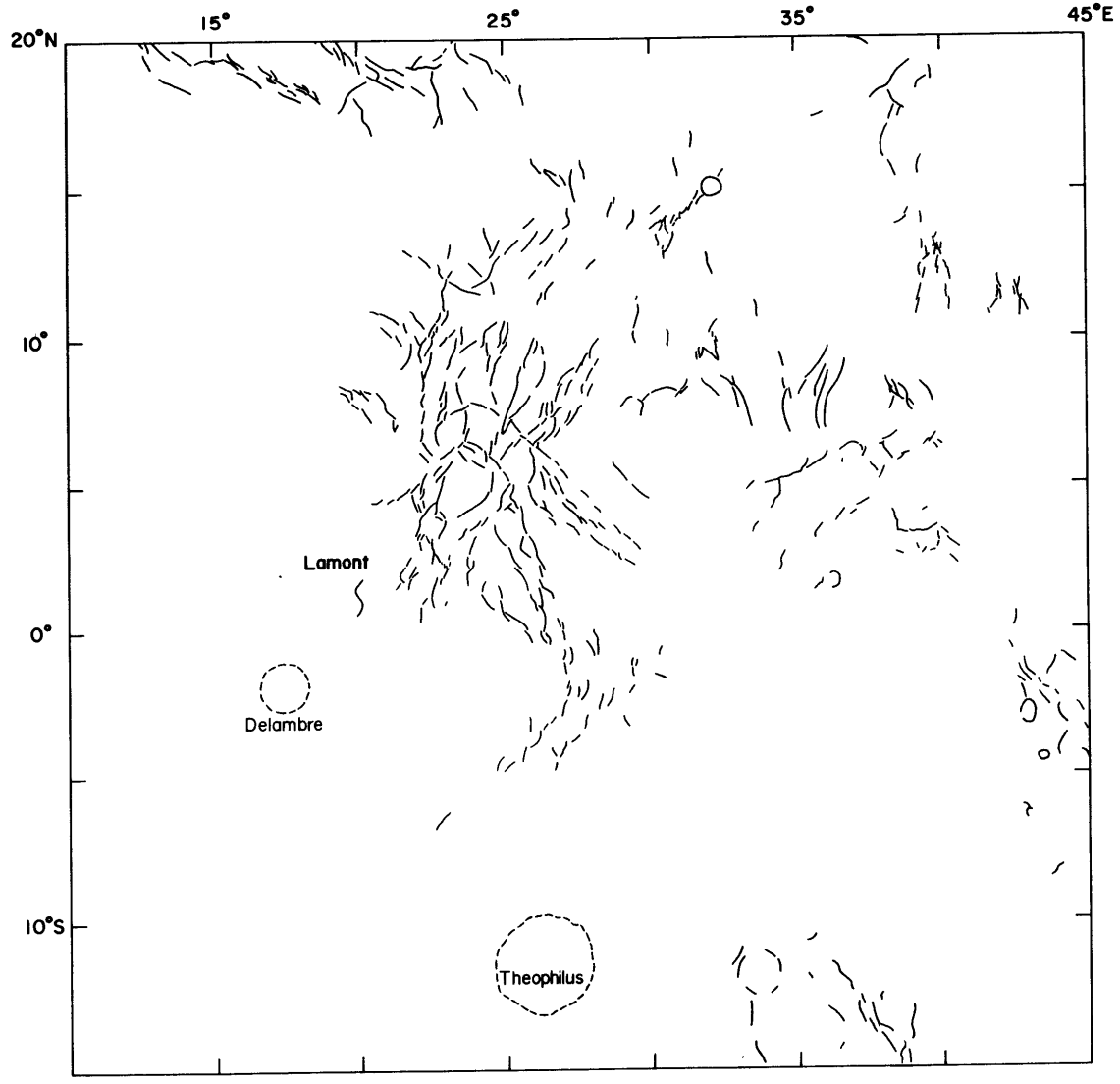

Figure 12c

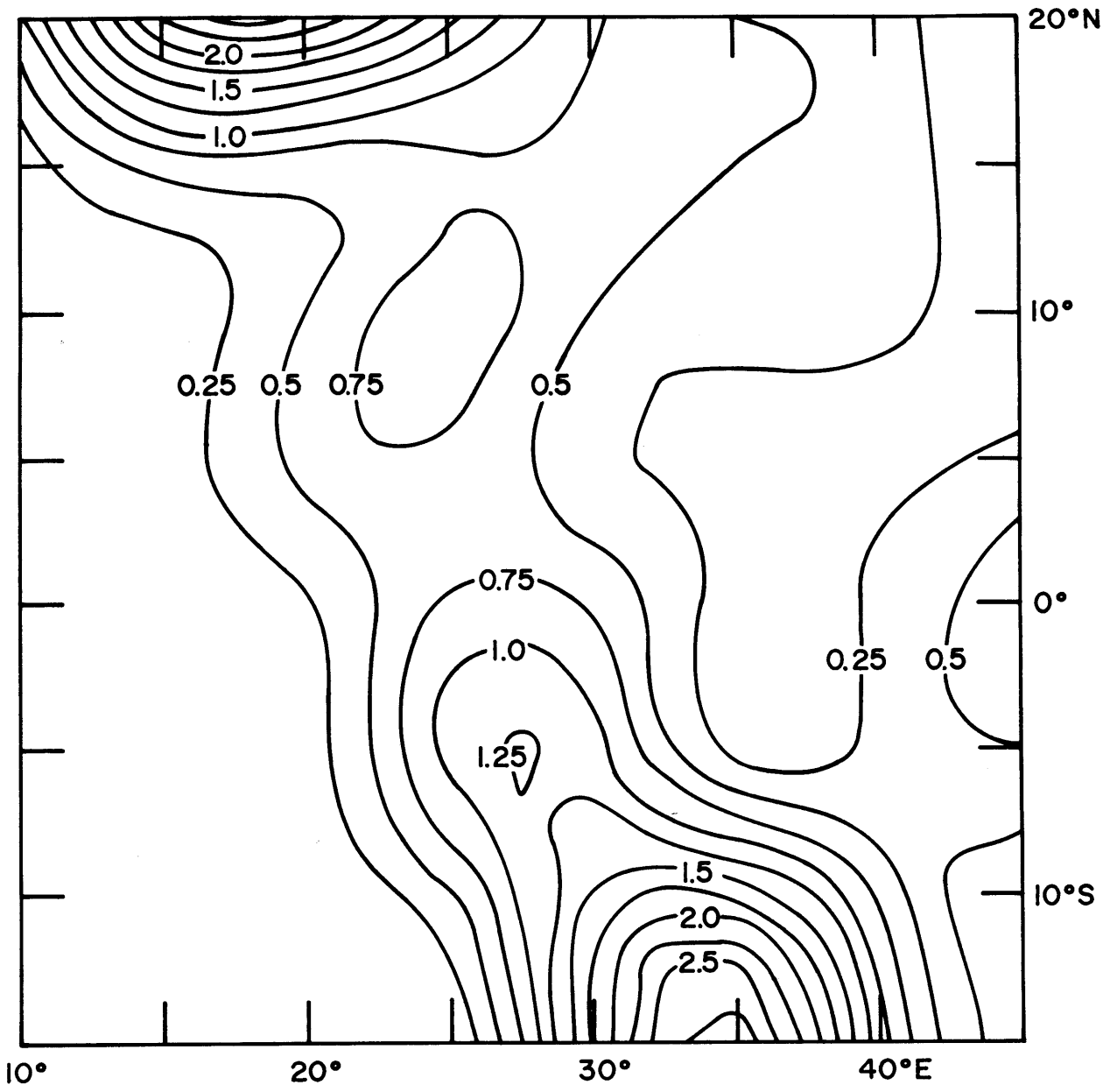
20°N
10°
0°
10°S
10°
20°
30°
40°E
2.0
1.5
1.0
0.25
0.5
0.75
0.5
0.75
1.0
0.25
0.5
1.25
1.5
2.0
2.5

Figure 13

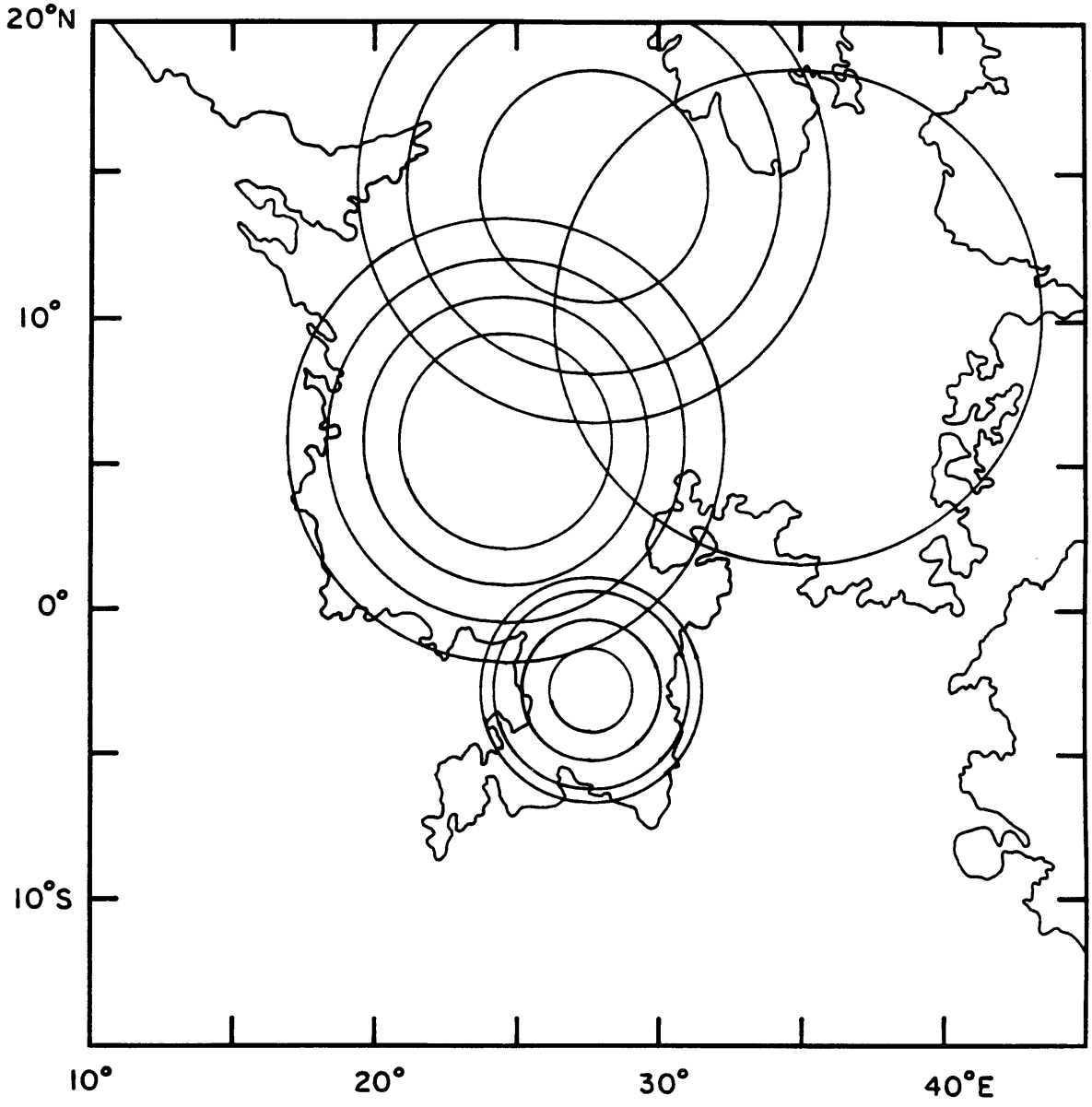

Figure 14

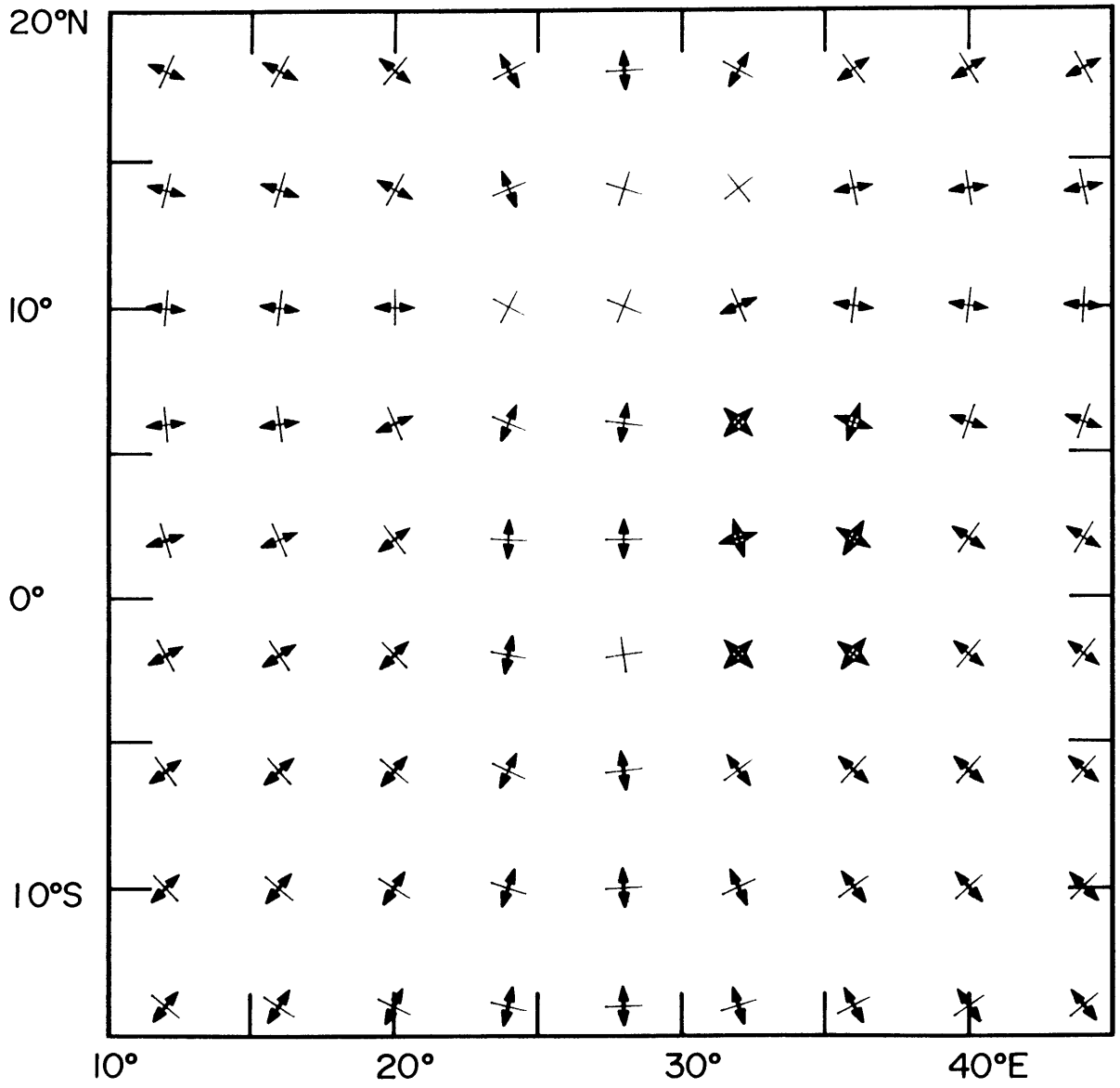

Figure 15a

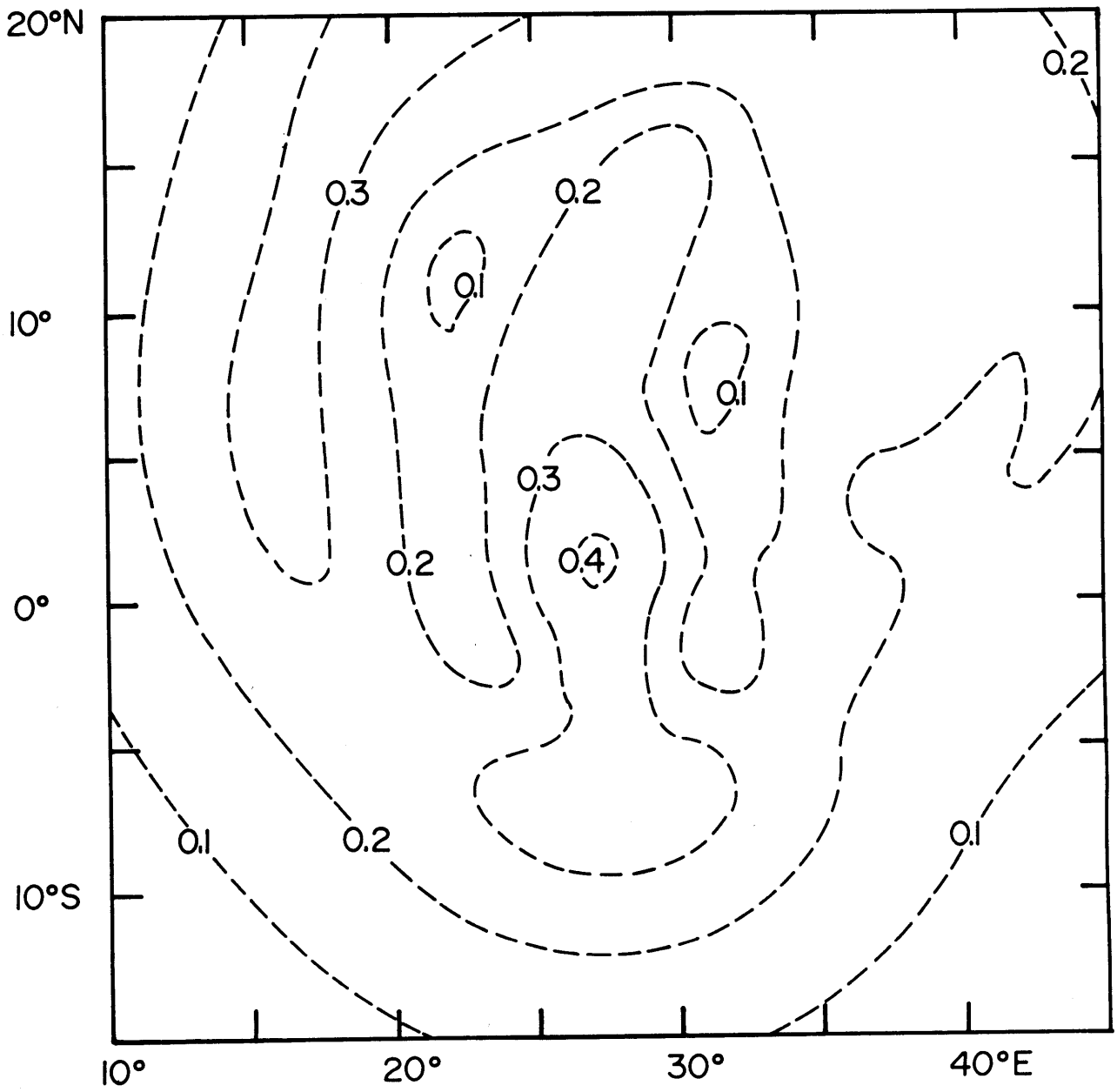

Figure 15b

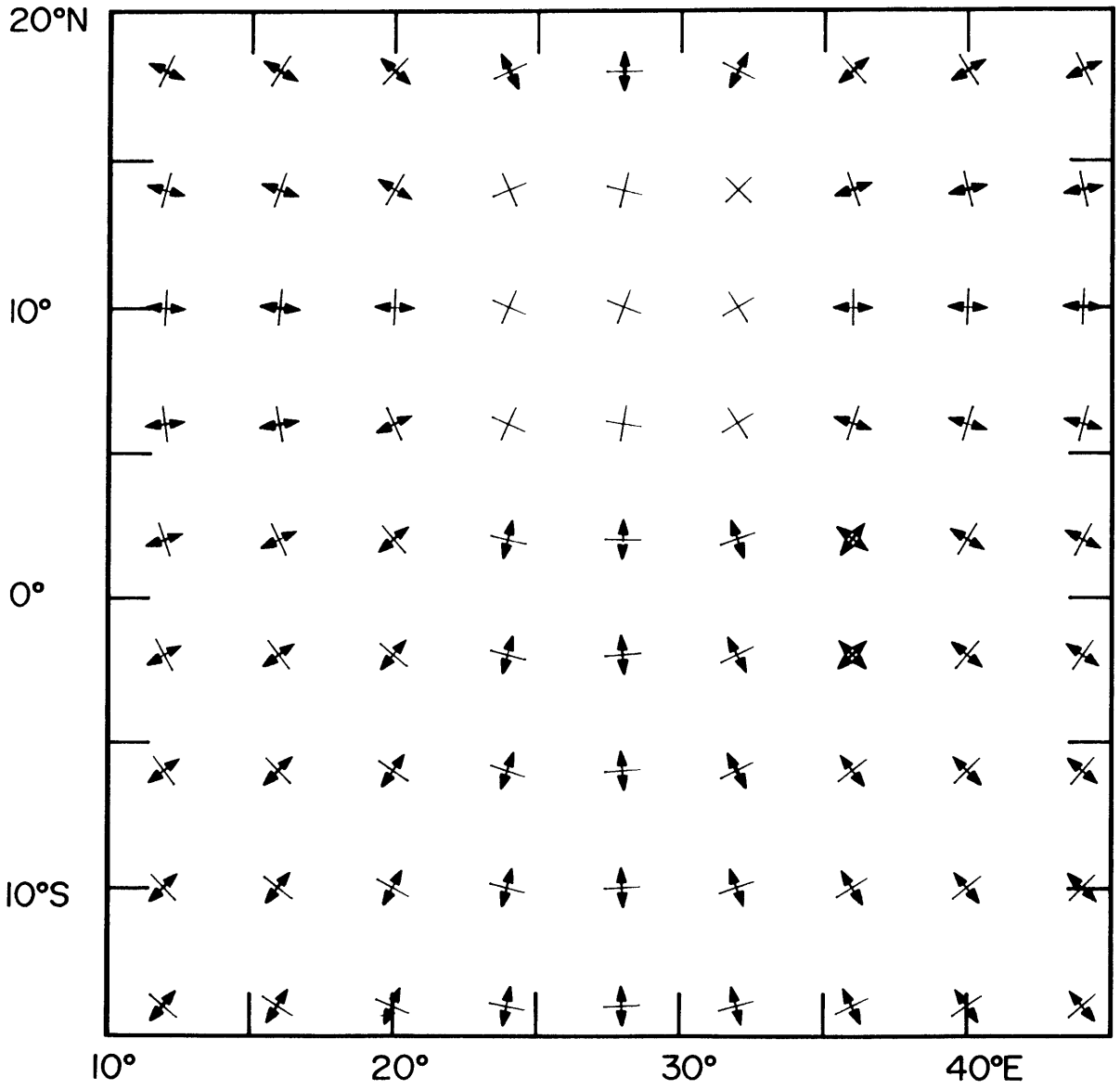

Figure 16a

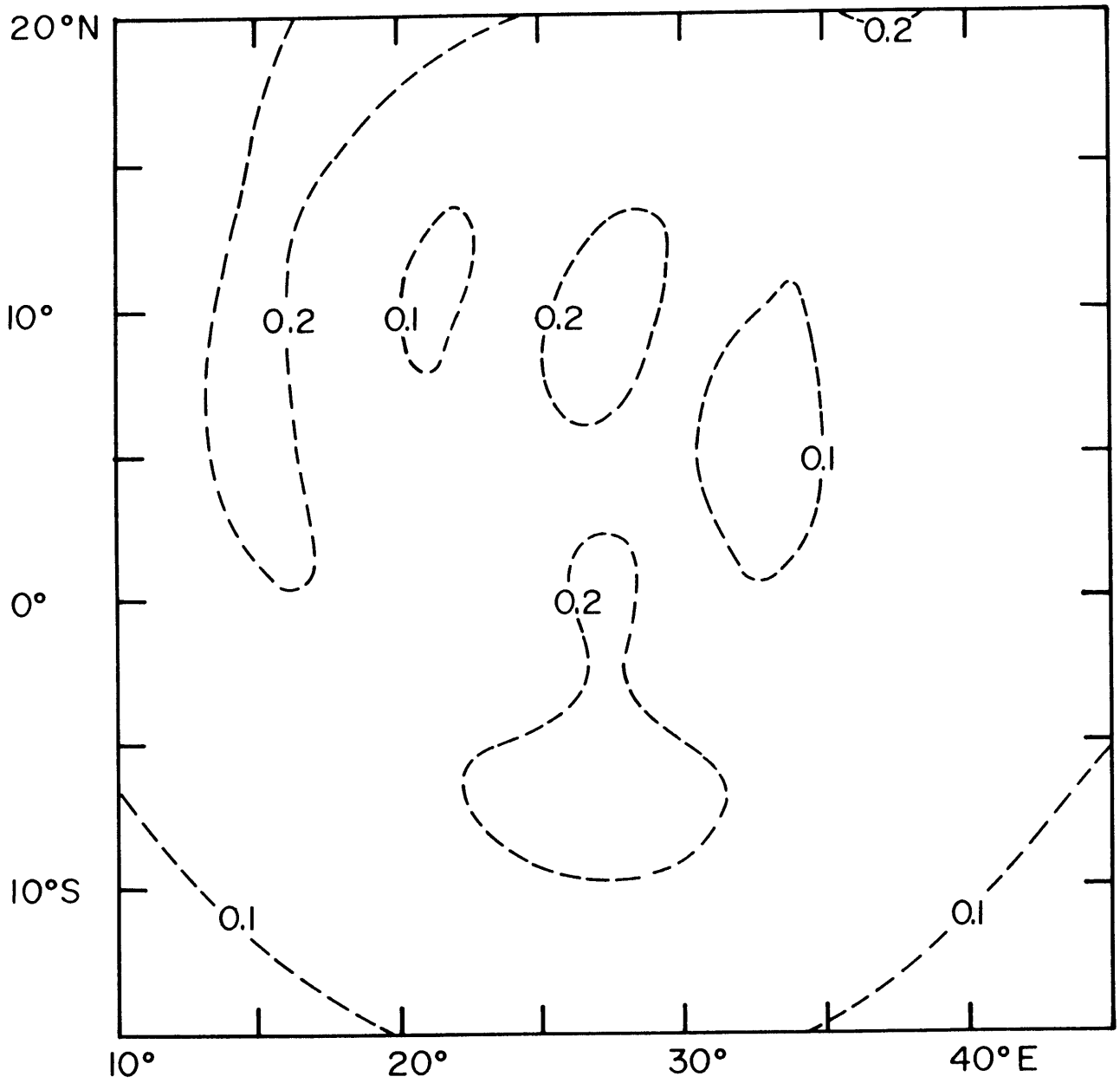

Figure 16b

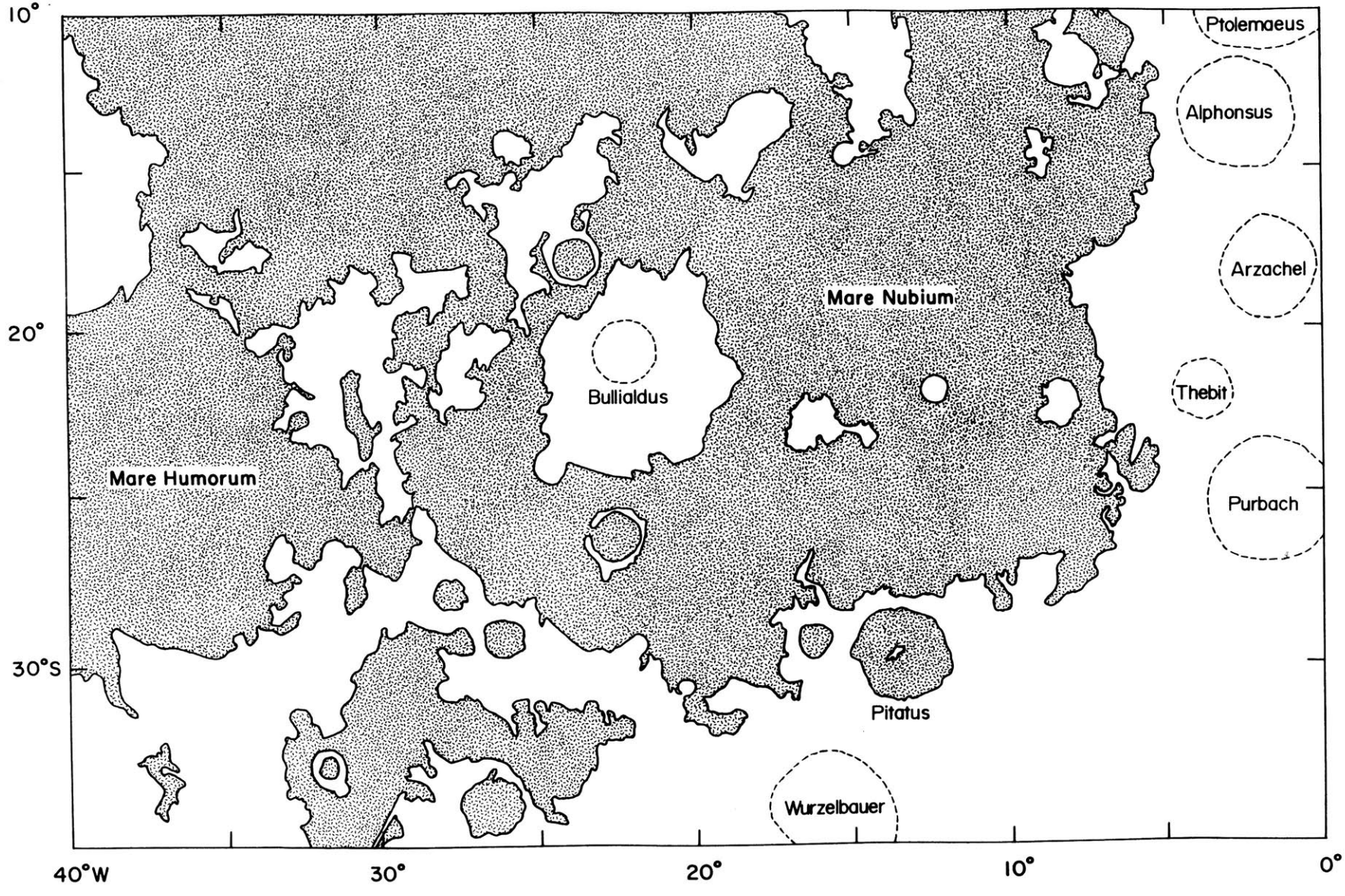
10°
20°
30°S
40°W
30°
20°
10°
0°
Ptolemaeus
Alphonsus
Arzachel
Thebit
Purbach
Mare Nubium
Bullialdus
Mare Humorum
Pitatus
Wurzelbauer

Figure 17a

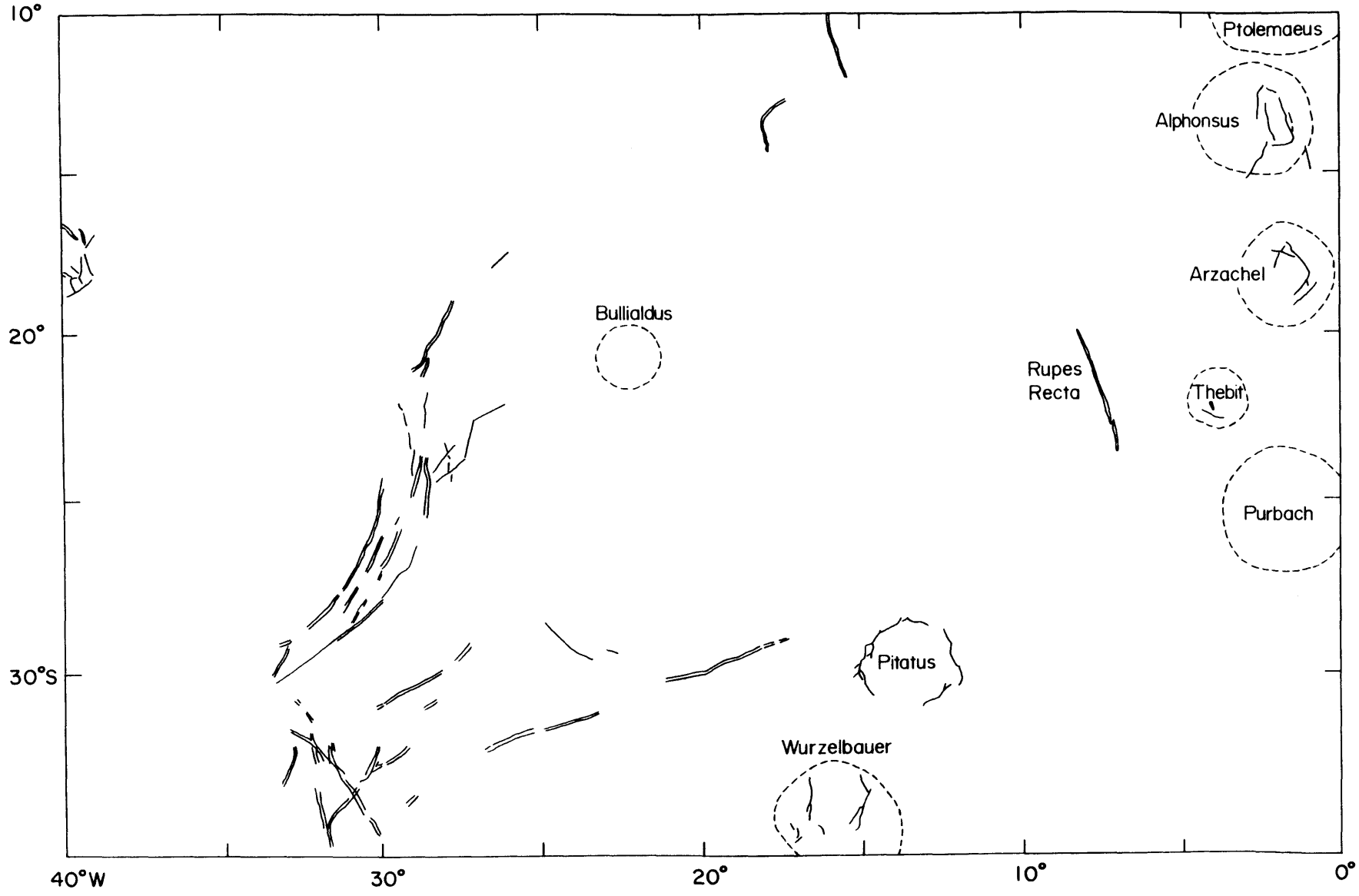
10°
20°
30°S
40°W
30°
20°
10°
0°
Ptolemaeus
Alphonsus
Arzachel
Bullialdus
Rupes
Recta
Thebit
Purbach
Pitatus
Wurzelbauer

Figure 17b

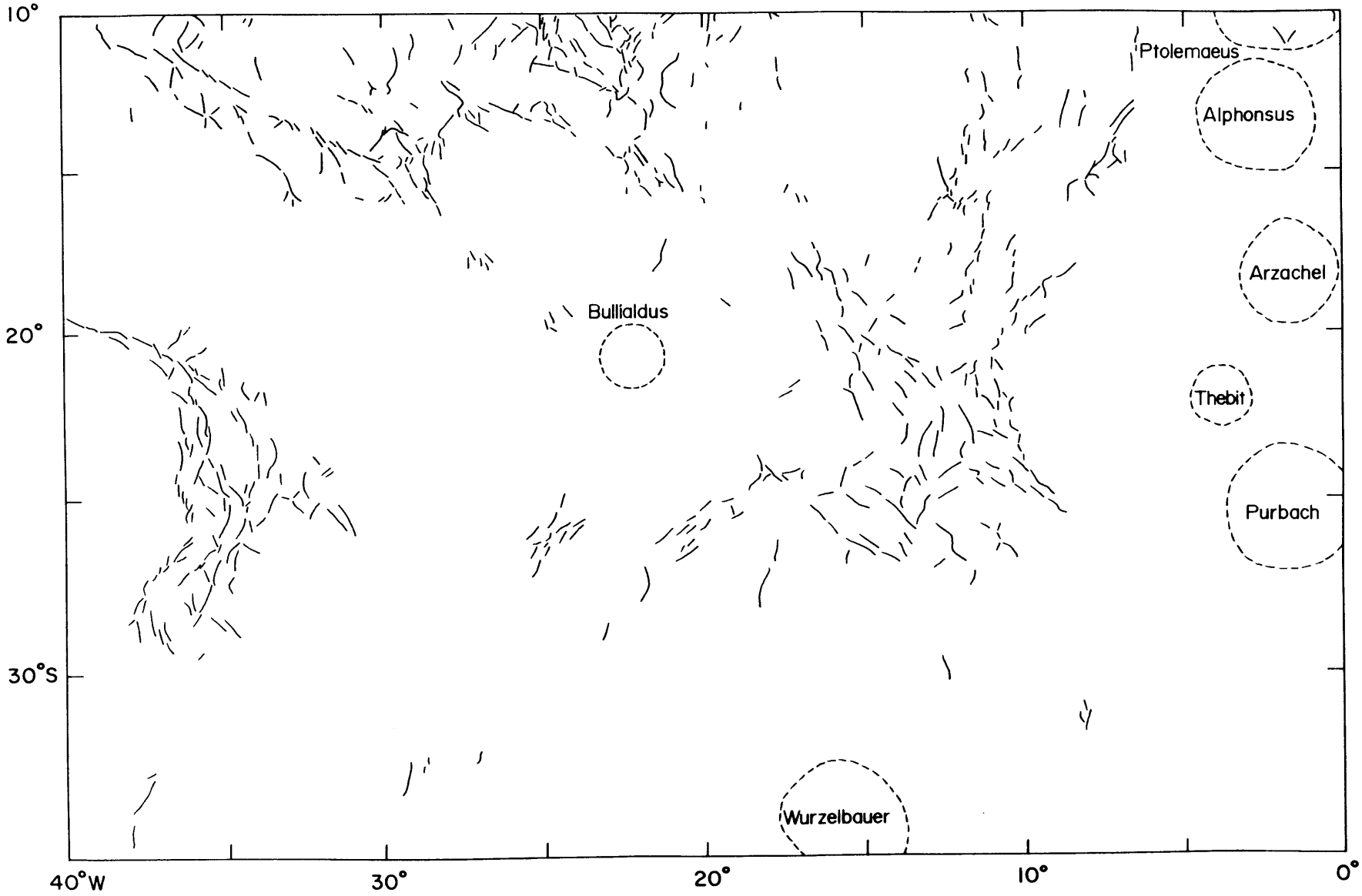
10°
20°
30°S
40°W
30°
20°
10°
0°
Ptolemaeus
Alphonsus
Arzachel
Bullialdus
Thebit
Purbach
Wurzelbauer

Figure 17c

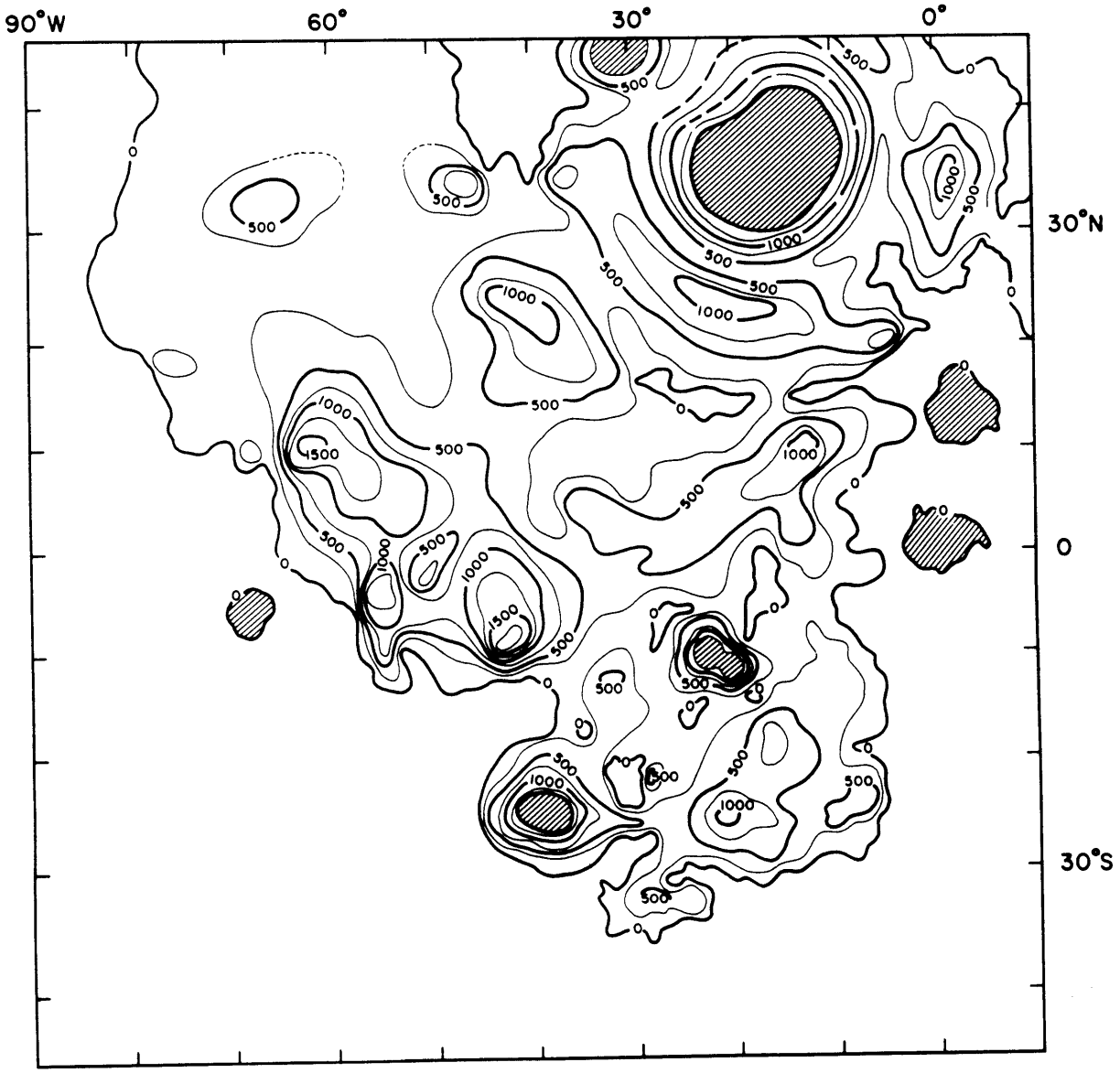

Figure 18

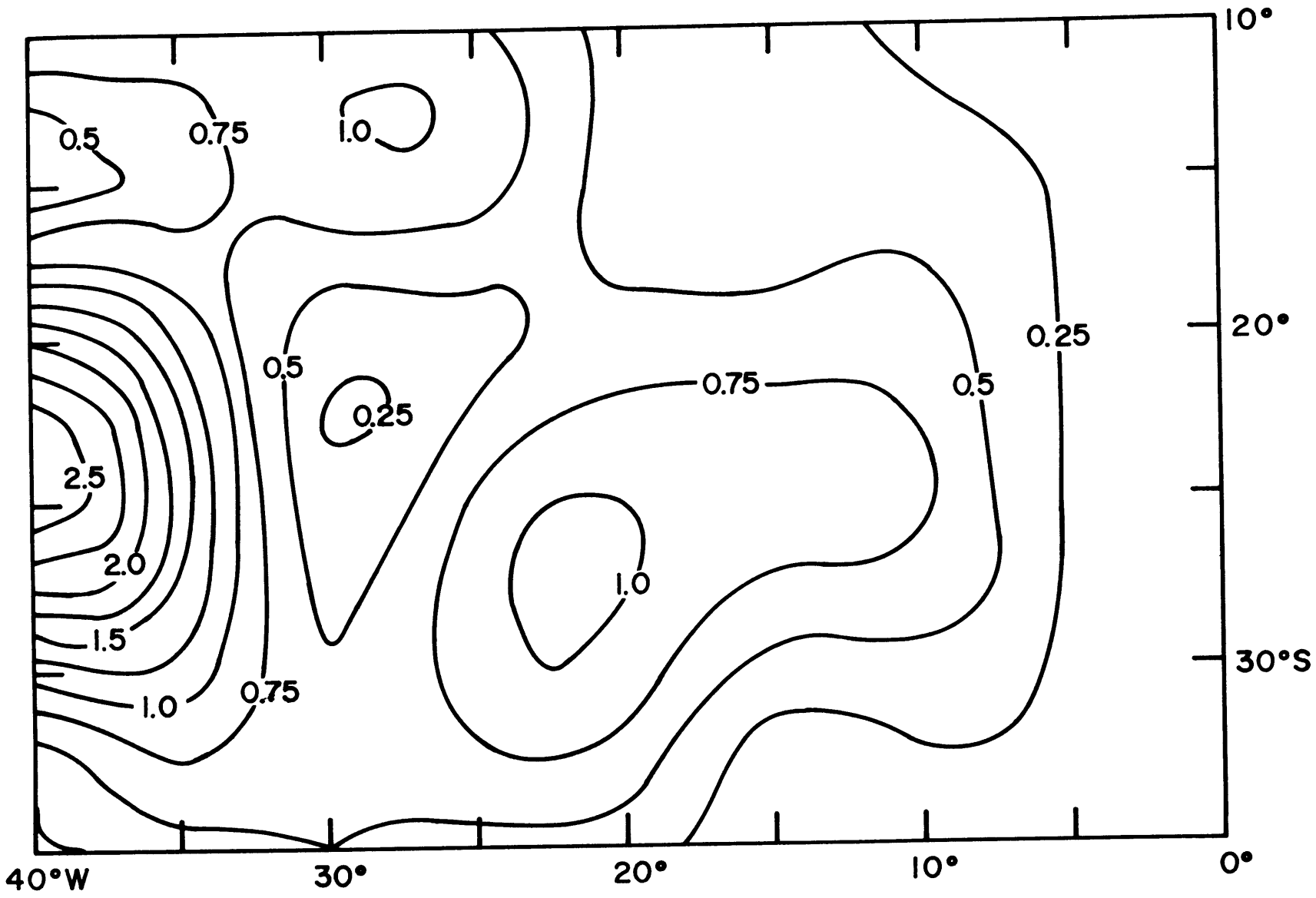
10°
20°
30°S
0°
10°
20°
30°
40°W
0.5
0.75
1.0
0.25
0.5
0.75
0.5
0.25
2.5
2.0
1.5
1.0
0.75
1.0

Figure 19

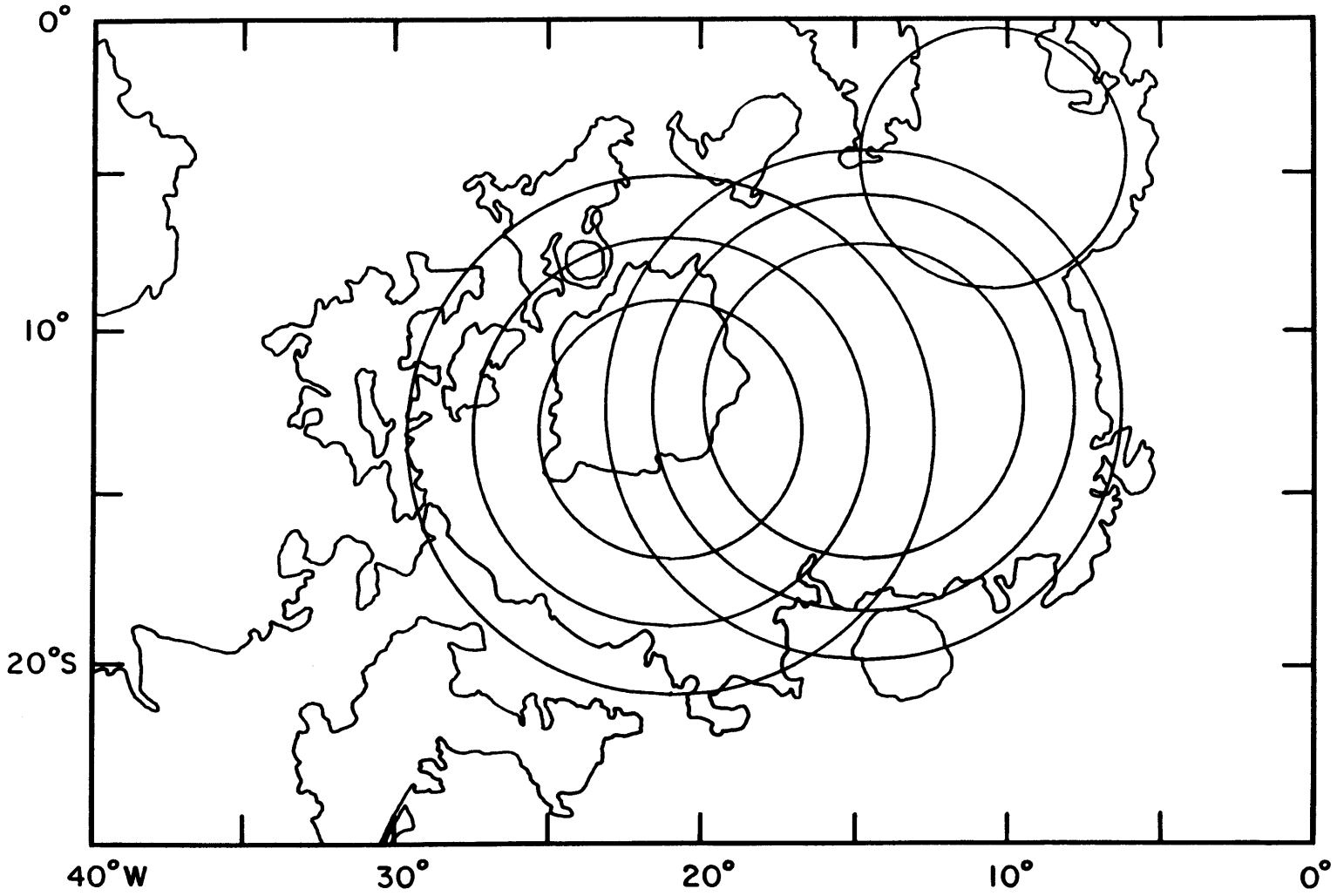

Figure 20

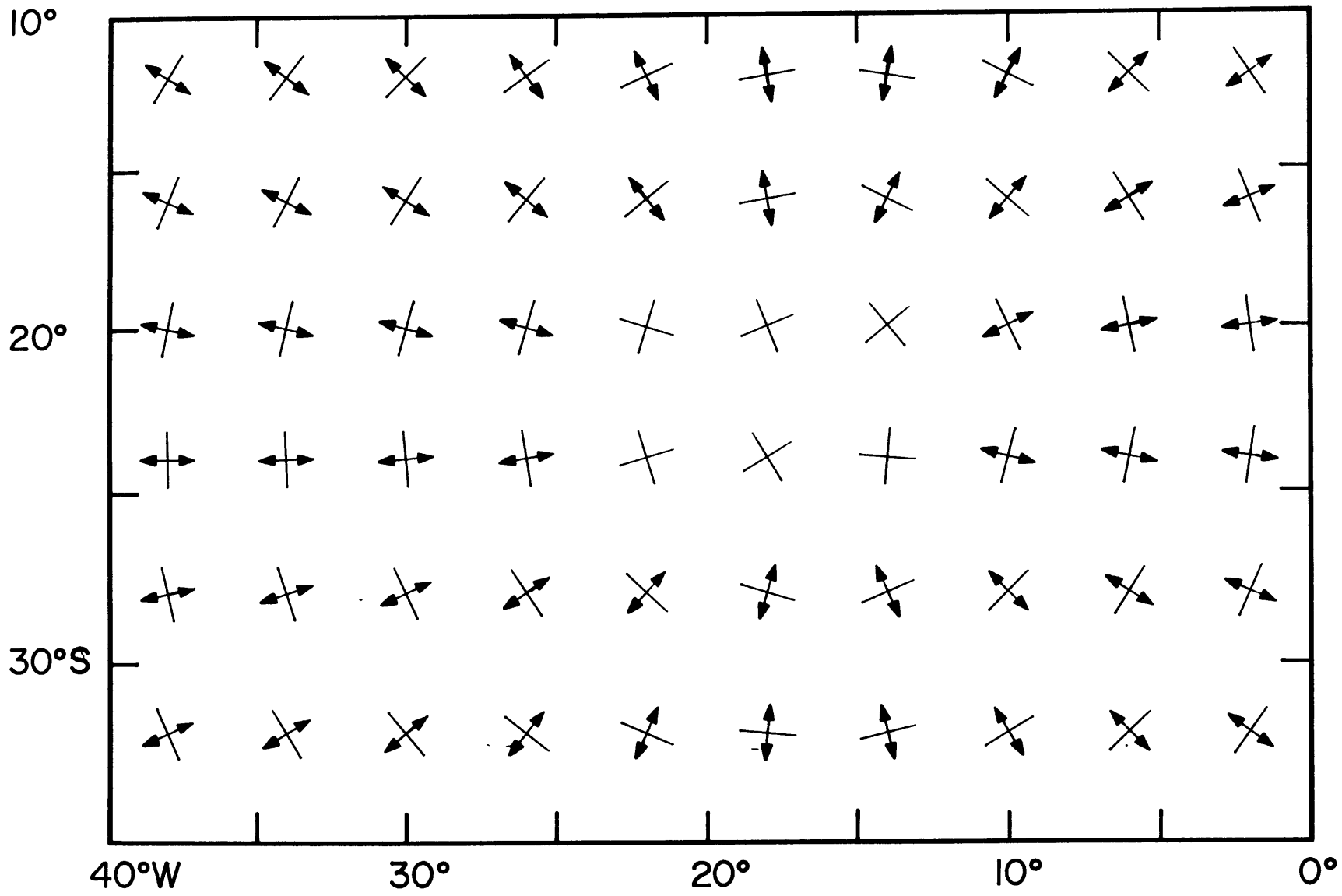

Figure 21a

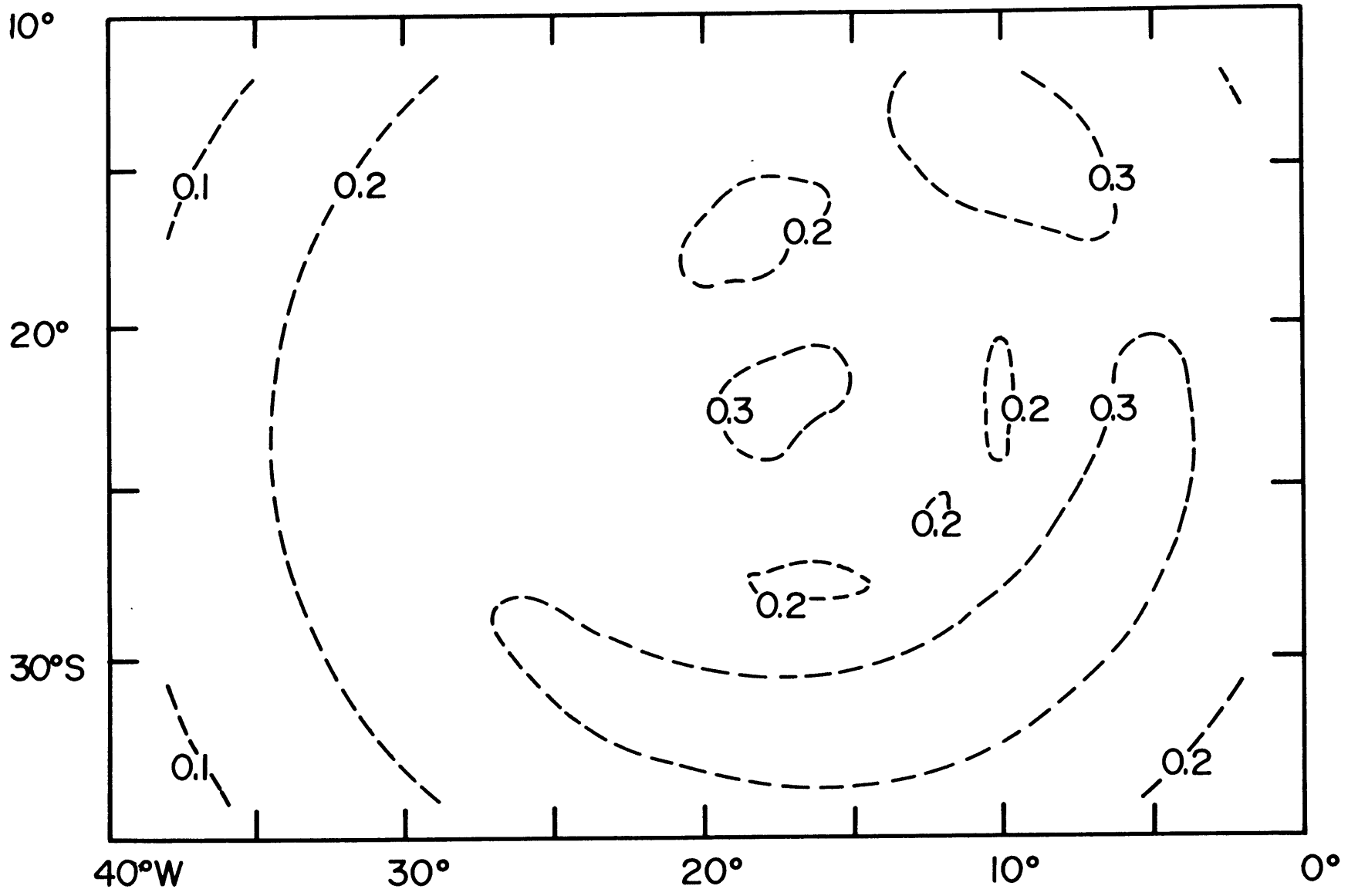

Figure 21b

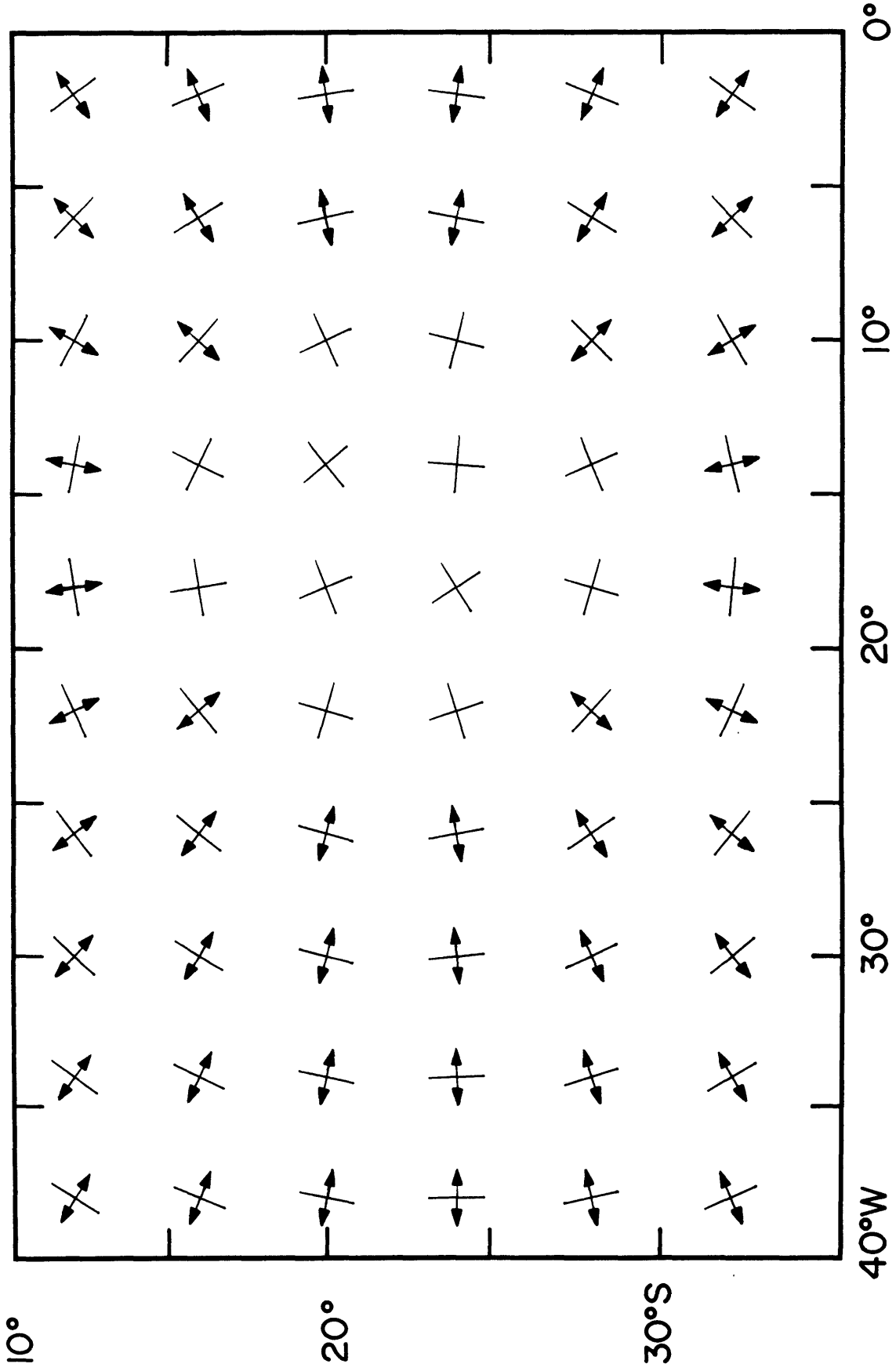

Figure 22a

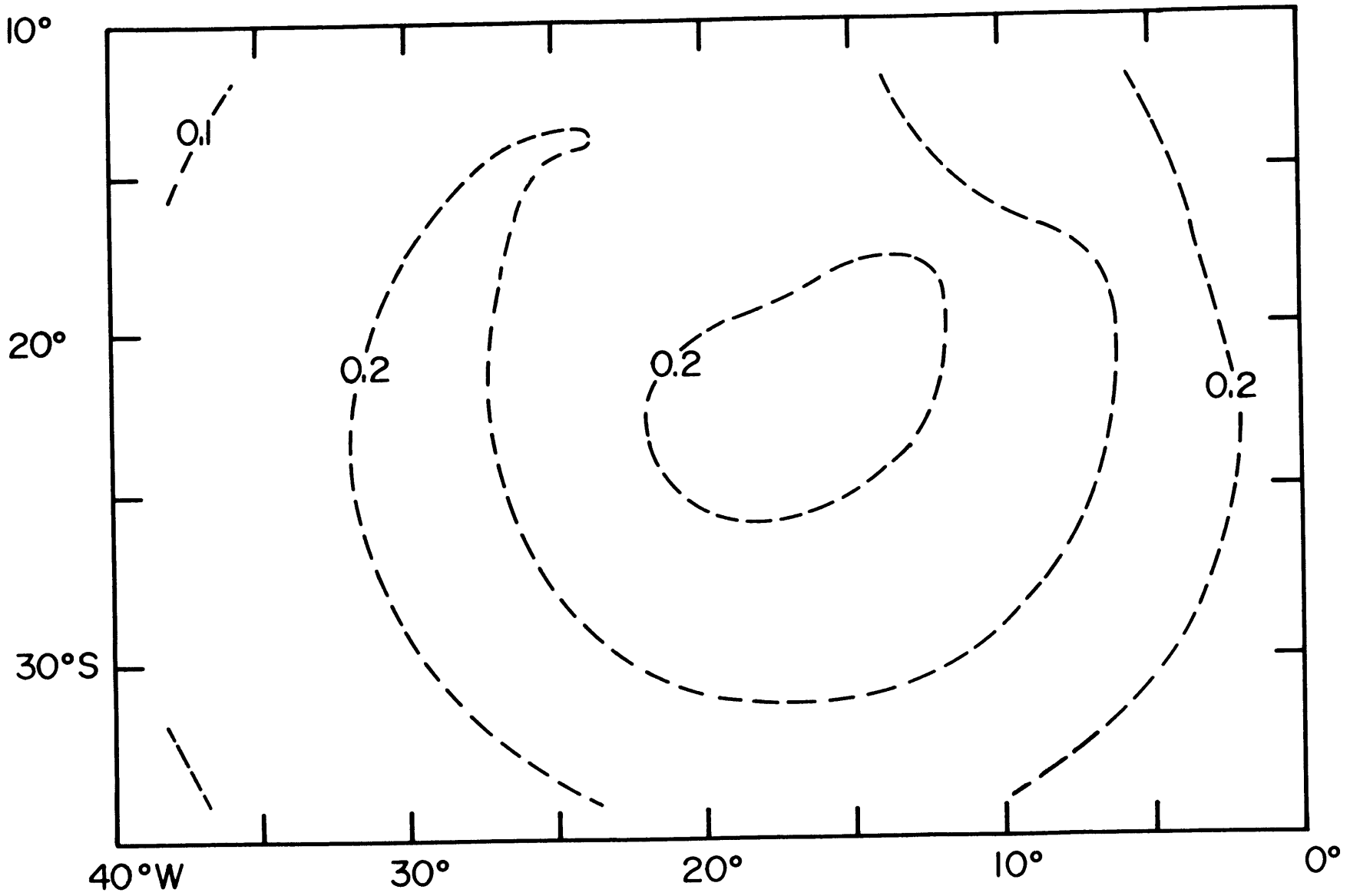

Figure 22b

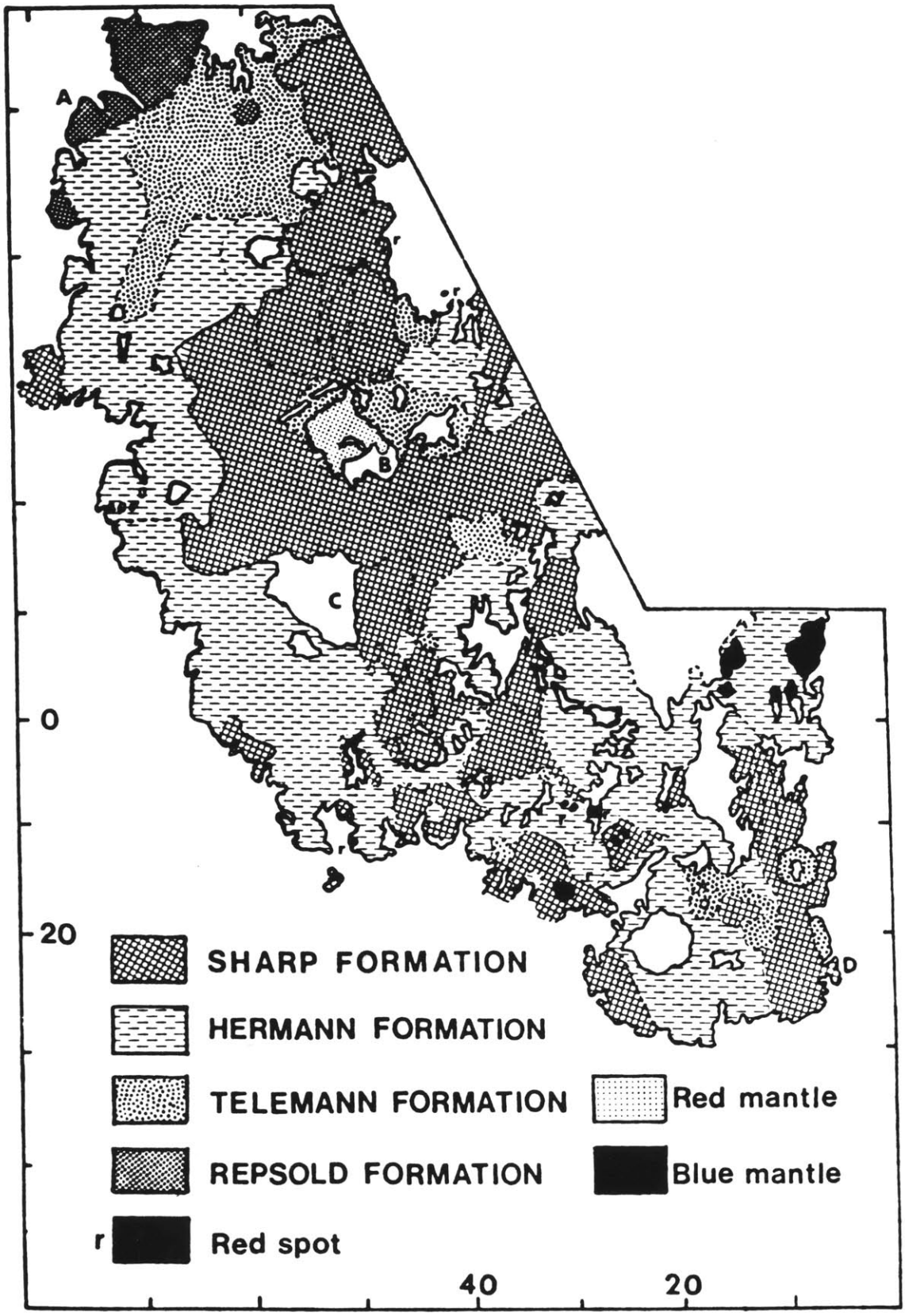
A
B
C
D
r
r
0
20
SHARP FORMATION
HERMANN FORMATION
TELEMANN FORMATION
REPSOLD FORMATION
r Red spot
Red mantle
Blue mantle
40
20

Figure 23

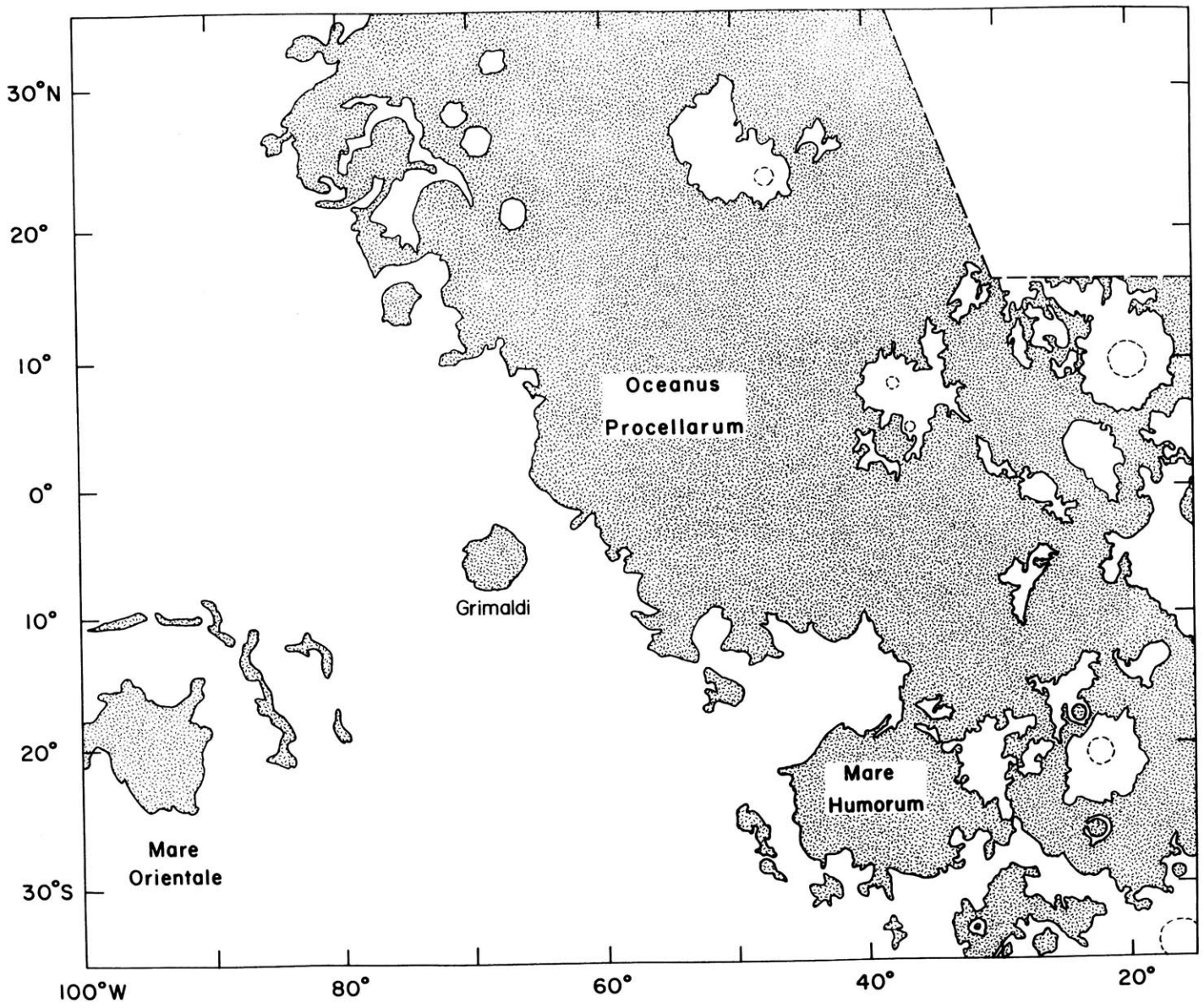
30°N
20°
10°
0°
10°
20°
30°S
100°W
80°
60°
40°
20°
Oceanus
Procellarum
Grimaldi
Mare
Humorum
Mare
Orientale

Figure 24a

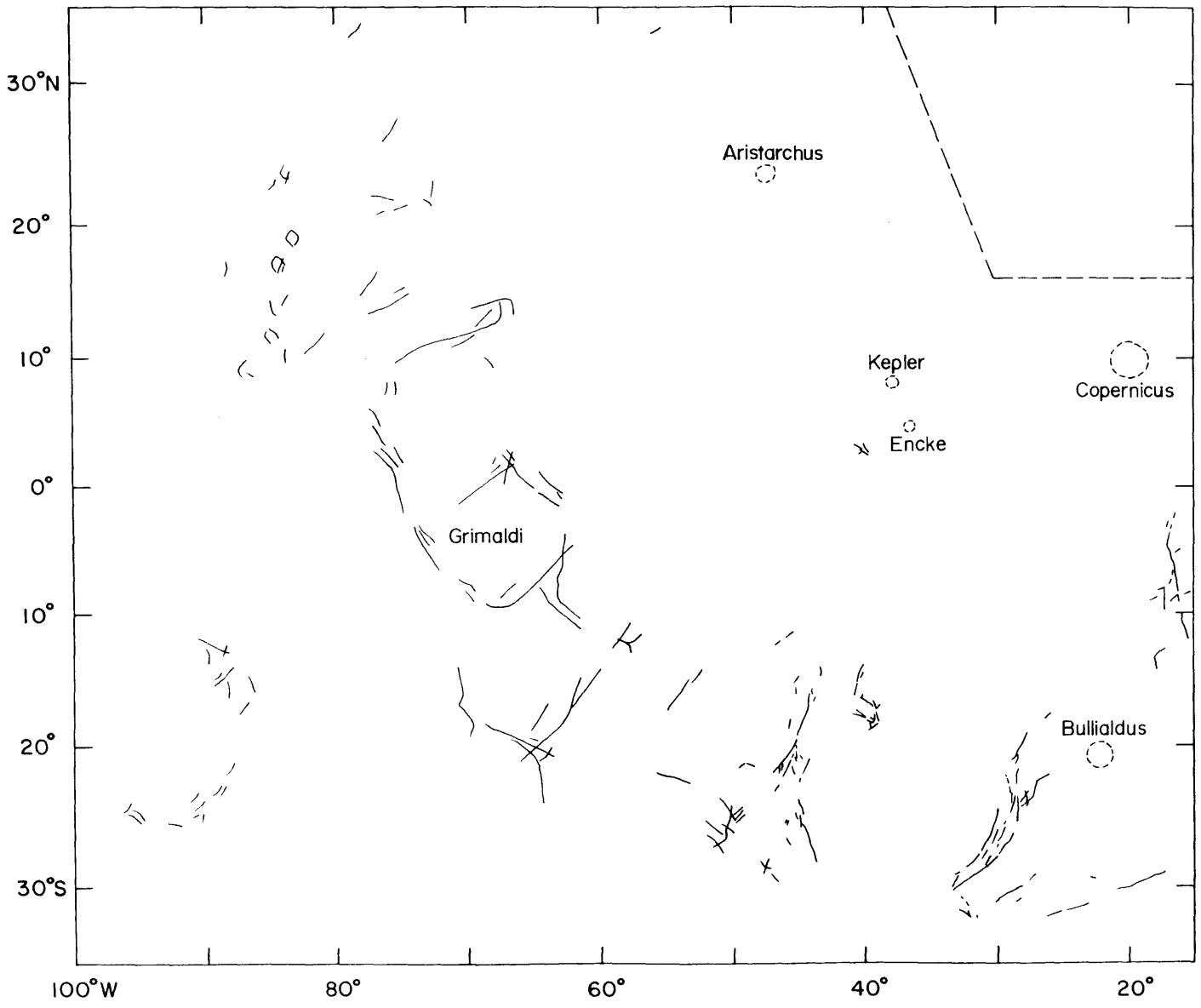
30°N
20°
10°
0°
10°
20°
30°S
100°W
80°
60°
40°
20°
Aristarchus
Kepler
Copernicus
Encke
Grimaldi
Bullialdus

Figure 24b

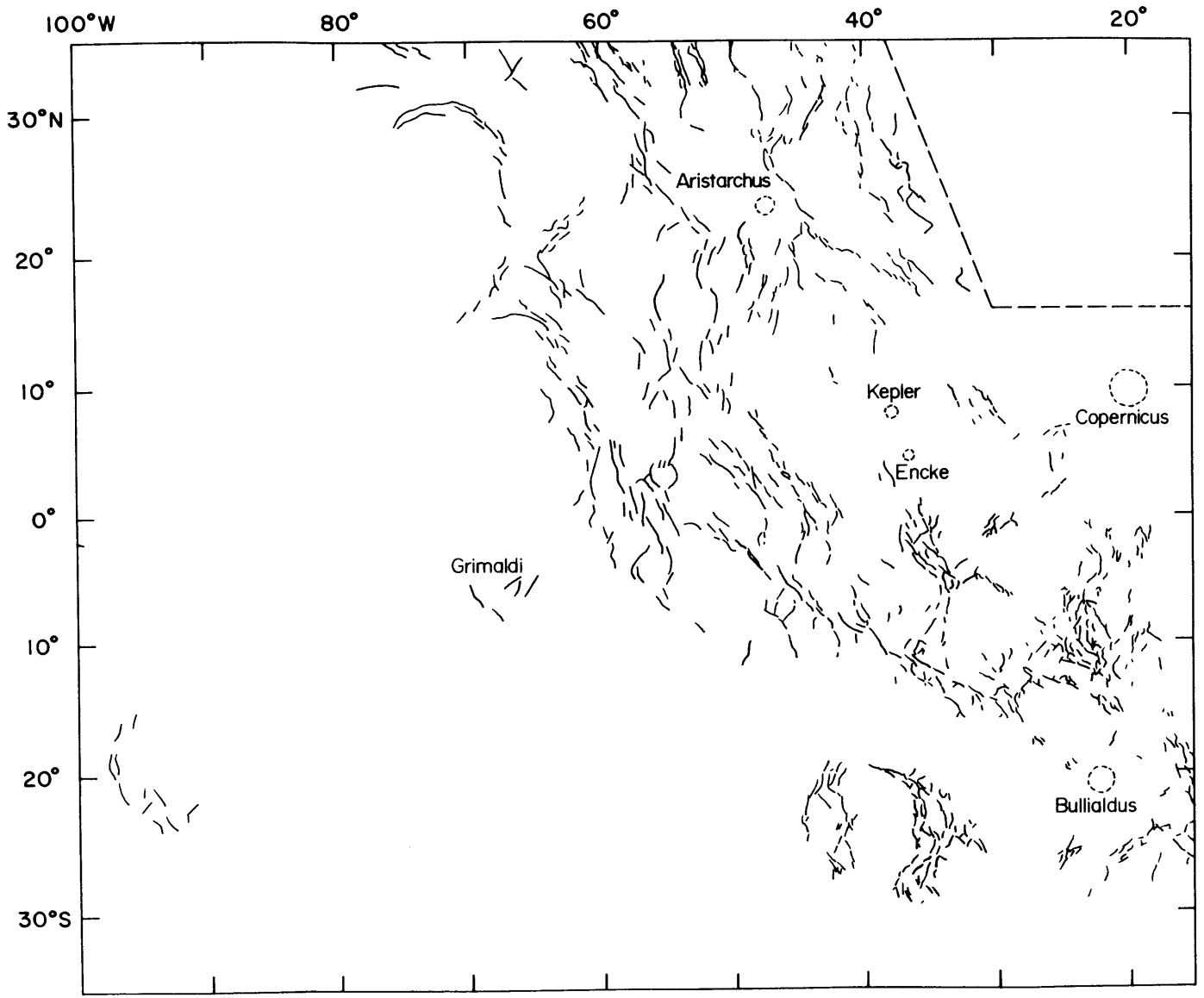
100°W
80°
60°
40°
20°
30°N
20°
10°
0°
10°
20°
30°S
Aristarchus
Kepler
Copernicus
Encke
Grimaldi
Bullialdus

Figure 24c

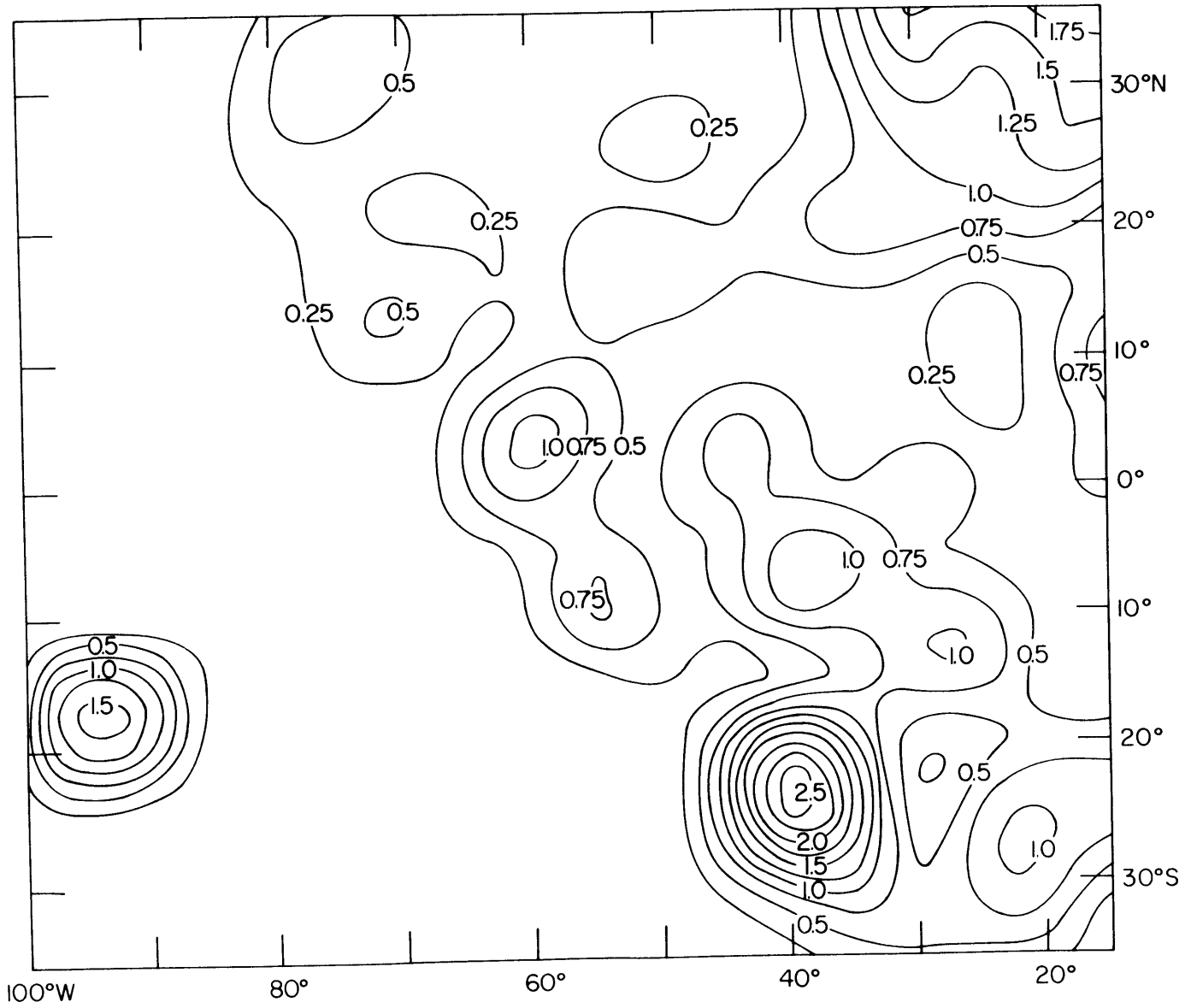
1.75
1.5
30°N
1.25
0.5
0.25
1.0
0.75
20°
0.5
0.25
0.25
0.5
10°
0.25
0.75
1.0 0.75 0.5
0°
1.0 0.75
0.75
10°
0.5
1.0
1.5
1.0
0.5
20°
0.5
2.5
2.0
1.5
1.0
1.0
30°S
0.5
100°W
80°
60°
40°
20°

Figure 25

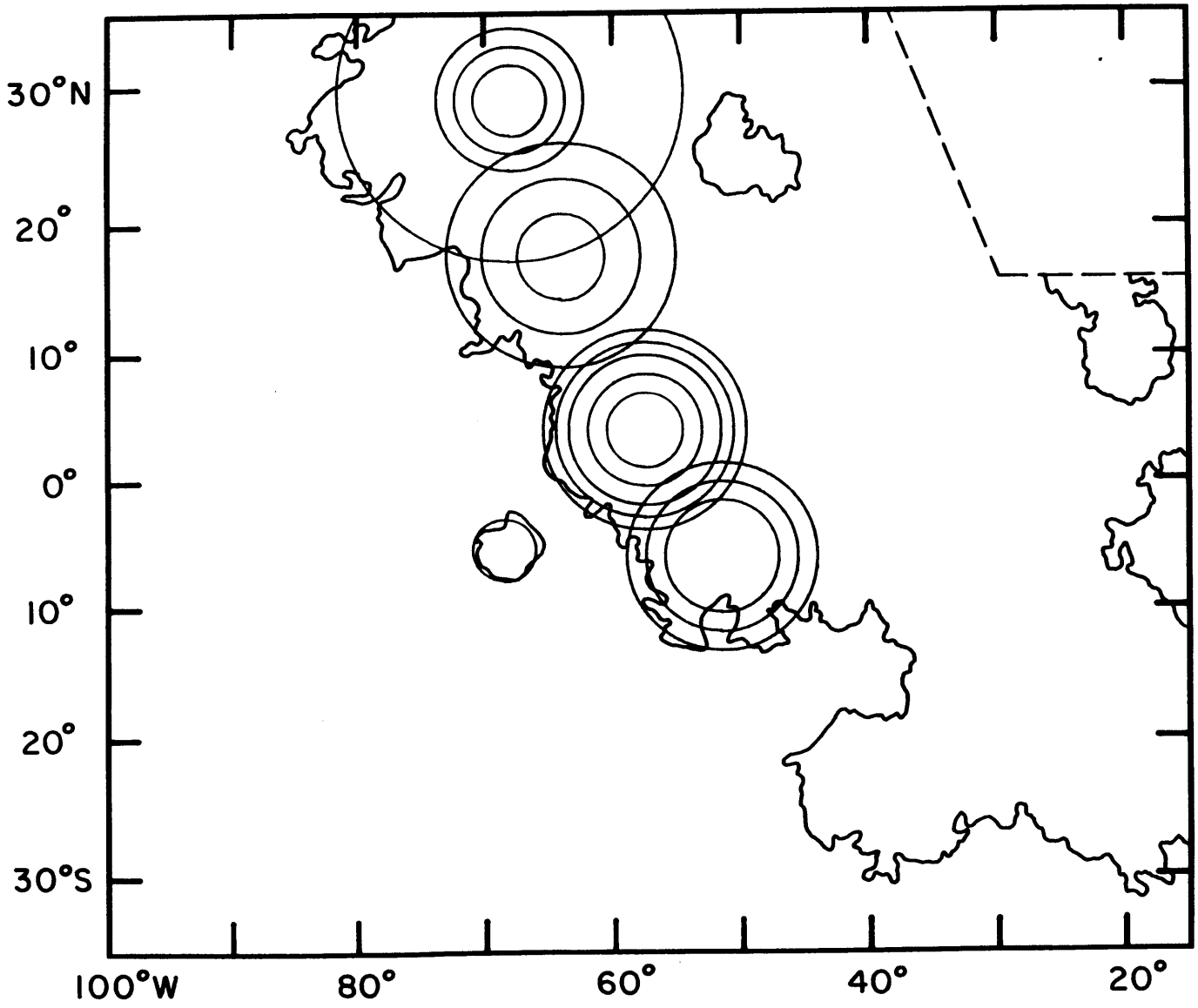

Figure 26

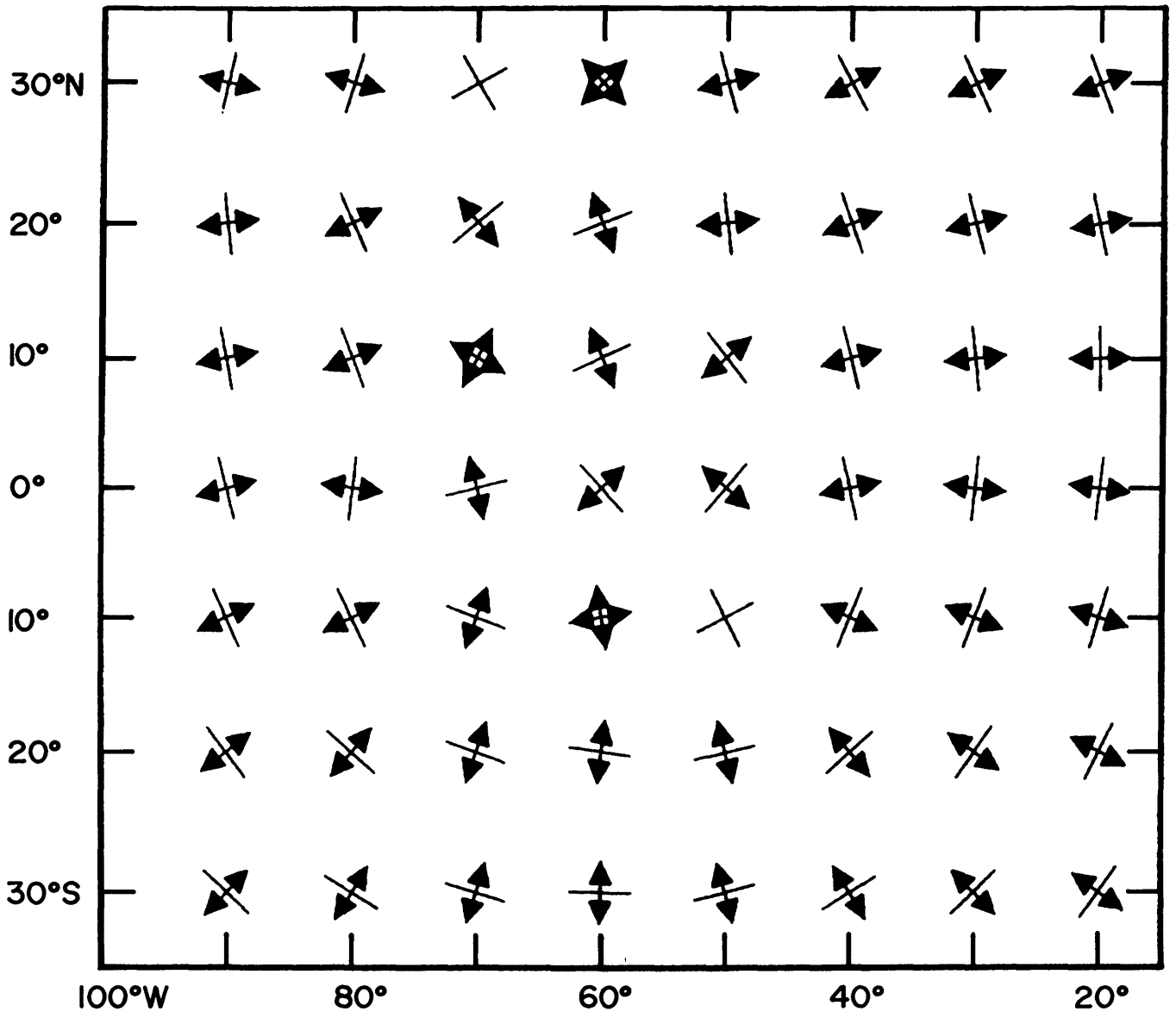

Figure 27a

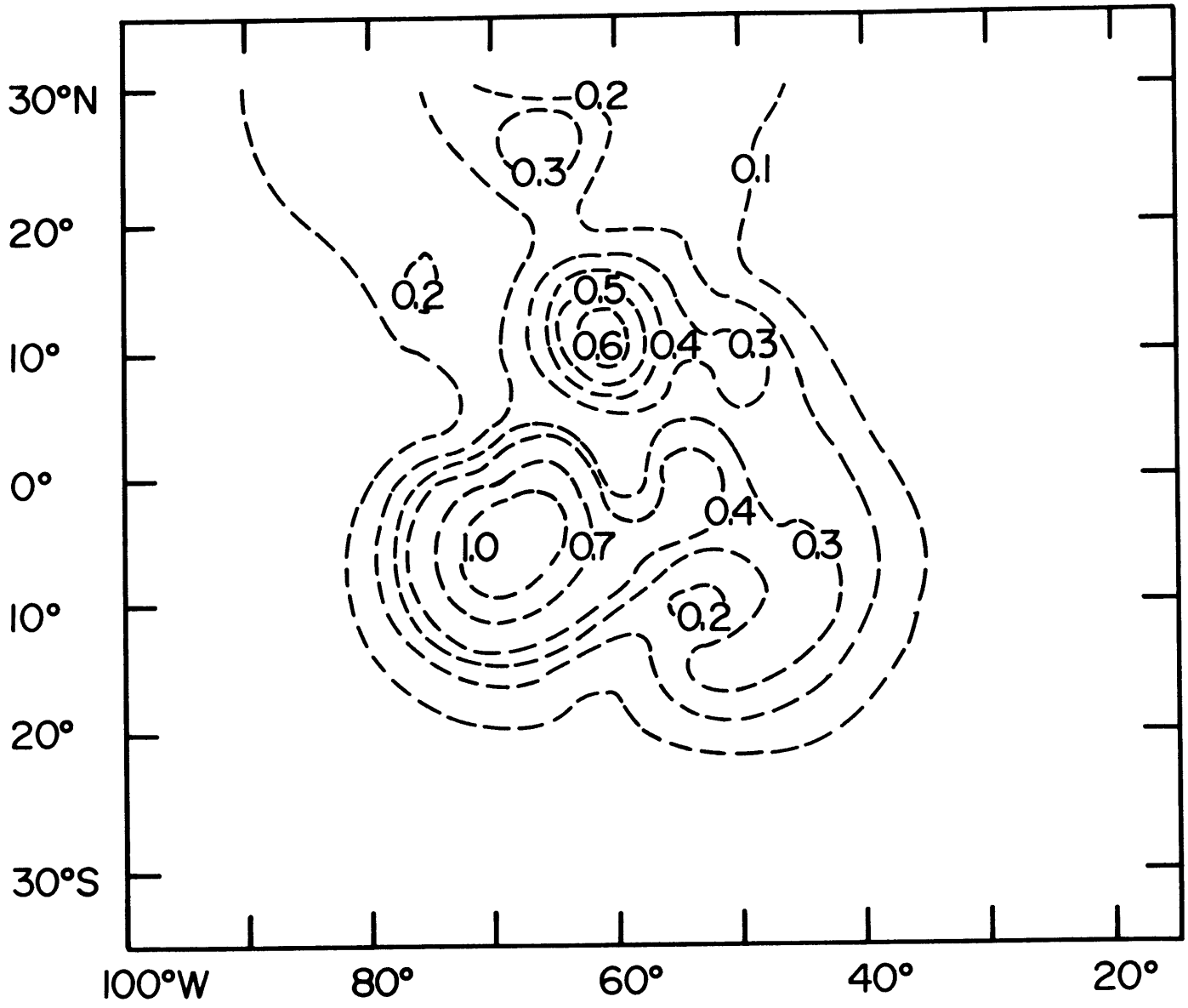
30°N
20°
10°
0°
10°
20°
30°S
100°W
80°
60°
40°
20°
0.2
0.3
0.1
0.2
0.5
0.6
0.4
0.3
0.4
1.0
0.7
0.3
0.2

Figure 27b

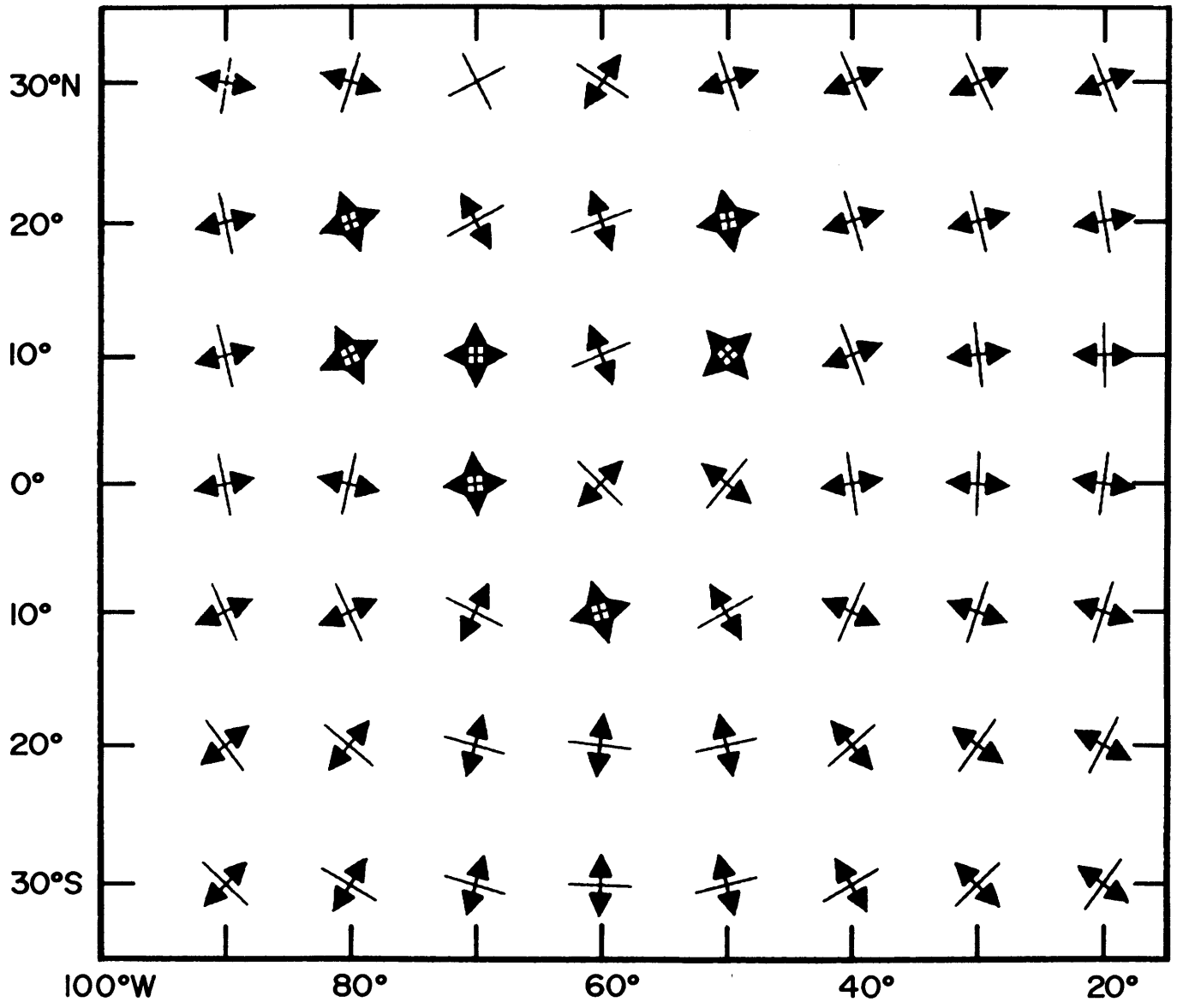

Figure 28a

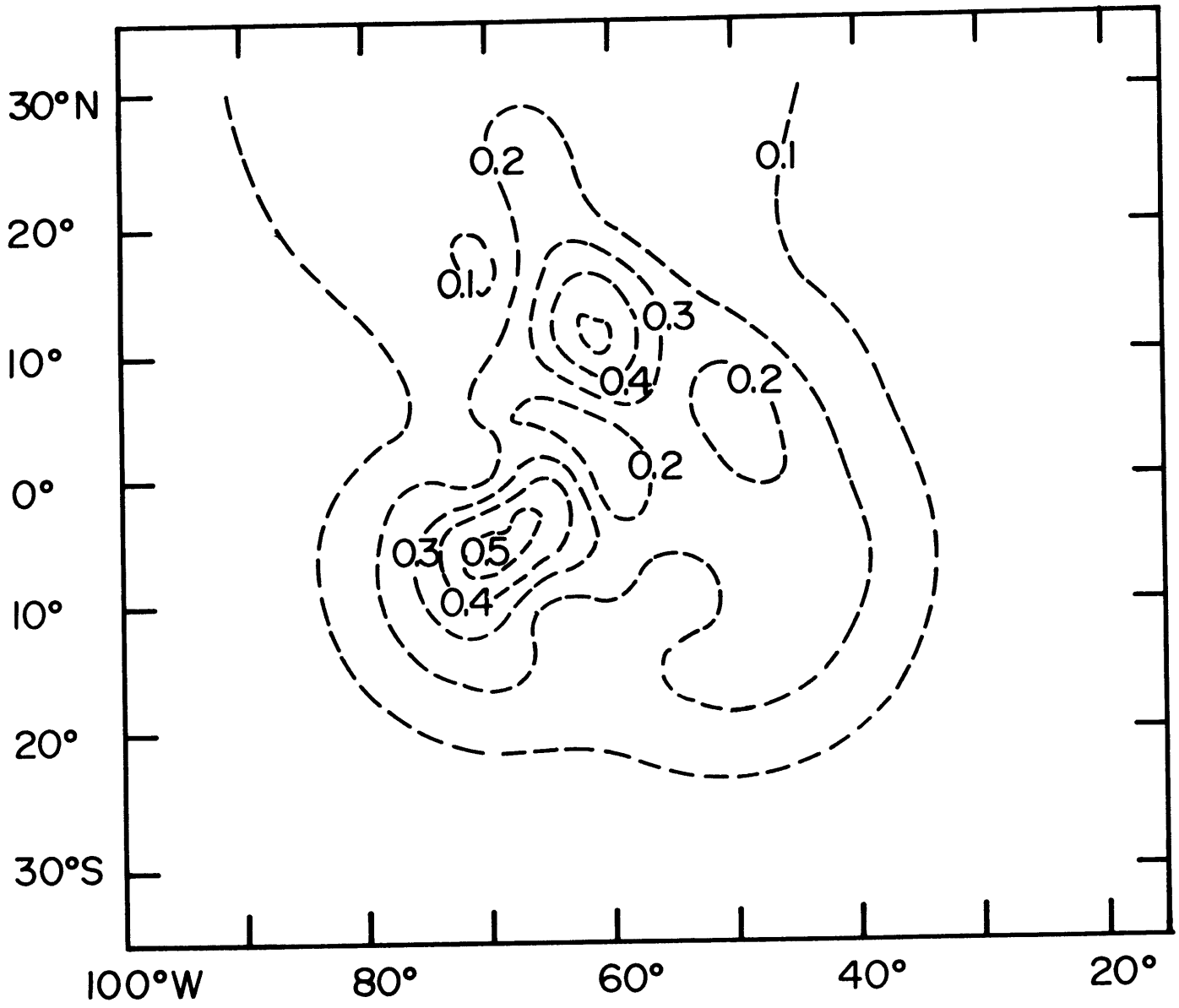

Figure 28b

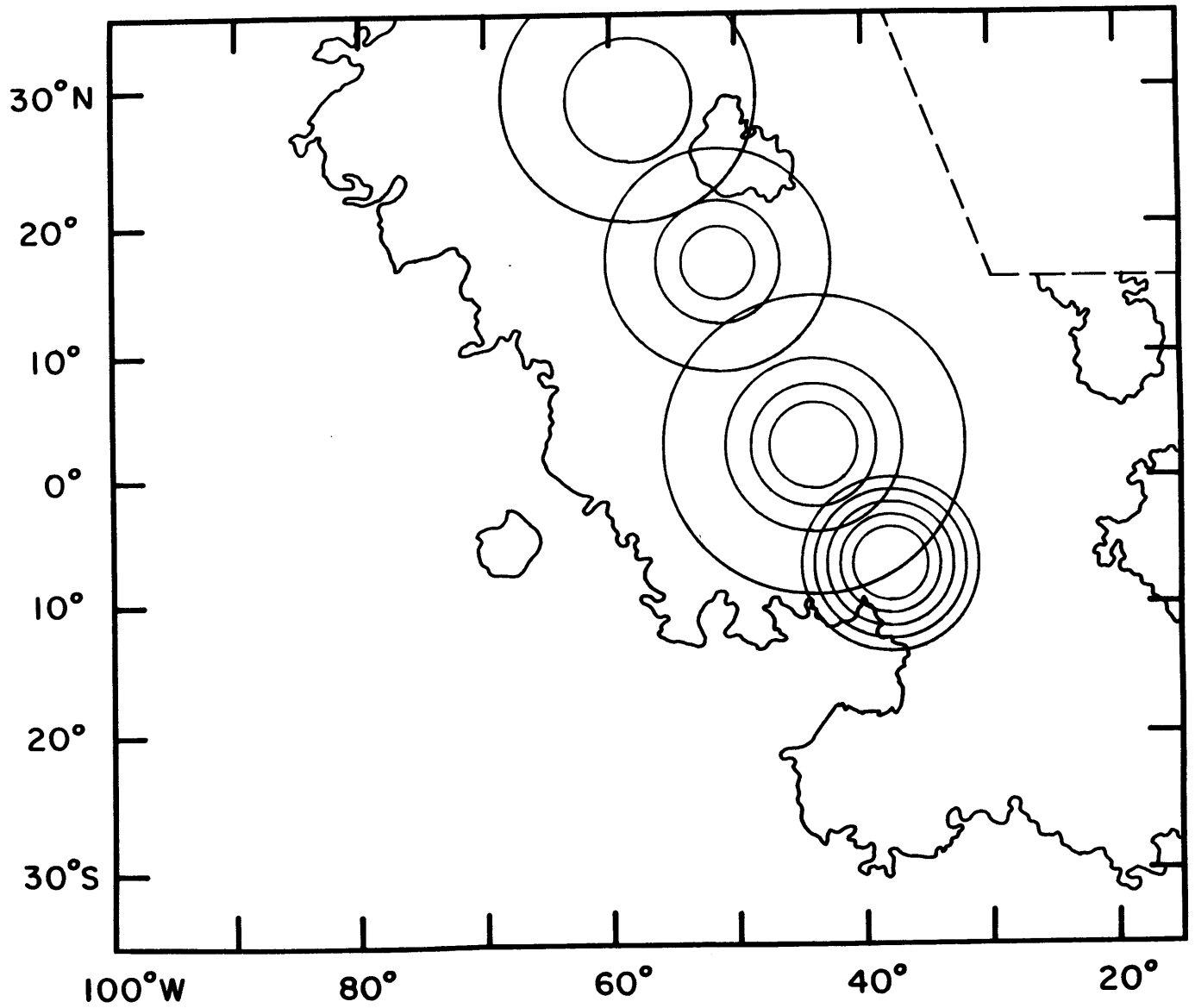

Figure 29

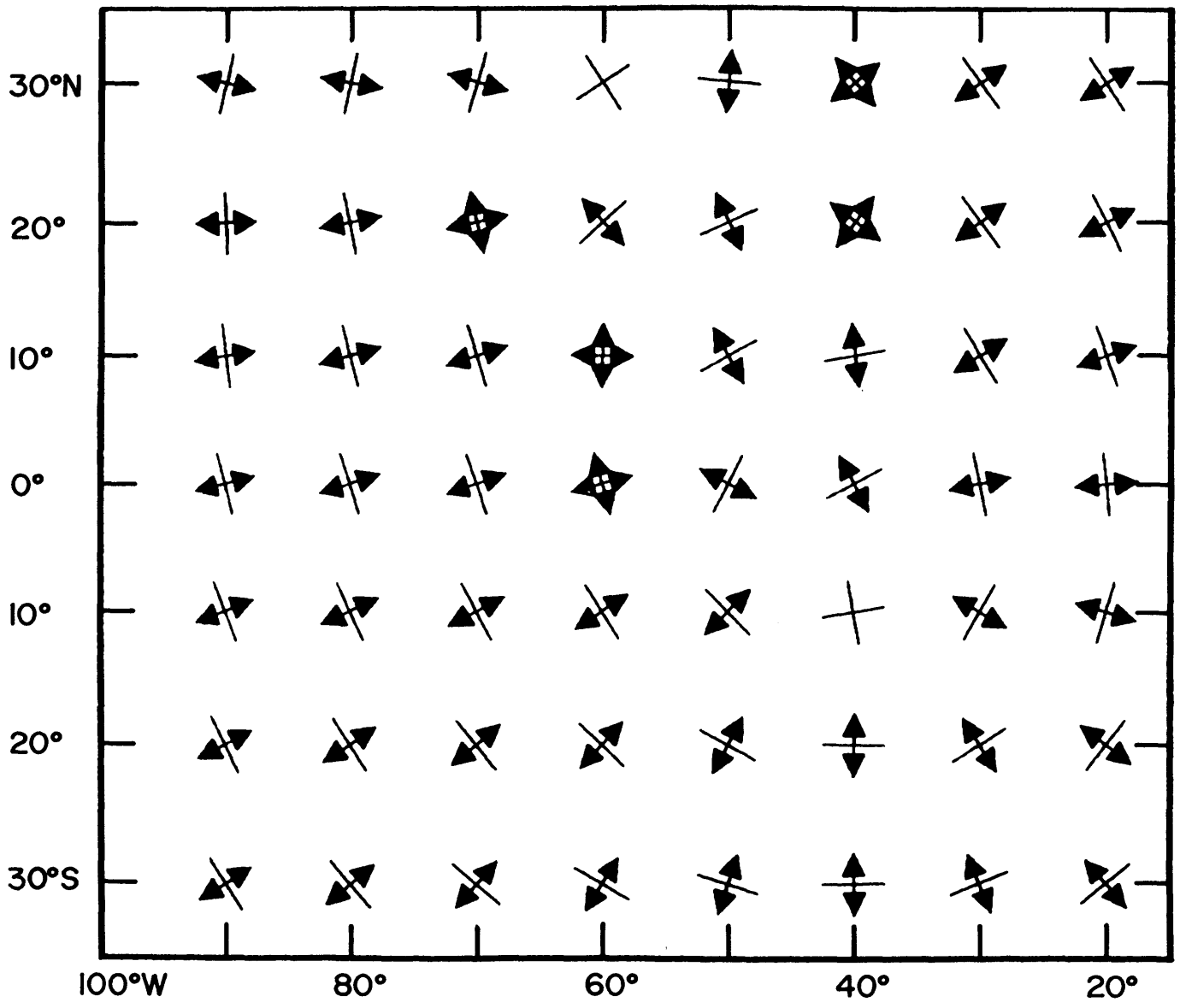

Figure 30a

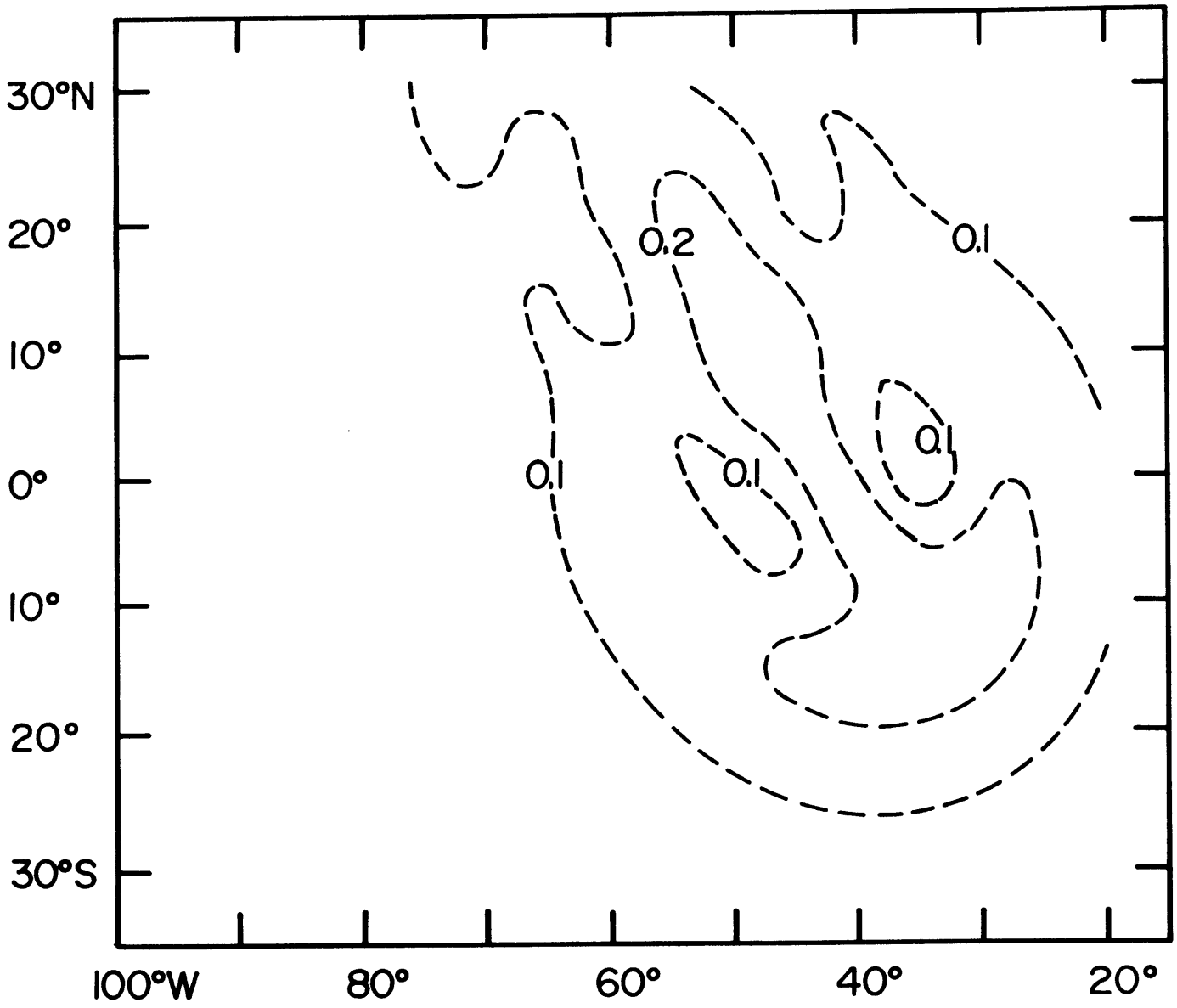

Figure 30b

CHAPTER 4

SOME RELATIONSHIPS AMONG LUNAR FLOOR-FRACTURED CRATERS, LITHOSPHERIC THICKNESSES AND LUNAR THERMAL HISTORY

"I can see nothing," said I...

"On the contrary, Watson, you can see everything. You fail, however, to reason from what you see. You are too timid in drawing your inferences."

-- Sir Arthur Conan Doyle,

The Adventure of the Blue Carbuncle

In Chapter 2 it was shown that the topography of floor-fractured craters is consistent with viscous relaxation of unmodified crater topography. We assume that near-surface temperature variations are the primary influence on near-surface viscosity variations. The effective viscosity is also a function of material composition and strain rate. Compared to the effect of temperature on viscosity, however, these are likely to be secondary effects [Solomon et al., 1982a]. The viscous relaxation of floor-fractured craters was probably restricted to fairly short time intervals (perhaps ten million years or less) over which high near-surface temperatures led to low effective viscosity and a thin elastic or brittle lithosphere. By this interpretation, the locations of most floor-fractured craters are indicative of small-scale heterogeneities in near-surface temperatures. The values of lithospheric thickness obtained for the irregular maria in this thesis (Chapter 3) and for the circular maria by Comer et al. [1979] and Solomon and Head [1979, 1980] are indicative of larger-scale variations in the thermal structure of the lunar crust and upper mantle and probably sample a somewhat greater interval of time. In this chapter, we discuss some of the implications of both sets of results for the thermal and volcanic history of lunar mare basins.

Lunar floor-fractured craters tend to be clustered around the edges of the lunar maria [Schultz, 1976] (Figure 1). The largest concentrations of floor-fractured craters are located along the western border of Oceanus Procellarum, around Mare Nectaris, and within and around the southern half of Mare

Smythii. Maria with few floor-fractured craters include Imbrium, Serenitatis, Tranquillitatis, Fecunditatis, and Crisium.

The locations of floor-fractured craters can be compared with both the ages of the mare basins and the ages of the mare basalt units filling those basins. In order of increasing age, the basins can be ranked as follows [Wilhelms, 1981]: Orientale, Imbrium, Serenitatis, Crisium, Humorum, Nectaris, Smythii, Nubium Fecunditatis, and Tranquillitatis (with the last three not distinguishably different in age). The nature of the Procellarum depression, as noted in Chapter 3, is still being debated; Wilhelms [1981] ranks it as the oldest lunar basin.

It can be seen (Figure 1) that floor-fractured craters are clustered around the old and intermediate-age basins Procellarum, Nectaris, and Smythii. There are fewer associated with the older Tranquillitatis and Fecunditatis basins, and almost none around the youngest basins (Orientale, Imbrium, Serenitatis, and Crisium). It is somewhat surprising that there are prominent concentrations of floor-fractured craters around Smythii and Nectaris but not around the older Tranquillitatis and Fecunditatis basins, which presumably formed at times when the near-surface temperatures were higher and thus the viscosity of near-surface material lower. The Tranquillitatis basin itself appears to have undergone significant viscous relaxation of its initial topography [Solomon et al., 1982a]. There are several possible explanations for this discrepancy. The Tranquillitatis and

Fecunditatis basins have both been heavily modified by subsequent nearby basin impacts, ejecta from which might have covered any fractures in the floors of craters which formed early in the basin history (during the time period soon after the basin-forming impact, when heat generated by the impact would lower near-surface viscosities). In addition, ejecta from Eratosthenian to Copernican age craters has obscured portions of these maria and their boundaries (as discussed in Chapter 3). Thus, we cannot be sure that if floor-fractured craters had formed early in the history of these basins that they would still be visible.

When the locations of floor-fractured craters are compared to the ages of mare units over the lunar surface [Boyce et al., 1974; Boyce, 1976; Boyce and Johnson, 1978], it appears that few floor-fractured craters are found in the areas of the youngest mare units. The mare basalts filling Mare Nectaris, for example, are dated at 3.75 b.y. by Boyce [1976]. For Mare Smythii the floor-fractured craters, which are found in the southern half of the mare, occur on the oldest mare unit, which is covered with the remnants of debris apparently related to the formation of Crisium and other nearby younger basins [Stewart et al., 1975]. The northern, younger mare units in Smythii do not contain floor-fractured craters. Mare Smythii is also surrounded by about ten dark-haloed craters. These craters may indicate the presence of ancient mare volcanic material [Schultz and Spudis, 1979]. If so, they are consistent with an early period of high near-surface

temperatures in that region. (However, the locations of dark-haloed craters do not in general correlate closely with the locations of floor-fractured craters; in particular, very few are found along the western edge of Oceanus Procellarum.) In Oceanus Procellarum, the mare surface in the area nearest the concentration of floor-fractured craters is much younger than the unit in Mare Smythii containing floor-fractured craters, but those surface units may be only a thin layer over much older mare units [Whitford-Stark and Head, 1980].

There is no obvious correlation between the location of floor-fractured craters and the lithospheric thicknesses at the time of tectonic feature formation (Figure 2) as estimated by Comer et al. [1979], Solomon and Head [1979, 1980], and in this thesis (Chapter 3). Although concentrations of floor-fractured craters are found adjacent to Oceanus Procellarum, for which there is evidence of an anomalously thin lithosphere, there are also concentrations of floor-fractured craters around the maria Nectaris and Smythii, for which Solomon and Head [1980] calculated minimum lithospheric thicknesses of 75 km at the time of formation of flexurally-induced graben elsewhere on the Moon.

The results of Chapters 2 and 3 are not inconsistent, however, when we consider them carefully. Viscous relaxation of crater topography requires only small-scale variations in near-surface temperatures occurring over a relatively limited period of time. The fact that there are only about 200 floor-fractured craters on the Moon indicates that conditions

favorable for their formation occurred only rarely. On the basis of basin thermal history models [Bratt et al., 1985b], these thermal anomalies most likely occurred early in each basin's history. The lithospheric thickness values derived from basalt load models, on the other hand, are based on the thicknesses of basalt accumulated throughout mare volcanic activity. There is no reason to expect that the results would correlate closely; they are indicators of the thermal environment at two different scales (local vs. regional) and at generally different times.

Considered in this sense, the floor-fractured craters around Mare Nectaris and Mare Smythii provide evidence that the thermal environment in each region changed over time. The floor-fractured craters presumably formed relatively soon after basin formation and then were "frozen in" as the lithosphere cooled and thickened, reaching a much greater thickness by the time the entire mare load was emplaced.

The presence and distribution of floor-fractured craters thus appear to be measures of the thermal state of portions of each basin soon after basin formation. The fact that the youngest basins have very few floor-fractured craters associated with them may indicate that by the time the youngest basins formed, the Moon had globally cooled and the lithosphere thickened to such an extent that impact heating alone was not sufficient to lower local viscosities to a sufficient degree and for a long enough time to favor viscous relaxation of crater topography. This conclusion is consistent with the

extent of topographic relief [Solomon et al., 1982a] and crustal thinning [Bratt et al., 1985a] preserved for younger and older impact basins, which also support a general decrease in crustal temperatures with time over the period of basin formation.

If we consider impact heating during basin formation to be a possible contributor to the high temperatures and low viscosities leading to viscous relaxation of crater topography, it is worthwhile to compare the time scales of crater relaxation with the time scale of basin cooling after impact. Bratt et al. [1985] estimated that impact heating during basin formation would lead to temperatures of order 1000°C or more beneath the center of a basin. They point out, however, that the spatial distribution of anomalous temperatures produced by impact heating is poorly constrained. If post-impact temperatures around basin margins reach 600°C, the effective viscosity of crustal material could lie in the range 10^{20}-10^{24} poise [e.g., Solomon et al., 1982a], with the exact value of η depending on the flow law and the strain rate. For the values of t/η calculated in this chapter, and for η less than about 10^{23} poise, the relaxation times t will be less than about 100 m.y. (possibly as low as 1 m.y., depending on the exact value of η). This is consistent with the time of most rapid basin cooling (~ 100 m.y.) estimated by Bratt et al. [1985b]. It is thus possible that basin impact heating is a significant

contributor to the formation of floor-fractured craters, especially in cases where cratering around the basin margin occurred soon after the basin impact itself.

A possible source of near-surface heating over much of the lunar nearside is the proposed Procellarum basin impact [Wilhelms, 1981]. While the implantation of heat by such an event can account for some of the variations seen in Figure 2, the concentration of floor-fractured craters around Mare Smythii lies outside the proposed basin.

We can summarize our arguments as follows: If the temperature variations leading to viscous relaxation of crater topography were solely temporal (due, say, to changes in the global near-surface thermal environment with time), we would expect to find floor-fractured craters scattered more or less randomly over the entire lunar surface. Although there are floor-fractured craters all over the Moon, the fact that they are concentrated around the edges of the maria means that they must be associated with spatial heterogeneities in temperature. The most likely sources for such spatial heterogeneities are basin impact heating and mare filling. Similarly, if these processes were the primary cause of lowered viscosities, we would expect to see floor-fractured craters around all mare basins (which we do not). Thus, it is plausible to ascribe the lowered viscosities leading to formation of floor-fractured craters to both spatial and temporal variations in temperature.

One possible scenario to explain the distribution of floor-fractured craters is that it is the result of the superposition of local (basin-related) heating to a time-dependent global temperature field which was warmer at the time of formation of the oldest basins than at that of the youngest.

FIGURE CAPTIONS

Figure 1. Spatial distribution of floor-fractured craters, showing the pronounced concentrations along the borders of the maria. From Schultz [1976].

Figure 2. Summary of determinations of the thickness T of the elastic lithosphere on the moon from mare tectonic features. In cases where two values are shown, the upper figure gives T in kilometers in the early interval of mare flooding (3.6-3.8 b.y. ago) during which rille formation occurred [Lucchitta and Watkins, 1978]; the lower figure gives T at a late stage in mare flooding (approximately 3.0-3.2 b.y. ago) when mare ridge formation and subsidence were continuing but rille formation had ceased. If only one figure is shown for the circular maria, it is the estimate of lithospheric thickness in the early period of flooding for maria lacking young volcanic flows. Values for the irregular maria Nubium, Tranquillitatis, Fecunditatis, and Oceanus Procellarum were estimated in Chapter 3; values for the circular maria (all others) are from Solomon and Head [1980]. The asterisk for eastern Oceanus Procellarum indicates that no range of T for the period of rille formation was calculated, because very young lava flows covering the region make it impossible to detect any early episodes of rille formation.

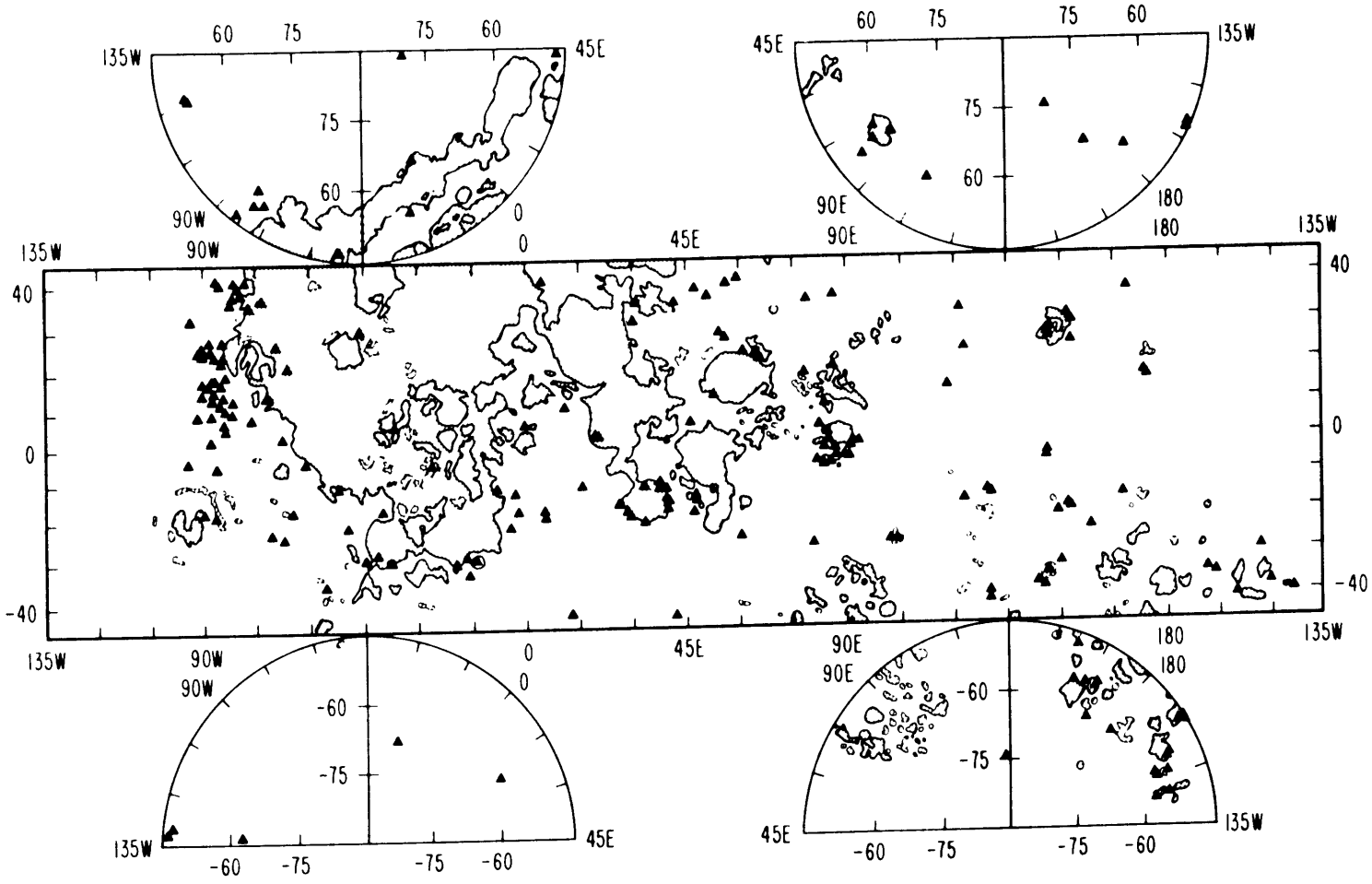

Figure 1.

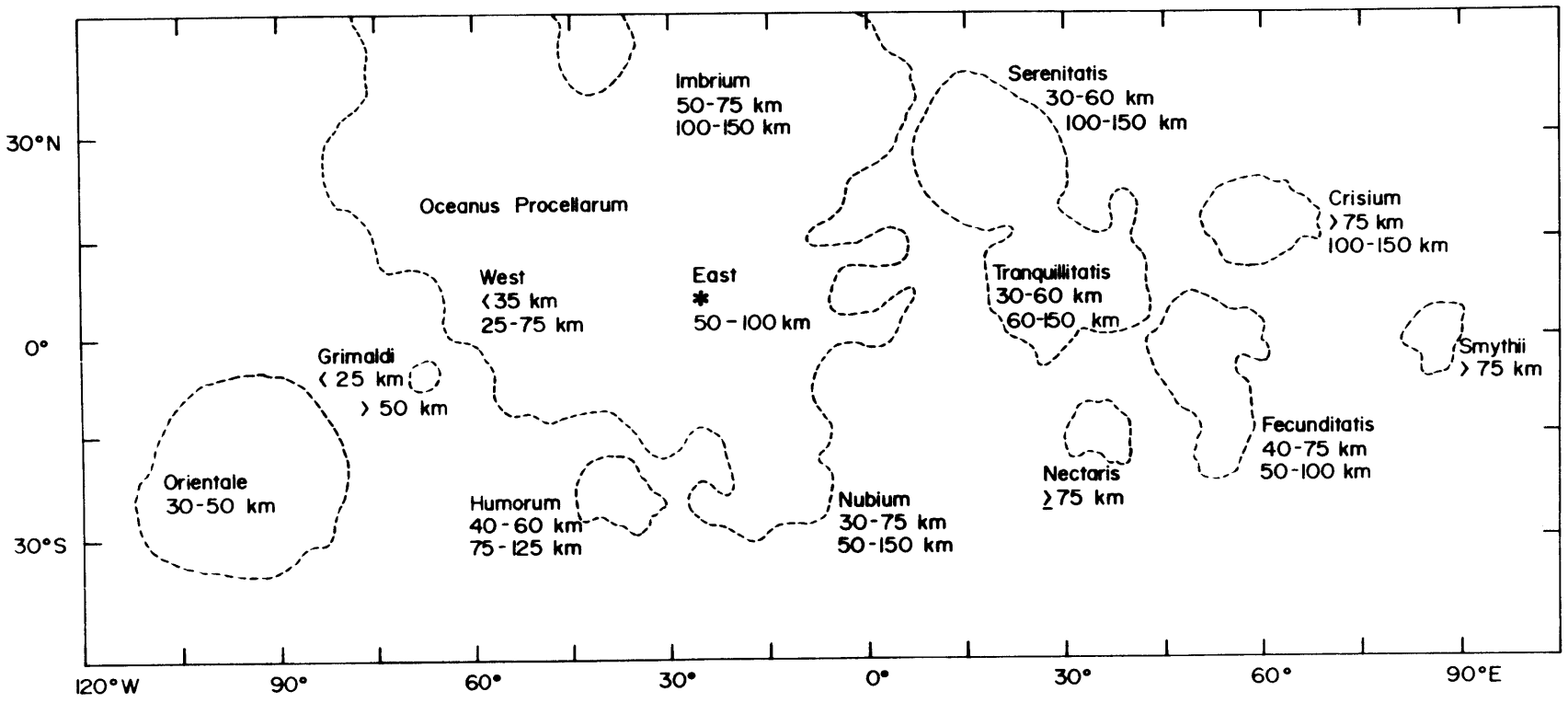
30°N
0°
30°S
120°W
90°
60°
30°
0°
30°
60°
90°E
Imbrium
50-75 km
100-150 km
Serenitatis
30-60 km
100-150 km
Oceanus Procellarum
Crisium
> 75 km
100-150 km
West
< 35 km
25-75 km
East
*
50 - 100 km
Tranquillitatis
30-60 km
60-150 km
Grimaldi
< 25 km
> 50 km
Smythii
> 75 km
Fecunditatis
40-75 km
50-100 km
Orientale
30-50 km
Nectaris
≥ 75 km
Humorum
40-60 km
75-125 km
Nubium
30-75 km
50-150 km

Figure 2

CHAPTER 5

ELYSIUM REGION, MARS: TESTS OF LITHOSPHERIC LOADING MODELS FOR THE FORMATION OF TECTONIC FEATURES

Mars is the third smallest planet and therefore of interest only to collectors. It is bleak and rocky with no coastline to speak of -- a feature that has made it one of the few beach areas within the financial grasp of this writer.

-- Fran Lebowitz, Metropolitan Life

INTRODUCTION

The tectonic history of the planet Mars has been dominated by the formation and evolution of several major volcanic provinces, notably those in the regions of Tharsis and Elysium. The Tharsis province, because it is the largest, has received the most attention. Two general categories of models have been proposed to explain the topography, gravity, and tectonic features of the Tharsis region. According to the first type of model, uplift of ancient crust caused by a chemical or thermal anomaly created a broad topographic dome and led to widespread fracturing and to the emplacement of relatively thin volcanic plains units and isolated volcanic shields [Hartmann, 1973; Carr, 1974; Mutch et al., 1976; Sleep and Phillips, 1979; Wise et al., 1979a,b,; Plescia and Saunders, 1980]. This uplift may have occurred isostatically or by a flexural uplift of the lithosphere [Banerdt et al., 1982]. In the second category, the Tharsis rise was created primarily by volcanic construction, and the tectonic features of the province are a signature of the response of the lithosphere to loading by these volcanic units [Solomon and Head, 1982; Willemann and Turcotte, 1982].

The generally radial pattern of graben and extensional faults centered on the Tharsis rise has been one of the primary pieces of evidence cited in support of uplift models. Such an argument has been based on the perceived similarity of the geometry of Tharsis fractures to fracture patterns associated with terrestrial domes [e.g., Hartmann, 1973; Carr, 1974a]. Radial extensional features would be expected for uplift of a

flat plate, whereas flexure of a flat plate in response to a generally circular downward load would give rise at the surface to circumferential extensional features. However, because the Tharsis region is so large (covering roughly 25 percent of the surface area of the planet), induced stresses are dominated by membrane stresses rather than the bending stresses that predominate for features of smaller dimensions [Turcotte et al., 1981; Willemann and Turcotte, 1981, 1982]. These membrane stresses are of different orientation and sign than the bending stresses for the corresponding uplift or loading problem. Large-scale flexural uplift models predict formation of radial compressional features, and are thus not consistent with the observed tectonics [Banerdt et al., 1982]. However, large-scale models of vocanic loading [Willemann and Turcotte, 1982; Banerdt et al., 1982] predict extensional fractures radiating from the center of Tharsis, generally consistent with many of the observed tectonic features.

Isostatic uplift models can also account for the present gravity and topography of Tharsis [Sleep and Phillips, 1979] as well as the distribution and type of some of the tectonic features in the region [Banerdt et al., 1982; Sleep and Phillips, 1985]. A purely thermal explanation for this uplift can be excluded because unreasonably large thermal anomalies (~ 3000°C) extending to great depths (~ 300 km) and persisting for billions of years would be required [Solomon and Head, 1982], but a compositional difference is a possible explanation [Sleep and Phillips, 1979, 1985]. The distribution of

extensional tectonic features in the Tharsis region appears to require distinct episodes of local isostatic support of the Tharsis rise and of partial support of the downward load by the finite strength of the Martian lithosphere; the temporal ordering of these episodes is not presently resolvable from the tectonics [Banerdt et al., 1982; Sleep and Phillips, 1985].

The second largest volcanic province on Mars lies in the Elysium region. Like the Tharsis region, the Elysium province is marked by both a topographic rise and a broad free-air gravity anomaly [Sjogren, 1979; Janle and Ropers, 1983]. The Elysium region also exhibits a complex assortment of tectonic and volcanic features. In this chapter we test the hypothesis that the tectonic features in the Elysium region are the product of stresses produced by loading of the Martian lithosphere.

We begin with a brief description of the physiographic features in the Elysium region which are of probable tectonic origin. We then test the hypothesis that these features are the product of loading of the lithosphere. We consider loading at three different scales: local volcanic loading (individual shields), regional loading of the lithosphere from above or below (at the scale of Elysium Planitia), and quasi-global loading by Tharsis. By comparing the predicted stress fields from such models with the distribution and orientation of tectonic features, we evaluate the relative importance of loading at these different scales, we constrain the mechanical properties of the Martian lithosphere, and we offer a step

toward a general understanding of the evolution of major volcanic provinces on Mars.

GEOLOGIC SETTING

The Elysium region (Figure 1) is the second largest volcanic province on Mars [Carr, 1973; Malin, 1977]. It consists of a broad topographic high, 2400 by 1700 km in extent and centered at about 25°N, 212°W , rising about 4 km above the 6.1-mbar reference equipotential surface [Batson et al., 1979]. On top of this rise sit the three volcanoes Elysium Mons, Hecates Tholus and Albor Tholus. The volcanic and tectonic characteristics of the region have been discussed by Scott and Allingham [1976], Malin [1977], and Mouginis-Mark et al. [1984].

On the basis of crater density, volcanic activity in the Elysium region ceased prior to the time of most recent activity in the Tharsis region. The plains of Elysium are more densely cratered than their Tharsis counterparts [Neukum and Wise, 1976; Malin, 1977]. Plescia and Saunders [1979] found that Elysium Mons has the oldest surface of the three volcanoes in the region, with Hecates Tholus younger, and Albor Tholus the youngest. Their area of study was limited to the summits of the volcanoes, however. Neukum and Hiller [1981] concluded that the crater densities on the Elysium Mons shield and adjacent lava plains indicate that flank activity on Elysium Mons may have continued for a significant time after summit activity ceased. The time of last volcanic activity in the Elysium region is poorly constrained, but the surfaces of the

three volcanic shields are estimated to be at least 1.0 b.y. old according to diverse models of the Martian cratering flux [Plescia and Saunders, 1979].

A broad positive free-air gravity anomaly is associated with the Elysium region. The anomaly is nearly centered over Elysium Mons, but is much broader than the volcano itself [Sjogren, 1979]. Gravity models of Janle and Ropers [1983] suggest that the topography of Elysium is isostatically compensated at wavelengths of 1000-2000 km. The fact that the topographic rise and gravity anomaly have persisted for so long after the cessation of volcanic activity suggests that a principally thermal mechanism for the origin of the present broad topographic rise of Elysium is unlikely [Solomon and Head, 1982].

Also found in the Elysium region, primarily to the northwest of Elysium Mons, are a number of sinuous depressions. Some of these features strongly resemble lunar sinuous rilles [Carr, 1981]; others are wide and channel-like, presumably erosional or fluvial in origin [Sharp and Malin, 1975; Malin, 1976; Mouginis-Mark and Brown, 1981; Carr, 1981; Baker, 1982; Mouginis-Mark et al., 1984]. Possible modes of formation that have been suggested for these types of features include lava erosion [Hulme, 1973, 1982; Carr, 1974b] and catastrophic melting of permafrost [Milton, 1973; Baker and Milton, 1974; Sharp, 1980; Baker, 1982]. Because these sinuous features do not have a significant tectonic component to their origin, they are not considered further here.

TECTONIC FEATURES IN ELYSIUM

A number of physiographic features in the Elysium region either are of tectonic origin or have likely been influenced by tectonic stress during their formation (Figure 1). These features may be grouped into four categories on the basis of morphology and location [Hall et al., 1983]: fractures concentric to Elysium Mons, narrow linear features, wide depressions, and ridges. Each type of feature is described in greater detail below. Identification of each feature was made using U.S.G.S. controlled photomosaics (Elysium quadrangle, and portions of Amenthes and Cebrenia quadrangles) and selected Viking Orbiter photographs.

Fractures concentric to Elysium Mons

An extensive set of concentric fractures and graben generally encircle Elysium Mons at distances of approximately 150 to 350 km from the volcano center (Figure 2). Some of these faults, particularly those to the west of the volcano, are quite fresh and sharply defined and apparently postdate the most recent volcanic units they cut. Others appear to have been mantled or partially buried by subsequent volcanic deposits. Because Elysium Mons is surrounded asymmetrically by geologic units of different ages [Mouginis-Mark et al., 1984] and because of the difficulty in assigning even relative ages to "inherited" fractures, differences in apparent freshness of the fractures and graben cannot be attributed solely to differences in the age of the features. On the basis of photogeologic mapping, Mouginis-Mark et al. [1984] conclude

that most of the circumferential fracturing occurred after formation of the intermediate-stage volcanic unit (the compound plains) but before the end of late stage effusive flank activity on Elysium Mons. One indication of this relationship is the fact that several fractures and graben on the lower flanks of Elysium Mons are truncated by the youngest major volcanic unit (the flood lavas).

The fractures concentric to Elysium Mons are consistent with the hypothesis that failure of the elastic lithosphere occurred in response to the load imposed by the volcanic construct [Thurber and Toksoz, 1978; Comer et al., 1985]. No comparable graben surround the other two volcanoes, but these constructs have been partially buried by extensive lava flows from the vicinity of Elysium Mons [Mouginis-Mark et al., 1984]. Any early episodes of fracturing around Hecates Tholus and Albor Tholus could thus have been obscured by these later flows.

Narrow linear depressions

A number of linear depressions in the Elysium region are sufficiently narrow so that they show no discernible floor in Viking Orbiter photographs (Figure 3). These features have a predominantly NW-SE trend. This category can be broken down into two subsets: the first consists of the narrow linear depressions of the Elysium Fossae (Figure 1), many of which are closely associated with erosional features such as braided channels. The second subclass includes a number of long, narrow depressions which in general have been previously

identified as faults: Hephaestus Fossae [Schumm, 1974; Hiller, 1979], Cerberus Rupes [Scott and Allingham, 1976; Scott and Carr, 1978], and the polygonal fracture set west-southwest of Elysium Mons (Figure 4). This category also includes two fractures which cut across the shield of Albor Tholus and are approximately, but not precisely, concentric to Elysium Mons. Their extreme distance from Elysium Mons and the fact that they are isolated from the rest of the concentric fracture systems, however, suggest that these features are unrelated to those in the first category. That we have grouped this assortment of features into a single category does not necesarily imply that they all have a single mode of origin.

Carr [1980, 1981] has suggested that many of the Elysium Fossae are of tectonic origin or tectonically controlled, but their association with the braided channels and other erosional features of northwest Elysium indicates that they have at the very least been modified by erosional processes. Possible modes of origin and modification, in addition to faulting, include collapse of lava tubes and subsidence along linear fracture zones due to melting of ground ice or magma withdrawal [Sharp and Malin, 1975]. The development of some Martian channels formed by erosional processes may have been guided by pre-existing fractures [Sharp and Malin, 1975]. Thus, even if some of the channels included in this category are of volcanic or fluvial origin, their consistent orientations may nonetheless be indicative of, and controlled by, the direction of the regional stress field at the time of their formation.

We also recognize the possibility, however, that some of the features in this category are not of tectonic origin at all, but rather are erosional features whose consistent orientations may reflect the direction of maximum topographic slope at the time of their formation [P.J. Mouginis-Mark, personal communication, 1983].

For the purposes of this paper we have taken as tectonic or tectonically controlled those narrow linear depressions lacking obvious signs of fluvial or volcanic activity. Sinuous rilles and systems of braided channels, for example, are excluded from this category. We assume that the mode of origin is less important than the consistent orientation of these features, which is taken to be indicative of the regional stress field.

Wide depressions

Nine flat-floored depressions with straight walls and widths up to 15 km are found in the Elysium region (Figures 5 and 6). Although these features have characteristics much like graben [Carr, 1980, 1981; Carr and Clow, 1981], it is not clear that they are entirely of tectonic origin. As with some of the narrow linear depressions, they may have been modified by volcanic or fluvial activity. Five of the depressions are found in the Elysium Fossae region to the west of Elysium Mons, while four are found to the east. All have a predominantly NW-SE trend. For the purposes of constraining stress models we treat these features as indicative of the orientation of the stress field at the time of their formation, despite their

possible later modification by fluvial or lava flow processes.

One such depression, 230 km long and 15 km wide, is located to the west of the Elysium Mons shield and is concentric to it (Figure 6). Its association with the concentric fracture system around Elysium Mons strongly suggests that it may be of tectonic origin or tectonically controlled. Because it is oriented approximately perpendicular to the topographic gradient, the depression is unlikely to have been formed solely by material flowing downslope. The feature may have originated as a member of the concentric fracture system and been subsequently modified.

Ridges

A system of ridges (Figure 7), similar to lunar mare ridges [Saunders and Gregory, 1980; Maxwell, 1982; Chicarro et al., 1983], is found at the eastern edge of Elysium Planitia (Figure 1), where the volcanic plains material merges with the older terrain of the Phlegra Montes [Gifford, 1981; De Hon, 1982]. The ridges are oriented approximately north-south, and the majority are located between latitudes 15°-40°N and longitudes 180° - 205°W [Gifford, 1981; Chicarro and Schultz, 1984].

Ridges such as these are taken to be evidence of horizontal compression of near-surface material [Howard and Muehlberger, 1973; Muehlberger, 1974; Lucchitta, 1976, 1977; Sharpton and Head, 1982a, 1983]. In the case of lunar mare basins, ridges can form as a result of the lithospheric compression and subsidence that accompanies loading of the

lithosphere by mare basalt material; load-induced stresses may perhaps be supplemented by a modest compressive stress field of global extent [Solomon and Head, 1979, 1980]. On Mars, the pattern of ridge systems suggests that they are more likely to be the result of larger scale regional or global stresses than of strictly local stresses [Maxwell and Gifford, 1981]. In particular, Martian ridge systems may be related to ancient impact structures [Schultz, 1984] or to a large-scale stress field, such as that generated by loading in the Tharsis region [Maxwell, 1982; Chicarro and Schultz, 1984; Watters, 1984]. The planet-wide predominance of north-south ridge orientations [Lucchitta and Klockenbrink, 1981; Gifford, 1981] has led some researchers to suggest that they are the product of a global compressive stress field, such as one generated by planetary thermal contraction [Solomon, 1978] or tidal despinning [Melosh, 1977]. According to Chicarro and Schultz [1984], the Elysium ridges are not concentric to the volcanic center, but rather to a center lying to the east of the constructs, possibly related to an ancient impact structure whose presence is inferred by Schultz [1984] from the distribution of massifs, knobby terrains, and scarps in the region. The fact that the ridges are found only on the eastern side of Elysium, in the direction of the Tharsis province, also suggests that the formation of the Elysium ridge system may have been influenced by tectonic processes in the Tharsis region.

In addition to the major ridge system in the eastern part of the Elysium province, there is a line of six mare-type ridge segments extending approximately 625 km across southwest

Elysium Planitia, trending northeast-southwest (Figure 1). Isolated narrow ridge segments are also found on the Elysium Mons shield [Malin, 1977; Gifford, 1981; Mouginis-Mark et al., 1984] and adjoining the edge of Hecates Tholus [Gifford, 1981]; because these isolated ridges do not closely resemble lunar mare ridges and are likely to be the result of local lava flow processes [Gifford, 1981], we have not included them as potential constraints on models of lithospheric stress.

STRESS MODELS

Our working hypothesis is that the tectonic features of the Elysium region are the result of stresses caused by loading of the lithosphere. The hypothesis that large-scale tectonic features associated with volcanic regions of the terrestrial planets are products of the flexural response to loading of the lithosphere has proven to be a fruitful approach for constraining the tectonic history of lunar mare basins [Melosh, 1978; Solomon and Head, 1979, 1980; Comer et al., 1979] and the regions surrounding individual Martian volcanoes [Thurber and Toksoz, 1978; Comer et al., 1985]. As noted earlier, this hypothesis can also account for the distribution and origin of many of the tectonic features in the Tharsis province [Willemann and Turcotte, 1982; Banerdt et al., 1982; Sleep and Phillips, 1985].

We anticipate that the present topography and the free-air gravity anomaly of the Elysium region are primarily the results of construction by volcanic material and of the response of the

lithosphere to this volcanism, including a possible contribution to the support of the volcanic load by finite lithospheric strength. Because the topographic and gravity anomalies of the Elysium region have survived for roughly 3.5 billion years since the cessation of volcanic activity [Plescia and Saunders, 1979], it is unlikely that the topography of the region is being supported at present by a thermal anomaly or by dynamic mantle processes [Solomon and Head, 1982]. While some of the tectonic features may have been formed in response to the present distribution of stresses, we also evaluate the hypothesis that some features may have formed during an early episode of uplift of the Elysium region.

We consider as specific models the load imposed by Elysium Mons, regional loading on the scale of Elysium Planitia and the other volcanoes, and the quasi-global loading of the Tharsis rise. For the loads of individual volcanoes, we use the theory of Brotchie and Silvester [1969] and Brotchie [1971] for flexure of a thin elastic shell overlying an inviscid fluid interior in response to an axisymmetric load. Because the flexure equation is linear, the stresses due to any distributed load can be represented by the superimposed stresses due to an equivalent distribution of circular loads. We use this approach to determine the stress distribution predicted by regional loading models, including the models proposed by Janle and Ropers [1983] to fit line-of-sight gravity data. For the Tharsis load, we use the spherical harmonic solutions of Banerdt et al. [1982] for displacement and stress in a thick elastic spherical shell given the topography and gravity.

The elastic theories used in these stress calculations are clearly idealizations of actual mechanical behavior, and it is important to recognize the limitations of these simplified descriptions of the stress field. Several distinct limitations of the theory may be identified. The local and regional stress models are based on thin shell theory and are valid only for loads of horizontal dimension small compared to the planetary radius. For all models, perfect elasticity is assumed for the lithosphere. Further, for each type of model the lithosphere is taken to have a uniform thickness or flexural rigidity. Such time-dependent effects as viscoelasticity and load growth are ignored. Finally, loads estimated from present topography and gravity need not be correct representations of loads at the time of formation of ancient tectonic features. In addition to these limitations on the model, of course, are uncertainties introduced by errors in topography and gravity and by imperfect and variable preservation of tectonic features. We discuss each of these limiting factors in turn.

The elastic flexure theory of Brotchie and Silvester [1969] and Brotchie [1971] is valid only for thin elastic shells and only for loads of small horizontal extent compared with the radius of curvature of the shell. The thin shell approximation is not a serious source of error for local loading problems [Melosh, 1978; Pullan and Lambeck, 1981; Comer, 1983], however, even for lithosphere several hundred kilometers in thickness such as that in the vicinity of Olympus Mons [Thurber and Toksoz, 1978; Comer et al., 1985]. The

approximation of horizontally limited loads in the Brotchie formulation of flexure presents no problem for individual volcanoes, which have diameters much less than the radius of curvature of the lithosphere. This approximation may introduce a small error, however, for loads on the scale of Elysium Planitia. Uncompensated portions of the volcanic load of Elysium Planitia may have a lateral dimension as great as 900 km, or 15° of arc [Janle and Ropers, 1983].

The assumption that the lithosphere behaves perfectly elastically does not take into account the fact that brittle fracture of the lithosphere (as demonstrated by the observed tectonic features) has acted to reduce stress. For the more plausible rheological models in which strength varies with depth [e.g., Goetze and Evans, 1979; Brace and Kohlstedt, 1980], however, the stress differences induced by flexure are supported by an elastic "core" of the plate even after near-surface failure, and the effective flexural rigidity is similar to that of the elastic core.

There may also be significant lateral variations in strength or in lithosphere thickness. If there are important variations in the thickness of the elastic lithosphere, then estimates of lithospheric thickness derived from a comparison of model predictions with observed tectonic features will be intermediate between the extremes in actual values [Pullan and Lambeck, 1981]. The models employed here do not include any zones of weakness in the lithosphere, which can act to concentrate deformation and faulting [e.g., Sykes, 1978].

The stress models of this paper are based on the premises that the volcanic load is emplaced instantaneously and does not change over time, neither of which is correct. Several time dependent effects have been considered by Comer et al. [1985] for the problem of loading by individual volcanoes, including an increase in the size of the volcanic load with time, lithospheric viscoelasticity, and a thickening of the elastic lithosphere with time. They found that neglect of load growth probably introduces the most serious source of error for the estimation of lithospheric thickness, because of the change in the distribution of stress and particularly the increase in stress magnitudes as the volcano grows. This problem can be minimized by considering only tectonic features comparable in age to the youngest constructional phase of the volcano [Comer et al. 1985]. In the Elysium region it is possible to identify concentric fractures on the youngest geologic unit around Elysium Mons, but over the rest of the region there is little detailed information about even the relative ages of the units on which tectonic features are found.

A somewhat related problem of temporal variability is that present topography and gravity must be used to constrain models for the stress fields that apparently gave rise to ancient tectonic features [Solomon and Head, 1982]. This is a particular difficulty for stress models [e.g., Banerdt et al., 1982] in complex tectonic provinces such as Tharsis, where many tectonic features predate the eruption of significant volumes of volcanic material. The simpler volcanic and tectonic

history of the Elysium province should lessen the impact of this problem on the models considered in this chapter.

The gravity and topographic data which provide the basis for our models also carry uncertainties. Recent earth-based radar measurements of Martian topography [Downs et al., 1982] indicate elevations substantially different from those on earlier U.S.G.S. topographic maps [Batson et al., 1979]. For the Elysium region, however, the difference is a nearly uniform downward shift of 1.7 km with little change to the shape of the topographic relief [Janle and Ropers, 1983]. Errors in estimated gravity anomalies are reflected primarily in the magnitudes of the loads adopted here and not in their relative areal distribution.

Elysium Mons Loading

We consider first the hypothesis that the circumferential fractures surrounding Elysium Mons are the product of flexure of the lithosphere in response to that load. For a simple model of the Elysium Mons load, Comer et al. [1985] found the thickness of the elastic lithosphere that predicts the distribution of deviatoric stresses most consistent with the observed distribution of concentric graben.

In this section we consider modifications to the assumed load model for Elysium Mons, and we assess the sensitivity of the predicted value of the elastic lithospheric thickness. We also evaluate the hypothesis [Solomon, 1985] that flexurally induced failure can account for the widths and inferred faulting depths of concentric graben.

For this type of calculation, the magnitude of the load is not critical, but a reliable model of the areal distribution of the load is essential. Determination of the areal distribution of the Elysium Mons load, however, is somewhat complicated by the fact that the Elysium Mons shield in many areas displays a gradual boundary with the surrounding plain, making precise estimates of the horizontal dimensions of the shield difficult. Further, the graben system is not concentric to the volcanic caldera, but rather to a point about 30 km to the north of the caldera center.

To estimate the size of the load-contributing portion of the shield, we have considered Viking Orbiter photographic evidence for the location of the shield boundary, the geologic boundary units as drawn by Mouginis-Mark et al. [1984], and the topographic contour data of Blasius and Cutts [1981]. We have excluded from consideration the thin mantle of lava flow material that can be traced for hundreds of kilometers from the caldera [Blasius and Cutts, 1981]. The shield radius estimated from photogeological considerations (r= 110 ± 10 km) coincides quite closely with an estimate derived from the 2-km elevation contour of Blasius and Cutts [1981] (r= 106 ± 12 km). Janle and Ropers [1983] used a uniform disk of similar dimensions (r= 105 km) for their calculations of the gravitational attraction of the volcano.

Comer et al. [1985] adopted as a model of the Elysium Mons load a stack of 20 coaxial disks simulating a conical volume and centered on the apparent center of fracturing; the largest

disk had a basal radius of 110 km and the total excess mass was 5.4 x 1020 g, obtained from the volume of the shield [Blasius and Cutts, 1981] and a scaling of excess mass to volume equal to that of Arsia Mons [Sjogren, 1979; Blasius and Cutts, 1981]. Using this model, Comer and coworkers formally inverted the range in radial distances of faults in the youngest major volcanic unit surrounding the shield, following the procedure of Comer et al. [1979]. They obtained a local thickness of the elastic lithosphere of 54 ± 6 km, with a formal lower bound of 48 km and a conservative upper bound of 110 km. The stress distribution for this model is shown in Figure 8a. A second model, with 20% of the excess mass contributed by a wider basal disk (r = 120 km), showed no significant difference in the predicted surface stresses.

The axially symmetric load model of Comer et al. [1985] is an idealized representation of the actual geometry of Elysium Mons, because it neglects the north-south elongation of the shield [Malin, 1977; Mouginis-Mark et al., 1984]. In an effort to test whether the results of Comer et al. [1985] depend on the assumption of axial symmetry, we have considered an alternative model in which the distribution of the load conforms more closely to the shape of the actual volcano. We used the elevation contours of Batson et al. [1979] as the basis for estimating the north-south elongation of the shield. We fit circles to the contours corresponding to the volcanic shield, and we estimated the coordinates of the centers of these circles. We then interpolated from these latitudes to

obtain the latitudes of a set of 20 disks (of the same radii as those in the coaxial models). The disks at the higher elevations are offset progressively to the south from the center of the largest disk (Table 1). The distance from the center of the northernmost disk to the center of the southernmost disk is 17 km. The stresses due to this load can be calculated by superposition of the stress fields due to the individual disk loads (see below).

This load model (Figure 8b) predicts stresses not significantly different from those of the axially symmetric model of Comer et al. [1985], for the same thickness of the elastic lithospere (Figure 8a). Principal stress directions are similar, and stress magnitudes differ by less than 10 percent. The stress field is thus not sensitive to moderate variations or uncertainties in the areal distribution of the load, and the lithospheric thickness estimate of Comer et al. [1985] is appropriate.

A further test of the hypothesis that the graben concentric to Elysium Mons are the result of flexure may be made by comparing the predicted stress magnitudes with the lithospheric strength. In the upper lithosphere of the terrestrial planets, strength is likely to be limited by friction on pre-existing faults [Goetze and Evans, 1979; Brace and Kohlstedt, 1980]. Byerlee [1968] demonstrated that frictional strength is well approximated by piecewise linear functions of depth under both horizontal extension and horizontal compression, relations that are largely independent

of temperature and rock type. The strength depends on the effective confining pressure, and thus on the presence of pore fluids.

Fluidized crater ejecta, chaotic terrain, and fluvial channels have been cited as evidence for extensive volcano-ground ice interactions within the Elysium region [Mouginis-Mark et al., 1984]. Because there may have been extensive melting of permafrost and ground ice during the time of volcanic activity in Elysium, the strength in both "wet" and "dry" situations should be considered.

If a flexural origin for the concentric graben is correct, then normal faulting should occur at radial positions and over depth intervals for which the flexural extensional stress exceeds the frictional strength [Solomon, 1985]. Golombek [1979] has proposed a simple rule to estimate the maximum depth of extensional faulting from graben widths. This method is based on the assumptions that the graben are the product of simple extension, that the faults bounding the graben dip at approximately 60°, and that faulting does not extend below the projected intersection at depth of the two faults. We measured graben widths at nine locations on six different graben (Figure 9). The measurement points are located 150 to 215 km from the load center; they are distributed around Elysium Mons from the northeast (N30°E) to the southwest (S30°W). Graben widths and wall widths were measured from Viking Orbiter photographs (VO541A30, VO844A19, VO846A16). Graben widths range from 1.0 ± 0.5 km to 3.0 ± 0.5 km. Wall widths in all

cases (both measured directly and determined by subtracting the floor width from the total graben width) were approximately 0.50 ± 0.25 km.

The inferred maximum depth of faulting ranges from 0.3 to 2.1 km for the various graben considered. These estimates have large uncertainties, however, particularly associated with uncertainties in the dip angles of the bounding faults. For assumed uncertainties of 10° in the fault dip and 5° in the slope of the graben walls, the range of possible fault intersection depths varies from 0.1 - 1.6 km for the narrowest graben measured to 0.6 - 5.1 km for the widest graben.

For each graben, the maximum depth of faulting may be compared to the depth at which flexural stresses fall below the extensional strength. The flexural stresses, including both bending and membrane stress contributions, are taken from the loading model for Elysium Mons of Comer et al. [1985]. As a rough measure of the uncertainties in the predicted stresses, we repeated the flexure calculations with a fixed flexural parameter while varying Young's modulus E and the load q by factors of 2 and 1.5, respectively, greater than and less than the values assumed by Comer et al. [1985]. These values represent our best estimate of uncertainties in the values of E and q.

One such comparison for one of the widest graben is shown in Figure 10. While the inferred maximum depth of normal faulting is somewhat shallower than that predicted from the intersection of the flexural stress distribution and Byerlee's

law for extensional strength under "dry" conditions, the two predicted depths agree to within the estimated uncertainties in both the maximum fault depth and the flexural stress magnitudes. If the difference in these depths is real, it may be due to partial release of stress by the formation of neighboring graben, finite extensional strength of relatively unfractured surficial volcanic material, or a superposition of stresses from other sources. In all cases the faulting depth predicted from the intersection of the flexural stress curve with the extensional strength distribution under "wet" conditions is greater than that inferred from graben geometry. This comparison suggests that the depth of faulting inferred for the formation of concentric graben is consistent with a flexural origin as long as there was no significant reduction of maximum effective pressure by near-surface pore fluids during the period of graben formation. However, because of the large uncertainties in the predicted flexural stresses, the presence of pore fluids cannot be completely excluded.

Regional-scale loading

The equations for stresses due to an arbitrary surface load $q(\underline{r})$ on a thin elastic shell were developed in Chapter 3. A number of different combinations of loads for Elysium Planitia volcanic units and constructs were examined (Table 2). Each of these individual loads corresponds to a surface excess mass in the gravity models of the Janle and Ropers [1983] for the Elysium region. The Elysium Mons and Hecates Tholus loads correspond to the disc loads TD5 and TD4 of Janle and Ropers

[1983], except that the excess mass for Elysium Mons is the slightly larger value assumed by Comer et al. [1985]. A separate load might also have been considered for Albor Tholus, but we did not do so because of its small size; its volume is less than that of Elysium Mons by nearly a factor of 20 [Blasius and Cutts, 1981]. The Elysium Planitia loads are based on topographic relief and correspond to the disc loads TD1-3 and TD6-7 of Janle and Ropers [1983]. Cylindrical discs, however, are poor approximations to the areal load distribution for loads of horizontal dimension at least comparable to the local flexural length. We therefore represented each load by a stack of cylinders approximating a cone for individual volcanoes and a truncated cone (or beveled disc) for larger volcanic units. In all of these representations, the total excess mass is preserved.

The stress field for one such regional load model is shown in Figure 11. The model includes loads for Elysium Mons and Hecates Tholus and a load (JR1 in Table 2) equivalent to about a 1.5-km-thick basalt unit over central Elysium Planitia. This model corresponds to the least compensated of the three-disc gravity models of Janle and Ropers [1983]. We also tested models with additional loads (Table 2). For each load model, stress fields were calculated for a range of values for the thickness of the elastic lithosphere.

All models with thicknesses of the elastic lithosphere less than approximately 150 km predict regional stresses of large magnitude, with the greatest extensional stress oriented

approximately radial to the center of mass of the total load (a point between Elysium Mons and Hecates Tholus). Such a stress field would give rise to strike-slip faulting. In the presence of additional stresses, graben circumferential to the Elysium rise or compressive features oriented approximately radial to the rise might also be produced. In addition, the simple model of Figure 11 fails to predict concentric graben around Elysium Mons at the distances observed, because the stress field in the vicinity of the shield is dominated by the compressive stress field of the regional Elysium Planitia load.

Janle et al. [1984] have made stress calculations similar to that shown in Figure 11. They have argued that such stress fields can account for the formation of the tectonic features in Figure 1, and they proceeded to make further inferences as to the thickness of the lithosphere and its lateral variation. In their comparison of predicted stresses with tectonic features, however, Janle et al. [1984] examined only the second invariant of the deviatoric stress tensor, which is a measure only of the magnitudes and not the directions of the principal deviatoric stresses. Although the regional stress models for thickness of the elastic lithosphere less than about 200 km do predict stress differences sufficient to induce faulting at shallow depths [Brace, 1964; Brace and Kohlstedt, 1980], the calculated stress trajectories are not consistent with the orientations and types of tectonic features observed.

We recognize the possibility that our loading models, based on the approximation of Brotchie [1971] in which the

dimension of the load is small compared with the planetary radius, will tend to underestimate the magnitude of membrane stresses for loads of large lateral extent. Turcotte et al. [1981] and Willemann and Turcotte [1981, 1982] have emphasized the importance of membrane stresses in the support of lithospheric loads on the terrestrial planets. Their analysis shows that membrane stresses act to support topography of long wavelength, while bending stresses are dominant in the support of short-wavelength topography. For each planet, the transition between bending-dominated and membrane-dominated stress fields depends on lithospheric thickness. They concluded that for Mars membrane stresses may be important in the support of loads with horizontal dimensions greater than about 2000 km [Willemann and Turcotte, 1981]. While the Elysium rise has approximately this dimension, the portion of the rise that may exert a load on the lithosphere is substantially smaller in extent, perhaps 900 km across [Janle and Ropers, 1983]. The analysis of Willemann and Turcotte [1981] indicates that for a load of this dimension the membrane stresses are not likely to be dominant in support of the load.

As a further check on the Brotchie [1971] formulation, we compared the calculated stress field with the stresses that would be predicted according to the model of Turcotte et al. [1981] in which membrane stresses are the sole source of support for the load. For a topographic load of the form

$$h = h_{oe}-(\phi/\phi o)^2 \qquad (1)$$

where ϕ_o is the angular radius of the load and h_o is the height of the topography at the center of the load, the radial and azimuthal components of the membrane stress field, in nondimensional form and positive in extension, are given by [Turcotte et al., 1981]

$$\begin{aligned} \bar{\sigma}_r &\equiv \frac{T(1+\tau)\sigma_r}{R\tau\rho_c g h_o} = -\frac{1}{2}\left(\frac{\phi_o}{\phi}\right)^2 \left[1 - e^{-(\phi/\phi_o)^2}\right] \\ \bar{\sigma}_t &\equiv \frac{T(1+\tau)\sigma_t}{R\tau\rho_c g h_o} = -e^{-(\phi/\phi_o)^2} + \frac{1}{2}\left(\frac{\phi_o}{\phi}\right)^2 \left[1 - e^{-(\phi/\phi_o)^2}\right] \end{aligned} \tag{2}$$

where R is the planetary radius, ρ_c is the crustal density, T is the thickness of the elastic lithosphere, g is the gravitational acceleration, and τ is the dimensionless quantity $\tau = Ed/[R^2 g(\rho_m - \rho_c)]$, where E is the Young's modulus of the lithosphere and ρ_m is the density of the mantle. The advantage of the nondimensional forms $\bar{\sigma}_r$ and $\bar{\sigma}_t$ is that they are not functions of the model parameters T, ρ_c, τ, and ϕ_o, but only of the distance ϕ/ϕ_o. Once $\bar{\sigma}_r$ and $\bar{\sigma}_t$ are known as functions of ϕ/ϕ_o, it is straightforward to determine dimensional membrane stresses σ_r and σ_t for any set of model parameters.

We have used (2) to calculate stresses due to a load with ϕ_o = 300 km and h_o = 2 km, parameters chosen to provide an approximate fit to the maximum uncompensated portion of Elysium Planitia relief [Janle and Ropers, 1983]. For comparison, we calculated the stresses using the Brotchie [1971] formulation for a load composed of a stack of cylinders of radii 100 to 500 km and with heights chosen to approximate (1). For

identical elastic constants and lithospheric thickness, the stresses predicted by the two models are quite similar (Figure 12). The radial stress components in the two models differ by less than 30%; this difference does not significantly alter conclusions derived from a comparison of predicted stress fields and tectonic features. For the regional Elysium Planitia load, therefore, the thin-shell flexure model of Brotchie [1971] is an acceptable representation of the stress field.

To summarize, we find no evidence in the distribution of tectonic features in Elysium for downward loading of the lithosphere by volcanic units at a regional scale. This implies either that the regional volcanic units are largely isostatically compensated [Janle and Ropers, 1981], or that the uncompensated portion of the load is supported by the strength of a very thick elastic lithosphere. The locally thinner lithosphere under Elysium Mons may be the result of heating associated with the formation of the volcanic shield itself. Similar lateral variations in lithospheric thickness have been estimated for the Tharsis region [Solomon and Head, 1982].

As an alternative to volcanic loading models, we next consider the possibility of flexural uplift on a regional scale. Such a possibility is suggested by the approximately radial trends of many of the extensional features on the Elysium rise (Figure 1). For Tharsis, the radial extensional features are not the consequence of large-scale flexural uplift [Banerdt et al., 1982]; this is because membrane stresses

dominate over bending stresses for lithospheric loads on the large scale of Tharsis [Turcotte et al., 1981; Willemann and Turcotte, 1981, 1982]. At the scale of the Elysium rise, however, the effects of bending stress are quite important and the analogy with plate flexure models is qualitatively appropriate.

A significant difference between our uplift models and those invoked to explain the Tharsis rise is that we are not attempting to match the present topography and gravity of the region with a flexural uplift model. The current topography and gravity are not generally appropriate constraints for models for formation of ancient tectonic features [Solomon and Head, 1982]. Even if regional uplift were responsible for some fracturing in the Elysium region, that uplift is likely to have been concentrated in an early stage in the evolution of the province, one that need not contribute appreciably to the present topographic rise.

The primary constraint on regional uplift models are the positions and orientations of the extensional tectonic features in Elysium Planitia. These features are found out to a radial distance of roughly 500 km from the center of the rise. This suggests that the area of uplift was also on the order of 500 km in radius, because extensional stress is predicted only over the uplifted area. The pattern and magnitude of uplift, or of equivalent upward load on the lithosphere, are otherwise poorly constrained. Presumably this upward load represents an excess pressure exerted on the base of the lithosphere by a mechanism such as thermal expansion of a volume of underlying mantle

material. Flexural uplift of the lithosphere creates stresses which balance the excess pressure; if the uplift is due to differential thermal expansion, the volume of thermally anomalous material and the percent volume change are not separately resolvable.

We have chosen a thickness of the elastic lithosphere of 100 km for the uplift models shown below. This value is largely arbitrary. A thicker lithosphere would require greater excess pressures in order to produce surface stresses of a given magnitude, while a thinner lithosphere would require lower excess pressures.

For an upward lithospheric load equal in magnitude, distribution, and location to the volcanic load JR1 in Table 2, the resulting stress field is generally consistent with the positions of radial extensional features. As shown in Figure 13, the greatest extensional stresses are approximately circumferential to the center of the Elysium rise and are significant in magnitude over the area in which those features are found. The predicted maximum upward deflection of the lithosphere for the assumed values of upward load and lithosphere thickness is approximately 1.0 km. Such an uplift could be the result of mantle thermal expansion for a temperature constrast of about 400°C extending to a depth of 100 km, values not unreasonable in comparison to

thermal anomalies associated with mid-ocean ridges on the earth [Parsons and Sclater, 1977]. Because this model is offered as a mechanism of formation of tectonic features rather than as an explanation of the regional topography and gravity, the thermal anomaly is not required to persist to the present. An uplift model in which the deformation matched the present topography (~ 4 km over the center of the rise) would predict very high several kbar) extensional surface stresses over most of the rise. With such high stresses it is difficult to account for the relatively small numbers of radial extensional tectonic features. It is thus likely that much of the present regional topography is due to construction rather than uplift. Radial fractures produced during an early uplift phase might later serve as preferred sites for fluvial erosion. This idea is supported by the observation of Carr [1981] that the graben-like wide depressions of central Elysium Fossae change downslope into sinuous channels of probable fluvial origin. Also, because the extensional stress field produced over the regional uplift adds constructively to the local extension produced by flexure in response to the Elysium Mons shield, the regional uplift model of Figure 13 is also consistent with the formation of graben concentric to Elysium Mons.

The uplift model of Figure 13 does not reproduce the azimuthal asymmetry in the distribution of extensional features, which are preferentially oriented NW-SE (Figure 1). The observed distribution of faulting could be due to corresponding asymmetries in the distribution of uplift (which

need not match the present topography) or in lithospheric thickness, but there is no means to test these possibilities at present.

Tharsis loading

Finally, we consider the effect on stress in the Elysium region of the long wavelength loading of the Martian lithosphere by the Tharsis rise. We employ the solutions of Banerdt et al. [1982] for displacement and stress in a self-gravitating elastic spherical shell overlying an inviscid fluid interior. Banerdt et al. [1982] use the formulation of Alterman et al. [1959] and Arkani-Hamed [1973], in which a spherical harmonic expansion of the gravity and topography, combined with a model for material properties and density of the medium, yield a representation of the internal deformation field, subject to the assumed spherical harmonic boundary conditions and the isostatic response function. The elements of the stress tensor are derived from the deformation via a generalized Hooke's law operator matrix [Arkani-Hamed, 1973]. For the calculation of stresses at the planetary surface, the operator equation reduces to the relation [W.B. Banerdt, personal communication, 1983]:

$$\begin{pmatrix} \sigma_{\theta\theta} \\ \sigma_{\phi\phi} \\ \sigma_{\theta\phi} \end{pmatrix}_{nm} = \begin{pmatrix} R_{21} & R_{23} \\ R_{31} & R_{33} \\ 0 & R_{63} \end{pmatrix}_{n} \begin{pmatrix} y_1 \\ y_3 \end{pmatrix}_{nm} S_{nm}(\theta,\phi) \qquad (3)$$

where the elements of the operator matrix $\underline{\underline{R}}$ are

$$R_{21} = R_{31} = \frac{2\mu}{r} \frac{(3\lambda + 2\mu)}{(\lambda + 2\mu)}$$

$$R_{23} = \frac{2\mu}{r}\left[\frac{\partial^2}{\partial\theta^2} - n(n+1)\left(\frac{\lambda}{(\lambda+2\mu)}\right)\right]$$

$$R_{33} = -\frac{2\mu}{r}\left[\frac{\partial^2}{\partial\theta^2} + 2n(n+1)\left(\frac{(\lambda+\mu)}{(\lambda+2\mu)}\right)\right]$$

$$R_{63} = \frac{2\mu}{r\sin\theta}\left[\frac{\partial^2}{\partial\theta\partial\phi} - \cot\theta\left(\frac{\partial}{\partial\phi}\right)\right]$$

and where the two components of $\underline{Y}_{nm}$ are the harmonic coefficients of radial and tangential displacement, respectively, S_{nm} is the unnormalized surface spherical harmonic of degree n and order m, and λ and μ are the Lame constants.

The stress models for Tharsis loading of Banerdt et al. [1982] are based on spherical harmonic expansions of gravity and topography to 4th degree and order from Sjogren et al. [1975] and Bills and Ferrari [1978], respectively. At these long wavelengths, there does not appear to be a significant contribution to either the gravity or the topography from the Elysium region. While Banerdt et al. [1982] did not show predicted stress trajectories in the Elysium region, W.B. Banerdt [personal communication, 1983] kindly provided us with the values of $\underline{Y}_{nm}$ for two of their models: their isostatic model and their flexural loading model. With these coefficients, we evaluated (3) by analytic differentiation of the surface spherical harmonics S_{nm}. (This procedure differs slightly from the one employed by Banerdt and colleagues.)

Surface stresses in the Elysium region for the isostatic model for compensation of Tharsis topography [Banerdt et al., 1982] are shown in Figure 14. This isostatic model, taken from Sleep and Phillips [1979], has a mean crustal thickness of 150

km and a (thermal or compositional) lithosphere 400 km thick. The Banerdt et al. [1982] formulation models variations in crustal and lithospheric thickness by using radial and lateral perturbations in density and radial variations in the material properties (see appendix). The stress distribution predicted for the isostatic model in the Tharsis region was shown by Banerdt et al. [1982] in their Figure 3b; these workers argued that the predicted stresses provide a good match to the observed distribution of tectonic features in the central Tharsis region.

In the Elysium region, the isostatic model of Banerdt et al. [1982] predicts that surface horizontal stresses are compressive over the entire area shown in Figure 14 except for the portion west of about 230°W. Between 230° and 248°W the stresses switch from compressional to extensional. The magnitude of the predicted stress difference ($\sigma_1 - \sigma_3$) decreases from east to west across Elysium. Stress differences between 200 and 250 bars are predicted between 180° and 195°W; to the west of about 210°W (including the region of extensional stress), the stress differences are less than 100 bars. In eastern Elysium the direction of maximum compressive stress is nearly E-W and would thus be consistent with the formation of the system of N-S trending ridges in the area (Figure 1). This is also the area in which the predicted stress differences are greatest (though only 200-250 bars). In western Elysium the stress differences are too small to have a significant effect on the formation of tectonic features.

Surface stresses in the Elysium region for the Tharsis flexural loading model of Banerdt et al. [1982] are shown in Figure 15. This model is based on an assumed 150 km thickness for the crust and 200 km thickness for the elastic lithosphere; the predicted stress distribution in the Tharsis region was shown by Banerdt et al. [1982] in their Figure 3c. In the Elysium region, this model predicts large extensional surface stresses in the eastern portion of Figure 13, with maximum extensional stresses oriented approximately N-S to NE-SW . Although these stresses are not consistent with the ridge system in eastern Elysium, they are roughly consistent with the orientation of linear extensional features in southeastern Elysium, including Cerberus Rupes (Figure 1).

In western Elysium, the flexural loading model predicts compressive horizontal stresses, with the direction of greatest compressive stress NW-SE, and the least compressive stress vertical. Such a stress field would not yield the NW-SE-trending extensional features observed in this region, but it might have been responsible for the isolated ridge segments seen in southwestern Elysium (Figure 1).

Combined models

It is, of course, unlikely that only one stress field (local, regional, or global) would be operating in the Elysium region during the time interval in which the tectonic features now visible were formed. Despite the greater surface age of the Elysium shields compared to their Tharsis counterparts, it is likely that the periods of major volcanic activity in the

two provinces overlapped. On the basis of a comparison of crater densities for the surfaces of the Elysium shields [Plescia and Saunders, 1979] with those for faulting centers identified in Tharsis [Plescia and Saunders, 1982], the surface of Elysium Mons appears to postdate the oldest unit cut by Tharsis faulting. The surfaces of Hecates Tholus and Albor Tholus are younger than Elysium Mons, but are still older than the most recent Tharsis faulting identified by Plescia and Saunders [1982]. Thus it is appropriate to consider the superposition of regional and local stress fields with the global-scale stress field due to loading by the Tharsis rise.

In constructing a variety of combined stress models we have also allowed for the addition of a horizontally isotropic stress field, such as would be introduced by planetary thermal expansion or contraction [Solomon, 1978]. This scheme permits an evaluation of principal stress trajectories and magnitudes for any linear combination of stresses due to Tharsis loading, regional and local loading, and horizontally isotropic stresses.

In no case does the stress field predicted by a single combined stress model achieve a simultaneously satisfactory fit to all of the observed tectonic features. There is no reason, of course, to expect that all tectonic features in the region formed contemporaneously. One of the better models consists of the Banerdt et al. [1982] isostatic model for Tharsis together with the regional uplift model and the individual volcanic loads of Elysium Mons and Hecates Tholus (Figure 16). This

model provides a reasonable fit to the ridge system in eastern Elysium, to the graben concentric to Elysium Mons, and at least qualitatively to the linear extensional features of the Elysium Fossae.

DISCUSSION

In this chapter we have tested three scales of lithospheric loading models for the formation of tectonic features of the Elysium region: local models of loading by Elysium Mons, regional models of loading on the scale of Elysium Planitia, and quasi-global models of loading by the Tharsis rise. Our lithospheric flexure calculations and the comparison of flexural stresses with lithospheric strength and the inferred maximum depth of faulting confirm the conclusion of Comer et al. [1985] that the concentric graben around Elysium Mons can be explained as the result of local flexure of an elastic lithosphere about 50 km thick in response to the volcano load.

The volcanic loading models on a regional scale predict stress fields inconsistent with all of the observed tectonic features, suggesting that loading by widespread emplacement of thick plains deposits was not an important factor in the tectonic evolution of the Elysium region, either because regional volcanic units were isostatically compensated without lithospheric loading or because the elastic lithosphere is sufficiently thick that it can support the regional load without surface stresses reaching levels which would cause fracture.

The linear extensional features may be the result of flexural uplift of the lithosphere on the scale of the Elysium rise. A regional uplift model can account for the formation of the linear depressions of the Elysium Fossae, which occur within 500 km of the center of the present topographic rise. The simple circularly symmetric model does not explain the NW-SE trends of the depressions; the asymmetry could be the result of heterogeneities in the lithospheric thickness over the region (with local thinning in the areas where fracturing occurs) or of unmodelled asymmetries in the extent of uplift.

Our attribution of the linear extensional features of Elysium to lithospheric uplift is made not without some irony. It had previously been argued [e.g., Carr, 1973; Scott and Allingham, 1976] that many of the tectonic features of the Elysium province are the result of regional uplift. These earlier arguments, however, were in general based on analogy with the Tharsis region, which is much larger but displays similar types of tectonic features. It is now recognized that at the long wavelengths of the Tharsis rise, radially oriented extensional features are the product of a stress field dominated by membrane stress and inconsistent with an origin by flexural uplift [Willemann and Turcotte, 1982; Banerdt et al., 1982]. For Elysium, the radial extensional features can be explained as the result of bending stresses produced by flexural uplift. It thus appears that while early arguments about the nature of Elysium tectonics were based on a faulty analogy, their ultimate conclusions concerning the origin of

many of the tectonic features may nonetheless have been correct. Previous uplift models for Elysium have in some cases also attempted to account for the current topographic rise and regional gravity anomaly. We make no such claim; because the uplift is called upon only for the origin of linear extensional features, the causative mechanism (such as a mantle thermal anomaly) is not required to have persisted to the present.

We also see some evidence for an influence of Tharsis-generated stresses on the tectonics of the Elysium region, particularly in eastern Elysium. One possibility suggested by our results is that the Elysium ridges may form an outlying western portion of the circum-Tharsis ridge system. While the majority of the Tharsis ridges are found in the eastern part of the province, ridges are found in western Tharsis as well [Maxwell, 1982; Watters and Maxwell, 1983]. Watters and Maxwell [1983] have analyzed cross-cutting relations between ridges and faults in the Tharsis region and have concluded that the ridges formed prior to the formation of the Tharsis radial fracture system. This finding, they suggest, is consistent with the Banerdt et al. [1982] scenario in which the ridges formed during an early isostatic stage in the evolution of the Tharsis province [Watters and Maxwell, 1983; Watters, 1984].

From a study of lunar mare ridges, however, Sharpton and Head [1982b] found that even in cases where the stratigraphic relationships clearly indicate that ridges postdate graben formation, the characteristic ridge morphology is subdued where the ridges and graben cross. This may be due to a change in

the material properties at the graben location, to the influence of graben faults on the near-surface stress field, or to mass-wasting of the depression walls which acts to erase or cover evidence of ridge morphology [Sharpton and Head, 1982b]. By this view, the observation that Tharsis faults appear to cut ridges need not imply that the ridges predate the graben. This ambiguity therefore leaves open the age relationship of the Tharsis models of Banerdt et al. [1982].

The comparison of stress models for Elysium with the preserved tectonic features is consistent with a succession of stress fields operating at different times in the region, but our ability to determine the order in which those stress fields were present is very limited. Because of the apparently limited extent of lithospheric extension in Elysium it is most reasonable to expect that flexural uplift of the lithosphere by a mantle thermal anomaly would have preceded or occurred contemporaneously with emplacement of the volcanic loads. While the ambiguity in relative ages of the different classes of tectonic features is permissive of this scenario, it does not permit its confirmation. The fact that some of the linear depressions in Elysium appear to have been modified by volcanic or fluvial flow processes means that the fracturing that created the original features occurred at least before the last stage of volcanic activity in the region. We also see evidence for a tectonic influence of the two stages of Tharsis evolution postulated by Banerdt et al. [1982]. The Elysium tectonic features do not resolve, however, the question as to which stage of Tharsis evolution occurred first [Banerdt et al., 1982; Sleep and Phillips, 1985].

CONCLUSIONS

A variety of tectonic or tectonically controlled features are present in the Elysium province of Mars, including graben and extensional fractures concentric to Elysium Mons, linear extensional features of several types with a predominantly NW-SE trend, and ridges of compressional origin in the eastern and southwestern parts of the province. All of these classes of tectonic features can be attributed to the response of the Martian lithosphere to loading at three distinct scales: local, regional, and quasi-global. Some temporal variation in the overall stress field is required, since no single combination of loads can account simultaneously for all observed tectonic features.

The distribution of graben concentric to Elysium Mons is consistent with fracturing of an elastic lithosphere approximately 50 km thick in response to the Elysium Mons load. A comparison of flexural stresses with lithospheric strength and with the maximum depth of faulting inferred from graben geometry [Golombek, 1979] provides additional support for this conclusion. We find no evidence for lithospheric loading by volcanic units on the scale of Elysium Planitia, because the predicted directions of the surface principal stresses are not consistent with the observed tectonic features.

The global stress field associated with the support of the Tharsis rise appears to have influenced the development of tectonic features in the Elysium region. The stress field predicted by the isostatic model for Tharsis of Banerdt et al. [1982] is generally consistent with the formation of the ridge

system of eastern Elysium; the flexural loading model for Tharsis [Banerdt et al., 1982] predicts extensional stresses generally consistent with the formation of the Cerberus Rupes system of linear extensional fault scarps and compressional stresses in western Elysium consistent with the formation of the ridges in that area.

The linear extensional features of the Elysium Fossae can best be explained as the result of modest flexural uplift of the lithosphere in the Elysium region, possibly in response to a mantle thermal anomaly beneath the volcanic province. That radial extensional fractures in Elysium can be attributed to lithospheric uplift while such an origin for similar features in Tharsis can be generally excluded [Willemann and Turcotte, 1982; Banerdt et al., 1982] is due to the smaller horizontal dimension of the Elysium province. We conjecture that the earliest tectonic activity in the Tharsis province may also have been the result of lithospheric uplift, but either the scale of such uplift was considerably smaller than the present horizontal extent of the Tharsis rise or the tectonic evidence of this uplift has been long since erased by subsequent volcanism and faulting.

FIGURE CAPTIONS

Figure 1. Sketch map of the Elysium region, showing major volcanic constructs and classes of features discussed in the text. Narrow lines indicate graben and narrow linear features; thicker darkened areas denote wide depressions and volcanic calderas; notched lines indicate ridges; and dotted lines outline the approximate edges of the volcanic shields. "Elysium Planitia" refers to the entire Elysium topographic rise, the boundaries of which are roughly 0°-40°N latitude, 180°-260°W longitude.

Figure 2. Viking Orbiter view of concentric fractures and graben west of Elysium Mons. Frame V0041AR2; width of image is 155 km.

Figure 3. Viking Orbiter view of narrow linear depressions south of Elysium Mons. Frame V0844A21; width of image is 315 km.

Figure 4. Viking Orbiter view of polygonal fractures located southwest of the Elysium Mons caldera. Frame V0844A43; width of image is 294 km.

Figure 5. Viking Orbiter view of wide depression east of Elysium Mons. Frame V0846A17; width of image is 300 km.

Figure 6. Viking Orbiter view of wide depression west-southwest of Elysium Mons. Frame V0844A20; width of image is 260 km.

Figure 7. Viking Orbiter view of ridge in the Phlegra Montes region of eastern Elysium. Frame V0580A09; width of image is 203 km.

Figure 8. Comparison of predicted stresses at the surface of the lithosphere for coaxial (8a) and non-coaxial (8b) models of the Elysium Mons load. Crosses indicate direction of horizontal principal stresses; arrowheads denote deviatoric extension. Dashed contours of the maximum stress difference $\sigma_1 - \sigma_3$ (in kbar) are also shown. Each load model consists of 20 disc loads of magnitude $q = 0.592 \times 10^8$ dyn/cm^2; circles show locations of selected disk loads. The thickness of the elastic lithosphere is taken to be 54 km for both calculations; Young's modulus and Poisson's ratio are assumed to be 10^{12} dyn/cm^2 and 0.25, respectively.

Figure 9. Sketch map of Elysium Mons and vicinity showing locations at which graben widths were measured, and the inferred depths (in km) at which the normal faults bounding each graben would intersect [Golombek, 1979].

Figure 10. Comparison of the maximum depth of faulting during the formation of graben circumferential to Elysium Mons inferred from graben width by the method of Golombek [1979] with that predicted from the intersection of the predicted flexural stress curve with a strength envelope calculated by the method of

Brace and Kohlstedt [1980]. The quantities σ_v and σ_H are the vertical principal stress and the most extensional horizontal principal stress, respectively; both are positive in extension. The extensional strength versus depth z under horizontal extension is shown under both dry and wet ($\lambda = 0.3$) conditions, where λ is the ratio of fluid pressure to lithostatic stress. The flexural stresses are from the Elysium Mons model of Comer et al. [1985] at the appropriate radial distance (r = 220 km), including the effects of uncertainties (indicated by arrows) in Young's modulus for the elastic lithosphere and in the magnitude of the load. The indicated uncertainties in the maximum depth of extensional faulting inferred from graben geometry are due principally to the uncertainty in fault dip. The shaded region indicates overlap in predicted maximum fault depths determined by the two methods.

Figure 11. Principal horizontal stress orientations and maximum stress differences for a load model consisting of Elysium Mons, Hecates Tholus, and a regional load of Elysium Planitia basalts approximately 900 km in horizontal extent (load JR1 in Table 2). The magnitudes of the loads are based on the gravity models of Janle and Ropers [1983]. The thickness of the elastic lithosphere is taken to be 100 km. Circles represent disk loads, with only the largest

disk shown for the individual volcanoes, and with the largest and smallest disks shown for the regional load. See Figure 8 for further explanation.

Figure 12. Comparison of radial (12a) and tangential (12b) stresses for the model of Turcotte et al. [1981], in which membrane stresses provide the sole support of the load, and that of Brotchie [1971], which is dominated by bending stresses. The loads for each model are chosen to provide an approximate fit to the maximum uncompensated portion of Elysium Planitia relief. Stress components are positive in extension. The thickness of the elastic lithosphere is taken to be 100 km, and Young's modulus and Poisson's ratio in the lithosphere are assumed to be 10^{12} dyn/cm^2 and 0.25, respectively.

Figure 13. Principal horizontal stress orientations and maximum stress differences for a model consisting of loading by Elysium Mons and Hecates Tholus superposed on a regional flexural uplift of Elysium Planitia; the upward load is approximately 900 km in extent and equal in magnitude to load JR1 used for the model in Figure 11. The thickness of the elastic lithosphere is taken to be 100 km. See Figure 8 for further explanation.

Figure 14. Principal horizontal stress orientations and maximum stress differences in the Elysium region predicted

by the isostatic model for Tharsis of Banerdt et al. [1982]. See Figure 8 for further explanation.

Figure 15. Principal horizontal stress orientations and maximum stress differences in the Elysium region predicted by the flexural loading model for Tharsis of Banerdt et al. [1982]. See Figure 8 for further explanation.

Figure 16. Principal horizontal stress orientations and maximum stress differences for a superposition of the volcano loading and regional uplift model of Figure 13 and the Banerdt et al. [1982] isostatic model for Tharsis from Figure 12. See Figure 8 for further explanation.

Table 1. Disk geometry in non-coaxial Elysium Mons load model.

Disk	Radius, km	Latitude, °N
1	110.0	25.21
2	104.5	25.21
3	99.0	25.21
4	93.5	25.18
5	88.0	25.14
6	82.5	25.10
7	77.0	25.07
8	71.5	25.04
9	66.0	25.00
10	60.5	24.98
11	55.0	24.96
12	49.5	24.93
13	44.0	24.92
14	38.5	24.94
15	33.0	24.95
16	27.5	24.96
17	22.0	24.96
18	16.5	24.96
19	11.0	24.96
20	5.5	24.96

Table 2. Contributions to Elysium Regional Load Models.

Load	Geometry	Radius, km	Lat., °N	Long., °W	Excess mass, 10^{21} g
Elysium Mons	Cone	100 (base)	25.2	213.5	0.54
Hecates Tholus	Truncated Cone	30 (top), 92 (base)	32.0	209.6	0.22
Elysium Planitia					
JR1	Beveled Disc	450 (top), 500 (base)	26.9	210.4	3.6
JR2	Beveled Disc	630 (top), 700 (base)	26.5	208.0	8.6
JR3	Beveled Disc	900 (top), 1000 (base)	25.5	204.8	8.8
JR6	Beveled Disc	510 (top), 570 (base)	16.5	176.5	1.4
JR7	Beveled Disc	430 (top), 480 (base)	33.8	176.5	1.0

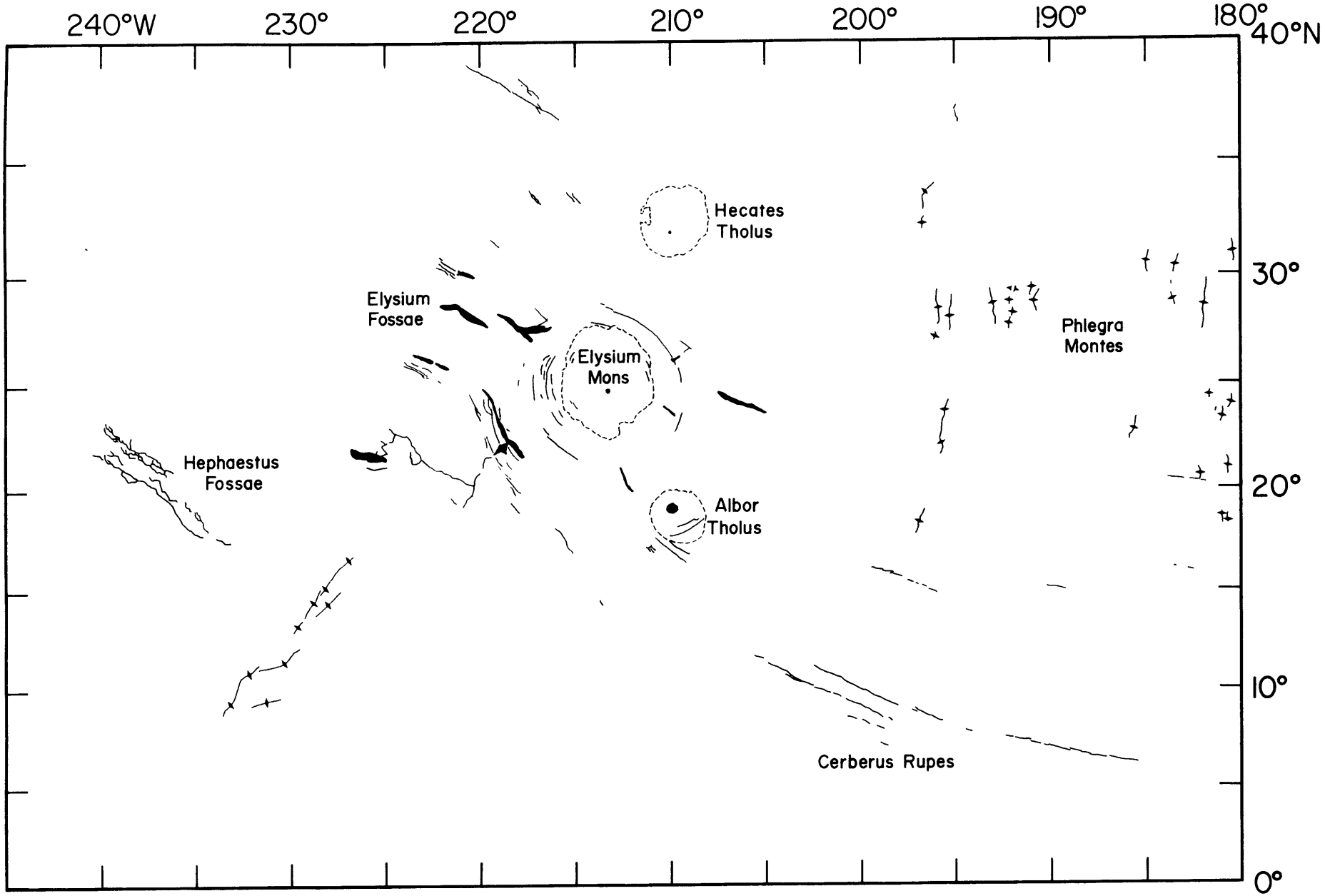
240°W
230°
220°
210°
200°
190°
180°
40°N
30°
20°
10°
0°
Hecates Tholus
Elysium Fossae
Elysium Mons
Phlegra Montes
Hephaestus Fossae
Albor Tholus
Cerberus Rupes

Figure 1

Figure 2

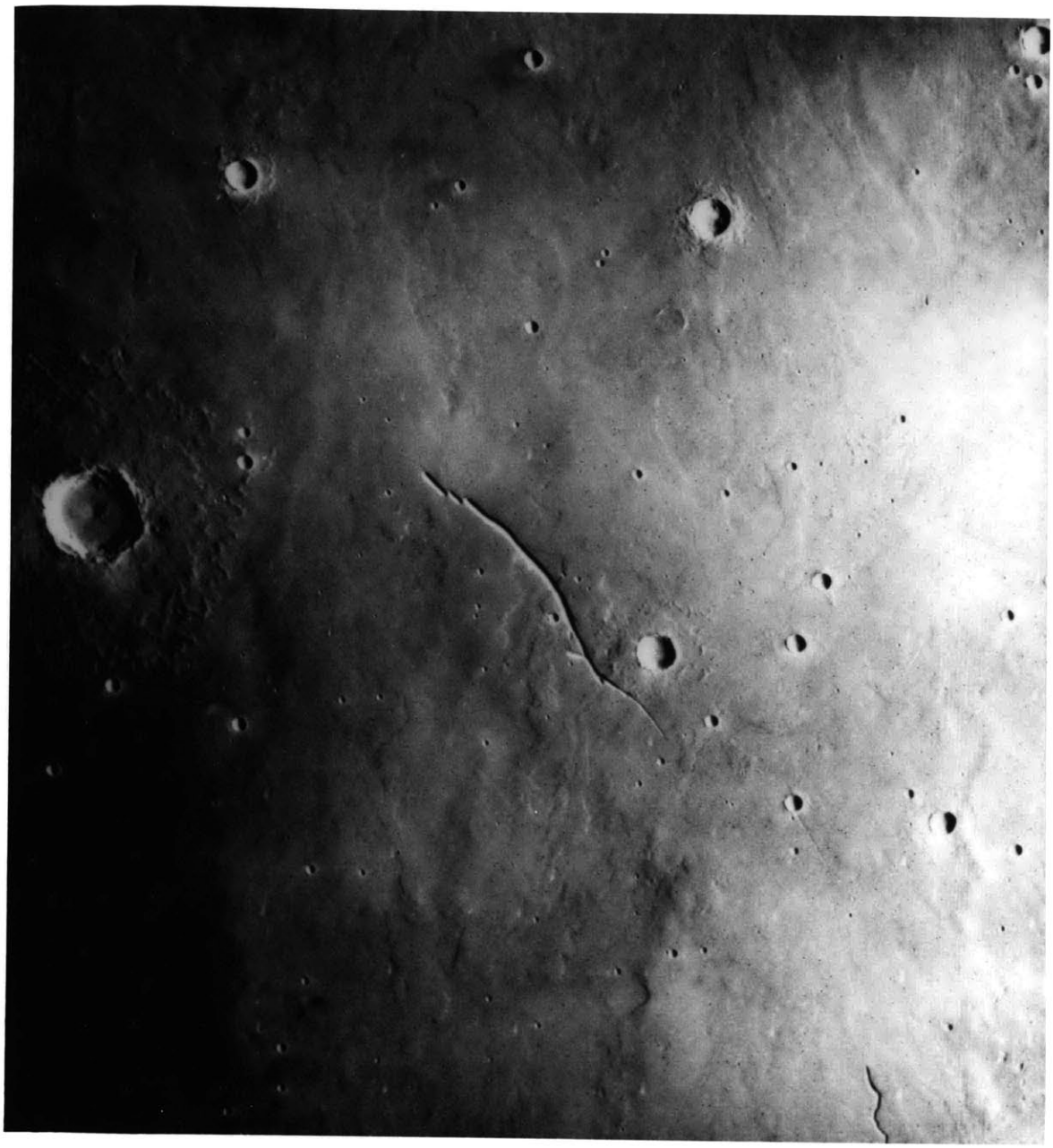

Figure 3

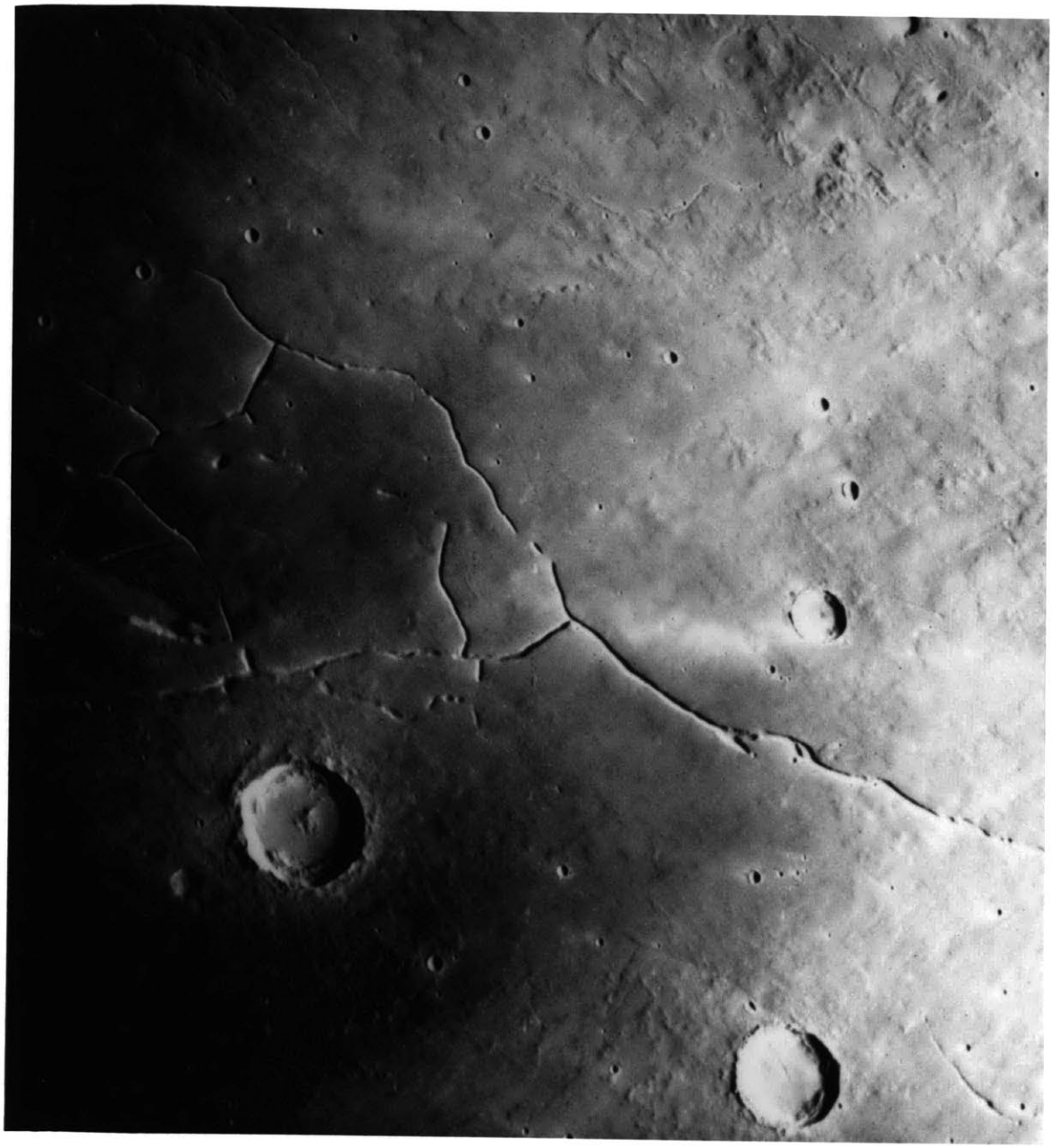

Figure 4

Figure 5

Figure 6

Figure 7

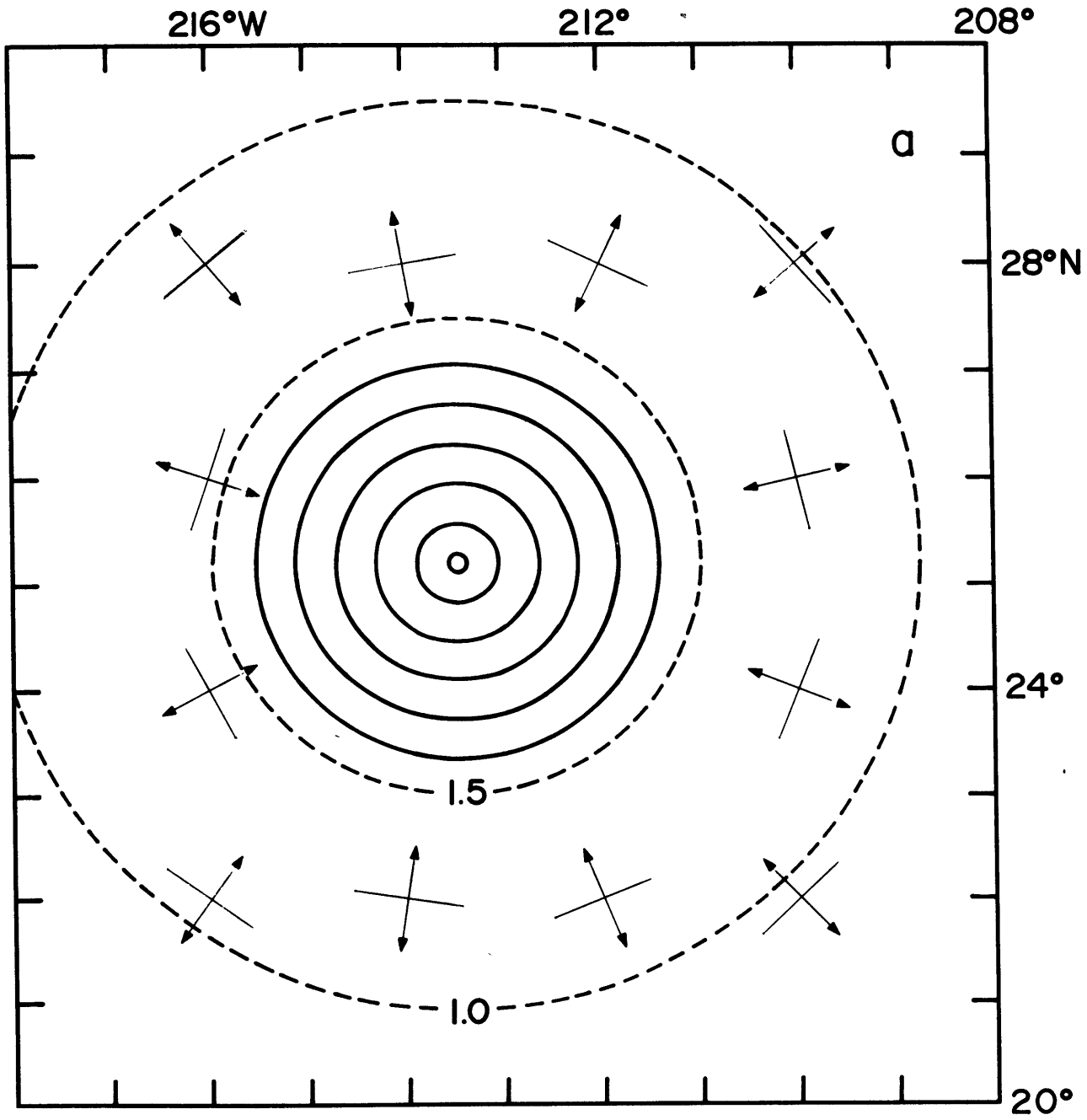

Figure 8a

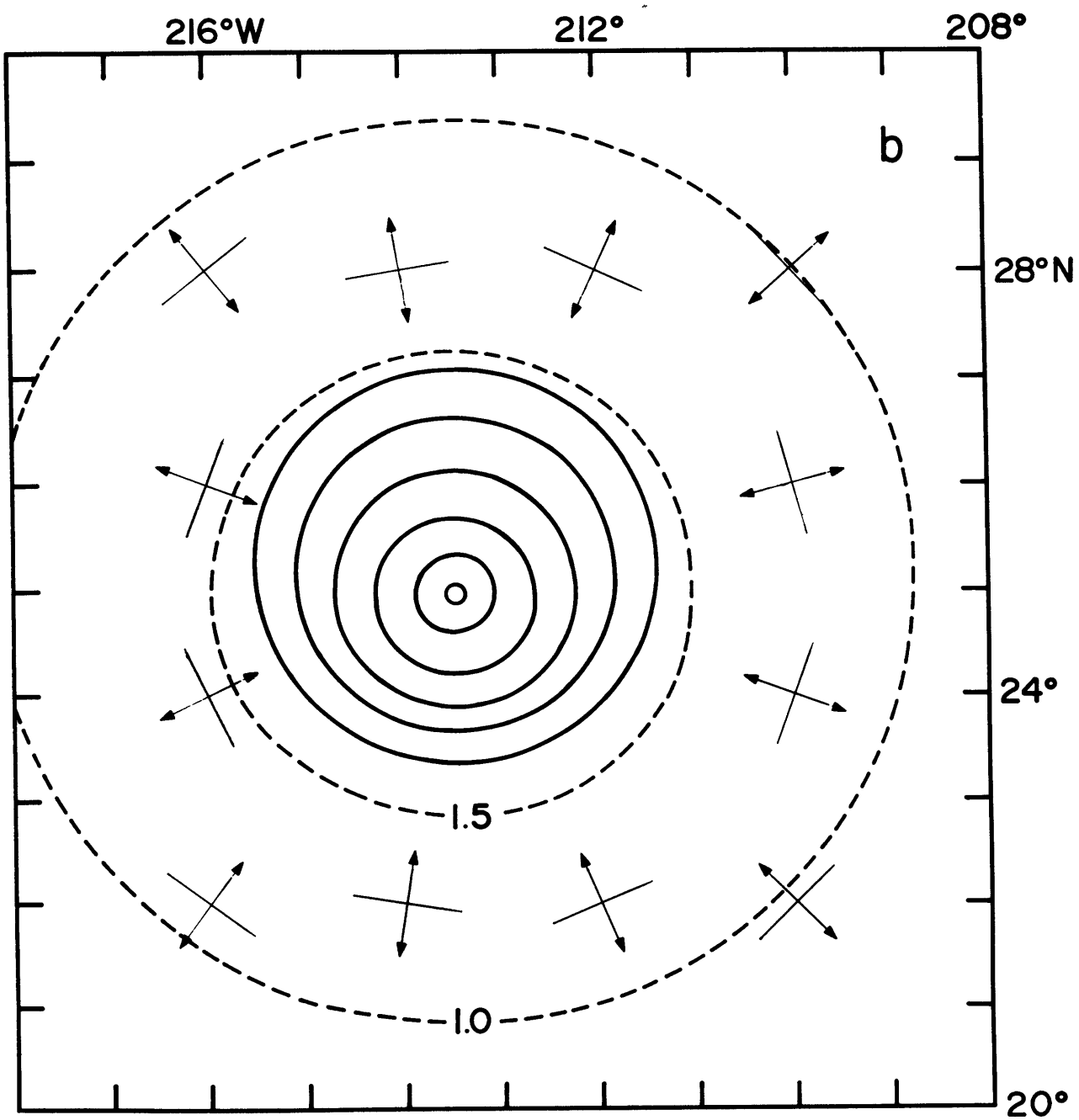

Figure 8b

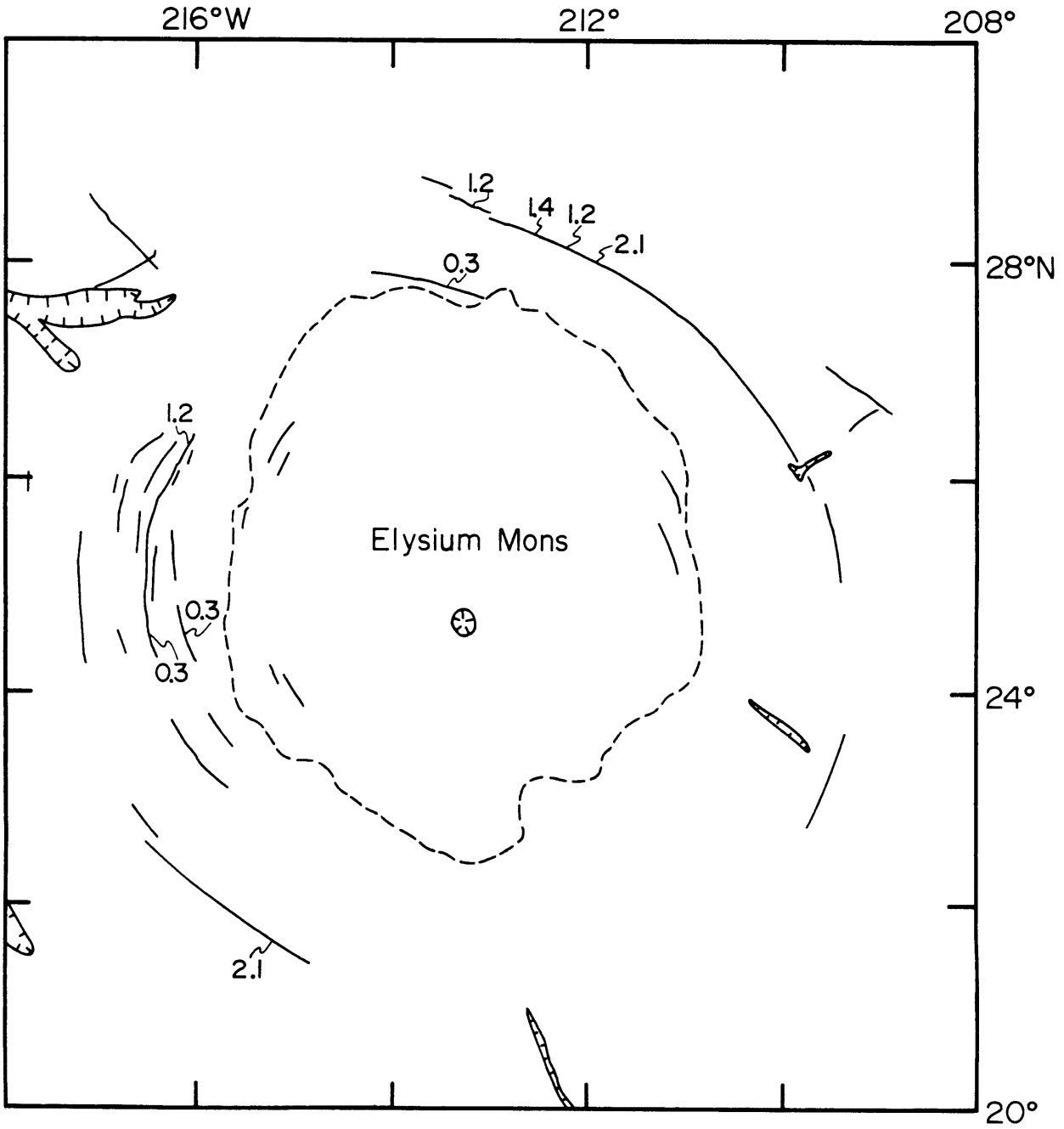

Figure 9

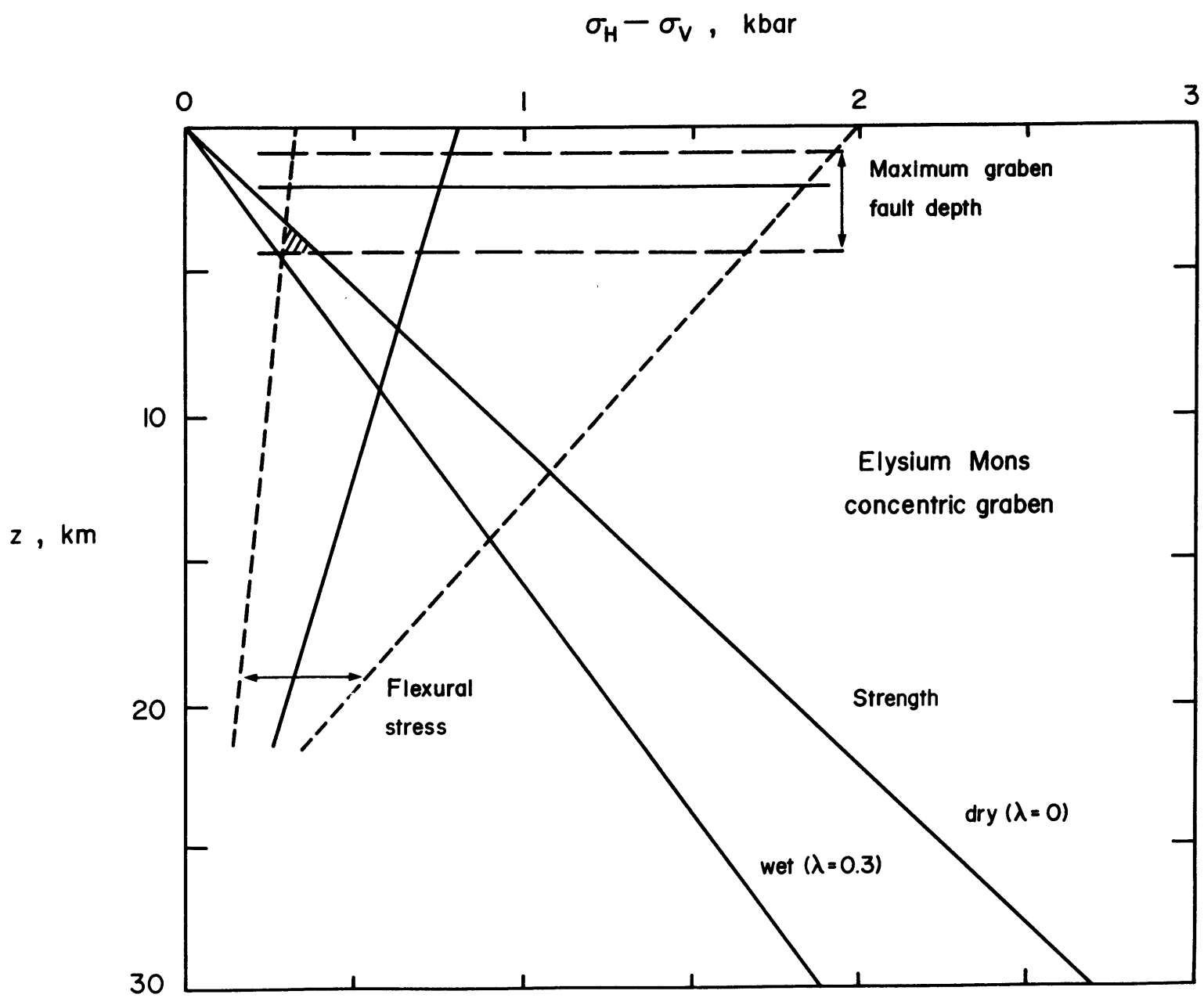
$\sigma_H - \sigma_V$, kbar
0
1
2
3
10
20
30
z , km
Maximum graben
fault depth
Elysium Mons
concentric graben
Flexural
stress
Strength
dry (λ = 0)
wet (λ = 0.3)

Figure 10

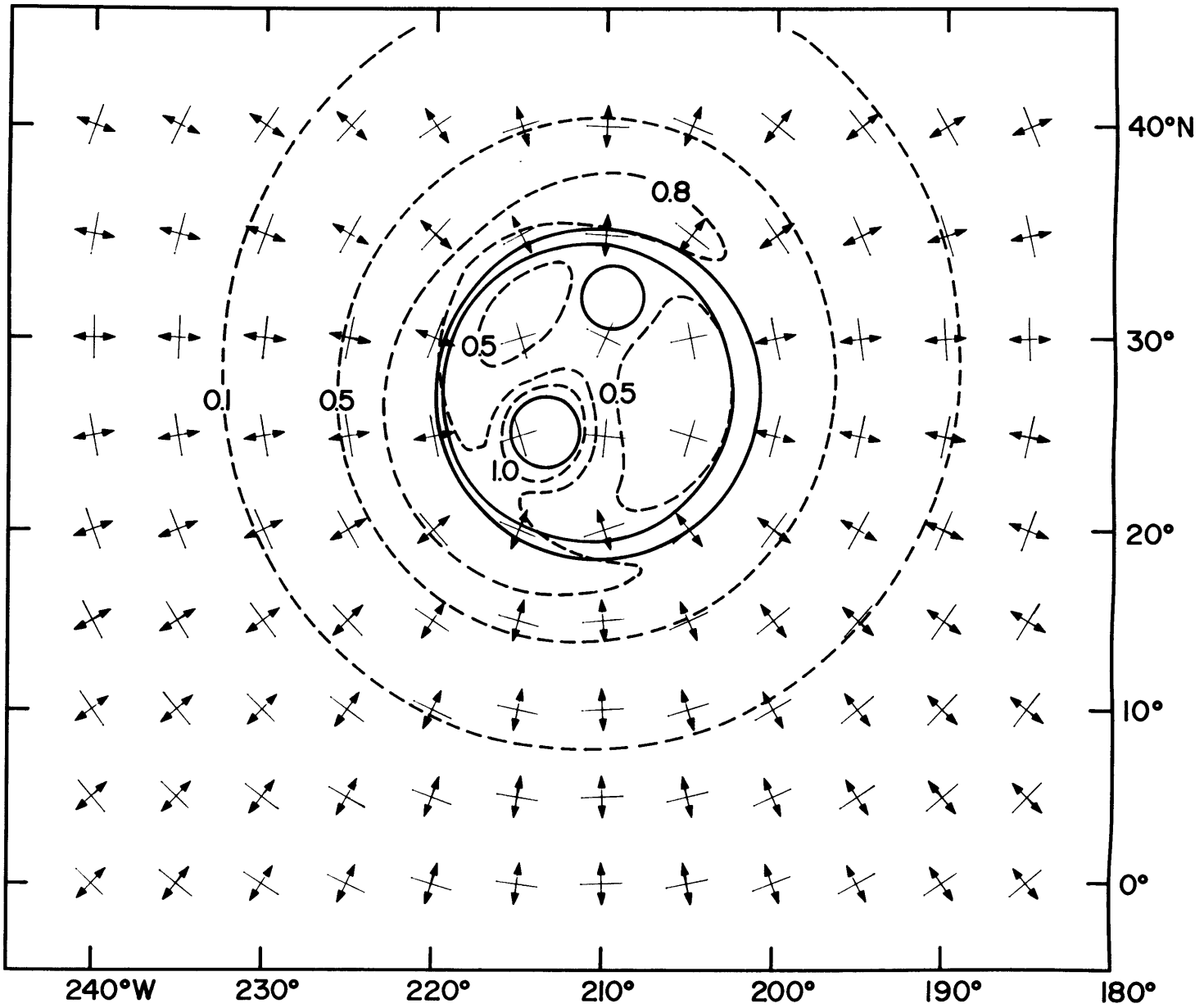

Figure 11

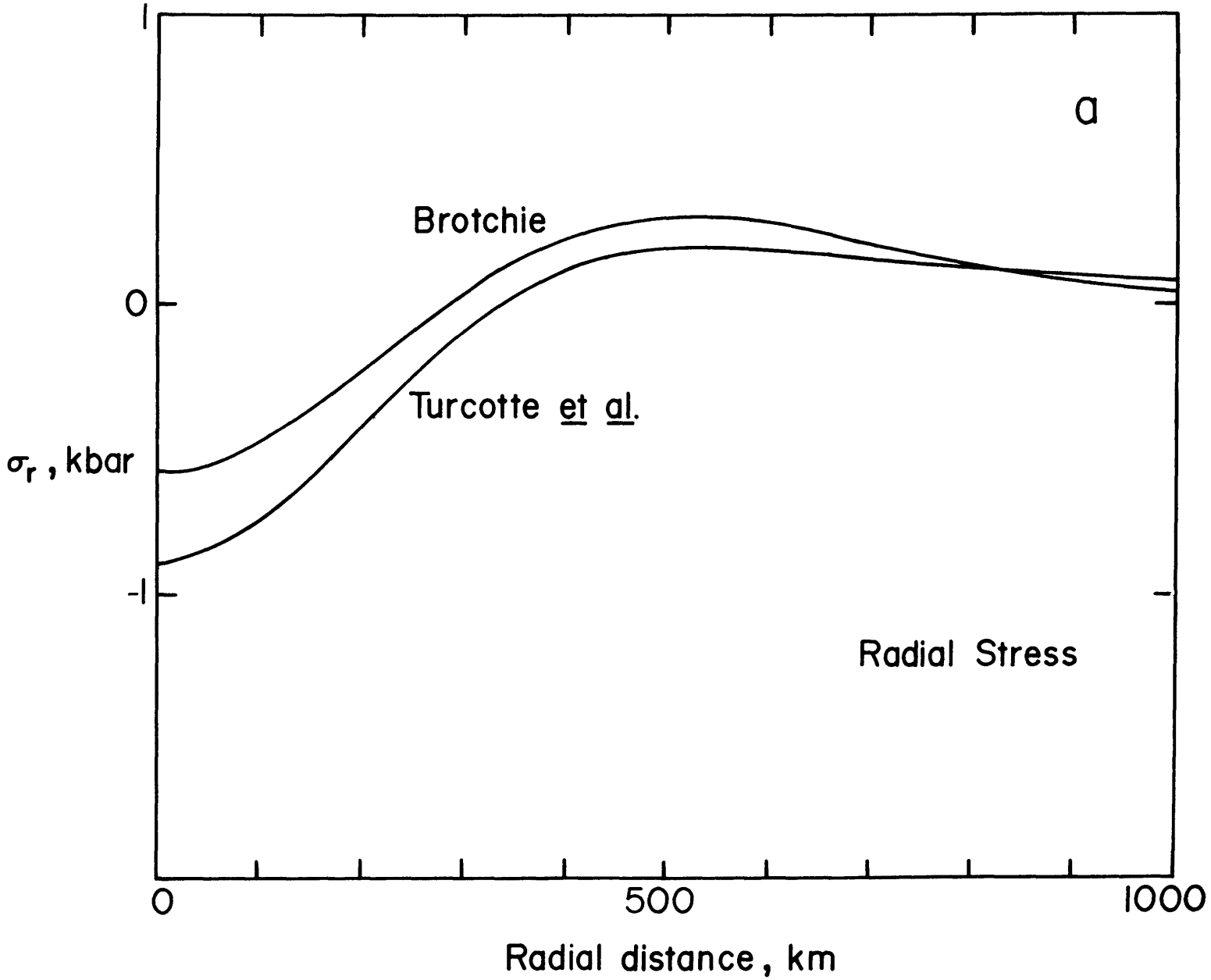
a
Brotchie
Turcotte et al.
σ_r, kbar
1
0
-1
Radial Stress
0
500
1000
Radial distance, km

Figure 12a

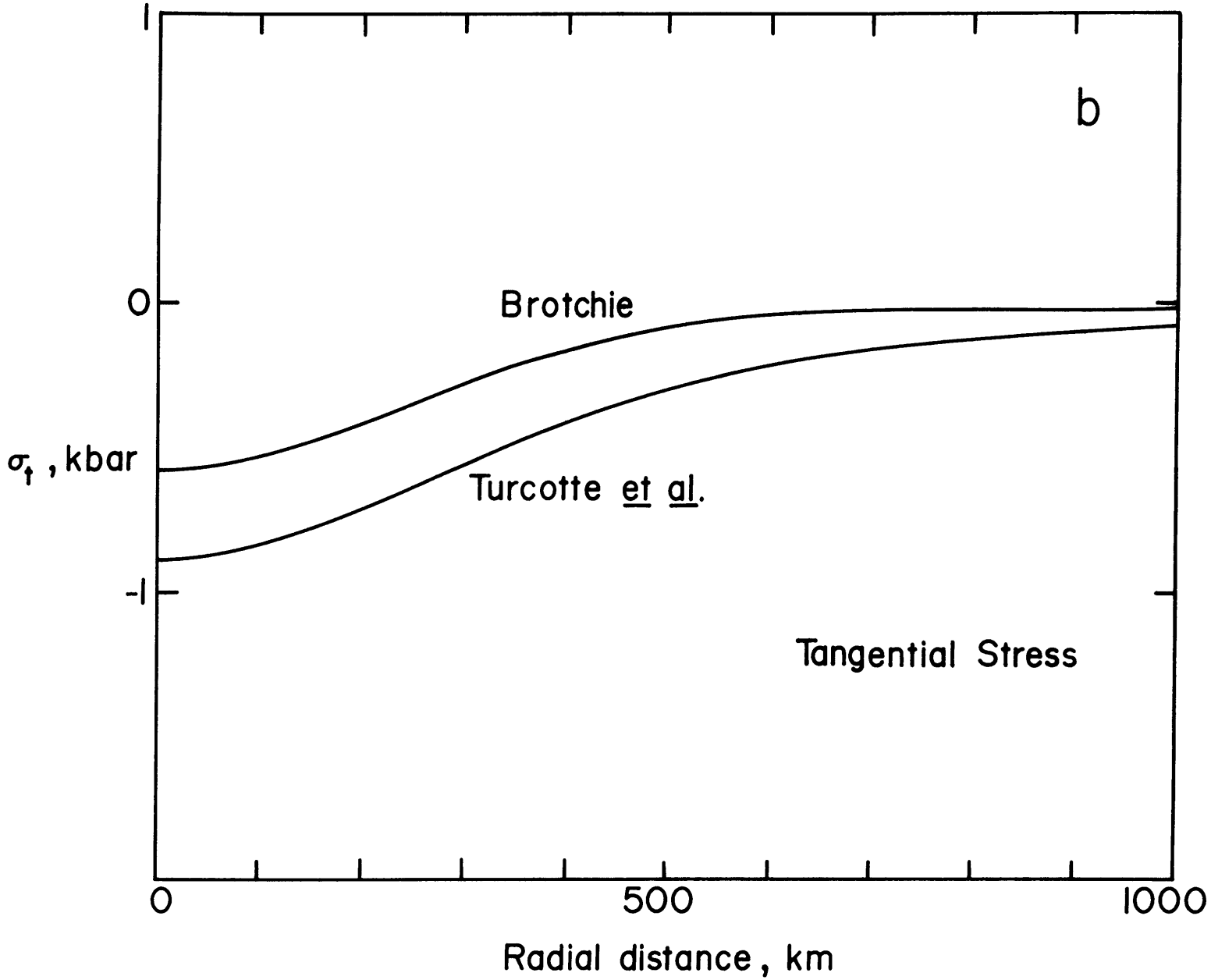
1
0
-1
b
Brotchie
Turcotte et al.
σ_t , kbar
Tangential Stress
0
500
1000
Radial distance , km

Figure 12b

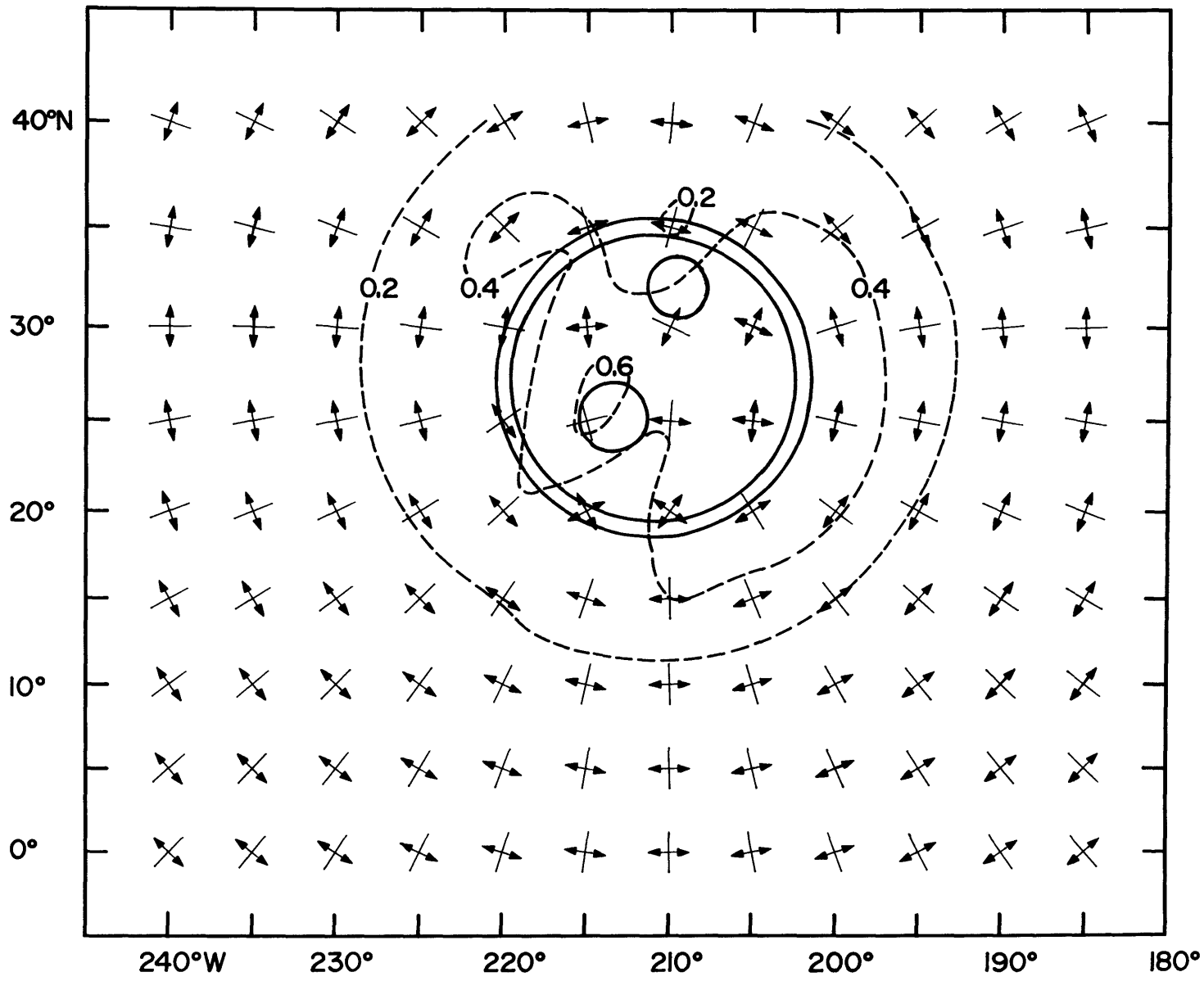

Figure 13

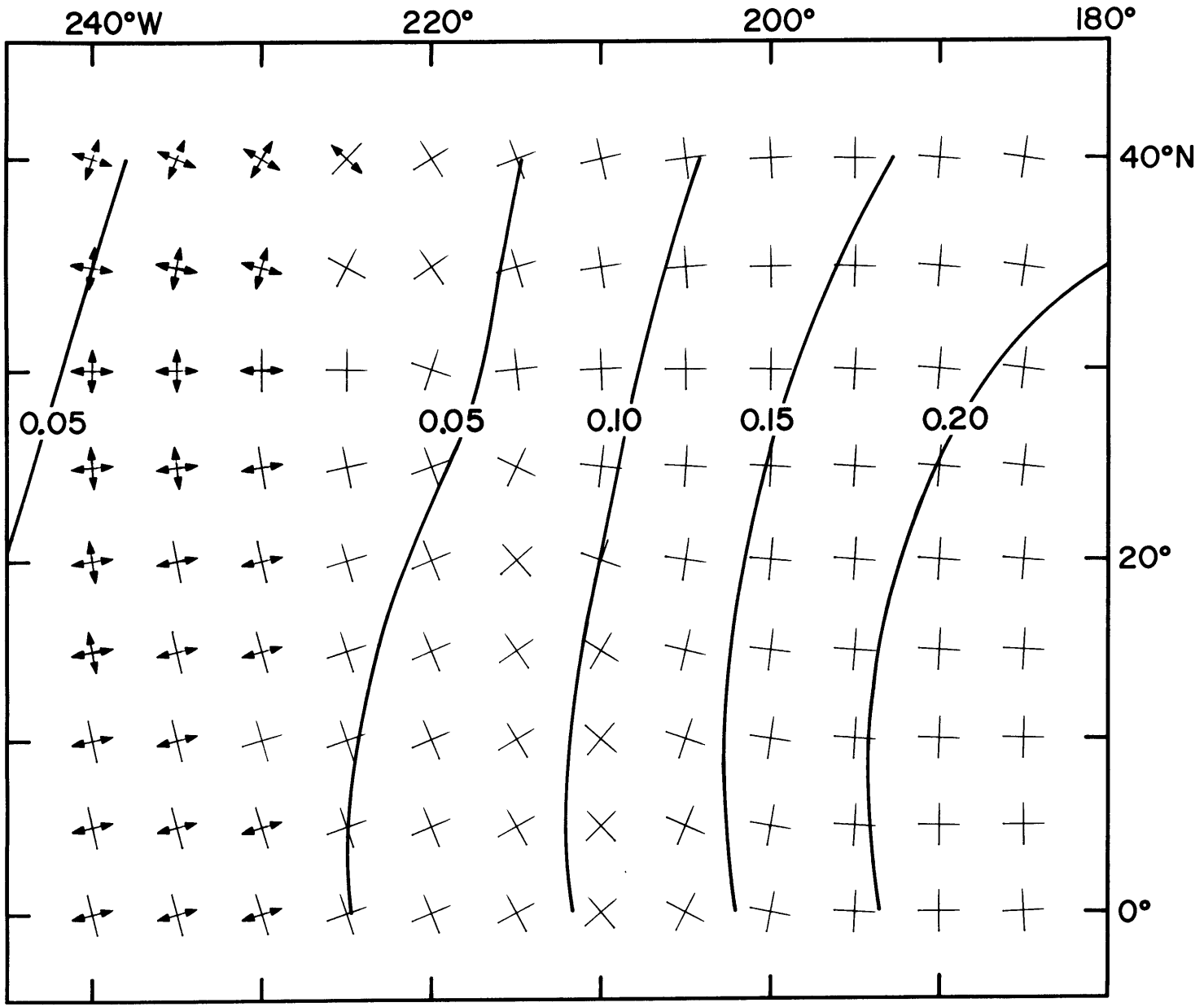

Figure 14

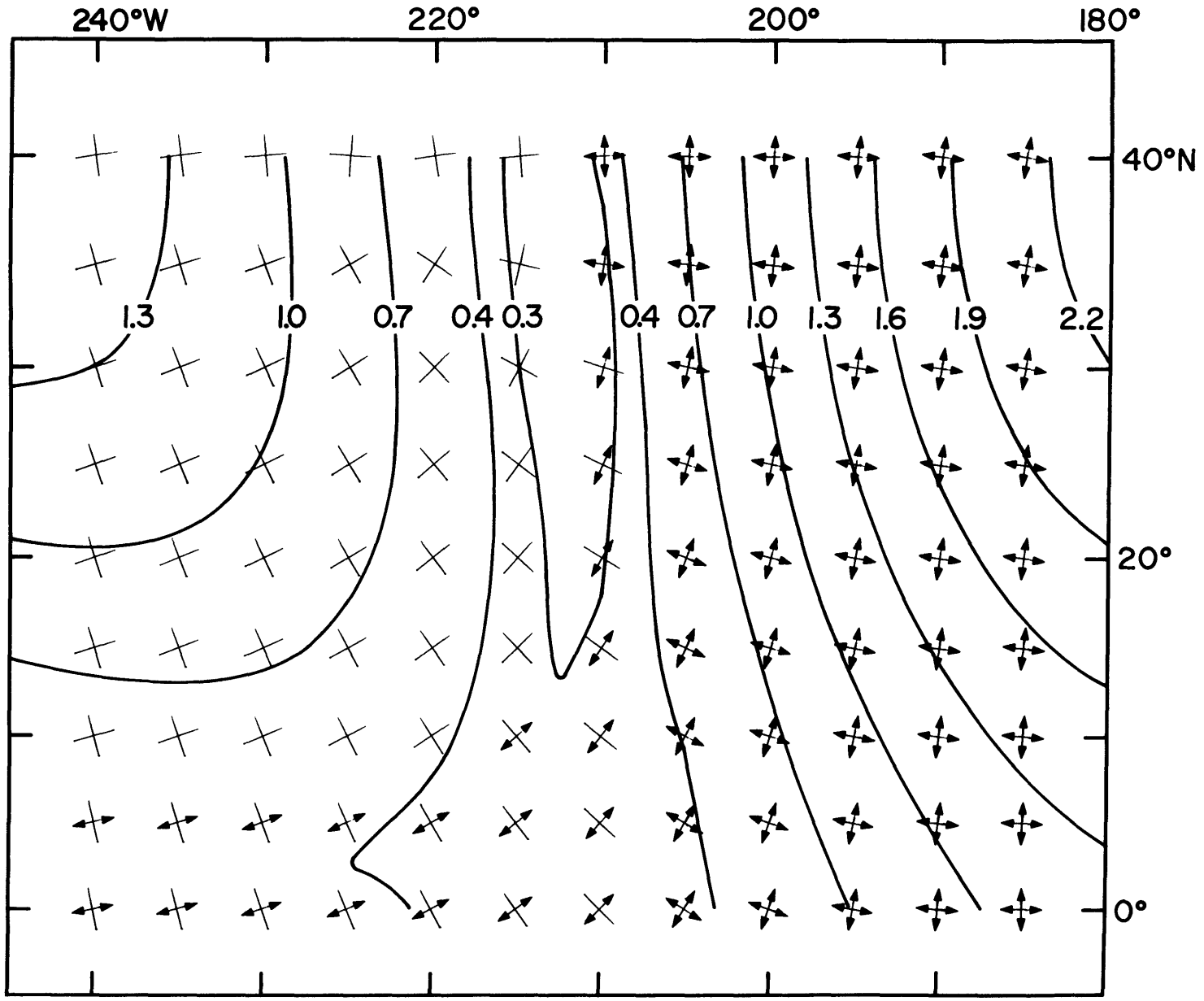

Figure 15

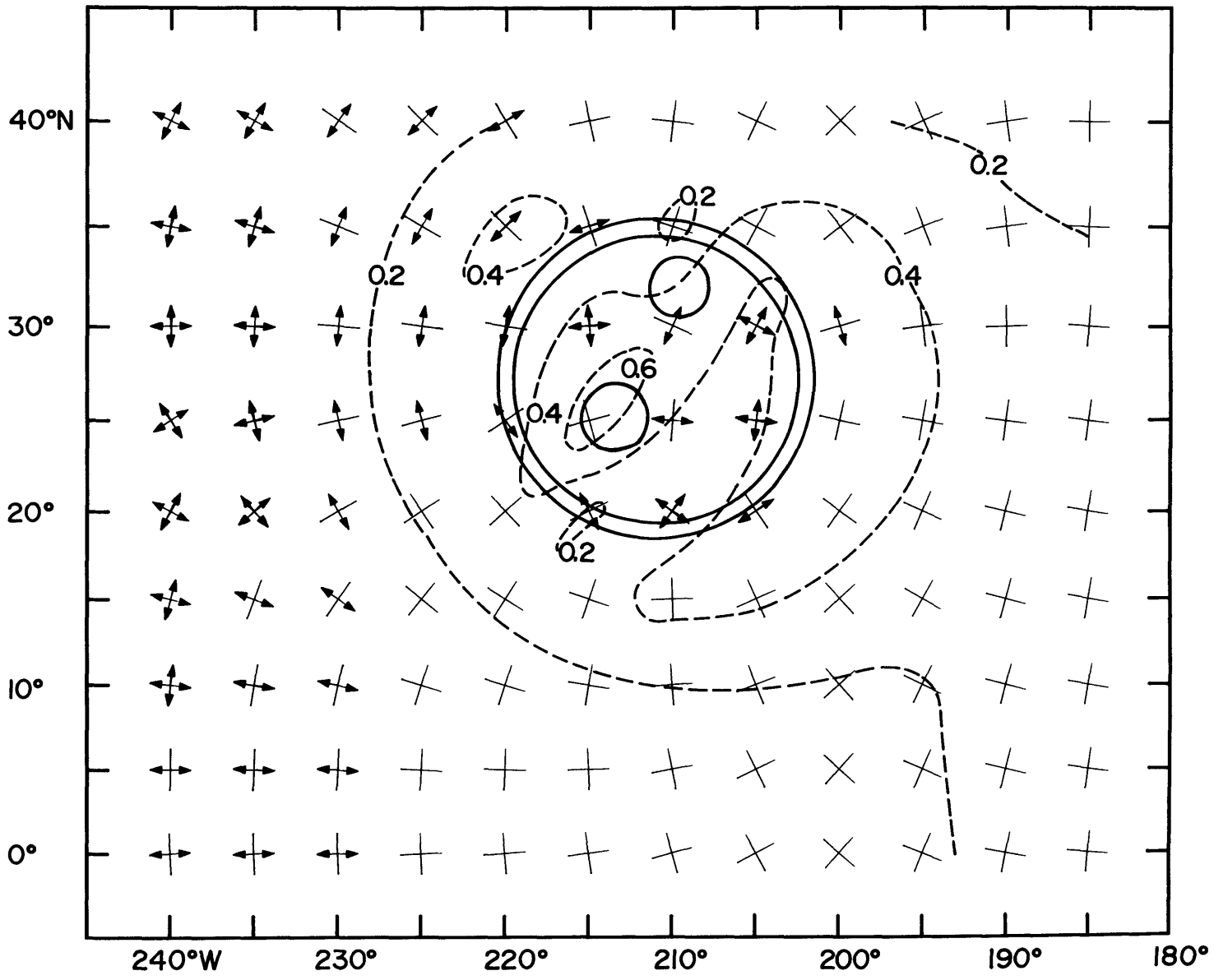

Figure 16

APPENDIX A: STRESSES IN A SELF-GRAVITATING, LATERALLY HETEROGENEOUS ELASTIC SPHERE

We explain here our adaptation of the method used by Banerdt et al. [1982], and in this thesis, to calculate the stresses in a self-gravitating, laterally heterogeneous elastic sphere.

We begin with an elastic sphere and perturb it by introducing lateral variations in the density of the upper mantle or in the depth of the crust-mantle boundary. Then we let the model deform under its own gravitational forces, and we calculate the stresses due to those displacements using a generalized form of Hooke's law. Spherical coordinates (r,θ,ϕ) are used throughout.

The following assumptions are made [Arkani-Hamed, 1973]: the initial model is a self-gravitating, non-rotating sphere which is isotropic and has a linearly elastic interior. The elastic moduli of the planet are functions of r only. The model stresses in the initial state (before perturbations are introduced) are purely hydrostatic, and thermal stresses are negligible. The model is subjected to a first-order perturbation from its initial state; this perturbation does not affect the elastic moduli. These assumptions are an idealization of the actual conditions within a planet. For instance, the mechanical behavior of a planet will be more complex than this simple elastic model, and during at least some portion of the planet's history the thermal stresses are likely to be non-negligible [Solomon and Chaiken, 1976; Solomon, 1978]. The deformation can be represented in terms of radius-dependent spherical harmonic

solutions of degree n and order m [Alterman et al., 1959; Kaula, 1963; Arkani-Hamed, 1973]:

$$\frac{d\underline{Y}_{nm}}{dr}(r) = \underline{\underline{M}}_n(r)\,\underline{Y}_{nm}(r) + \underline{D}_{nm}(r) \qquad (1)$$

where the elements of the 6-vector $\underline{Y}_{nm}(r)$ are y_1 = radial displacement, y_2 = radial stress, y_3 = tangential displacement, y_4 = tangential stress, y_5 = the perturbation to the gravitational potential (due to the density perturbations), and y_6 = gradient of the perturbed gravitational potential minus the contribution to the potential of the radial displacement.

The 6 x 6 matrix $\underline{\underline{M}}$ is of the form

$$\underline{\underline{M}}_n = \begin{vmatrix} M_{11} & M_{12} & M_{13} & 0 & 0 & 0 \\ M_{21} & M_{22} & M_{23} & M_{24} & 0 & M_{26} \\ M_{31} & 0 & M_{33} & M_{34} & 0 & 0 \\ M_{41} & M_{42} & M_{43} & M_{44} & M_{45} & 0 \\ M_{51} & 0 & 0 & 0 & 0 & M_{56} \\ 0 & 0 & M_{63} & 0 & M_{65} & M_{66} \end{vmatrix} \qquad (2)$$

with the elements of $\underline{\underline{M}}$ defined as follows:

$$M_{11} = \frac{-2\lambda}{r(\lambda+2\mu)}$$

$$M_{12} = \frac{1}{(\lambda+2\mu)}$$

$$M_{13} = \frac{n(n+1)\lambda}{r(\lambda+2\mu)}$$

$$M_{21} = \frac{-4\rho_o g_o}{r} + \frac{4\mu(3\lambda+2\mu)}{r^2(\lambda+2\mu)}$$

$$M_{22} = \frac{-4\mu}{r(\lambda+2\mu)}$$

$$M_{23} = n(n+1)\left[\frac{\rho_o g_o}{r} - \frac{2\mu(3\lambda+2\mu)}{r^2(\lambda+2\mu)}\right]$$

$$M_{24} = \frac{n(n+1)}{r}$$

$$M_{26} = -\rho_o$$

$$M_{31} = -\frac{1}{r}$$

$$M_{33} = \frac{1}{r}$$

$$M_{34} = \frac{1}{\mu}$$

$$M_{41} = \frac{\rho_o g_o}{r} - \frac{2\mu(3\lambda+2\mu)}{r^2(\lambda+2\mu)}$$

$$M_{42} = \frac{-\lambda}{r(\lambda+2\mu)}$$

$$M_{44} = \frac{-3}{r}$$

$$M_{45} = \frac{-\rho_o}{r}$$

$$M_{51} = 4\pi G\rho_o$$

$$M_{56} = 1$$

$$M_{63} = \frac{-4\pi G\rho_o n(n+1)}{r}$$

$$M_{65} = \frac{n(n+1)}{r}$$

$$M_{66} = \frac{-2}{r}$$

where $\lambda(r)$ and $\mu(r)$ are the Lame constants, ρ_o is density of the unperturbed medium, g_o is the gravitational acceleration at the surface, and G is the gravitational constant.

The vector $\underline{D}_{nm}(r)$ is given by [Banerdt et al., 1982]

$$\underline{D}_{nm}(r)T = \left(0, \frac{g_o(r)\ \varepsilon_{nm}}{d}, 0, 0, 0, \frac{-4\pi G\ \varepsilon_{nm}}{d}\right) \qquad (3)$$

where (ε_{nm}/d) is the parameter used by Banerdt et al. [1982] to represent the desired variations in density or in the depth of the crust-mantle boundary, and T denotes transpose. The quantity ε_{nm}, which has dimensions of density times length, is an eigenvalue of the solution to (1) subject to constraints by the appropriate boundary conditions. The variable d is an integration constant with dimensions of length [Banerdt et al., 1982].

Equation (1) is solved subject to boundary conditions at the surface and in the interior. These boundary conditions define the models for which we wish to predict the stress fields. The vector $\underline{Y}$ is in turn used to calculate the stress tensor.

At the surface the boundary conditions are the Dirichlet and Neumann conditions for the gravitational potential, and the vanishing of normal and tangential stress at the free surface. The condition for tangential stress at the free surface,

$$y_4 = 0 \qquad (4)$$

is applied at the deformed surface. This means that the influence of the variation in elastic properties of the topography on the deformation of the lithosphere is ignored. The error introduced is of the order of the ratio of the load thickness to the lithosphere thickness [Banerdt et al., 1982]. The condition on normal stress is also applied at the deformed surface and includes the observed topography plus that part of the topography taken up by the radial displacement y_1:

$$y_2 + g_o \rho_s (Rh_{nm} + y_1) = 0 \qquad (5)$$

where ρ_s is the density of the topography, R is the planetary radius, and h_{nm} is a normalized spherical harmonic coefficient for the observed topography.

In the isostatic case, ε_{nm} is specified such that there is isostatic balance in the lithosphere. In this case, the Dirichlet boundary condition is omitted to keep the system from being overdetermined, but ε_{nm} is chosen such that this condition is satisfied implicitly [Banerdt et al., 1982].

Once the values for the vector $\underline{Y}$ for a particular model are obtained, we can calculate the stress tensor by means of a generalized Hooke's law operator matrix [Arkani-Hamed, 1973]:

$$\begin{bmatrix} \bar{\sigma}_{rr} \\ \sigma_{\theta\theta} \\ \sigma_{\phi\phi} \\ \sigma_{r\theta} \\ \sigma_{r\phi} \\ \sigma_{\theta\phi} \end{bmatrix}_{nm} = \underline{\underline{T}}_{nm}(r,\theta,\phi) = \underline{\underline{R}}_n(r,\theta,\phi)\underline{Y}_{nm}(r)S_{nm}(\theta,\phi) \tag{6}$$

where

$$\underline{\underline{R}}_n = \begin{bmatrix} 0 & R_{12} & 0 & 0 \\ R_{21} & R_{22} & R_{23} & 0 \\ R_{31} & R_{32} & R_{33} & 0 \\ 0 & 0 & 0 & R_{44} \\ 0 & 0 & 0 & R_{54} \\ 0 & 0 & R_{63} & 0 \end{bmatrix} \tag{7}$$

and the elements of $\underline{\underline{R}}$ are defined as

$$R_{21} = R_{31} = \frac{2\mu(3\lambda+2\mu)}{r(\lambda+2\mu)}$$

$$R_{12} = 1$$

$$R_{22} = \frac{\lambda}{\lambda+2\mu}$$

$$R_{22} = R_{32} = \frac{2\mu}{r}\left[\frac{\partial^2}{\partial\theta^2} - n(n+1)\frac{\lambda}{\lambda+2\mu}\right]$$

$$R_{33} = \frac{-2\mu}{r}\left[\frac{\partial^2}{\partial\theta^2} + 2n(n+1)\frac{(\lambda+\mu)}{(\lambda+2\mu)}\right]$$

$$R_{44} = \frac{\partial}{\partial\theta}$$

$$R_{54} = \frac{1}{\sin\theta}\,\frac{\partial}{\partial\phi}$$

$$R_{63} = \frac{2\mu}{r\sin\theta}\left[\frac{\partial^2}{\partial\theta\,\partial\phi} - \cot\theta\,\frac{\partial}{\partial\phi}\right]$$

The full stress tensor is then obtained from

$$\underline{\underline{T}}(r,\theta,\phi) = \sum_{n=1}^{n_{max}} \sum_{m=1}^{n} \underline{\underline{T}}_{nm}(r,\theta,\phi)$$

In this thesis we calculate stresses only at the planetary surface, where only three stress components are non-zero: $\sigma_{\theta\theta}$, $\sigma_{\phi\phi}$, and $\sigma_{\theta\phi}$. In this case equation (6) simplifies to:

$$\begin{pmatrix} \sigma_{\theta\theta} \\ \sigma_{\phi\phi} \\ \sigma_{\theta\phi} \end{pmatrix}_{nm} = \begin{pmatrix} R_{21} & R_{23} \\ R_{31} & R_{33} \\ 0 & R_{63} \end{pmatrix}_n \begin{pmatrix} y_1 \\ y_3 \end{pmatrix}_{nm} S_{nm}(\theta,\phi) \qquad (8)$$

We evaluate (8) by applying the R operators analytically to $S_{nm}(\theta,\phi)$, leaving one equation for each stress component. The stresses at any point are found by substituting the appropriate value of (θ,ϕ) into the stress equations.

The method used by Banerdt et al. [1982] differs in that they calculate numerical values for the terms of R_nS_{nm} at each (θ,ϕ), and then calculate the values of the stresses numerically from (6).

CHAPTER 6

CONCLUDING REMARKS

"Under the law, the Quest for Ultimate Truth is quite clearly the inalienable prerogative of your working Thinkers. Any bloody machine goes and actually finds it and we're straight out of a job, aren't we?"

"That's right," shouted Vroomfondel. "We demand rigidly defined areas of doubt and uncertainty!"

-- Douglas Adams,

The Hitchhiker's Guide to the Galaxy

In this thesis we have examined processes leading to the formation of tectonic features on the Moon and Mars. The topography of lunar floor-fractured craters has been shown to be consistent with the viscous relaxation of unmodified crater topography, probably over short time intervals during which the effective viscosity was low and the thickness of the elastic lithosphere was small. Thus, the presence of floor-fractured craters around certain lunar maria indicates the existence of spatial and temporal thermal anomalies. We also found that lithospheric loading by volcanic units can account for many of the tectonic features associated with the lunar irregular maria; this is consistent with previous results for the circular maria [Comer et al., 1979; Solomon and Head, 1979, 1980]. The two models (viscous relaxation and flexure of an elastic lithosphere under a load) are not necessarily inconsistent. The relatively small number (~ 200) of floor-fractured craters suggests that they formed in an atypical situation, and are most likely the result of thermal anomalies limited in both space and time. The filling of large impact basins to form the maria, on the other hand, occurred over a much longer period of time (hundreds of millions of years as opposed to tens of millions of years for crater relaxation) and is spatially a reflection of regional rather than local rheology.

For the Elysium region of Mars, we found that several tectonic signatures can be identified. At the local scale, the concentric graben around Elysium Mons can be attributed to

loading by the Elysium Mons shields. At the regional scale, the linear features of the Elysium Fossae are consistent with modest regional lithospheric uplift. Finally, we see evidence for the influence of quasi-global Tharsis stresses on Elysium tectonics; these stresses are consistent with a two-stage model for Tharsis evolution, such as that of Banerdt et al. [1982].

The simple viscous relaxation model used in chapter 2 provides a good fit to the observed topography of lunar floor-fractured craters, but more elaborate physical models might provide more detailed information on the processes which created floor-fractured craters and on the lunar near-surface thermal environment. Future models should incorporate an effective viscosity that is a function of temperature and perhaps also of stress or strain rate. Viscoelastic models would more closely simulate the mechanical behavior of lunar near-surface material than does a simple viscous model. Parmentier and Head [1981] described how the topography of relaxed craters on Ganymede and Callisto could be used to infer variations in viscosity with depth. As yet this technique has not been applied to the Moon, although research to this effect is underway [P. Roberts, unpublished manuscript]. Further work is also needed to determine the timing of crater floor fracturing more precisely, in order to constrain the times over which high temperatures (and thus low viscosities) existed at shallow depths on the Moon. Because most floor-fractured craters have been extensively modified, however, it is not generally possible to date crater age from crater morphology

alone (as is done for fresh craters). It should be possible to date the surfaces on which the craters are found, which would provide an estimate of the maximum age of each crater; some estimate of the timing of crater modification and fracture formation will also be necessary, but will be more difficult to obtain. In addition, our study of lunar floor-fractured craters was limited by the availability of detailed topographic data. For example, there are no Lunar Topographic Orthophotomaps for the region on the western boundary of Oceanus Procellarum, where large numbers of floor-fractured craters are located. Another outstanding omission is the large floor-fractured crater Humboldt, which would provide an interesting subject of study because of its large size. Future lunar missions (if they occur) or ground-based radar studies could provide the topographic data needed to extend this work.

Lithospheric loading models were used in chapter 3 to model the formation of tectonic features associated with the major irregular lunar maria, and to estimate the lithospheric thickness for each mare at the time tectonic features were formed. The major limitation of the flexural loading model used in this thesis is that the effects of heterogeneities in lithospheric thickness cannot be included. Such heterogeneities clearly exist from basin to basin on the Moon. What effects would variations in the lithospheric thickness between the maria or across an individual mare have on the predicted stress field? Our loading models are also limited by the representation of the lunar interior as an elastic shell of

constant mechanical properties over a liquid-filled interior. More sophisticated loading models might include a viscoelastic rather than a purely elastic lithosphere; and they could include variations in physical properties with depth. Temporal as well as spatial changes in lithospheric thickness could also be explicitly modeled. Most of these improvements would require numerical solutions to the loading problem (e.g., finite element techniques) rather than the analytical solutions employed here.

Other questions relating to large-scale lunar tectonics also remain unanswered. Besides the stresses due to lithospheric loading, significant stresses are associated with the impact itself [Mason et al., 1976; Fleitout and Thomas, 1983], and with the thermal after-effects of impact heating [Bratt et al, 1985b]. To what extent are the patterns of tectonic features around the lunar maria affected by impact-generated stresses? A first approach to this problem might be to examine the tectonic features associated with unfilled impact basins on the lunar farside.

The nature of the depression filled by Oceanus Procellarum is still a mystery. It has been suggested (by Cadogan [1974], Whitaker [1981], and Wilhelms [1983], among others) that it originated in a single enormous impact. If this is true, why doesn't the thin elastic lithosphere inferred for western Oceanus Procellarum continue beneath other areas within the proposed basin? Conversely, if the Procellarum depression did not originate in a single impact, what process thinned the

lithosphere in western Procellarum? The mechanical effects of an impact by a body large enough to form the proposed Procellarum basin are unknown. Some stress models are available for the Imbrium basin-forming event [Fleitout and Thomas, 1982]. Would the tectonic effects of formation of a much larger Procellarum basin be similar?

In Chapter 5 we examined the tectonic history of the Elysium region of Mars, using loading models at local, regional, and global scales. The tectonic features of Elysium bear a superficial resemblence to those of the much larger Tharsis volcanic province, but because of the difference in lateral dimension of the two regions, the radial extensional features in Tharsis are the result of lithospheric loading or isostasy [e.g., Banerdt et al., 1982] while similar features in Elysium are consistent with a stage of modest regional flexural uplift of the lithosphere. What would be the tectonic signature of a load intermediate in size between those in which the stresses are dominated by bending stresses (such as the lunar maria, or the Elysium region on Mars) and membrane-stress-dominated (such as Tharsis)? Would the Tharsis province have passed through this intermediate stage as the load grew early in the history of the region? If the tectonic signature of the intermediate stage can be determined, it would be possible to examine the photogeologic data for traces of this signature. There is also evidence for the influence of Tharsis tectonics on Elysium, consistent with a two-stage model for Tharsis evolution including both an isostatic stage and a

flexural loading phase. Still to be resolved are questions dealing with the relative timing of tectonic events in Tharsis, which are complicated by the difficulty in determining relative ages of intersecting ridges and faults [Sharpton and Head, 1982b].

An important limitation of models for the tectonic history of both the Tharsis and Elysium regions is that they are based on the current gravity and topography. Thus they do not model adequately the early tectonic history of each region. Improvements to the current models could be made by reconstructing the early topography of the region, "peeling away" surface volcanic units and estimating the extent and magnitude of the load at different stages of its evolution. This use of photogeologic techniques to estimate changes in the load magnitude with time was applied to the lunar mascon maria by Solomon and Head [1979, 1980]. Scott and Tanaka [1980,1981] have applied photogeologic techniques to estimate the lateral extent of various volcanic units emplaced through the history of the Tharsis province; a first step in modelling the tectonic evolution of the Tharsis province might be to derive time-dependent load models based on their work.

The areally largest volcano on Mars is Alba Patera, which is located in the northern part of the Tharsis region. The radius of the volcanic shield is at least several hundred kilometers, although it is difficult to define the edge of the topographic shield exactly because the available topographic data are poor. The topographic relief of the shield is also

poorly known, but is probably several kilometers [Carr, 1976a]. Although Comer et al. [1985] estimated the lithospheric thickness beneath Alba Patera from the graben positions around the volcano, the poor topographic data result in large uncertainties in their solution. Future Mars orbital missions could provide improved topographic and gravity data needed to continue the analysis of martian tectonic history.

At this time we have no direct information on the ages of geologic units on the martian surface. Dating of surface units is done by crater density studies and by superposition relationships. Crater density studies are notoriously assumption-dependent, and for Mars they are complicated by the fact that on Mars (unlike the Moon) erosion by wind, ice, and water may have acted to degrade and erase craters. In the Elysium region the numerous and elaborate sinuous channels provide evidence for the complex history of erosion in the region. Further research is needed to determine age relationships and the sequence of tectonic events in Elysium and throughout Mars; absolute dating, however, will have to wait for sample return and analysis.

REFERENCES

Alterman, Z., H. Jarosch, and C.L. Pekeris, Oscillations of the Earth, Proc. R. Soc. London, Ser. A, 252, 80-95, 1959.

Arkani-Hamed, J., Stress differences in the Moon as evidence for a cold Moon, Moon, 6, 135-163, 1973.

Baker, V.R., The Channels of Mars, University of Texas Press, Austin, 198 pp., 1982.

Baker, V.R., and D.J. Milton, Erosion by catastrophic floods on Mars and Earth, Icarus, 23, 27-41, 1974.

Baldwin, R.B., The Measure of the Moon, University of Chicago Press, 488 pp., 1963.

Baldwin, R.B., Rille pattern in the lunar crater Humboldt, J. Geophys. Res., 73, 3227-3229, 1968.

Baldwin, R.B., Rima Goclenius II, J. Geophys. Res., 76, 8459-8465, 1971a.

Baldwin, R.B., The question of isostasy on the Moon, Phys. Earth Planet. Inter., 4, 167-179, 1971b.

Banerdt, W.B., R.J. Phillips, N.H. Sleep, and R.S. Saunders, Thick shell tectonics on one-plate planets: Applications to Mars, J. Geophys. Res., 87, 9723-9733, 1982.

Batson, R.M., P.M. Bridges, and J.L.Inge, Atlas of Mars, NASA SP-438, NASA Scientific and Technical Information Branch, 146 pp., 1979.

Bills, B.G., and A.J. Ferrari, A harmonic analysis of lunar topography, Icarus, 31, 244-259, 1977.

Bills, B.G., and A.J. Ferrari, Mars topography and geophysical implications, J. Geophys. Res., 83, 3497-3508, 1978.

Blasius, K.R., and J.A. Cutts, Topography of Martian central volcanoes, Icarus, 45, 87-112, 1981.

Bowin, C., B. Simon, and W.R. Wollenhaupt, Mascons: A two-body solution, J. Geophys. Res., 80, 4947-4955, 1975.

Boyce, J.M., Ages of flow units in the lunar nearside maria based on Lunar Orbiter IV photographs, Proc. Lunar Sci. Conf. 7th, 2717-2728, 1976.

Boyce, J.M., A.L. Dial, and L.A. Soderblom, Ages of the lunar nearside light plains and maria, Proc. Lunar Sci. Conf. 5th, 11-23, 1974.

Brace, W.F., Brittle fracture of rocks, in State of Stress in the Earth's Crust, ed. by W.R. Judd, Elsevier, New York, pp. 110-178, 1964.

Brace, W.F., and D.L. Kohlstedt, Limits on lithospheric stress imposed by laboratory experiments, J. Geophys. Res., 85, 6248-6252, 1980.

Bratt, S.R., S.C. Solomon, J.W. Head, and C.H. Thurber, The deep structure of lunar basins: Implications for basin formation and modification, J. Geophys. Res., 90, 3049-3064, 1985a.

Bratt, S.R., S.C. Solomon, and J.W. Head, The evolution of impact basins: Cooling, subsidence, and thermal stress, submitted to J. Geophys. Res., 1985b.

Brennan, W.J., Modification of premare impact craters by volcanism and tectonism, Moon, 12, 449-461, 1975.

Brotchie, J.F., Flexure of a liquid-filled spherical shell in a radial gravity field, Mod. Geol., 3, 15-25, 1971.

Brotchie, J.F., and R. Silvester, On crustal flexure, J. Geophys. Res., 74, 5240-5252, 1969.

Bryan, W.B., Wrinkle ridges as deformed surface crust on ponded mare lava, Proc. Lunar Sci. Conf. 4th, 93-106, 1973.

Bryan, W.B., and M.L. Adams, Volcanic and tectonic features of crater Aitken (abstract), Lunar Sci., 5, 95-96, 1974.

Bryan, W.B., P.A. Jezek, and M.L. Adams, Volcanic and tectonic evolution of crater Goclenius, western Mare Fecunditatis, Proc. Lunar Sci. Conf. 6th, 2563-2569, 1975.

Byerlee, J.D., Brittle-ductile transition in rocks, J. Geophys. Res., 73, 4741-4750, 1968.

Cadogan, P.H., Oldest and largest lunar basin?, Nature, 250, 315-316, 1974.

Cadogan, P.H., The Gargantuan basin - Some implications (abstract), Lunar Sci., 6, 123-124, 1975.

Cameron, W.S., and J.L. Padgett, Possible lunar ring dikes, Moon, 9, 249-294, 1974.

Carr, M.H., Geologic map of the Mare Serenitatis region of the Moon, Map I-489, U.S. Geol. Surv., Reston, VA, 1966.

Carr, M.H., Volcanism on Mars, J. Geophys. Res., 78, 4049-4062, 1973.

Carr, M.H., Tectonism and volcanism of the Tharsis region of Mars, J. Geophys. Res., 79, 3943-3949, 1974a.

Carr, M.H., The role of lava erosion in the formation of lunar rilles and Martian channels, Icarus, 22, 1-23, 1974b.

Carr, M.H., The morphology of the Martian surface, Space Sci. Rev., 25, 231-284, 1980.

Carr, M.H., The Surface of Mars, Yale University Press, New Haven, CT, 232 pp., 1981.

Carr, M.H., and G.D. Clow, Martian channels and valleys: Their characteristics, distribution and age, Icarus, 48, 91-117, 1981.

Cathles, L.M., The Viscosity of the Earth's Mantle, Princeton University Press, Princeton, NJ, 386 pp., 1975.

Chicarro, A.F., and P.H. Schultz, Global and regional ridge patterns on Mars (abstract), Lunar Planet. Sci., 15, 146-147, 1984.

Chicarro, A.F., P.H. Schultz, and P. Masson, Basin control of ridge patterns on Mars (abstract), Lunar Planet. Sci., 14, 105-106, 1983.

Colton, G.W., K.A. Howard, and H.J. Moore, Mare ridges and arches in southern Oceanus Procellarum, Apollo 16 Preliminary Science Report, NASA SP-315, pp. 29-90 to 29-93, 1972.

Comer, R.P., Thick plate flexure, Geophys. J. R. Astron. Soc., 72, 101-113, 1983.

Comer, R.P., S.C. Solomon, and J.W. Head, Elastic lithosphere thickness on the moon from mare tectonic features: A formal inversion, Proc. Lunar Planet. Sci. Conf. 10th, 2441-2463, 1979.

Comer, R.P., S.C. Solomon, and J.W. Head, Mars: Thickness of the lithosphere from the tectonic response to volcanic

loads, Rev. Geophys., 23, 61-92, 1985.

Danes̆, Z.F., Rebound processes in large craters, Astrogeologic Studies, Ann. Prog. Rept., pt. A, pp. 81-100, U.S. Geol. Surv., Washington, DC, 1965.

Danes̆, Z.F., and D.R. McNeely, Possibility of a layered Moon, Icarus, 15, 314-318, 1971.

DeHon, R.A., Cauldron subsidence in lunar craters Ritter and Sabine, J. Geophys. Res., 76, 5712-5718, 1971.

DeHon, R.A., Thickness of mare material in the Tranquillitatis and Nectaris basins, Proc. Lunar Sci. Conf. 5th, 53-59, 1974.

DeHon, R.A., Mare Fecunditatis: Basin configuration (abstract), in Papers Presented to the Conference on Origins of Mare Basalts and Their Implications for Lunar Evolution, pp. 32-34, Lunar Science Institute, Houston, TX, 1975a.

DeHon, R.A., An isopach map of the eastern mare basalts (abstract), in Papers Presented to the Conference on Origins of Mare Basalts and Their Implications for Lunar Evolution, pp. 29-31, Lunar Science Institute, Houston, TX, 1975b.

DeHon, R.A., Mare Humorum and Mare Nubium: Basalt thickness and basin-forming history, Proc. Lunar Sci. Conf. 8th, 633-641, 1977.

DeHon, R.A., Thickness of the western mare basalts, Proc. Lunar Planet. Sci. Conf. 10th, 2935-2955, 1979.

DeHon, R.A., Thickness of Tharsis volcanic materials, J. Geophys. Res., 87, 9821-9828, 1982.

DeHon, R.A., and J.D. Waskom, Geologic structure of the eastern mare basins, Proc. Lunar Sci. Conf. 7th, 2729-2746, 1976.

Downs, G.S., P.J. Mouginis-Mark, S.H. Zisk, and T.W. Thompson, New radar-derived topography for the northern hemisphere of Mars, J. Geophys. Res., 87, 9747-9754, 1982.

Dvorak, J., and R.J. Phillips, The nature of the gravity anomalies associated with large young lunar craters, Geophys. Res. Lett., 4, 380-382, 1977.

Dvorak, J., and R.J. Phillips, Lunar Bouguer gravity anomalies: Imbrium age craters, Proc. Lunar Planet. Sci. Conf. 9th, 3651-3668, 1978.

Dvorak, J., and R.J. Phillips, Gravity anomaly and structure associated with the Lamont region of the Moon, Proc. Lunar Planet. Sci. Conf. 10th, 2265-2275, 1979.

Eggleton, R.E., Geologic map of the Riphaeus mountains region of the Moon, Map I-458, U.S. Geol. Surv., Reston, VA, 1965.

Elston, D.P., Geologic map of the Columbo quadrangle of the Moon, Map I-714, U.S. Geol. Surv., Reston, VA, 1972.

Fagin, S.W., D.M. Worral, and W.R. Muehlberger, Lunar mare ridge orientations: Implications for tectonic models, Proc. Lunar Planet. Sci. Conf. 9th, 3473-3479, 1978.

Fielder, G., Topography and tectonics of the lunar Straight Wall, Planet. Space Sci., 11, 23-30, 1963.

Fleitout, L., and P.G. Thomas, Far-field tectonics associated with a large impact basin: Applications to Caloris on Mercury and Imbrium on the Moon, Earth Planet. Sci. Lett., 58, 104-115, 1982.

Gifford, A.W., Ridge systems of Mars, Advances in Planetary Geology, NASA TM 84412, pp. 220-363, 1981.

Goetze, C., and B. Evans, Stress and temperature in the bending lithosphere as constrained by experimental rock mechanics, Geophys. J. R. Astron. Soc., 59, 463-478, 1979.

Golombek, M.P., Structural analysis of lunar grabens and the shallow crustal structure of the Moon, J. Geophys. Res., 84, 4657-4666, 1979.

Golombek, M.P., Fault type predictions from stress distributions on planetary surfaces: Importance of fault initiation depth, J. Geophys. Res., 90, 3064-3074, 1985.

Greeley, R., P.H. Schultz, and C.L. Wilbur, Volcanic features of the Smythii basin (abstract), Lunar Sci., 8, 371-373, 1977.

Guest, J.E., and G. Fielder, Lunar ring structures and the nature of the maria, Planet. Space Sci., 16, 665-673, 1968.

Guest, J.E., and J.B. Murray, Volcanic features of the nearside equatorial lunar maria, J. Geol. Soc. Lond., 132, 251-258, 1976.

Hackman, R.J., Geologic map and sections of the Kepler region of the Moon, Map I-355, U.S. Geol. Surv., Reston, VA, 1962.

Hall, J.L., S.C. Solomon, and J.W. Head, Lunar floor-fractured craters: Evidence for viscous relaxation of crater topography, J. Geophys. Res., 86, 9537-9552, 1981.

Hall, J.L., S.C. Solomon, J.W. Head, and P.J. Mouginis-Mark, Elysium region, Mars: Characterization of tectonic features (abstract), Lunar Planet. Sci., 14, 275-276, 1983.

Hartmann, W.K., Martian surface and crust: Review and synthesis, Icarus, 19, 550-575, 1973.

Hartmann, W.K., and C.A. Wood, Moon: Origin and evolution of multi-ring basins, Moon, 3, 3-78, 1971.

Head, J.W., Processes of lunar crater degradation, Moon, 12, 299-329, 1975.

Head, J.W., Lunar volcanism in space and time, Rev. Geophys. Space Phys., 14, 265-300, 1976.

Head, J.W., Lava flooding of ancient planetary crusts: Geometry, thickness, and volumes of flooded lunar impact basins, Moon Planets, 26, 61-88, 1982.

Head, J.W., and S.C. Solomon, Lunar basin structure: Possible influence of variations in lithospheric thickness (abstract), Lunar Planet. Sci., 11, 421-423, 1980.

Head, J.W., S.C. Solomon, and J.L. Whitford-Stark, Oceanus Procellarum region: Evidence for an anomalously thin early lunar lithosphere (abstract), Lunar Planet. Sci., 11, 424-425, 1980.

Hiller, K.H., Geologic map of the Amenthes quadrangle of Mars, Map I-1110, U.S. Geological Survey, Reston, VA, 1979.

Hodges, C.A., Geologic map of the Langrenus quadrangle of the Moon, Map I-739, U.S. Geol. Surv. Reston, VA, 1973a.

Hodges, C.A., Geologic map of the Petavius quadrangle of the Moon, Map I-794, U.S. Geol. Surv., Reston, VA, 1973b.

Holt, H.E., Geologic map of the Purbach quadrangle of the Moon, Map I-822, U.S. Geol. Surv., Reston, VA, 1974.

Horz, F., How thick are lunar mare basalts?, Proc. Lunar Planet. Sci. Conf. 9th, 3311-3331, 1978.

Howard, K.A., and H. Masursky, Geologic map of the Ptolemaeus quadrangle of the Moon, Map I-566, U.S. Geol. Surv., Reston, VA, 1968.

Howard, K.A., and W.R. Muehlberger, Lunar thrust faults in the Taurus-Littrow region, in Apollo 17 Preliminary Scientific Report, NASA Spec. Publ., SP-330, pp. 31-22 to 31-25, 1973.

Hubbard, N., and C.G. Andre, Magma genesis in a battered Moon: Effects of basin-forming impacts, Moon Planets, 29, 15-37, 1983.

Hulme, G., Turbulent lava flow and the formation of lunar sinuous rilles, Mod. Geol., 4, 107-117, 1973.

Innes, M.J.S., The use of gravity methods to study the underground structure and impact energy of meteorite craters, J. Geophys. Res., 66, 2225-2239, 1961.

Janle, P., Structure of lunar impact craters from gravity models, J. Geophys., 42, 407-417, 1977.

Janle, P., A lunar crustal gravity model across the Triesnecker-Hyginus area, Mare Tranquillitatis, and Mare Fecunditatis, Moon Planets, 24, 441-451, 1981.

Janle, P., and J. Ropers, Investigation of the isostatic state of the Elysium dome on Mars by gravity models, Phys. Earth Planet. Inter., 32, 132-145, 1983.

Janle, P., F. Roth, and J. Voss, Limits of the lithospheric thickness of the Elysium area on Mars from correlations of surface stresses with the lineament system (abstract), Lunar Planet. Sci., 15, 401-402, 1984.

Johnson, T.V., and T.R. McGetchin, Topography on satellite surfaces and the shapes of asteroids, Icarus, 18, 612-620, 1973.

Kaula, W.M., Elastic models of the mantle corresponding to variations in the external gravity field, J. Geophys. Res., 68, 4967-4981, 1963.

Kuiper, G.P., R.G. Strom, E.A. Whitaker, J.W. Fountain, and S.M. Larson, Consolidated Lunar Atlas, Contrib. 4, Lunar and Planet. Lab., Univ. of Ariz., Tucson, 1967.

Kunze, A.W.G., Creep response of the lunar crust in mare regions from an analysis of crater deformation, Ph.D. thesis, Penn. State Univ., University Park, PA, 1973.

Lucchitta, B.K., Mare ridges and related highland scarps -a result of vertical tectonism? Proc. Lunar Sci. Conf. 7th, 2761-2782, 1976.

Lucchitta, B.K., Topography, structure, and mare ridges in southern Mare Imbrium and northern Oceanus Procellarum, Proc. Lunar Sci. Conf. 8th, 2691-2703, 1977.

Lucchitta, B.K., and J.A. Watkins, Age of graben systems on the Moon, Proc. Lunar Planet. Sci. Conf. 9th, 3459-3472, 1978.

Lucchitta, B.K., and J.L. Klockenbrink, Ridges and scarps in the equatorial belt of Mars, Moon Planets, 24, 415-429, 1981.

Malin, M.C., Age of Martian channels, J. Geophys. Res., 81, 4825-4845, 1976.

Malin, M.C., Comparison of volcanic features of Elysium (Mars) and Tibesti (Earth), Geol. Soc. Amer. Bull., 88, 908-919, 1977.

Marshall, C.H., Thickness of the Procellarian system, Letronne region of the Moon, U.S. Geol. Surv. Prof. Paper 424-D, 208-211, 1961.

Marshall, C.H., Geologic map and sections of the Letronne region of the Moon, Map I-385, U.S. Geol. Surv., Reston, VA, 1963.

Mason, R., J.E. Guest, and G.N. Cooke, An Imbrium pattern of graben on the Moon, Proc. Geol. Assn., 87, 161-168, 1976.

Masursky, H., A preliminary report on the role of isostatic rebound in the geologic development of the lunar crater Ptolemaeus, Astrogeologic Studies, Ann. Prog. Rept., pt. A, pp. 102-134, U.S. Geol. Surv., Washington, DC, 1964.

Maxwell, T.A., Orientation and origin of ridges in the Lunae Palus-Coprates region of Mars, Proc. 13th Lunar Planet. Sci. Conf., Part 1 , J. Geophys. Res., 87, Suppl., A97-A108, 1982.

Maxwell, T.A., and A.W. Gifford, Ridge patterns of large craters and basins on Mars (abstract), Lunar Planet. Sci., 12, 673-675, 1981.

Maxwell, T.A., F. El-Baz, and S.H. Ward, Distribtution, morphology, and origin of ridges and arches in Mare Serenitatis, Bull. Geol. Soc. Am., 86, 1273-1278, 1975.

McCauley, J.F., Geologic map of the Grimaldi quadrangle of the Moon, Map I-740, U.S. Geol. Surv., Reston, VA, 1973.

McCauley, J.F., and D.H. Scott, The geologic setting of the Luna 16 landing site, Earth Planet. Sci. Lett., 13, 225-232, 1972.

McGill, G.E., Attitudes of fractures bounding straight and arcuate rilles, Icarus, 14, 53-58, 1971.

McKinnon, W.B., An investigation into the role of plastic failure in crater modification, Proc. Lunar Planet. Sci. Conf. 9th, 3965-3973, 1978.

Melosh, H.J., On the origin of features radial to lunar basins, Proc. Lunar Sci. Conf. 7th, 2967-2982, 1976.

Melosh, H.J., Global tectonics of a despun planet, Icarus, 31, 221-243, 1977a.

Melosh, H.J., Crater modification by gravity: A mechanical analysis of slumping, in Impact and Explosion Cratering, ed. by D.J. Roddy, R.O. Pepin, and R.B. Merrill, pp. 1245-1260, Pergamon Press, NY, 1977b.

Melosh, H.J., The tectonics of mascon loading, Proc. Lunar Planet. Sci. Conf. 9th, 3513-3525, 1978.

Milton, D.J., Geologic map of the Theophilus quadrangle of the Moon, Map I-546, U.S. Geol. Surv., Reston, VA, 1968.

Milton, D.J., Water and processes of degradation in the Martian landscape, J. Geophys. Res., 78, 4037-4047, 1973.

Moore, H.J., Geologic map of the Aristarchus region of the Moon, Map I-465, U.S. Geol. Surv., Reston, VA, 1965.

Morris, E.C., and D.E. Wilhelms, Geologic map of the Julius Caesar quadrangle of the Moon, Map I-510, U.S. Geol. Surv., Reston, VA, 1967.

Mouginis-Mark, P.J., and S.H. Brown, An unusual volcanic center in western Elysium Planitia, Mars (abstract), Lunar Planet. Sci., 12, 729-731, 1981.

Mouginis-Mark, P.J., L. Wilson, J.W. Head, S.H. Brown, J.L. Hall, and K.D. Sullivan, Elysium Planitia, Mars: Regional geology, volcanology, and evidence for volcano/ground ice interactions, Earth Moon Planets, 30, 149-173, 1984.

Muehlberger, W.R., Structural history of southeastern Mare Serenitatis and adjacent highlands, Proc. Lunar Sci. Conf. 5th, 101-110, 1974.

Muller, P.M., and W.L. Sjogren, Mascons: Lunar mass concentrations, Science, 161, 680-684, 1968.

Mutch, T.A., R.E. Arvidson, J.W. Head III, K.L. Jones, and R.S. Saunders, The Geology of Mars, Princeton University Press, Princeton, NJ, 400 pp., 1976.

Neukum G., and K. Hiller, Martian ages, J. Geophys. Res., 86, 3097-3121, 1981.

Neukum, G., and D.U. Wise, Mars: A standard crater curve and possible new time scale, Science, 194, 1381-1387, 1976.

O'Keefe, J.D., and T.J. Ahrens, Impact-induced energy partitioning, melting, and vaporization on terrestrial planets, Proc. Lunar Sci. Conf. 8th, 3357-3374, 1977.

Olson, A.B., and D.E. Wilhelms, Geologic map of the Mare Undarum quadrangle of the Moon, Map I-837, U.S. Geol. Surv., Reston, VA, 1974.

Parmentier, E.M., and J.W. Head, Internal processes affecting surfaces of low-density satellites: Ganymede and Callisto, J. Geophys. Res., 84, 6263-6276, 1979.

Parmentier, E.M., and J.W. Head, Viscous relaxation of impact craters on icy planetary surfaces: Determination of viscosity variations with depth, Icarus, 47, 100-111, 1981.

Parsons, B., and J.G. Sclater, An analysis of the variation of ocean floor bathymetry and heat flow with age, J. Geophys. Res., 82, 803-827, 1977.

Passey, Q.R., and E.M. Shoemaker, Craters and basins on Ganymede and Callisto: Morphological indicators of crustal evolution, in Satellites of Jupiter, ed. by D. Morrison, pp. 379-434, University of Arizona Press, 1982.

Phillips, R.J., and K. Lambeck, Gravity fields of the terrestrial planets: Long-wavelength anomalies and tectonics, Rev. Geophys. Space Phys., 18, 27-76, 1980.

Phillips, R.J., and R.S. Saunders, Interpretation of gravity anomalies in the irregular maria (abstract), Lunar Sci., 5, 596-597, 1974.

Pieters, C.M., J.W. Head, J.B. Adams, T.B. McCord, S.H. Zisk, and J.L. Whitford-Stark, Late high-titanium basalts of the western maria: Geology of the Flamsteed region of Oceanus Procellarum, J. Geophys. Res., 85, 3913-3938, 1980.

Pike, R.J., Meteoritic origin and consequent endogenic modification of large lunar craters - A study in analytical geomorphology, Ph.D. Thesis, Univ. of Michigan, Ann Arbor, 404 pp., 1968.

Pike, R.J., Genetic implications of the shapes of Martian and lunar craters, Icarus, 15, 384-395, 1971.

Pike, R.J., Simple to complex impact craters: The transition on the Moon (abstract), Lunar Sci., 7, 700-702, 1976.

Pike, R.J., Size-dependence in the shape of fresh impact craters on the Moon, in Impact and Explosion Cratering, ed. by D.J. Roddy, R.O. Pepin, and R.B. Merrill, pp. 489-509, Pergamon Press, NY, 1977.

Pike, R.J., Geometric interpretation of lunar craters, U.S. Geol. Survey Prof. Paper 1046-C, pp. C1-C77, 1980.

Plescia, J.B., and R.S. Saunders, The chronology of the Martian volcanoes, Proc. Lunar Planet. Sci. Conf. 10th, 2841-2859, 1979.

Plescia, J.B., and R.S. Saunders, Estimation of the thickness of the Tharsis lava flows and implications for the nature of the topography of the Tharsis plateau, Proc. Lunar Planet. Sci. Conf. 11th, 2423-2436, 1980.

Plescia, J.B., and R.S. Saunders, Tectonic history of the Tharsis region, Mars, J. Geophys. Res., 87, 9775-9791, 1982.

Pullan, S., and K. Lambeck, Mascons and loading of the lunar lithosphere, Proc. Lunar Planet. Sci., 12B, 853-865, 1981.

Quaide, W., Rilles, ridges, and domes - Clues to maria history, Icarus, 4, 374-389, 1965.

Raitala, J., Tectonic implications of the mare-ridge pattern of the central parts of Oceanus Procellarum on the Moon, Moon Planets 23, 307-321, 1980.

Saunders, R.S., and T.E. Gregory, Tectonic implications of Martian ridged plains (abstract), in Reports of Planetary Geology Program - 1980, NASA TM 82385, 93-94, 1980.

Saunders, R.S., and D.E. Wilhelms, Geologic map of the Wilhelm quadrangle of the Moon, Map I-824, U.S. Geol. Surv., Reston, VA, 1974.

Schimerman, L.A. (ed.), Lunar Cartographic Dossier, Defense Mapping Agency Aerospace Center, St. Louis, MO, 1973.

Schmitt, H.H., N.J. Trask, and E.M. Shoemaker, Geologic map of the Copernicus quadrangle of the Moon, Map I-515, U.S. Geol. Surv., Reston, VA, 1967.

Schultz, P.H., Floor-fractured lunar craters, Moon, 15, 241-273, 1976.

Schultz, P.H., Impact basin control of volcanic and tectonic provinces on Mars (abstract), Lunar Planet. Sci., 15, 728-729, 1984.

Schultz, P.H., and H. Glicken, Impact crater and basin control of igneous processes on Mars, J. Geophys. Res., 84, 8033-8047, 1979.

Schultz, P.H., and M.H. Mendenhall, On the formation of basin secondary craters by ejecta complexes (abstract), Lunar Planet. Sci., 10, 1078-1080, 1979.

Schultz, P.H., and P.D. Spudis, Evidence for ancient mare volcanism, Proc. Lunar Planet. Sci. Conf. 10th, 2899-2918, 1979.

Schultz, P.H., and P.D. Spudis, Procellarum basin: A major impact or the effect of Imbrium? (abstract), Lunar Planet. Sci., 16, 746-747, 1985.

Schumm, S.A., Structural origin of large Martian channels, Icarus, 22, 371-384, 1974.

Scott, D.H., The geologic significance of some lunar gravity anomalies, Proc. Lunar Sci. Conf. 5th, 3025-3036, 1974.

Scott, D.H., and J.W. Allingham, Geologic map of the Elysium quadrangle of Mars, Map I-935, U.S. Geological Survey, Reston, VA, 1976.

Scott, D.H., and M.H. Carr, Geologic map of Mars, Map I-1083, U.S. Geological Survey, Reston, VA, 1978.

Scott, D.H., and R.E. Eggleton, Geologic map of the Rumker quadrangle of the Moon, Map I-805, U.S. Geol. Surv., Reston, VA, 1973.

Scott, D.H. and H.A. Pohn, Geologic map of the Macrobius quadrangle of the Moon, Map I-799, U.S. Geol. Surv., Reston, VA, 1972.

Scott, D.H., and K.L. Tanaka, Mars Tharsis region: Volcanotectonic events in the stratigraphic record, Proc. Lunar Planet. Sci. Conf. 11th, 2403-2421, 1980.

Scott, D.H., amd K.L. Tanaka, Mars: Paleostratigraphic reconstruction of buried surfaces in Tharsis Montes, Icarus, 45, 304-319, 1981.

Scott, D.H., J.M. Diaz, and J.A. Watkins, The geologic evolution and regional synthesis of metric and panoramic photographs, Proc. Lunar Sci. Conf. 6th, 2531-2540, 1975.

Scott, D.H., J.F. McCauley, and M.N. West, Geologic map of the west side of the Moon, Map I-799, U.S. Geol. Surv., Reston, VA, 1977.

Scott, R.F., Viscous flow of craters, Icarus, 7, 139-148, 1967.

Settle, M., and J.W. Head, Radial variation of lunar crater rim topography, Icarus, 31, 123-135, 1977.

Sharp, R.P., Geomorphological processes on terrestrial planetary surfaces, Ann. Rev. Earth Planet. Sci., 8, 231-261, 1980.

Sharp, R.P., and M.C. Malin, Channels on Mars, Geol. Soc. Amer. Bull., 86, 593-609, 1975.

Sharpton, V.L., and J.W. Head, Stratigraphy and structural evolution of southern Mare Serenitatis: A reinterpretation based on Apollo Lunar Sounder Experiment Data, J. Geophys. Res., 87, 10,983-10,998, 1982a.

Sharpton, V.L., and J.W. Head, Mare ridge morphology at structural and stratigraphic boundaries: Implications for determining age sequence (abstract), Lunar Planet. Sci., 13, 714-715, 1982b.

Sharpton, V.L., and J.W. Head, Tectonic origin of mare ridges: Evidence from basalt stratigraphy in Mare Imbrium (abstract), Lunar Planet. Sci., 14, 690-691, 1983.

Sjogren, W.L., Mars gravity: High resolution results from Viking Orbiter II, Science, 203, 1006-1010, 1979.

Sjogren, W.L., P. Gottlieb, P.M. Muller, and W.R. Wollenhaupt, Lunar gravity via Apollo 14 Doppler radio tracking, Science, 175, 165-168, 1972a.

Sjogren, W.L., P.M. Muller, and W.R. Wollenhaupt, S-band transponder experiment, in Apollo 16 Preliminary Science Report, NASA SP-315, pp. 24-1 to 24-7, 1972b.

Sjogren, W.L., W.R. Wollenhaupt, and R.N. Wimberly, S-band transponder experiment, in Apollo 17 Preliminary Science Report, NASA SP-330, pp. 14-1 to 14-4, 1973.

Sjogren, W.L., R.N. Wimberly, and W.R. Wollenhaupt, Lunar gravity via the Apollo 15 and 16 subsatellites, Moon, 9, 115-128, 1974a.

Sjogren, W.L., R.N. Wimberly, and W.R. Wollenhaupt, Lunar gravity: Apollo 16, Moon, 11, 35-40, 1974b.

Sjogren, W.L., J. Lorell, L. Wong, and W. Downs, Mars gravity field based on a short arc technique, J. Geophys. Res., 80, 2899-2908, 1975.

Sleep, N.H., and R.J. Phillips, An isostatic model for the Tharsis Province, Mars, Geophys. Res. Lett., 6, 803-806, 1979.

Sleep, N.H., and R.J. Phillips, Gravity and lithospheric stress on the terrestrial planets with reference to the Tharsis region of Mars, J. Geophys. Res., 90, 4469-4489, 1985.

Smith, B.A., L.A. Soderblom, T.V. Johnson, A.P. Ingersoll, S.A. Collins, E.M. Shoemaker, G.E. Hunt, H. Masursky, M.H. Carr, M.E. Davies, A.F. Cook, II, J. Boyce, G.E. Danielson, T. Owen, C. Sagan, R.F. Beebe, J. Veverka, R.G. Strom, J.F. McCauley, D. Morrison, G.A. Briggs, and V.E. Suomi, The Jupiter system through the eyes of Voyager 1, Science, 204, 951-972, 1979.

Solomon, S.C., On volcanism and thermal tectonics on one-plate planets, Geophys. Res. Lett., 5, 461-464, 1978.

Solomon, S.C., The elastic lithosphere: Some relationships among flexure, depth of faulting, lithospheric thickness, and thermal gradient (abstract), Lunar Planet. Sci., 16, 799-800, 1985.

Solomon, S.C., and J. Chaiken, Thermal expansion and thermal stress in the Moon and terrestrial planets, Proc. Lunar Sci. Conf. 7th, 3229-3243, 1976.

Solomon, S.C., and J.W. Head, Vertical movement in mare basins: Relation to mare emplacement, basin tectonics, and lunar thermal history, J. Geophys. Res., 84, 1667-1682, 1979.

Solomon, S.C., and J.W. Head, Lunar mascon basins: Lava filling, tectonics, and evolution of the lithosphere, Rev. Geophys. Space Phys., 18, 107-141, 1980.

Solomon, S.C., and J.W. Head, Evolution of the Tharsis province, Mars: The importance of heterogeneous lithospheric thickness and volcanic construction, J. Geophys. Res., 87, 9755-9774, 1982.

Solomon, S.C., J.W. Head, and R.P. Comer, Thickness of the martian lithosphere from tectonic features: Evidence for lithospheric thinning beneath volcanic provinces (abstract), in Reports of Planetary Geology Program, 1978-1979, NASA TM 80339, pp. 60-62, 1979.

Solomon, S.C., R.P. Comer, and J.W. Head, The evolution of impact basins: Viscous relaxation of topographic relief, J. Geophys. Res., 87, 3975-3992, 1982a.

Solomon, S.C., S.K. Stephens, and J.W. Head, On Venus impact basins: Viscous relaxation of topographic relief, J. Geophys. Res., 87, 7763-7771, 1982b.

Spudis, P.D., and P.H. Schultz, The proposed lunar Procellarum basin: Some geochemical inconsistencies (abstract), Lunar Planet. Sci., 16, 809-810, 1985.

Stewart, H.E., J.D. Waskom, and R.A. DeHon, Photogeology and basin configuration of Mare Smythii, Proc. Lunar Sci. Conf. 6th, 2541-2551, 1975.

Strom, R.G., Lunar mare ridges, rings, and volcanic ring complexes, Mod. Geol., 2, 133-157, 1972.

Stuart-Alexander, D.E., and K.A. Howard, Lunar maria and circular basins - A review, Icarus, 12, 440-456, 1970.

Stuart-Alexander, D.E., and R. W. Tabor, Geologic map of the Fracastorius quadrangle of the Moon, Map I-720, U.S. Geol. Surv., Reston, VA, 1972.

Sykes, L.R., Intraplate seismicity, reactivation of preexisting zones of weakness, alkaline magmatism, and other tectonism postdating continental fragmentation, Rev. Geophys. Space Phys., 16, 621-688, 1978.

Thurber, C.H., and S.C. Solomon, An assessment of crustal thickness variations on the lunar near side: Models, uncertainties, and implications for crustal differentiation, Proc. Lunar Planet. Sci. Conf. 9th, 3481-3497, 1978.

Thurber, C.H., and M.N. Toksoz, Martian lithospheric thickness from elastic flexure theory, Geophys. Res. Lett., 5, 977-980, 1978.

Titley, S.R., Geologic map of the Mare Humorum region of the Moon, Map I-495, U.S. Geol. Surv., Reston, VA, 1967.

Trask, N.J., and S.R. Titley, Geologic map of the Pitatus region of the Moon, Map I-485, U.S. Geol. Surv., Reston, VA, 1966.

Turcotte, D.L., and G. Schubert, Geodynamics: Applications of Continuum Physics to Geological Problems, John Wiley and Sons, New York, 450 pp., 1982.

Turcotte, D.L., R.J. Willemann, W.F. Haxby, and J. Norberry, Role of membrane stresses in the support of planetary topography, J. Geophys. Res., 86, 3951-3959, 1981.

Watters, T.R., Gravity induced compressive stress in the Tharsis region of Mars (abstract), Lunar Planet. Sci., 15, 898-899, 1984.

Watters, T.R., and T.A. Maxwell, Crosscutting relations and relative ages of ridges and faults in the Tharsis region of Mars, Icarus, 56, 278-298, 1983.

Whitaker, E.A., The lunar Procellarum basin, in Multi-Ring Basins, Proc. Lunar Planet. Sci., 12A, pp. 105-111, 1981.

Whitford-Stark, J.L., Internal origin for lunar rilled craters and the maria?, Nature, 248, 573-575, 1974.

Whitford-Stark, J.L., The gravity anomalies of Oceanus Procellarum (abstract), in Reports of Planetary Geology Program, 1979-1980, NASA TM 81776, pp. 22-24, 1980.

Whitford-Stark, J.L., A comparison of the origin and evolution of a circular and an irregular lunar mare, in Advances in Plantary Geology, NASA TM 85630, pp. 127-353, 1983.

Whitford-Stark, J.L., and J.W. Head, Oceanus Procellarum: Volcanic and tectonic evolution (abstract), Lunar Sci., 8, 1011-1013, 1977a.

Whitford-Stark, J.L., and J.W. Head, The Procellarum volcanic complexes: Contrasting styles of volcanism, Proc. Lunar Sci. Conf. 8th, 2705-2724, 1977b.

Whitford-Stark, J.L., and J.W. Head, Stratigraphy of the Oceanus Procellarum basalts: Sources and styles of emplacement, J. Geophys. Res., 85, 6579-6609, 1980.

Wilhelms, D.E., Geologic map of the Taruntius quadrangle of the Moon, Map I-722, U.S. Geol. Surv., Reston, VA, 1972.

Wilhelms, D.E., Relative ages of lunar basins (II): Serenitatis (abstract), in Reports of Planetary Geology Program - 1981, NASA TM 84211, pp. 405-407, 1981.

Wilhelms, D.E., Procellarum, a giant planetary basin (abstract), in Reports of Planetary Geology Program - 1982, NASA TM 85127, pp. 111-113, 1982.

Wilhelms, D.E., Effects of the Procellarum basin on lunar geology, petrology, and tectonism (abstract), Lunar Planet. Sci., 14, 845-846, 1983.

Wilhelms, D.E., and J.F. McCauley, Geologic map of the near side of the Moon, Map I-703, U.S. Geol. Surv., Reston, VA, 1971.

Willemann, R.J., and D.L. Turcotte, Support of topographic and other loads on the moon and on the terrestrial planets, Proc. Lunar Planet. Sci., 12B, 837-851, 1981.

Willemann, R.J., and D.L. Turcotte, The role of lithospheric stress in the support of the Tharsis rise, J. Geophys. Res., 87, 9793-9801, 1982.

Wise, D.U., M.P. Golombek, and G.E. McGill, Tharsis province of Mars: Geologic sequence, geometry, and a deformation mechanism, Icarus, 38, 456-472, 1979a.

Wise, D.U., M.P. Golombek, and G.E. McGill, Tectonic evolution of Mars, J. Geophys. Res., 84, 7934-7939, 1979b.

Wolfe, R.W., and F. El-Baz, Photogeology of the multi-ringed crater Haldane in Mare Smythii, Proc. Lunar Sci. Conf. 7th, 2903-2912, 1976.

Wood, C.A., and J.W. Head, Comparison of impact basins on Mercury, Mars, and the Moon, Proc. Lunar Sci. Conf. 7th, 3629-3651, 1976.

Young, R.A., Lunar volcanism: Fracture patterns and rilles in marginal premare craters, in Apollo 16 Preliminary Science Report, NASA SP-315, p. 29-89 to 29-90, 1972.

Young, R.A., W.J. Brennan, R.B. Wolfe, and D.J. Nichols, Volcanism in the lunar maria, Apollo 17 Preliminary Science Report, NASA SP-330, pp. 31-1 to 31-11, 1973.

BIOGRAPHICAL NOTE

I was born in Marietta, Georgia, in 1956, the oldest child of Mary Ann and Al Hall. My interest in planetary science began with a pre-school fascination with the space program. From age 6 to 18 I attended the John McEachern Schools in Powder Springs, Georgia. From the 6th grade on, I spent most of my free time playing the clarinet (I was a member of the All-State Band in my senior year). I seriously considered a career as a classical musician, but was discouraged by the cutthroat competitiveness of the music world (don't ask me why I thought academic science would be any better!). I graduated from high school in 1974 as a National Merit Scholar and a Presidential Scholar, and entered M.I.T. as a freshman in September, 1974. I received my S.B. in Earth and Planetary Sciences in June, 1978, and that fall I began working on my Ph.D. in geophysics at M.I.T. My first year in graduate school was funded by an Ida Green Fellowship. My work experience outside M.I.T. includes summers spent as a policy analyst for the U.S. Geological Survey (1980), and as a AAAS Mass Media Science Fellow at Newsweek magazine (1981).

After completing my doctorate I'm going to spend a month in Europe, where I plan to gain back all the weight (10 pounds) I lost during my thesis crunch. After that I plan to work as a freelance writer, although I expect that it will take most of my first year of freedom to purge my brain of the writing style I had to adopt for this thesis. Right now my main goal in life is to have no major goals for a while -I just want to enjoy life (for a change)!

Besides writing, my interests include running, film, food, theater, music, travel, quiltmaking, and tap dancing.

I was married in 1978 to Rick Buxton, who also holds two degrees from M.I.T. (in physics). Rick works as a medical physicist at Mass. General Hospital. Together we are the proud parents of two cats, Holmes and Watson (combined weight approximately 30 pounds).

POPULAR PUBLICATIONS:

"The Human Side of Science" (review of Scientific Temperaments, by Philip J. Hilts), Technology Review, July, 1983.

"Networking for Success" (review of Winning the Games Scientists Play, by Carl J. Sindermann), Technology Review, May/June, 1983.

"Science From the Inside Out" (review of Science Observed, by Jeremy Bernstein), Technology Review, October, 1982.

"On the Demise of the Dinosaur", Technology Review, Feb./Mar., 1982.

reporting credits:

"How to Build a Bomb", Newsweek, June 22, 1981.

"Cooling Without Kilowatts", Newsweek, August 3, 1981.

"NSA's Cryptic Alliance", Newsweek, August 24, 1981.

SCIENTIFIC PUBLICATIONS:

Hall, J.L., S.C. Solomon, and J.W. Head, Lunar floor-fractured craters: Evidence for viscous relaxation of crater topography, J. Geophys. Res., 86, 9537-9552, 1981.

Hall, J.L., S.C. Solomon, and J.W. Head, Elysium region, Mars: Tests of lithospheric loading models for the formation of tectonic features, submitted to J. Geophys. Res., 1985.

Mouginis-Mark, P.J., L. Wilson, J.W. Head, S.W. Brown, J.L. Hall, and K.D. Sullivan, Elysium Planitia, Mars: Regional geology, volcanology, and evidence for volcano/ground ice interactions, Earth Moon Planets, 30, 149-173, 1984.